Elaboration of 4′-Phosphopantetheine Adenylyltransferase inhibitors and Benzoxaboroles as antimalarial agents

Mokhitli Morake

Supervisor: **Professor Kelly Chibale**

Co-supervisor: **Dr Gregory S Basarab**

Thesis presented for the Degree of

Doctor of Philosophy

in the Department of Chemistry

UNIVERSITY OF CAPE TOWN

May 2022

DECLARATION

I, **Mokhitli Morake**, hereby:

(i) grant the University of Cape Town free license to reproduce this thesis, in whole or in part, for the purpose of research.

(ii) I declare that this thesis is my own unaided work, both in concept and execution, and that apart from the normal guidance from my supervisor/s, I have received no assistance except as acknowledged.

(iii) I declare that neither the substance nor any part of this thesis has been in the past, or is being, or is to be submitted for a degree at this University, or any other university.

Signature: Signed by candidate **Date:** May 1, 2022

TABLE OF CONTENTS

LIST OF FIGURES

LIST OF SCHEMES

LIST OF TABLES

DEDICATION

To my Mother Mme MaMoleboheng Morake for the sacrifices you made over the years for me and my siblings. You believed in education and with nothing but prayer you helped us to reach this far.

To my late father Ntate Morake who would have loved to see this work and for the support he provided during the time our Lord allowed us to have with him.

To my Grandmother Mme MaThoko for unconditional love and support even though not understanding what PhD is.

ACKNOWLEDGEMENTS

I would like to thank my supervisor Professor Kelly Chibale for accepting me into his research group and for a wonderful opportunity to be his student. I am grateful for the support you have provided and the many things I learnt from you in terms of chemistry and drug discovery. Thank you for always making the time to discuss work and other matters with me. I will forever draw from the life lessons you always imparted during our one-on-one meetings. You have challenged me to be a hard worker, to think, to be responsible, to strive for excellence, to be kind and grateful in all circumstances. Thank you for the jokes and laughter that lightened the journey and your contagious smile that always makes you so approachable.

I am grateful to my co-supervisor Dr Greg Basarab from H3D who shared his over 30 years of experience with me. You challenged me to think and to understand what I am doing. Nothing escaped your critical mind and you fostered attention to details in me. I will forever be grateful for how you prioritized my work amongst your busy schedule and for the support throughout this PhD.

I would like to thank my lab mentor Dr Gurminder Kaur who helped me settle in the lab and taught me some tricks. A special thanks to my mentor Dr Lutete "Peguy" Khonde who always made time to talk about work. You have taught me more than science and professional skills I learnt from you have translated into my personal life.

I would like to thank the H3D staff who have been supportive throughout my journey. Thank you for sharing your experience in drug discovery with me and for the many lessons I learnt from you. A special thanks to Dr Preshen Govender who helped with lab techniques, Dr Grant Boyle who was my mentor and kept encouraging me and, Dr Nchinda Nchinda for honest conversations. I also like to thank Mrs Elaine Rutherfoord-Jones for her help with lots of administrative work. Thanks to Mrs Saroja Naicker and Mrs Deidre van Rooyen for the support with many organizational work.

Thank you to our collaborators who supported the project with other aspects: Professor Lynn-marie Birkholtz lab at the University of Pretoria and Dr Sergio Wittlin's lab at Swiss Tropical and Public Health institute who conducted antiplasmodium screening assays. Dr Marcus Lee's lab at the Wellcome Sanger Institute for the barcoded mutant lines screenings. Professor Manuel Llinás lab at the Penn State University for kindly conducting the metabolomics studies. To the

special team at UCT led by Dr Dale Taylor and assistance with chemical rescue assays by Dr Devasha Redhi. Thanks to Professor Timothy Egan's lab for support and the department of Chemistry for facilities.

Thank you to Kelly Chibale Academic Group for the fun we had in the lab even when things were tough. Thank you to all of you for your support. A special thanks to Dr Godwin Dziwornu for always making the time to share his experience. Thank you to Radwan Alnajjar for your support in learning the computational chemistry and Dr Stephen Fienberg who provided invaluable support with CADD. I am grateful to Drs Lauren Arendse and Kathryn Wicht who helped with accessing overseas collaborators.

Thanks to the Sotho Trio Drs Lebu Taleli, Donald Seanego and Mmakwena Mmonwa who helped me with chemistry and explained it in my mother tongue. Thank you for your contribution, criticism of my work and thinking, challenging me to excel and master my work. You pushed for excellence!

Thank you to National Research Foundation for generous support with the PhD scholarship, the UCT Postgraduate Funding Office for funding and the Harry Crossley Foundation. Another big thanks to Professor Chibale for additional support through his research funds. I am grateful to Keystone Symposia for the travel grant to attend the conference at Addis Ababa and Stellenbosch University for funding to attend the StellenCoA 2018 meeting.

Thank you to my "guardian angels" Dr Thabi Melamu, Dr Disa Mogashana and Mr Lucky Mogashana who believed in me even when I thought I can't make it. Your presence in my life has been a blessing. Thanks to Dr Tinashe Chikowore who is beyond a friend but a big brother and a mentor. God bless.

I would like to thank my friends Prince Morake, Teboho Mosidi, Paballo Pule, Dr Thabo Mpotje, Drs Siphiwe (my personal doctor) and Tsoany Makhanye for the love and support you have shown over the years. It is unconditional and I am forever grateful.

Thank you to the Mowbray SDA Church Family for the support, family spirit and the prayers. You have made this PhD journey bearable. Special thanks to Auntie Chuma, Auntie Hannah, Uncle Amuka and Auntie Albie for the prayers and giving me an ear when I needed to confide.

Thank you to my Mum Mme MaMoleboheng Morake for the love and support. I have come this far because of you. I am divinely favoured to have you in my life. Thank you to my siblings Mokhitlinyane, Moleboheng, Mannini and Fusi Morake for encouragement and support throughout my PhD as well as my Grandma, Aunts, Cousins and Uncles who believe in me.

To Akhona Njara, a special person in my life, for your prayers, support, and love. You have made the journey enjoyable and you have been a pillar of strength in many aspects.

I thank God for strengthening me through the journey: “Now unto Him that is able to do exceedingly abundantly above all we can ask or think of be glory forever”.

CONFERENCES ATTENDED

1. **Mokhitli Morake**, Greg Basarab & Kelly Chibale. "Elaboration of 4'-Phosphopantetheine Adenylyltransferase inhibitors as antimalarial agents". Presented at the *StellenCoA2018 Conference*, Stellenbosch, South Africa, 28 October – 1 November 2018. (Poster presentation).
2. **Mokhitli Morake**, Greg Basarab & Kelly Chibale. "Elaboration of 4'-Phosphopantetheine Adenylyltransferase inhibitors as antimalarial agents". Presented at the *Malaria Symposium*, Stellenbosch, South Africa, 30 September – 1 October 2019. (Poster presentation).
3. **Mokhitli Morake**, Greg Basarab & Kelly Chibale. "Elaboration of 4'-Phosphopantetheine Adenylyltransferase inhibitors as antimalarial agents". Presented at *The Malaria Endgame: Innovation in Therapeutics, Vector Control and Public Health Tools (G1-2020)*, Addis Ababa, Ethiopia, 28 October – 1 November 2019. (Poster presentation).

ABSTRACT

Malaria continues to be one of the leading causes of morbidity and mortality in the impoverished parts of the world with majority of the disease burden in Sub-Saharan Africa. The World Health Organization (WHO) 2021 report estimates at least 241 million cases and 627 000 deaths due to malaria in 2020. This is an increase compared to 2019 (227 million cases and 558 000 deaths), and it is also attributed to plateaued declines in malaria cases since 2015 and the 2020 COVID-19 pandemic. The WHO African region accounts for about 95% of the cases, and the mortality in children under 5 years of age is still alarmingly high. Further complicating the situation is the rise in drug-resistant species of the causative agent of the most lethal malaria, *Plasmodium falciparum* (*P. falciparum*). *P. falciparum* has developed resistance against almost all clinically used antimalarials, and there are mounting reports of resistance to artemisinins which are currently the most commonly used antimalarials. Artemisinins are fast-acting and are coupled with longer-acting partner drugs in artemisinin combination therapy (ACT). In South-East Asia, slow parasite clearances and high recrudescence rates following ACT have been reported and resistance to artemisinin partner drugs have been established. Resistance markers to artemisinins have also been identified even in Africa. Therefore, novel antimalarials with better activity against resistant parasites not quickly prone to rapid resistance development are urgently needed. These drugs must have novel modes of actions and act against novel targets in the parasite.

To that end, this PhD project explored novel scaffolds on which to base future antimalarial drug discovery projects. A 500-member compound library of the bacterial 4′-Phosphopantetheine adenylyltransferase (PPAT) inhibitors obtained from AstraZeneca (AZ) containing two chemical series, viz. Ugi and cyclohexyl pyrimidine series, was subjected to the medium-throughput screening at the University of Cape Town (UCT)'s Holistic Drug Discovery and Development Centre (H3D). PPAT is a previously unexplored target in *P. falciparum*, and the current study aimed to reposition both the target and the bacterial PPAT inhibitors for malaria. As such, four hits (two from each series) with moderate antiplasmodium activity against the drug-sensitive *Pf*NF54 strain with IC_{50}'s between 1.04 μM and 2.9 μM were identified. These compounds were resynthesized but were found not to validate with the exception of one compound **2/MM1-19** from the Ugi series, albeit at 2-fold less activity than the hit (IC_{50} = 5.2 μM). The structure-activity relationship (SAR) based on this compound summarized in **Figure 1** yielded compounds with abrogated

antiplasmodium activity (IC_{50}'s >6 μM, which is the highest concentration tested in this assay).

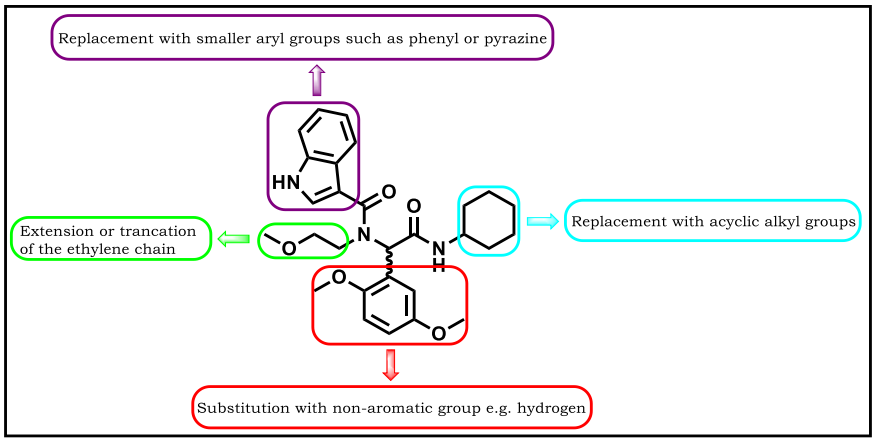

Figure 1: SAR study of the Ugi series-based hit compound 2/MM1-19

In addition to the aforementioned series, bacterial PPAT inhibitors reported by Novartis were explored, and a similar triazolopyrimidine series resulted in a hit compound **28/MM2-145** with *Pf*NF54 IC_{50} = 2.2 μM. Formal hit assessment study of this compound with the SAR strategy proposed in **Figure 2** resulted in compounds with low antiplasmodium activity.

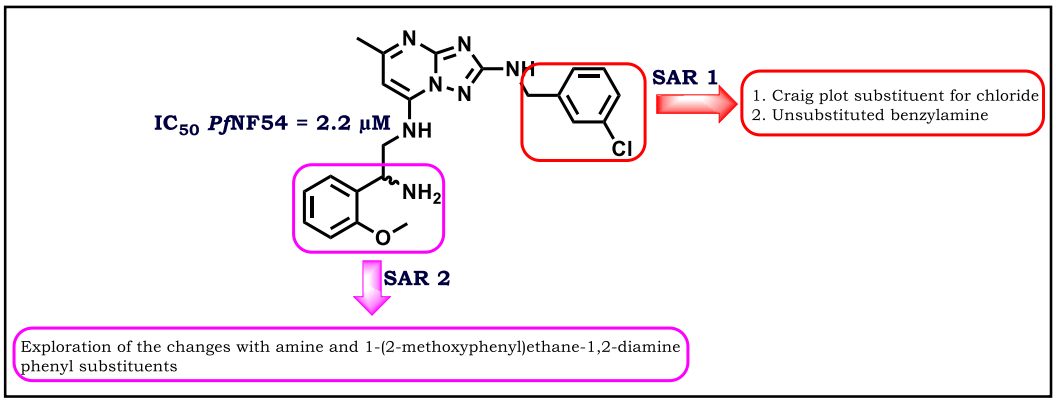

Figure 2: SAR study of the Triazolopyrimidine series-based hit compound 28/MM2-145

The Ugi series compound **2/MM1-19** and the triazolopyrimidine series compound **28/MM2-145** were found not to possess gametocytocidal activity when tested against the early and late-stage gametocytes. The compounds were also not found to be acting on the coenzyme A (CoA) biosynthesis pathway and thus unlikely inhibiting the *Pf*PPAT when subjected to chemical rescue experiments in the presence of high concentration of metabolites of the pathway or the end-product CoA. The metabolomics data showed that compound **2/MM1-19** caused an increase in pyrimidine biosynthesis precursors *N*-carbamoyl-L-aspartate (*N*-Carb-Asp) and

dihydroorotate (DHO) and a marked decrease in a number of peptides. **28/MM2-145** was found to cause an increase in pyrimidine biosynthesis precursors. The increase in pyrimidine biosynthesis precursors implicates pathways similar to those targeted by known antimalarials like atovaquone whose action is along the mitochondrial electron transport chain. Compound **2/MM1-19** did not inhibit β-hematin formation (IC_{50} =1541 µM) as seen by decreased peptides in the parasite culture. In summary, the proposed PPAT inhibitors studied in this thesis were found to exhibit weak antiplasmodium activity and to be acting on different pathways beyond those involving Co-A biosynthesis.

Penicillin binding protein (PBP) inhibitors from an antibacterial programme at H3D were screened for antiplasmodium activity. This identified a hit compound **H3D006145** (**43/MM2-92**) with activity against *Pf*NF54 (IC_{50} = 1.06 µM) and no cytotoxicity against Chinese Hamster Ovarian (CHO) and HepG2 cell lines at the highest concentration tested (IC_{50}'s >50 µM). A formal hit assessment was undertaken for this compound with the proposed SAR plan summarized in **Figure 3**.

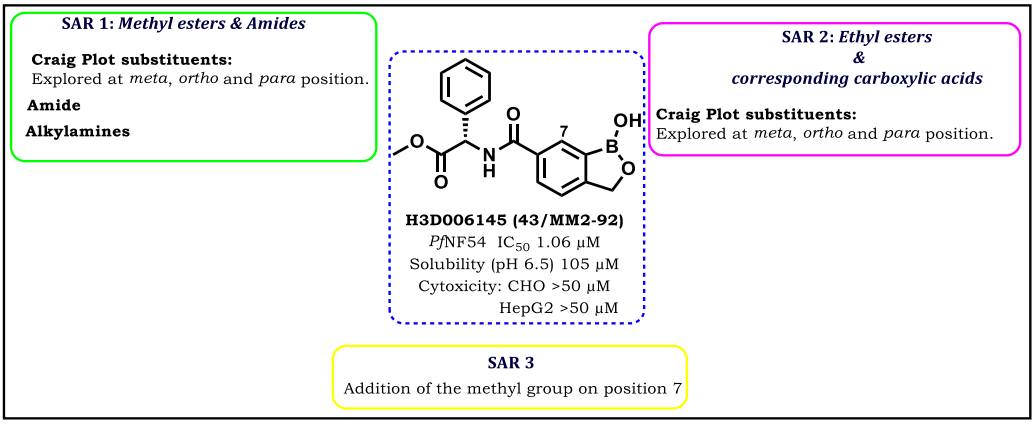

Figure 3: SAR design for compounds in the benzoxaboroles series

The SAR explorations showed that the methyl esters (*Pf*NF54 IC_{50}'s between 0.4 and >6 µM) had better activity than the ethyl esters (*Pf*NF54 IC_{50}'s between 1.21 and >6 µM) and the carboxylic acids were more active than the former two series (*Pf*NF54 IC_{50}'s = 0.12–2.6 µM). These three series were all found to have no gametocytocidal activity against the early and late stages of gametocyte development and were non-cytotoxic against mammalian CHO and HepG2 cell-lines at the maximum concentration tested (IC_{50}'s >50 µM). The investigation of the possible pathways targeted by this class of benzoxaboroles through metabolomics resulted in

ambiguous metabolomic profiles which could not identify the exact metabolites resulting from the parasite treatment. Furthermore, the assessment of a selected representative analogue **45/MM2-91** for cross-resistance in a pool of barcoded resistant mutants with parasites resistant to known antimalarials and those in clinical development showed that the compound was not cross-resistant. This benzoxaboroles class was also found to have high *in vitro* microsomal stability when incubated with human, rat, and mouse liver microsomes with 91–99%, 90–99% and 87–97% of the compound remaining at 30 min, respectively. Retrospective rationalization of the binding mode in the editing domain of the *P. falciparum* Leucyl-tRNA (LeuRS) showed that these compounds have favourable interactions similar to previously reported related compounds. Lastly, the investigation of physicochemical properties determined both computationally and experimentally showed that the benzoxaborole series reported in this thesis possess drug-like characteristics. In conclusion, this study identified a new class of benzoxaboroles with sub-micromolar antiplasmodium activity and properties that supports its progression to a proof-of-concept *in vivo* efficacy study in a mouse infection model.

LIST OF ABBREVIATIONS AND SYMBOLS

δ	Chemical shift
J	Coupling constants
°C	degree Celsius
µW	Microwave
ACT	Artemisinin-based Combination Therapy
ACT	Artemisinin combination therapy
ADME	Absorption, Distribution, Metabolism and Excretion
AZ	AstraZeneca
B2pin2	bis(pinacolato)diboron
boc	*tert*-Butyloxycarbonyl
CADD	Computer-aided drug discovery
CaP	calcium pantothenate
C-C	Carbon-carbon
CHMI	Controlled Human Malaria Infection
CoA	Coenzyme A
COSY	Homonuclear correlation spectroscopy
Cpm	Counts per minute
CQ	Chloroquine
Da	Daltons
DeCoA	dephospho-Coenzyme A
DHODH	Dihydroorotate dehydrogenase
DIPEA	*N,N*-Diisopropylethylamine
DMF	*N,N*-Dimethylmethanamide
EDCI	1-Ethyl-3-(3-dimethylaminopropyl)carbodiimide
eq.	Equivalent
ESI-MS	Electrospray ionization-Mass Spectroscopy
FDA	Food and Drug Administration
G6PD	Glucose-6-Phosphate Dehydrogenase
GSK	GlaxoSmithKline
h	Hour
H3D	Holistic Drug Discovery and Development Centre
HMBC	Heteronuclear Multiple Bond Correlation
HOBt	*N*-Hydroxybenzotriazole
HPLC	High-performance liquid chromatography

HSQC	Heteronuclear Single Quantum Coherence
HTS	High–throughput screening
Hz	Hertz
IRS	Indoor-residual spraying
LC-MS	Liquid Chromatography and Mass spectroscopy
LDH	Lactate dehydrogenase
LeuRS	LeucyltRNA synthetase
LiOH	Lithium hydroxide
LLINs	Long-lasting insecticidal nets
MCRs	Multicomponent Reactions
MDA	Mass Drug Administration
MMV	Medicines for Malaria Venture
MS	Mass spectroscopy
mtETC	mitochondrial electron transport chain
MTS	Medium-throughput screening
NAD^+	Nicotinamide Adenine Dinucleotide
NMR	Nuclear Magnetic Resonance
NPP	New Permeability Pathways
NTDs	Neglected tropical diseases
PanK	Phosphopantetheine kinase
PfCRT	*Plasmodium falciparum* chloroquine resistant transporter
PfCRT	*Pf* chloroquine resistant transporter
*Pf*DHFR	*Plasmodium falciparum* dihydrofolate reductase
*Pf*DHPS	*Plasmodium falciparum* dihydropteroate synthetase
PFI	Property forecast index
*Pf*mdr-1	*Pf* multi-drug resistant
PPAT	4'–phosphopantetheine adenylyltransferase
ppm	Parts per million
RS	Aminoacyl transfer Ribonucleic Acid Synthetase
RTS,S	RTS,S-ASO1
SAR	Structure-activity relationship
SCID	Severe Combined Immunodeficiency
SM	Suzuki-Miyaura
SNPs	Single-nucleotide polymorphisms
TCP	Target Candidate Profile

TLC	Thin Layer Chromatography
TPP	Target Product Profile
tRNA	transfer Ribonucleic acid
U-4CR	Ugi four-component reaction
US$	United States Dollar

Chapter 1: Introduction and literature review

1.1 Chapter Overview

This chapter begins with a review of malaria including a brief history of the disease and its epidemiology. The species *Plasmodium,* which is responsible for the disease, its life cycle, as well as the vector and pathogenesis of malaria are also discussed. The current antimalarial control and preventive strategies are reviewed and the challenges facing their use are highlighted. This is followed by a review of future antimalarials with a specific focus on the newly defined target candidate and target product profiles, as well as a review of the current antimalarial drug pipeline. A brief section on the discovery of antimalarials and the use of metabolomics in drug discovery to identify targets and/or pathways is also included. The biosynthesis of coenzyme A (CoA) and inhibitors of enzymes along this pathway in the context of malaria research is also reviewed. Some background is provided on aminoacyl transfer ribonucleic acid synthetases (RSs), and inhibitors of certain RSs in malaria research are discussed. Emphasis is placed on leucyl tRNA synthetase- and benzoxaborole-based inhibitors and their proposed mechanisms of inhibition. The chapter concludes by highlighting details of this research programme including the justification of the study, objectives, research questions, and specific aims.

1.2 The history and origin of malaria

Malaria has coexisted with humanity for eons and infections are thought to have been driven by continued changes in agricultural practices during the Neolithic revolution. These are thought to have created breeding niches for *Anopheles* mosquito species.[1] The existence of malaria was recorded as early as 2700 BC in China, 2000 BC in Mesopotamia, 1570 BC in Egypt, and in 6th century Hindu texts.[2]

Recent DNA-based analyses have shed some light on the genetic origin of human malaria. Resultant from the interaction between humans and their environment, human malaria parasites share genetic similarities with those infecting wild apes and gorillas from central and west Africa. These findings suggest that human malaria has its origins in these species and not in birds, as was previously proposed.[3, 4] Indeed, the discovery of *Plasmodium knowlesi (P. knowlesi)* as a zoonotic species infecting humans is one example that may shed light on the origin of malaria. Liu *et*

al. analyzed DNA sequences in the feces of wild apes from sub-Saharan Africa and found that *Plasmodium spp.*, including *Plasmodium falciparum (P. falciparum)*, were transmitted to humans from gorillas.[5]

In the 19th century, Charles Louis Alphonse Laveran examined blood smears of soldiers who presented with fever and discovered that the causative agent of human malaria was the protozoan *Plasmodium.*[1, 2] Subsequent studies showed that female *Anopheles* mosquitoes transmitted *Plasmodium relictum* to birds and elucidated the transmission cycle of malaria.[6] These works laid the foundation for research in the following decades and the current understanding of the disease, and informed prevention measures.[2]

1.3 Epidemiology of malaria

Malaria continues to plague humanity with least 50% of the world's population at risk of being infected. However, there have been significant declines in malaria-related morbidity and mortality since 2000.[7] These gains can largely be attributed to intensified efforts for mass distribution of insecticide-treated nets and artemisinin combination therapy (ACT) drug regimens in most endemic countries during the turn of the millennium. In addition, chemoprevention strategies during rainy seasons and the availability of rapid diagnostic tests together with microscopy in endemic regions have assisted progress. There has also been an increase in surveillance and funding, although shortfalls still exist in malaria prevention and elimination strategies.[8]

Despite these gains, infections, and deaths due to malaria remain high. This burden is mostly pronounced in people residing in resource-limited regions of Africa, South-East Asia, and Central and South America (**Fig. 1.1**). There were an estimated 241 million malaria cases in 2020 according to the 2021 World Health Organization (WHO) malaria report compared to 227 million cases in 2019.[9] The majority of these cases were reported in the WHO African Region (95%), followed by South-East Asia (3%) and the Eastern Mediterranean Region (2.1%). The burden of cases is concentrated in 19 countries of the WHO African Region and India, which together make up 85% of global cases. In addition, there were an estimated 627 000 deaths due to malaria in 2020 compared to 558 000 deaths in 2019. The WHO African Region accounted for 95% of deaths despite a significant decrease in the number of deaths compared to the year 2000. The report also shows that 85% of global deaths

were reported from 20 countries in Africa and India. The scourge is mostly felt by children under 5 years, which accounted for 67% of deaths.[9] Malaria kills approximately 1200 children per day in Africa, and this necessitates finding solutions towards the eradication of this disease.[10]

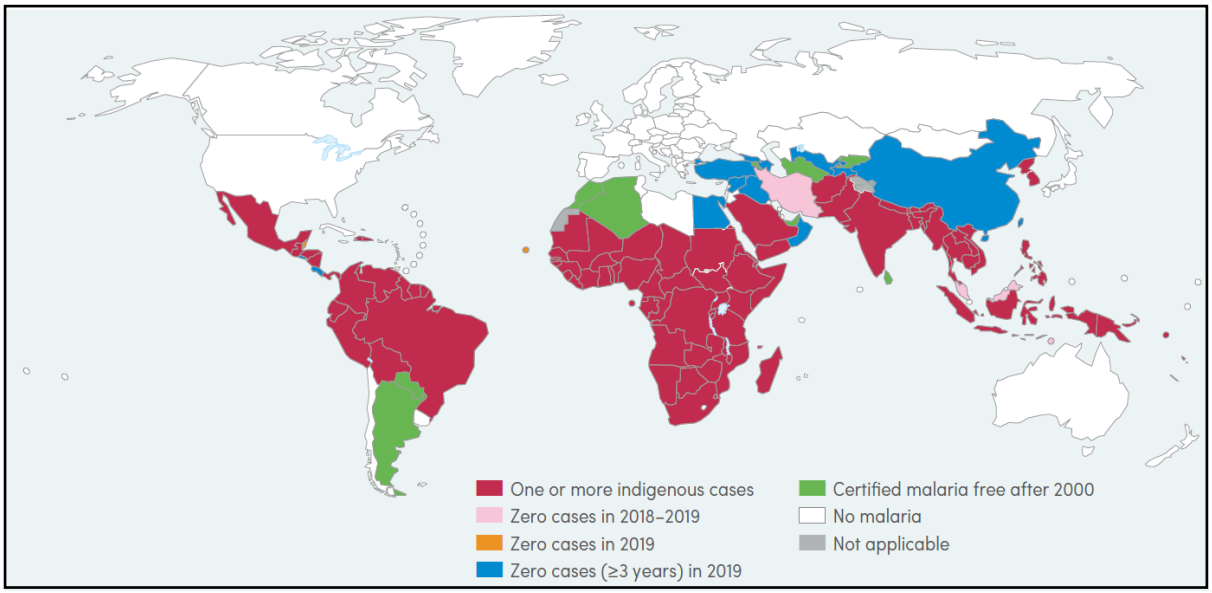

Figure 1.1: Distribution of global malaria cases in 2019[9]

Because of its geographical distribution, malaria is a complicated disease to prevent and treat. In most low-income countries, co-morbidities with human immunodeficiency virus (HIV), tuberculosis (TB), and helminth infections are common.[11] HIV increases the risk of severe malaria and deaths while helminths, which infect >50% of people in endemic areas, increase parasitemia.[12, 13] In addition, pregnant women are also vulnerable to infection and are at high risk.[14] While great strides have been made towards the elimination of malaria, there has been meagre success in lowering the number of malaria cases and deaths has since 2014.[15] This is concerning and threatens to reverse the gains already made, especially in the light of growing parasite resistance to insecticides and antimalarials.

1.4 Malaria parasites, vectors, and pathogenesis

1.4.1 Parasite and vector species that cause human malaria

Malaria is transmitted to humans by a mosquito vector. Female mosquitoes of the genus *Anopheles* are responsible for the transmission of malaria pathogens to humans. There are at least 40 species of *Anopheles* that transmit malaria parasites to humans. Single-celled eukaryotes belonging to the apicomplexan *Plasmodium spp.* cause malaria, and *Plasmodium malariae*, *P. knowlesi*, *Plasmodium ovale*, *Plasmodium vivax (P. vivax)* and *P. falciparum* are the five *Plasmodium* species that infect humans.[14] *P. knowlesi* is of zoonotic origin and is associated with severe cases of malaria in South-East Asia.[16, 17] *P. ovale* and *P. vivax* are associated with disease relapse as they can exist in dormant forms in the liver known as hypnozoites. This is particularly problematic because *P. vivax* can survive in temperate climates and thus exists in many parts of the world.[18, 19] *P. falciparum* is the most virulent of the *Plasmodium* species and accounts for majority of fatalities resulting from malaria especially in sub-Saharan Africa.[15, 20]

1.4.2 Malaria parasite life cycle

The life cycle of the malaria parasite is very complicated and takes place in both human and mosquito hosts (**Fig. 1.2**). The infection begins when a female *Anopheles* mosquito feeds on human blood, releasing needle-like parasite forms known as sporozoites.[8, 14] Sporozoites are taken up the lymphatic system, and some migrate to the liver where they infect hepatocytes. In the liver, these sporozoites undergo multiple fission events (schizogony), thus generating thousands of merozoites. In the case of *P. ovale* and *P. vivax*, some of these sporozoites differentiate into dormant hypnozoites which can later reactivate and reignite infection. Merozoites are released into the bloodstream where they invade red blood cells and replicate rapidly. Merozoites differentiate into ring forms that become trophozoites. The trophozoites differentiate into schizonts and later into merozoites, which are released from ruptured erythrocytes to invade other erythrocytes. This is the stage of malaria infection during which symptoms manifest. An individual may present with low fever, shaking chills, or digestive symptoms, which can progress to drenching sweats, exhaustion, and high fever. These symptoms coincide with the rupture of erythrocytes.[14] In some cases, the disease progresses to severe malaria because of

the obstruction of capillaries by parasitized erythrocytes. Disease complications may manifest as coma, severe anemia, end organ damage, pulmonary complications, and hypoglycemia.[8]

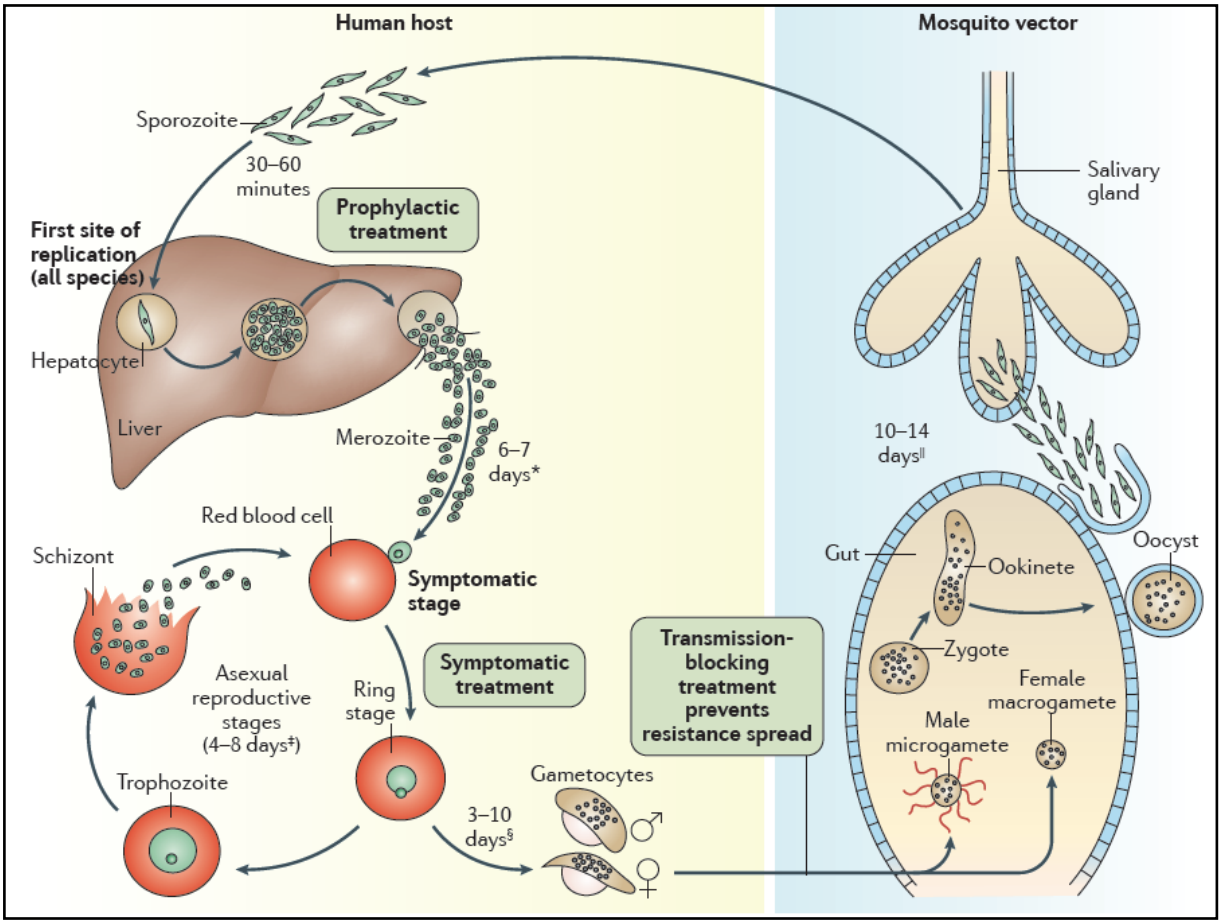

Figure 1.2: Diagram of the malaria life-cycle, including number days for each stage and stages for treatment interventions[14]

Some of the merozoites entering red blood cells differentiate into committed male and female gametocytes. The gametocytes concentrate in skin capillaries where they are taken up by a female *Anopheles* mosquito during a blood meal. Once the gametocytes enter the mosquito gut, they differentiate into microgametes (from male gametocytes) and macrogametes (from female gametocytes), due to the change in environmental conditions. The microgametes are motile and fuse with macrogametes to form a diploid zygote. A diploid zygote differentiates into an ookinete, which exits the mosquito gut's lumen as an oocyst. Oocysts replicate multiple times to form sporozoites, which migrate to the salivary glands where they await transfer into a

human host during a blood meal. This completes the parasite's life cycle between human and mosquito.[8, 14]

1.5 Malaria prevention and treatment

1.5.1 Control and preventive strategies

Strategies for vector control

Targeting the vector involved in malaria transmission has been a strategy prioritized in the fight against malaria. The use of insecticide-treated nets, particularly long-lasting insecticidal nets (LLINs), and indoor-residual spraying (IRS) are integral strategies in the *Global Technical Strategy for Malaria 2016–2030*.[15, 21-23] Scaling up these interventions in many endemic countries has led to a significant decline in disease burden, and it is thought that universal coverage will assist in accelerating malaria eradication.[24] The concurrent use of LLINs with non-pyrethroid IRS has an added benefit in endemic areas in that mosquitoes that successfully bite an infected individual can be targeted by IRS while resting on treated surfaces upon exit from the household, thus interrupting the spread of the disease.[21, 25] Despite their obvious benefit in controlling malaria, these strategies are threatened by the parasite's increasing resistance to insecticides. The insecticides most commonly used are organochlorides, organophosphates, carbamates, and pyrethroids, with the latter being the most extensively used.[26] Resistance to these insecticides will greatly hamper progress towards eradication and universal coverage for the use of LLINs and IRS. The WHO encourages countries to continue tracking resistance and recommends investment in finding new types of insecticides.[27]

In addition to the aforementioned strategies, the use of biological vector control is considered a crucial part of malaria eradication programs. Biological vector control can be achieved using biological tools such as entomopathogenic fungi, bacteria, viruses, and larvivorous fish.[28] These strategies are enhanced when used together with LLINs and IRSs, considering growing resistance towards insecticides. An advantage of using biological vector controls in integrated vector management programs is that they do not appear to contaminate the environment nor suffer resistance from *Anopheles* mosquitoes. A recent review on the use of bacterial larval control in sub-Saharan Africa showed that in low to moderate transmission settings, larviciding was well accepted, specific to mosquitoes, cost-effective, and

complementary to other vector control strategies.[29] Therefore, it is important that this strategy be incorporated in eradication programs.

Vaccination

The discovery of a malaria vaccine will positively impact disease control and will be a significant step towards malaria eradication. RTS,S-ASO1 (RTS,S) is the first malaria vaccine to be approved by the WHO for clinical use.[30] GlaxoSmithKline (GSK) has worked on this vaccine since 1987 and their efforts are starting to pay off 30 years later.[31] RTS,S-ASO1 is a combination of the RTS,S which is a protein expressed on the surface of sporozoites and a hepatitis B surface antigen, while the ASO1 is an adjuvant. RTS,S targets invasion of sporozoites in the liver by generating antibodies that recognise sporozoites and provide immunity against this infectious form. The main challenge facing this vaccine is the short time needed by sporozoites to infect the liver (approximately 30 min), which implies that the immune response must be developed as quickly as possible.[32] Phase III clinical trials showed that the protective efficacy of RTS,S is suboptimal as it protects only 30% of children, and 40% of children with severe malaria. Despite its recent approval, an RTS,S pilot study launched in Ghana, Kenya, and Malawi is still ongoing.[33] Data from this study show that RTS,S is safe and prevents malaria in children in moderate-to-high transmission areas, and the WHO has therefore recommended its integration into prevention programs.[30] Besides RTS,S, other vaccines are now in early phases of clinical trials, including vaccines that target the pre-erythrocytic stage (R21 and modified parasites, *Pf*SPZ), the blood stage (RH5), and the transmission stage (*Pf*S230).[34]

Chemoprophylaxis

Chemoprophylaxis is a preventive strategy that is used particularly by travellers to malaria-endemic areas who have never been exposed to malaria. Chemoprophylaxis targets blood-stage active schizonticides. The use of these drugs is required for days or weeks before the traveller leaves their country, daily or weekly during their stay in an endemic country, and for days or weeks after their return. The main challenges facing effective chemoprophylaxis are lack of compliance and adverse effects. Policies guiding recommended drugs used for chemoprophylaxis vary between countries, although the main drugs used are mefloquine, doxycycline, atovaquone-proguanil, and primaquine. However, these have varying efficacy and may be tolerated

differently in individuals, leading to problems associated with non-compliance.[35, 36] For instance, doxycycline requires daily administration once in an endemic area and mefloquine requires weekly administration, and this often leads to inconsistent compliance as these drugs must be taken at specified times. Other issues include contraindications associated with these drugs: for example, mefloquine may cause neuropsychiatric disorders, doxycycline is contraindicated during pregnancy and may lead to skin photosensitivity, and primaquine poses a risk of severe haemolytic anaemia in glucose-6-phosphate dehydrogenase (G6PD)-deficient individuals. The recently approved primaquine analogue tafenoquine has a longer half-life (15 days) and is active against both *P. falciparum* and *P. vivax*.[36] A long half-life will minimize dosing frequency and thus improve compliance. However, like primaquine, tafenoquine is contraindicated in G6PD-deficient individuals.[37, 38]

Mass drug administration and seasonal malaria control

Mass drug administration (MDA) with effective doses of antimalarial drugs is encouraged to the entire population residing in areas of low transmission to eliminate malaria.[39, 40] The therapeutic advantages of this strategy are clearance of the parasite from the blood and prophylaxis against future infections. However, MDA increases the risk of rapid development of drug resistance. Although this is possible, it is proposed that parasites that have selected for resistance are likely to be the cause of resistance rather than treated individuals. MDA is therefore more beneficial when applied as an elimination strategy in a circumscribed location with low transmission rather than as part of a control program in high-transmission settings. This reduces the risk of selecting for resistance. Furthermore, the mass treatment of symptomatic individuals who carry a high parasite load contributes to lowering the spread of parasites and leads to decreased malaria transmission and infections in a specific endemic setting.[39-41] Although successful MDA programs have been reported in the small island of Aneityum in the South Pacific Ocean with a small population below 1000, this strategy has not achieved the goal of complete elimination in Africa and there have been reports of failure and development of resistance.[41, 42]

1.5.2 Current antimalarial drugs and challenges facing malaria treatment

There are different classes of antimalarials in clinical use which differ according to their structures and the stage of infection against which they act. These classes are discussed in this section and the chemical structures of the drugs are shown in **Figure 1.3**.[43]

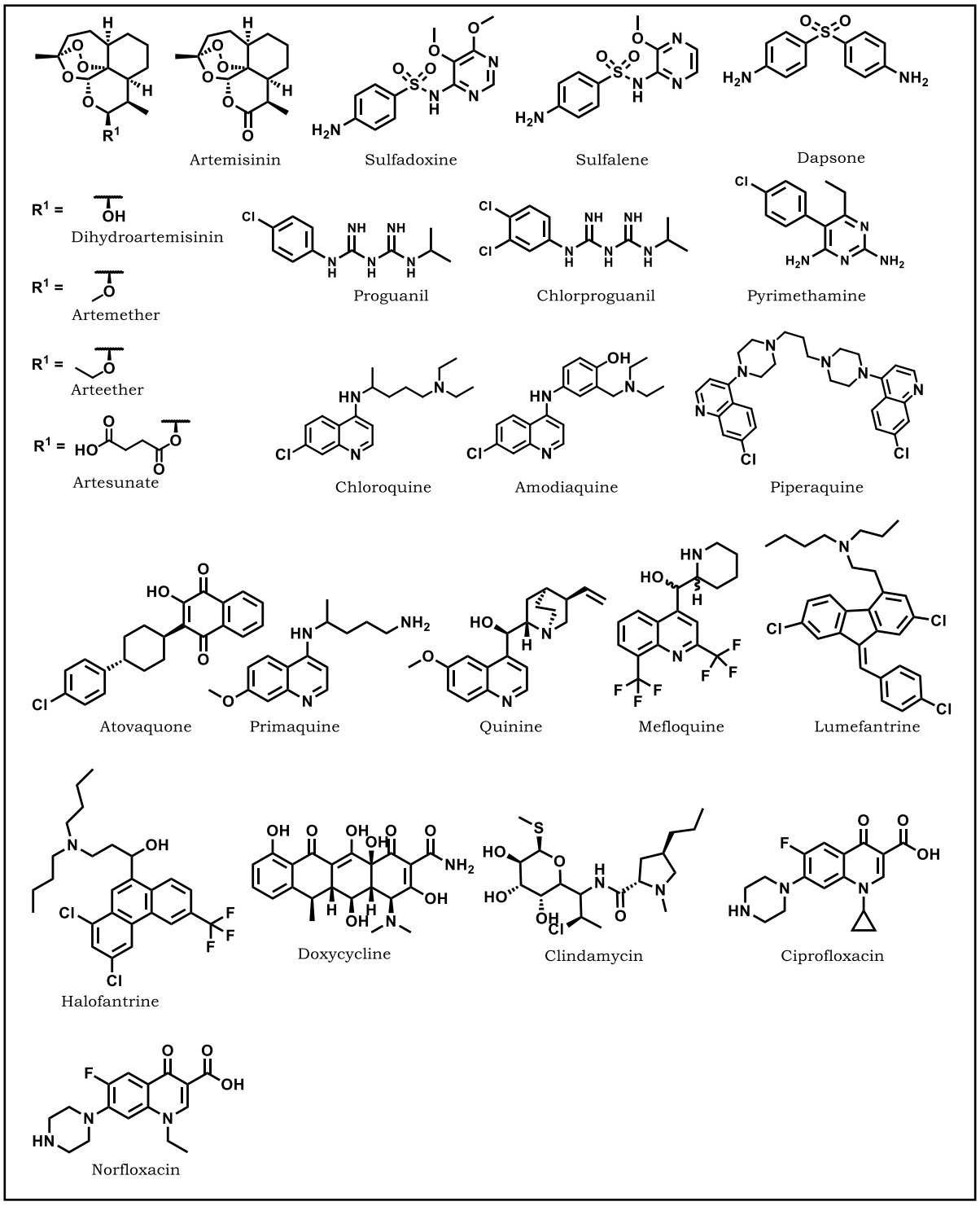

Figure 1.3: Antimalarial drugs in clinical use

Current antimalarial drugs

Artemisinin was discovered from *Artemisia annua* in the 1970s in an effort to identify new antimalarials in the wake of emerging chloroquine resistance. As artemisinin is poorly soluble, first-generation derivatives (collectively called artemisinins) were synthesized, viz. the water-soluble artesunate and the lipid-soluble arteether and artemether (**Fig. 1.3**).[44-47] These compounds are fast-acting with a short half-life of approximately 45 min to 7 h and are rapidly cleared.[48] They are all prodrugs of the most active metabolite dihydroartemisinin.[49] Artemisinins are effective blood schizonticides and have potential activity against the early sexual stage.[50, 51] Artemisinins are not used in monotherapy but rather in combination with other antimalarials as part of ACT for the treatment of uncomplicated malaria. The rationale behind ACT is that the fast-acting artemisinin component may rapidly reduce parasite biomass while the long-acting partner drug can continue to clear parasites after concentrations of the artemisinin partner decrease.[52] This strategy was also aimed at delaying the development of resistance against artemisinins. However, there have been reports of delayed parasite clearance in treated patients and increasing recrudescence following ACT treatment in South-East Asia.[8, 53, 54] These are largely due to parasites carrying mutations on the *Pf*Kelch13 gene. This is in addition to established resistance against partner drugs such as mefloquine and sulfadoxine-pyrimethamine.[55-58] Similar resistance markers have started to emerge in several African countries although ACTs remain efficacious at various sites.[59-62] However, this threatens to render ACTs ineffective in the near future.

Other key antimalarials in clinical use today have their origin in quinine, which was first isolated in 1820 from the Cinchona tree. The bark of this tree was used for the treatment of malaria by missionaries working in Peru as early as the 1600s.[63] These compounds include various classes such as aryl amino alcohols (quinine, mefloquine, halofantrine, and lumefantrine), 4-aminoquinolines (chloroquine and amodiaquine), and 8-aminoquinoline (primaquine; **Fig. 1.3**).[64] Chloroquine, a 4-aminoquinoline synthesized in 1934, was a cornerstone of antimalarial treatment in the 1950s until resistance developed against it. Other derivatives played a major role in the treatment of malaria and remain important antimalarials with activity against the erythrocytic stage of infection. However, primaquine is active against the hepatic forms of *P. vivax* and *P. ovale* as well as against gametocytes.[65] Resistance to quinoline-based antimalarials has since developed but these drugs remain useful

and are important constituents of ACT in the treatment of uncomplicated *P. falciparum* malaria in endemic areas.[56, 66]

Folate biosynthesis inhibitors are also important antimalarials that interfere with the synthesis of DNA precursors and cell multiplication.[67] These antifolates target *P. falciparum* dihydropteroate synthetase (*Pf*DHPS) and dihydrofolate reductase (*Pf*DHFR).[68] The *Pf*DHPS inhibitors are sulfur-based drugs such as sulfadoxine, sulfalene, and dapsone (**Fig. 1.3**), which compete with para-aminobenzoic acid for the active site of *Pf*DHPS. *Pf*DHFR inhibitors include chlorproguanil (converted to active metabolite chlorcycloguanil), proguanil (converted to the active metabolite cycloguanil), and pyrimethamine (**Fig. 1.3**), which compete with dihydrofolate for the active site of *Pf*DHFR.[69] Antifolates are used in combination because they act synergistically with nanomolar-active *Pf*DHPS inhibitors, potentiating the micromolar-active *Pf*DHFR inhibitors.[69] Combination therapies currently in clinical use include Fansidar® (pyrimethamine and sulfadoxine), Metakelfin® (pyrimethamine and sulfalene), Malarone® (proguanil and atovaquone), and Lapdap® (chlorproguanil and dapsone). Resistance to antifolates is also established,[56, 70, 71] however, these remain important partner drugs in ACT.[72]

Antibiotics have emerged as useful antimalarials for the treatment of uncomplicated drug-resistant *P. falciparum* infections. These are slow-acting and exert a delayed death effect.[73, 74] This class comprises tetracyclines (doxycycline), macrolides (clindamycin and azithromycin), and fluoroquinolones (ciprofloxacin and norfloxacin; **Fig. 1.3**). Antibiotics are recommended for use in combination with fast-acting antimalarials, such as clindamycin-quinine, for the treatment of uncomplicated *P. falciparum* infection during pregnancy. Their use is important in regions with ongoing resistance, and they are also used in causal prophylaxis to target both blood- and liver-stage parasites.[73, 75, 76]

Challenges for malaria treatment

In the absence of an effective vaccine against malaria, antimalarial chemotherapy remains the cornerstone of malaria treatment and prevention. There are currently no drugs active against all stages of *Plasmodium* development. The majority of current antimalarials act against erythrocytic stages of infection and a few are active against the pre-erythrocytic stage, thus showing potential for prophylaxis.[77]

Chemoprotection relies solely on the schizonticidal combination of atovaquone-proguanil as the development of drugs that can target both dormant hepatic forms associated with *P. vivax* and *P. ovale* and the transmittable gametocyte stage are not yet available.[53, 78, 79] Quinine-based antimalarials such as chloroquine, primaquine, and mefloquine have been the mainstay of antimalarial chemotherapy for decades but suffer from safety liabilities. Mefloquine induces severe neuropsychiatric toxicity and quinine itself is known to cause cinchonism, manifesting as tinnitus, blindness, dizziness amongst other complications.[80] Primaquine, which shows anti-relapse potential against *P. vivax* and *P. ovale* infections and is used in malaria prophylaxis, causes severe hemolysis in individuals with G6PD deficiency.[37] Its derivative tafenoquine, which also shows anti-relapse potential and which was recently approved for use in relapse prevention and prophylaxis, is subject to the same toxicity risk. Other antimalarials have varying toxicity profiles and may cause neurotoxicity and/or ototoxicity.[81-83] These safety concerns have the unfortunate consequence of limiting their use in vulnerable groups such as pregnant women and young children, with the latter bearing the brunt of the annual malaria cases and deaths. Antibiotics also have adverse effects on both pregnant women and children.[84]

Another challenge facing malaria chemotherapy is the emergence of resistance that has decreased the efficacy of almost all antimalarials.[85] Resistance to chloroquine is widespread and there are reports of ACT treatment failure in parts of South-East Asia, resulting from a loss of efficacy of some partner drugs. Mefloquine-only and mefloquine-artesunate treatment failure has been reported in this area.[86, 87] Although ACT remains effective, resistance markers on *PfKelch13* associated with slow parasite clearance by artemisinins have also been identified in some parts of Africa.[61] In addition to this, the availability of counterfeit and substandard antimalarials in circulation in low-income African and Asian countries fuels resistance selection.[88] The loss of artemisinin efficacy would be hugely detrimental to the goal of eliminating malaria and novel antimalarials are thus urgently needed. Some of the antimalarials currently in advanced clinical trials are discussed in the following section.

1.6 Future antimalarials: newly defined target candidate and target product profiles

One of the major impediments to the complete eradication of malaria is the emergence of parasite strains resistant to current antimalarials. This has made

malaria the first priority tropical disease in the WHO portfolio. The development of new antimalarials and the effective use of current antimalarials in combination therapy is a top priority towards malaria. An ideal antimalarial drug will be one that is active against all stages of malaria, can be administered as a short-course or single-dose treatment, is well tolerated in vulnerable groups such as pregnant women and young children, is affordable to poor populations, and is refractory to drug resistance.[67, 77, 79, 89]

Newly defined target candidate profiles (TCPs) and target product profiles (TPPs) envisage that quality molecules enter clinical trials, quality medicines be used in combination therapies, and their formulations be delivered for clinical use.[14] According to the Medicines for Malaria Venture (MMV), preclinical candidates have 8% chance of successfully becoming a product and approximately 2% only of the drugs entering clinical trials will reach late-stage development.[14, 90, 91] The main attributes of new medicines as guided by the TCP and TPP are briefly discussed below.

1.6.1 Combination therapy towards the elimination and eradication of malaria

The future of malaria chemotherapy will be based on combination therapy in order to delay the inevitable development of parasite resistance to drugs. Such combinations will have to be collated based on the efficacy, propensity to resistance, safety of each component, and compatibility with co-formulation.[91] The current failure of some ACTs in the clinic has encouraged research into single exposure with triple combinations (addition of a third partner drug to ACT) and multiple first-line therapies that will rotate ACTs in a specific area.[87, 92-94] An ideal antimalarial combination will require molecules with activity against more than one stage of the parasite life cycle, as current regimens mostly comprise drugs active against the blood stage. This highlights an urgent need for compounds with transmission-blocking potential (acting against late-stage gametocytes) and chemoprotection (inhibiting hepatic schizonts).[14, 91] Additionally, a combination that includes anti-relapse antimalarials will greatly assist in eradication of *P. vivax*- and *P. ovale*-associated malaria.[89, 91]

1.6.2 Resistance-proofing

New molecules should be active against all five *Plasmodium* species, viz. *P. falciparum*, *P. malariae*, *P. vivax*, *P. ovale*, and *P. knowlesi*. There are always risks of *Plasmodium* species developing resistance against new molecules in the future.[95] Therefore, new molecules should only be used in combination to delay selection for resistance by parasites.[94] These compounds must also be assessed for cross-resistance against different existing parasite strains. Indeed, new guidelines and assays have now been developed to assess resistance markers in these molecules. Among these are laboratory-adapted mutant strains raised under drug pressure to test compounds against field isolates and assess cross-resistance through DNA-barcoded mutant strain technologies.[62] These will also help in identifying combinations of molecules that do not show cross-resistance with one another. Ultimately, new antimalarials must be developed such that they may withstand parasite resistance and enhance or protect the efficacy of artemisinins until other active compounds are identified for future front-line treatment.[91, 96]

1.6.3 Safety and cost

Eradicating malaria will require treatment of the entire population at risk. However, drugs safety studies are difficult to carry out in pregnant women and very young children. Further complicating this is the prevalence of co-infections with diseases such as HIV/AIDS and TB amongst high-risk populations.[79] In the case of HIV/AIDS, co-treatment may increase risks of drug-drug interactions through cytochrome P450-mediated metabolic pathways with consequently reduced efficacy or enhanced drug exposure, causing increased adverse side effects.[97] Ideally, new molecules would also address complicated severe malaria, which will often require parenteral administration in the absence of injectable alternatives, rather than oral administration as a patient may be unconscious. New molecules should also be inexpensive as the populations that most need them tend to be impoverished. The use of combination therapy may include complex formulations, which will inevitably increase the cost of production and thus affect access by the target population.[91, 97]

1.7 Antimalarial pipeline

Product development partnerships such as MMV (founded in 1999) and Drugs for Neglected Diseases Initiative (DNDi, founded in 2003) have been established to integrate efforts towards the discovery and development of new antimalarials. These partnerships are funded through philanthropic and public agencies and have managed to leverage expertise from pharmaceutical and academic sectors to accelerate the discovery of novel antimalarials.[98] MMV publishes regular updates on its website on the progress of new antimalarials traversing through the drug pipeline and highlights the clinical trial stage of each candidate. Clinical trials can be divided into three phases following the discovery and preclinical phases, viz. Phase I, Phase II, and Phase III. In Phase I clinical trials, drug safety is assessed in a small group of healthy volunteers (n = 20–80) without the disease. Phase II is a proof-of-concept study for efficacy in diseased patients (n = 100–300). This is followed by a further efficacy study in Phase III in diseased patients (n > 1000) in a randomized double-blind study comparing the test drug to an existing drug.[99] A recent update on some of the compounds traversing through the MMV pipeline (**Fig. 1.4**) is briefly discussed and we focus on molecules in human volunteers and patient exploratory stages (**Fig. 1.5**).[100]

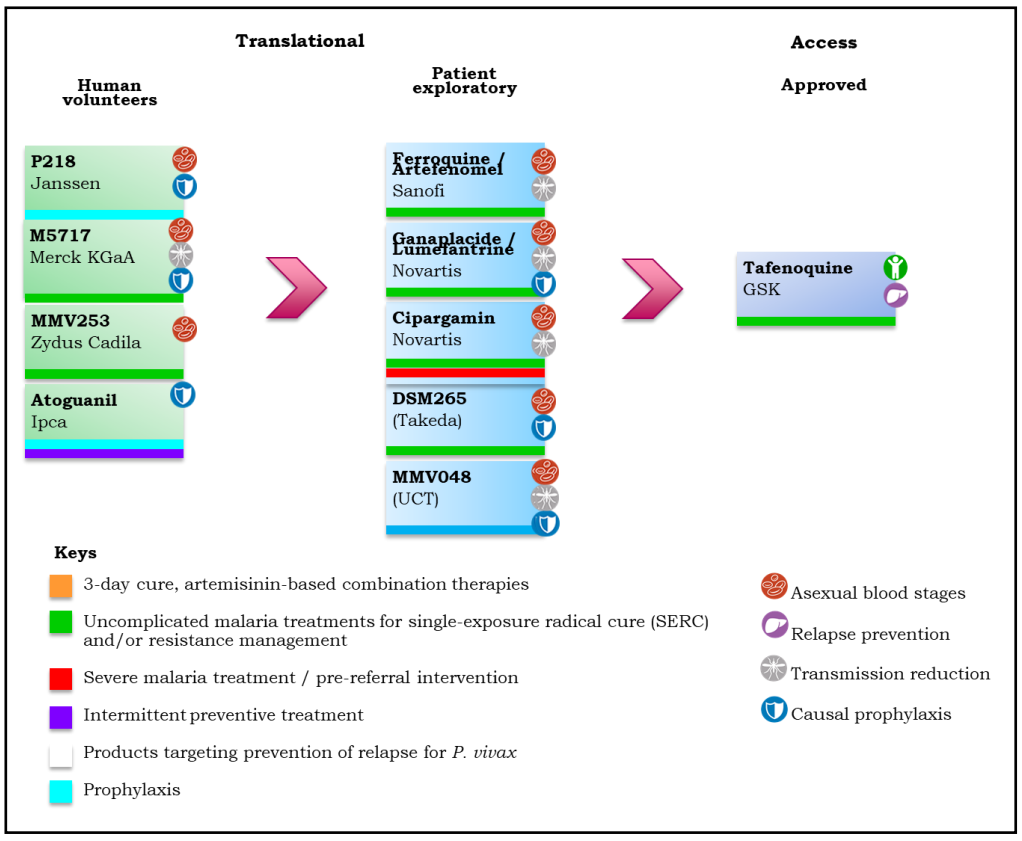

Figure 1.4: Recent MMV antimalarial pipeline

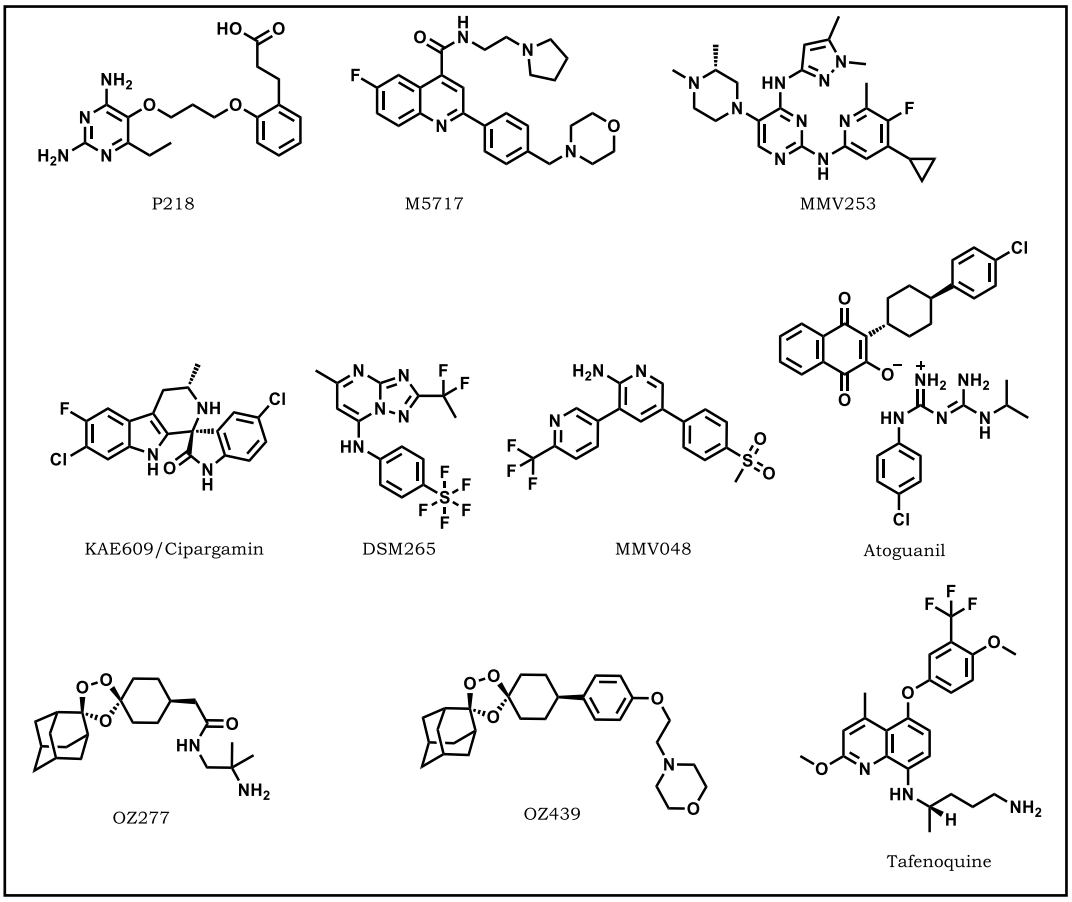

Figure 1.5: Structures of antimalarials currently in the drug pipeline

1.7.1 Human volunteers

Drug candidate P218 (**Fig. 1.5**), a 2,4–diaminopyrimidine antifolate, has completed Phase I clinical trials and is envisioned for deployment in prophylaxis with potential use in combination treatment as an alternative for pyrimethamine or as a long-acting agent through injectable formulation.[49, 101] Another promising candidate is the 2,6–disubstituted quinoline–carboxamide M5717 (**Fig. 1.5**), which has demonstrated multi-stage activity and transmission-blocking potential. This compound's promising pharmacokinetic profile in preclinical species and acceptable safety properties enabled its first-in-human studies.[102] The projected low cost of production per treatment (approximately US$1) is an asset as target patients typically reside in low-income countries.[49] The first-in-human studies for MMV253 began in February 2019, and this compound has potential to be used in combination therapies owing to its predicted long half-life of 36 h in humans. Future milestones will assess human pharmacokinetics and efficacy.[49, 103]

The developmental combination therapy Atoguanil comprising atovaquone and proguanil is set for completion of bioavailability studies. This combination is intended for intermittent preventive therapy and prophylaxis, and to offer a cheaper alternative to atovaquone in low-income malaria-endemic areas.[100, 104]

1.7.2 Patient exploratory studies

Several diverse antimalarials are also progressing along the patient exploratory stages (**Fig. 1.5**). KAE609/cipargamin belongs to the spiroindolone class and a Phase II clinical study showed that administration of a 30 mg dose for 3 days in adults with uncomplicated *P. falciparum* and *P. vivax* achieved parasite clearance. The compound has a half-life of 12 h[8] and parenteral studies are currently ongoing. Also in Phase II clinical trials is the triazolopyrimidine DMS265, which shows excellent oral bioavailability and low clearance.[105] In Peru, a Phase IIa study was completed in controlled human malaria infection (CHMI) with *P. falciparum* and *P. vivax* and DSM265 was found to clear these parasites after administration of a single dose only. It is currently being explored for use in combination with OZ439 in a CHMI study.[106]

MMV048 is the first antimalarial developed in Africa to reach clinical trials. It was discovered through optimization of the phenotypic screening lead of a BioFocus Kinase library at the University of Cape Town's Drug Discovery and Development Centre (H3D). It is part of the 2-aminopyridine class of compounds and was shown to target the ATP-binding pocket of phosphatidylinositol 4–kinase (PI4K).[107] This compound was well tolerated in humans and shows a promising pharmacokinetic profile, with potential for use in prophylaxis and single-dose cure. It had begun Phase IIa clinical trials in Ethiopia in adults with acute, uncomplicated *P. falciparum* or *P. vivax*,[108] but development was discontinued due to toxicity concerns later identified in animal studies (unpublished).

Emerging resistance and the high cost of production required for artemisinins necessitate replacement with cheaper alternatives.[109] The ozonide compound OZ439 (artefenomel) is an optimized analogue of OZ277 (arterolane, discovered in 2004) that is currently in Phase II clinical trials in combination with the 4-aminoquinoline ferroquine. This combination is balanced by the fact that OZ439 is fast-acting (elimination half-life: 46–62 h) but shows slower clearance than artemisinins (0.5–4

h), while ferroquine is long-acting (elimination half-life: 16 days).[89, 110] This combination is expected to result in a single-exposure radical cure.

Tafenoquine, an 8–aminoquinoline, was approved by the US Food and Drug Administration (FDA) in 2018 for the treatment of malaria, especially in *P. vivax*-associated relapses.[111] Although it has single-exposure radical cure potential, it is recommended to be co-administered with blood schizonticides. Like primaquine, tafenoquine is contraindicated in patients with G6PD.[112] This drug is currently under development by GSK and is under review in four endemic countries.[100]

There are other compounds with desired structural diversity, novel mechanisms of action, and activity against novel drug targets in the MMV antimalarial pipeline (**Fig. 1.5**). The pipeline also shows a number of new combination therapies recently approved for deployment in clinic.

1.8 Drug discovery approaches and target pathway identification

1.8.1 Phenotypic screening

There is an urgent need for effective drug discovery in tropical diseases such as malaria considering their deleterious impact on human lives. However, research into such diseases does not offer much return on investment due to their geographic distribution. Indeed, drug discovery is a long and costly endeavour lasting 13–15 years and costing approximately US$2–3 billion.[113, 114] Against the backdrop of this long timeframe and exorbitant cost is the low rate at which new drugs enter the market, with 20–30 drugs approved by the FDA per annum.[115, 116] As such, methods used to identify drugs for tropical diseases should include cost mitigations as funding will likely stem from governmental or philanthropic contributions. There are several strategies applied to the discovery of new drugs including whole-cell phenotypic screening, target-based screening, computer-aided drug discovery, and structure-based design.[117] The contributions of each of these strategies towards the discovery of new drugs differ. An analysis of drugs approved by the FDA between 1999 and 2008 showed that phenotypic screening produced more drugs than target-based drug discovery approaches. The latter was also attributed to high attrition rate in clinical phases and low productivity in overall pharmaceutical research and development.[118]

High-throughput screening (HTS) of libraries containing thousands to hundreds of thousands of compounds has become a central strategy in many pharmaceutical industries to identify new chemical entities. Advances in HTS technologies have enabled the development of robust whole-cell phenotypic and target-based HTS campaigns.[119] Both these screening methods show advantages and disadvantages. The complementarity of these two strategies is increasingly embraced by the drug discovery community.[120, 121] While target-based screening received attention over the past three decades, whole-cell phenotypic screening is experiencing a revival because of new genomic tools that enable the study of targets of new chemical entities. Whole-cell phenotypic screening yields hits endowed with lead-like properties such as the ability to enter cells and this is advantageous in finding new lead molecules. However, the disadvantage of this strategy is that the target of the compounds remains unknown and will require a target-deconvolution step to identify the target and elucidate the drug's mechanism of action (MoA). Several strategies including chemoproteomics, generation of *in vitro* mutations under drug pressure followed by whole-genome sequencing analysis, cellular thermal shift assay, knockdown models, chemoinformatics, and metabolomics have been developed to better understand the targets of antimalarials.[122, 123]

1.8.2 Metabolomics

Metabolomics is an "omics" technique that focuses on the study of small molecules (<1 kDa) through the analysis of cellular metabolites. Metabolomics can provide a complementary representation of the molecular phenotype of health and disease to other omics approaches, including genomics, transcriptomics, and proteomics.[124] It enables the prediction of enzymatic activities in cells and the study of metabolites as end-products of cellular processes whose levels reflect ultimate responses to genetic changes.[125, 126] Its application in drug discovery and development enables scientists to predict the mode of action of drug molecules and to identify the metabolic pathways involved. Metabolite concentrations are thought to reflect enzymatic activity and provide a greater understanding of the overall phenotype of the system. This may accelerate drug discovery and development by informing scientists about pathways and target proteins perturbed by drug treatment, thus allowing for structure-based drug discovery and target identification.[126-130]

There are two approaches through which metabolomics studies are designed, viz. targeted and untargeted metabolomics. Targeted metabolomics is hypothesis-driven and metabolites are measured to test a specific biochemical hypothesis.[131] Therefore, targeted metabolomics attempts to provide insight into the effect of drugs or genetic modifications on a specific enzyme or pathway under study. Conversely, untargeted metabolomics is an unbiased study of global metabolic profiles in a biological sample with the aim of gaining a greater understanding of the effect of drugs.[131]

Recent studies have used metabolomics in antimalarial drug discovery to identify metabolic perturbations in the parasite following treatment with novel antimalarials. Metabolomic profiles can match those of known antimalarials and may reveal changes in the intermediates formed in critical cellular pathways.[127, 132] Metabolomics has helped uncover pathways targeted by antimalarial compounds to provide insight into the mechanisms of action. Untargeted metabolomics was applied to provide an unbiased, hypothesis-free understanding of the actions of these compounds.[132] In one study using hypothesis-driven targeted hydrophilic metabolomics, metabolomic fingerprints (metaprints) were defined based on projections of log2-fold changes in values following metabolic perturbation by a specific compound. Metaprints provided a simple way of visualizing metabolic changes induced by each compound and delivered a unique overview of the compound's phenotype. This study defined four main metabolic processes affected by perturbation: cellular homeostasis, folate biosynthesis, mitochondrial electron transport chain (mtETC)/pyrimidine synthesis, and hemoglobin catabolism.[127] The significance of this technique is its ability to accelerate the discovery phase of novel antimalarials by uncovering target pathways.[127] An understanding of pathways will ultimately guide identification of target proteins and will help triage next-generation antimalarials.

1.9 The coenzyme A biosynthesis pathway and its enzymes as drug targets

1.9.1 Coenzyme A biosynthesis pathway

Coenzyme A (CoA) is an essential cofactor for all eukaryotic and prokaryotic species that acts as an acetyl carrier and carbonyl activating group in many metabolic pathways. The prosthetic 4′-phosphopantetheine group is incorporated into a variety of biosynthesis pathways including fatty acids biosynthesis, the tricarboxylic acid

cycle, non-ribosomal protein biosynthesis, and membrane biogenesis.[133, 134] The centrality of this essential biomolecule makes its biosynthesis and utilization an attractive area of research as none of the current antimalarials are known to target CoA biosynthesis and/or uptake.

Pioneering works by William *et al.* (1933) demonstrated that pantothenic acid was required for the growth of *Saccharomyces cerevisiae* in culture and, subsequently, for the growth of a variety of organisms.[133] Pantothenic acid is a precursor of CoA, and it is converted to CoA through enzymatic processes. *P. falciparum* is a pantothenic acid auxotroph that acquires this molecule exogenously.[135] The first studies that were successful in culturing erythrocytic-stage malaria parasites revealed that *P. falciparum* has an absolute requirement for pantothenic acid.[136] Uninfected red blood cells were found to be impermeable to pantothenic acid whereas infected red blood cells were permeable. The latter is attributed to new permeability pathways (NPP) created by the parasite in the erythrocyte membrane to allow for the trafficking of nutrients, metabolic waste, and inorganic ions.[133] The NPP allow for the transport of pantothenic acid into the erythrocyte where it is shuttled into the parasitophorous vacuole. From here, pantothenic acid is taken up into the parasite down a H^+-transport electrochemical gradient.[137, 138]

The CoA biosynthesis pathway (**Fig. 1.6**) starts with pantothenate being first phosphorylated to 4′-phosphopantothenate by 4′-phosphopantothenate kinase (PanK) in an ATP-mediated process. *P. falciparum* PanK has high affinity for pantothenate (K_m = 0.3 μM) and this helps in the retention and phosphorylation of this biomolecule.[137] From PanK, 4′-phosphopantothenate is taken up by 4′-phosphopantothenate cysteine synthetase (PPCS), which fuses it with cysteine to form 4′-phosphopantothenoylcysteine. This molecule is decarboxylated on its cysteine appendage by 4′-phosphopantothenoylcysteinoyl decarboxylate (PPCDC) to form 4′-phosphopantotheine. Once the 4′-phosphopantotheine has been taken up by 4′-phosphopantotheine adenylyltransferase (PPAT), it is adenylated through nucleophilic attack by 4′-phosphate on the α-phosphate of ATP to form dephospho–CoA. Dephospho-CoA is phosphorylated on its adenosine 3′-hydroxyl by dephospho–CoA kinase (DPCK). The first four enzymes of the pathway are said to be localized in the cytosol, while the last enzyme has been suggested to reside in the apicoplast. This implication for DPCK adds to the fact that synthesized CoA feeds directly into the fatty acid biosynthesis, which takes place in the apicoplast.[133, 139]

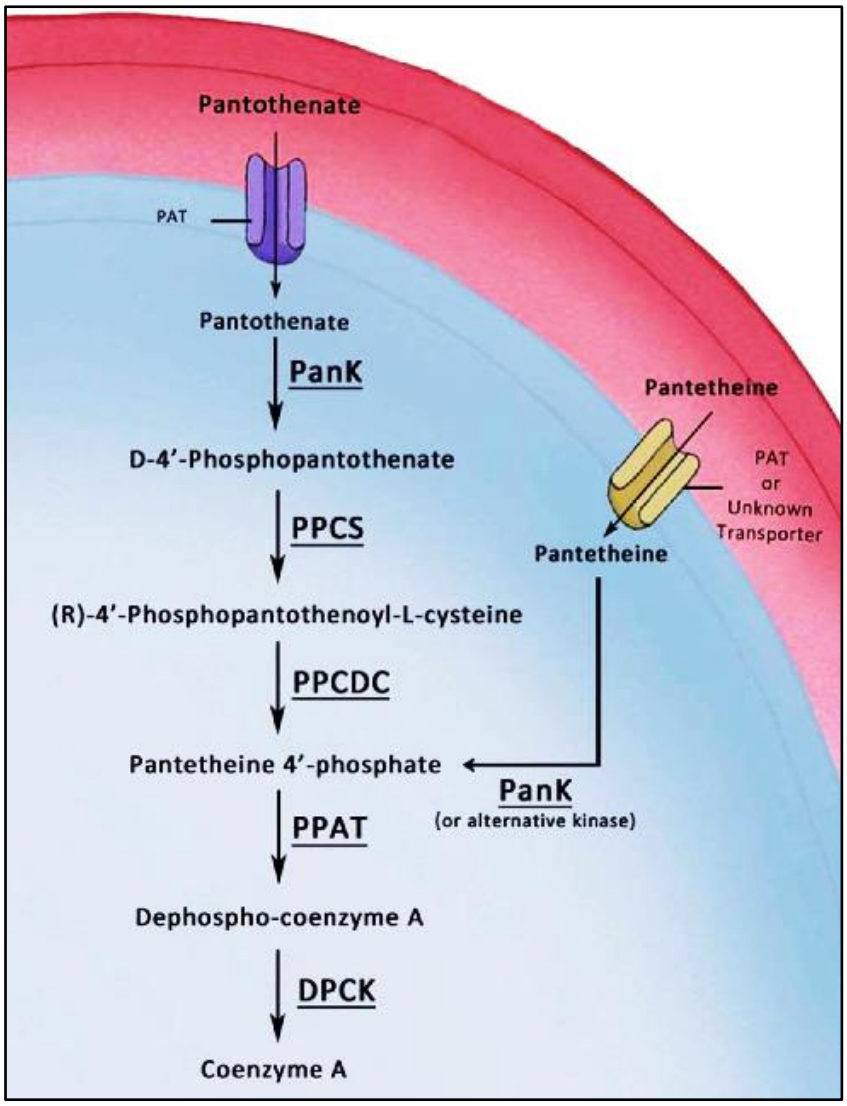

Figure 1.6: The coenzyme A biosynthesis pathway

PanK, pantothenate kinase; PPCS, phosphopantothenoylcysteine synthetase; PPCDC, phosphopantothenoylcysteine decarboxylase; PPAT, pantetheinephosphate adenylyltransferase; DPCK, dephospho-coenzyme A kinase; PAT, putative pantothenate transporter.[140]

There is variability in the amino acid sequence of enzymes involved in CoA biosynthesis across eukaryotes and prokaryotes, although their function is conserved. In particular, *Plasmodium* PPAT differs from its human counterpart in its amino acid sequence.[133] In most mammalian cells, PPAT and DPCK are encoded as a bifunctional enzyme system known as CoA synthase. These differences mean that drugs can be developed against this enzyme without acting on human PPAT. Furthermore, *Plasmodium* PPAT is obligatory for CoA biosynthesis during erythrocyte development and cannot be by-passed, unlike the preceding enzymes on the CoA biosynthesis pathway.[140] This emphasizes the importance of targeting this enzyme in antimalarial drug discovery efforts.

1.9.2 CoA biosynthesis enzyme inhibitors

Pioneering work towards the development of the CoA biosynthesis inhibitors was based on pantothenate analogues, including pantoyltaurine and pantoyltauramides (**Fig. 1.7**). Their ability to supress avian malaria parasites and the observation that their inhibitory effect could be negated by administration of high concentrations of pantothenate was essential for current research in this area.[133] In addition, the success of establishing *in vitro* assay conditions for intraerythrocytic *Plasmodium coatneyi* (monkey malaria parasite) and *P. falciparum* maintenance further assisted in the discovery of active pantothenate analogues.[133] These breakthroughs laid a foundation that enabled 21st century research into CoA biosynthesis inhibitors.

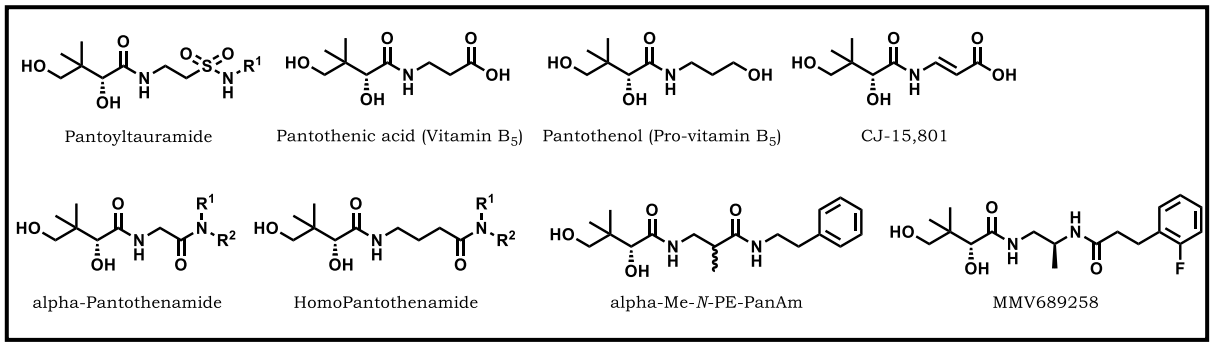

Figure 1.7: The coenzyme A biosynthesis pathway inhibitors

Several such inhibitors have been reported. Saliba *et al.* have reported that pantothenol (pro-vitamin B_5) and a fungal natural product CJ-15,801 (**Fig. 1.7**)

showed activity against *in vitro* intraerythrocytic *P. falciparum*.[135, 141] The antiplasmodium activity of these compounds was mediated by the pantothenate-metabolizing pathway in *P. falciparum*.[142] Other pantothenic acid analogues (*N*-pantothenamides) have also showed high antiplasmodium activity and do not show toxicity against mammalian cells (**Fig. 1.7**).[143, 144] Despite high *in vitro* antiplasmodium activity, these compounds were prone to pantetheinase degradation in the culture medium, although this liability could be overcome by using heat-deactivated medium or via chemical modifications. The heat-deactivated medium resulted in improved antiplasmodium activity (*Pf*3D7 IC_{50} = 20-150 nM compared to 44–166 μM in fresh medium).[144] Chemical modifications also resulted in compounds with resistance to pantetheinase degradation by shifting the position of the scissile amide bond.[143] The frontrunner compound identified in these works is the alpha-Me-*N*-PE-PanAm (**Fig. 1.7**; *Pf*3D7 IC_{50} = 29 nM in aged culture medium, and *Pf*3D7 IC_{50} = 52 nM in fresh culture medium).[145]

Although initial studies have implicated that *N*–pantothenamides were inhibitors of PanK, de Villiers *et al.* have recently reported that the compounds were phosphorylated by PanK to metabolically active analogues. These either inhibit the subsequent enzymes along the pathway or are converted into CoA antimetabolites that interfere with CoA utilization.[146] None of these compounds have progressed to preclinical stages but a recent report highlights a preclinical candidate of the *N*-pantothenamides class of compounds.[147] This compound (MMV689258; **Fig. 1.7**) is a pantothenamide bioisostere with a reversed amide, which makes it more resistant to pantetheinase degradation and produces high *in vitro* antiplasmodium activity (*Pf*NF54 IC_{50} = 5 nM). MMV689258 also shows gametocidal activity and transmission-blocking potential. It displayed a desirable pharmacokinetics profile and suppressed *P. falciparum* parasitemia in a severe combined immunodeficient (SCID) mouse infection model with 99.9% activity at 50 mg/kg/day and 99.8% at 25 mg/kg/day over four days.[147] In agreement with the findings by de Villiers *et al.*, MMV689258 acted downstream in the pathway and did not inhibit PanK. The metabolomic fingerprint of this compound suggested that the acetyl-CoA pathway was targeted and analysis of *in vitro*-derived resistant mutants revealed acetyl-CoA synthetase as the target.[147] The progression of MMV689258 to preclinical development validates CoA-metabolizing enzymes as potential antimalarial targets and reveals a new class of promising antimalarials.

1.10 Aminoacyl transfer ribonucleic acid synthetases (RSs)

1.10.1 Cellular role of RSs

Protein synthesis is vital for the survival of organisms.[148] Proteins serve many functions in the organism and facilitate enzymatic reactions involved in various metabolic functions of the cell, such as the formation and synthesis of membranes, regulation of cellular homeostasis, and many other processes.[149] However, protein synthesis is also a specialized process, and, as proteins are made of amino acid sequences, cells add amino acids through controlled mechanisms during protein synthesis. A family of proteins known as RSs are important in driving protein synthesis across cells, making valuable proteins during the organism's life-time.[150] Inhibition of these proteins may stall protein synthesis and adversely affect the viability of organisms.[151, 152]

There are 20 RSs in eukaryotic cells, one for each of the 20 amino acids. In *P. falciparum*, protein synthesis occurs in three compartments (the apicoplast, cytoplasm, and mitochondria), involving a total of 36 RSs.[151, 153] Although there should theoretically be 20 RSs in each of these translation compartments, *P. falciparum* has adapted to use 36 RSs with varying distribution. Sixteen of the RSs compartmentalize to the cytoplasm, fifteen to the apicoplast, one to the mitochondria, and the remaining four have dual residence in both the cytoplasm and apicoplast (**Fig. 1.8**, referred to as aaRSs).[152] RSs play an important role in the cell by attaching a specific amino acid to its cognate transfer ribonucleic acid (tRNA) before engaging with the ribosome for protein synthesis.[148] RSs are divided into two classes (class I and class II, 10 in each class) based on their protein fold, sequence conservation in the catalytic sites, and mechanism of tRNA aminoacylation. Class I RSs aminoacylate on the 2′-OH of the 3-terminal of the terminal ribose's adenosine (Ade 76), while class II RSs aminoacylate on the 3′-OH.[148, 153]

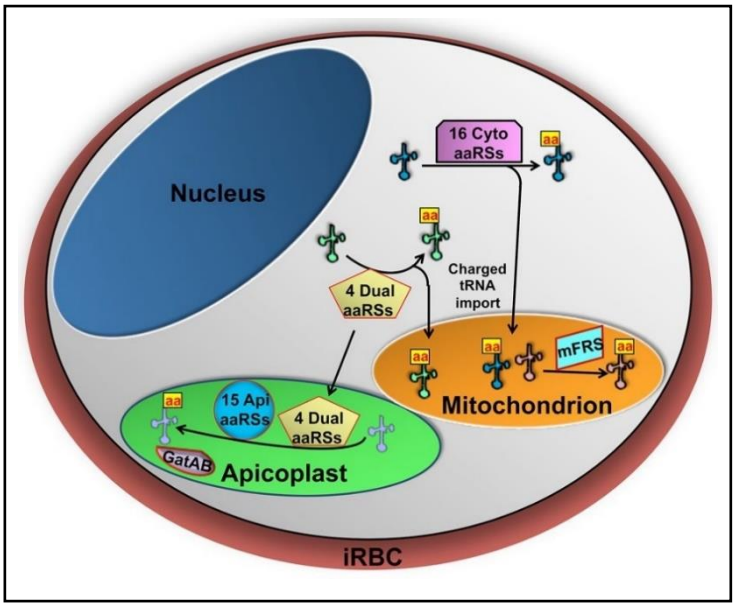

Figure 1.8: Red blood cell infected with malaria parasite showing localization of aminoacyl tRNA synthetases in the parasite
aa, amino acid; aaRSs, aminoacyl tRNA synthetases referred to throughout the text as RS; Api, apicoplast; cyto, cytoplasm; GatAB, glutamyl-tRNA amidotransferase; iRBC, infected red blood cell; mFRS, mitochondrial phenylalanyl-tRNA synthetase[151]

A recent bioinformatics study showed that there is low sequence identity (≈40%) and key structural and functional conservation differences between human and *Plasmodium* RSs.[153] This study showed that the localization of human RSs is such that 17 reside in the mitochondria, 16 in the cytoplasm, and three in both.[153] In addition, the druggable sites of *Pf*ArgRS, *Pf*MetRS, and *Pf*ProRS showed low sequence conservation and high variation when compared to their human homologues. These key differences warrant targeting the *Plasmodium* RSs as drug targets, as such drugs may be selective relative to mammalian RSs and thus avoid target-based toxicity.[154]

1.10.2 RSs as drug targets

RS inhibitors

There has been a recent surge in the development of inhibitors that target RSs, as genomic data has provided a clearer understanding of these enzymes.[152] Some of these RSs inhibitors include prolyl-RS inhibitors (febrifugine, halofuginone, and (2*S*,2*R*,3*S*)-halofuginol), cladosporin (lysyl-RS inhibitor), borrelidin (threonyl-RS

inhibitor), bicyclic azetidine BRD7929 (phenylalanyl-RS inhibitor), and isoleucyl-RS inhibitors (mupirocin and thiaisoleucine; **Fig. 1.9**).[148, 155] This is by no means an exhaustive list considering the large number of RSs that are present in *P. falciparum* and which can be explored as antimalarial drug targets. More important are the dual-localized RSs (AlaRS, ThrRS, GlyRS, and CysRS), whose inhibition will consequently halt protein synthesis in multiple compartments.[151, 153] Recent antimalarial drug discovery efforts into RS inhibitors identified the high activity of leucyl-tRNA (LeuRS) inhibitors and delivered the first antimalarial RS inhibitor preclinical candidate.[156] This new class of RS inhibitors is discussed in the following section.

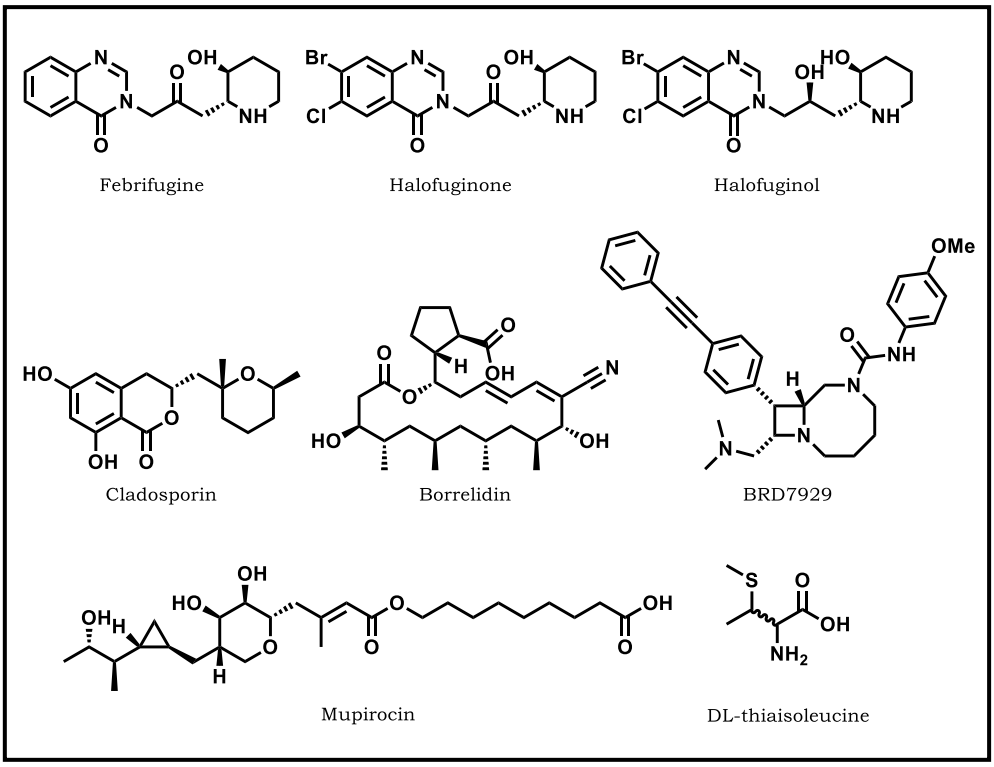

Figure 1.9: Structures of RS inhibitors

LeuRS inhibitors

Several potent LeuRS inhibitors have been developed against protozoan, fungus, and bacterial infections.[155, 157] LeuRS is found in the apicoplast and the cytoplasm of many eukaryotic and prokaryotic cells. This class II RS contains a distinct editing domain in addition to the catalytic and tRNA binding domains. LeuRS facilitates aminoacylation of the leucyl-tRNA with cognate amino acid leucine.[151] However, due to structural similarities between leucine, isoleucine, and valine, leucyl-tRNA may be

mischarged with one of these other amino acids. As such, the editing domain of LeuRS has evolved to proofread mis-incorporation and to hydrolyse mismatched amino acids to release tRNA for the correct uptake of leucine.[158] This domain has also become an essential target for the development of antimalarial agents.

A new class of antimicrobial, antifungal, and antimalarial compounds called benzoxaboroles has been shown to target the editing domain of LeuRS (**Fig. 1.10**).[157, 159] Benzoxaboroles are heterocyclic boron-containing analogues of phenylboronic acid in with the boron-oxygen bond incorporated into a five-membered ring and possesses high hydrolytic stability.[160] An empty p-orbital in the boron atom confers strong Lewis acidity, thus making it amenable to attack by nucleophiles within biological systems. Furthermore, the boron centre in the benzoxaborole is in the neutral trigonal sp^2 hybridization state and converts to a tetrahedral sp^3-hybridized form as it forms dative bonds with biological nucleophiles. The tight incorporation of the boron atom into the five-membered ring may be attributed to the pKa of the benzoxaborole system (pKa = 7–8), which is lower than that of acyclic boron-containing systems (pKa = 8–10).[160, 161] These properties are important for the reactivity or the proposed mechanism by which benzoxaboroles inhibit biological systems.

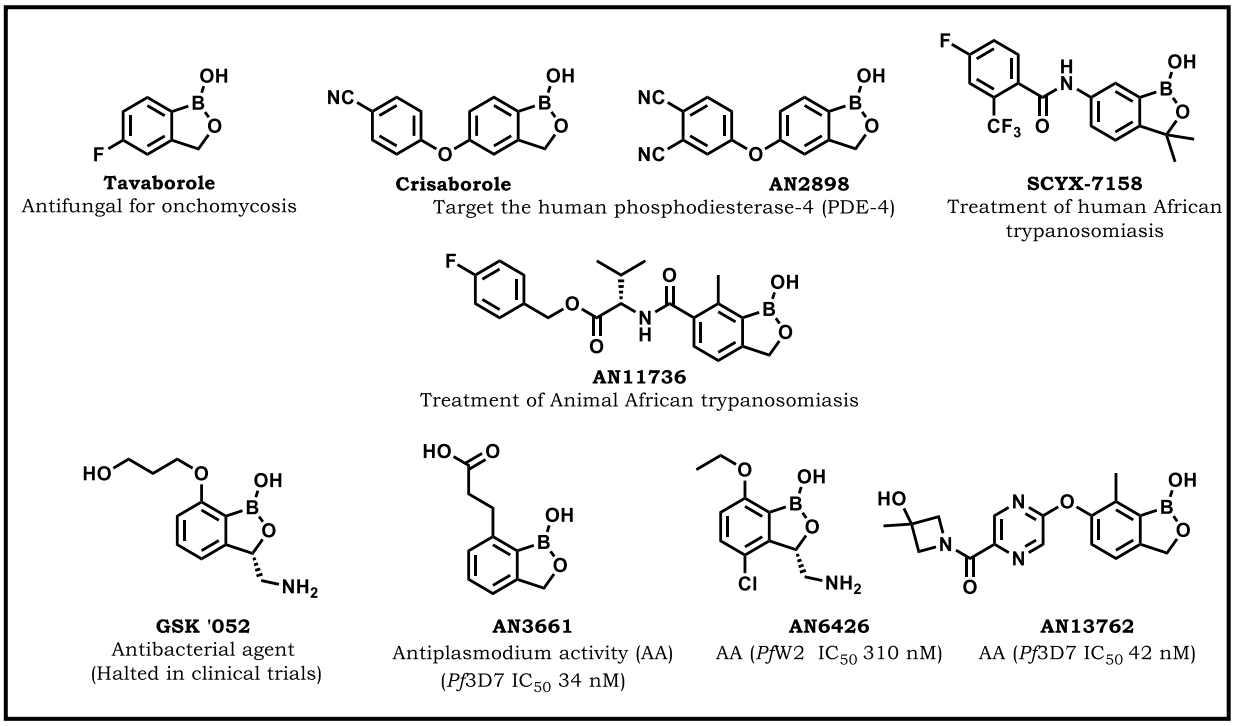

Figure 1.10: Benzoxaboroles currently in clinical trials and clinical use
Pf, Plasmodium falciparum; IC_{50}, 50% inhibitory concentration

Benzoxaboroles in development and clinical use

Crisaborole (Eucrisa®; **Fig. 1.10**) is an anti-inflammatory benzoxaborole used in the treatment of mild to moderate atopic dermatitis, operating via inhibition of phosphodiesterase-4.[162] Tavaborole (Kerydin®; **Fig. 1.10**) is a clinically approved antifungal benzoxaborole that is used to treat onchomychosis. It targets LeuRS by inhibiting protein synthesis, thus arresting fungal growth.[163, 164] Other benzoxaboroles have been explored in other indications including bacterial and protozoan infections. Indeed, success has already been seen with acoziborole (SCYX-7158) and AN11736 (**Fig. 1.10**), which are in advanced clinical development for the treatment of African trypanosomes in humans (human African trypanosomiasis, HAT) and animals (animal African trypanosomiasis, AAT). Acoziborole was found to be active against *Trypanosoma brucei*, the parasite causing HAT, with proof-of-concept data allowing its application for investigational new drug application and subsequently Phase I clinical trials.[165] AN11736 inhibited the growth of *Trypanosoma congolense* and *Trypanosoma vivax* parasites with 100% efficacy at 10 $mg.kg^{-1}$ in a *T. congolense* infection mouse model. Recent genomic data confirmed that these compounds target the nuclear mRNA-processing endonuclease required for mRNA maturation before export to the cytoplasm for protein translation (cleavage and polyadenylation specificity factor 3, CPSF3).[166]

Benzoxaboroles have also shown potential in antibacterial drug discovery and development programs.[167, 168] GSK2251052 (**Fig. 1.10**) was a clinically advanced LeuRS inhibitor developed for the treatment of Gram-negative bacteria. However, this compound was withdrawn from Phase II clinical trials due to the rapid development of resistance.[168]

The first report of benzoxaboroles active against *P. falciparum* was published in 2011 with AN3661 (*in vitro* IC_{50} in *Pf*3D7 = 26 nM; **Fig. 1.10**).[169] Further studies showed that this compound was active against a panel of other multidrug-resistant *Plasmodium* strains (mean IC_{50} = 32 nM) and field isolates (mean IC_{50} = 64 nM). It also showed efficacy in *P. berghei*- and *P. falciparum*-infected SCID mouse models (ED_{90} = 0.34 and 0.57 mg kg^{-1} on day 4, respectively).[170] Probing of the MoA through *in vitro* selection of resistance under drug pressure and CRISPR-Cas9-mediated introduction of mutations supported by homology modelling confirmed that AN3661 acts against nuclear CPSF3.[171] High *in vitro* activity and efficacy in mouse models

coupled with genomic data of this compound suggested that the benzoxaborole scaffold may be further investigated to identify new antimalarials with novel MoAs.

AN13762 advanced to the preclinical development stage but was recently withdrawn due to toxicity in animals (**Fig. 1.10**).[172] Biochemical and genomic studies to elaborate the MoA of this compound were complicated by intracellular *P. falciparum* prodrug activation during which the amide of AN13762 was hydrolysed to the acid, perhaps by an identified resistant determinant, the *P. falciparum* prodrug activation and resistance esterase. Higher level resistant mutants showed mutations in several genes encoding enzymes for CPSF3, ubiquitination, and sumoylation, implicating multiple targets. The activity of AN13762 was more pronounced against ring and trophozoite parasites, and treated parasites did not grow beyond trophozoites.[172] In another study, two benzoxaboroles (AN6426 and AN8432, **Fig. 1.10**) were shown to inhibit LeuRS. These compounds also showed *in vivo* efficacy against a *P. berghei* murine infection model.[170]

Proposed MoA of benzoxaboroles in LeuRS

Benzoxaboroles are also proposed to act against LeuRS through oxaborole-tRNA trapping (OBORT) of the LeuRS in the editing site (**Fig. 1.11**).[160, 167] The strong Lewis acidity of the boron atom allows it to react readily with nucleophiles such as hydroxyls. The proposed mechanism involves attack by two cis-diols on the ribose of the 3′-terminal tRNA adenosine in the LeuRS editing domain on the boron centre. This results in a spiro-complex that is tetrahedral about the boron atom. It is stable enough to prevent exit of the tRNA from the editing site and entry to the active site. The complex also prevents other tRNAs from accessing the enzyme and consequently stopping protein synthesis.[160]

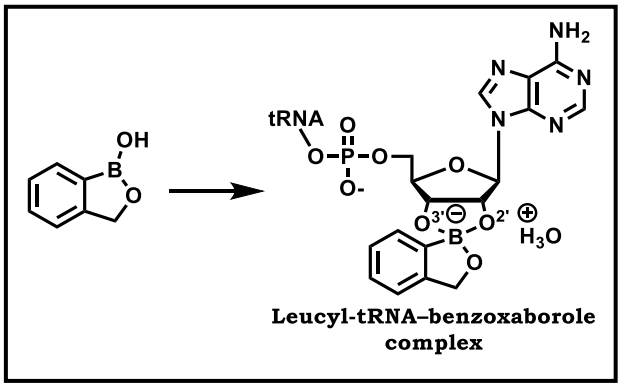

Figure 1.11: Proposed mechanism of inhibition of LeuRS by benzoxaboroles

1.11. Research Programme

Justification for the study

The scourge of malaria is still felt by many people living in resource-limited areas of the world. A lack of promising returns on investment for diseases endemic in such settings discourages investment by pharmaceutical industries. A rise of drug resistant species against frontline drugs in ACTs are concerning and threaten their future utility against malaria.[173] More daunting are recent and growing reports of delayed clearance of the parasite biomass following ACTs as a result of possible resistance against artemisinins. As such, new antimalarials are urgently needed to address these concerns. New antimalarials entering the drug development pipeline need to be based on novel chemotypes, act against novel drug targets, preferably be able to provide single radical cure and should be able to treat vulnerable groups such as pregnant women and young children.[91]

Previously untargeted pathways such as the CoA biosynthesis pathway have the potential to bring forth novel drugs acting by novel modes of action. There are currently no CoA biosynthesis pathway inhibitors in the clinic, and only recently has a preclinical candidate proposed to target the first of the five enzymes along the CoA biosynthesis been reported.[147] There are five enzymes involved in the metabolism of pantothenate to CoA.[133] The penultimate enzyme, 4′–phosphopantetheine adenylyltransferase (PPAT), of the pathway offers an advantage in that it cannot be by–passed through shunt pathways and it is central to CoA biosynthesis in *Plasmodium.*[140] Furthermore, the mammalian PPAT homologue of the *P. falciparum* PPAT is dissimilar on a sequence level, and therefore offers an opportunity that compounds thus developed against the latter would not be toxic to humans.[174] Current work applies the repositioning strategy, which is the use of the compounds developed for one indication for use as templates for the design of compounds for another indication. This builds on the idea that the bacterial PPAT inhibitors previously explored were found to selectively inhibit the bacterial PPAT over the human homologue. The sequence level of PPAT of various species including bacteria and *Plasmodium* have been proposed to be dissimilar, however, the function is known to be conserved as with other enzymes of the CoA biosynthesis pathway.[19, 140] The antibacterial campaigns at AstraZeneca and Novartis developed bacterial PPAT inhibitors and the current study aims to reposition these inhibitors as potential *P. falciparum* PPAT inhibitors.[175-177]

In addition, the development of boron–containing drugs is receiving attention, and a few are currently in clinical use for treating cancers as well as bacterial and parasitic infections.[160] Of these, benzoxaboroles are the most interesting in that they possess promising properties for development as novel antimalarials. The work in the malaria space was first reported in 2011.[169] No benzoxaborole compound has entered human clinical studies, and one preclinical candidate has been withdrawn due to toxicity in animal trials.[172] Benzoxaboroles have the potential to be developed as a new class of antimalarials acting against novel targets and would therefore not be cross–resistant with current antimalarials. These features are in line with the objectives of finding novel scaffolds for antimalarials and a potential for identification of novel targets.

Research question

The research question is whether a series of bacterial PPAT inhibitors can be repositioned as antimalarial agents and whether PPAT inhibition can be implicated in the antimalarial action. The next research question is to assess antiplasmodium activity of benzoxaboroles initially designed as penicillin-binding protein-3 (PBP-3) and their potential inhibition of *P. falciparum* LeuRS as their mode of action.

Objectives

The objective of this study is to reposition a series of bacterial PPAT inhibitors as antiplasmodium agents and to investigate antiplasmodium activity of benzoxaborole compounds.

Specific aims

i. Resynthesize hits from an AstraZeneca collection of bacterial PPAT inhibitors screened against *Pf*NF54 and reassess them against *Pf*NF54 to validate activity and then conduct a Formal Hit Assessment (FHA) program. Synthesize select published bacterial PPAT inhibitors from Novartis.
ii. Profile the antiplasmodium activity, solubility, cytotoxicity, and microsomal stability of relevant synthesized compounds.
iii. Assess attenuation of antiplasmodium activity of PPAT inhibitors with high concentrations of selected CoA biosynthesis pathway substrates and CoA in a chemical rescue assay to implicate PPAT inhibition as the mode of action.

iv. Conduct metabolomics studies to investigate if PPAT inhibitors act along the CoA biosynthesis pathway and to establish the metabolomic fingerprint of benzoxaboroles.

v. Assess if LeuRS or other RSs are targets of benzoxaboroles in knockdown models.

vi. Derive SARs in conjunction with mode of action studies to form the basis for a future hit-to-lead optimization program.

1.12. References

1. Bynum, B., A history of malaria. *Lancet* **2008**, *371* (9622), 1407-1408.
2. Cox, F. E., History of the discovery of the malaria parasites and their vectors. *Parasites Vectors* **2010**, *3* (1), 5.
3. Rich, S. M.; Leendertz, F. H.; Xu, G.; LeBreton, M.; Djoko, C. F.; Aminake, M. N.; Takang, E. E.; Diffo, J. L. D.; Pike, B. L.; Rosenthal, B. M.; Formenty, P.; Boesch, C.; Ayala, F. J.; Wolfe, N. D., The origin of malignant malaria. *Proc. Natl. Acad. Sci. U. S. A.* **2009**, *106* (35), 14902.
4. Rayner, J. C.; Liu, W.; Peeters, M.; Sharp, P. M.; Hahn, B. H., A plethora of Plasmodium species in wild apes: a source of human infection? *Trends Parasitol.* **2011**, *27* (5), 222-229.
5. Liu, W.; Li, Y.; Learn, G. H.; Rudicell, R. S.; Robertson, J. D.; Keele, B. F.; Ndjango, J. B.; Sanz, C. M.; Morgan, D. B.; Locatelli, S.; Gonder, M. K.; Kranzusch, P. J.; Walsh, P. D.; Delaporte, E.; Mpoudi-Ngole, E.; Georgiev, A. V.; Muller, M. N.; Shaw, G. M.; Peeters, M.; Sharp, P. M.; Rayner, J. C.; Hahn, B. H., Origin of the human malaria parasite Plasmodium falciparum in gorillas. *Nature* **2010**, *467* (7314), 420-425.
6. Cox, F. E., History of the discovery of the malaria parasites and their vectors. *Parasites Vectors* **2010**, *3* (1), 1-9.
7. Njoroge, M.; Njuguna, N. M.; Mutai, P.; Ongarora, D. S.; Smith, P. W.; Chibale, K., Recent approaches to chemical discovery and development against malaria and the neglected tropical diseases human African trypanosomiasis and schistosomiasis. *Chem. Rev.* **2014**, *114* (22), 11138-11163.
8. White, N. J.; Pukrittayakamee, S.; Hien, T. T.; Faiz, M. A.; Mokuolu, O. A.; Dondorp, A. M., Malaria. *Lancet* **2014**, *383* (9918), 723-735.
9. WHO, World Malaria Report 2020: 20 Years of Global Progress and Challenges. Geneva, 2020. https://apps.who.int/iris/handle/10665/337660 (11 October 2021).
10. Maitland, K., Severe malaria in African children—the need for continuing investment. *N. Engl. J. Med.* **2016**, *375* (25), 2416-2417.
11. Vitoria, M.; Granich, R.; Gilks, C. F.; Gunneberg, C.; Hosseini, M.; Were, W.; Raviglione, M.; De Cock, K. M., The global fight against HIV/AIDS, tuberculosis, and malariacurrent status and future perspectives. *Am. J. Clin. Pathol.* **2009**, *131* (6), 844-848.
12. Butera, J. A., Phenotypic Screening as a Strategic Component of Drug

Discovery Programs Targeting Novel Antiparasitic and Antimycobacterial Agents: An Editorial: Miniperspectives Series on Phenotypic Screening for Antiinfective Targets. *J. Med. Chem.* **2013**, *56* (20), 7715-7718.

13. Cohen, C.; Karstaedt, A.; Frean, J.; Thomas, J.; Govender, N.; Prentice, E.; Dini, L.; Galpin, J.; Crewe-Brown, H., Increased prevalence of severe malaria in HIV-infected adults in South Africa. *Clin. Infect. Dis.* **2005**, *41* (11), 1631-1637.14. Phillips, M.; Burrows, J.; Manyando, C.; van Huijsduijnen, R.; Van Voorhis, W.; Wells, T., Malaria. *Nat. Rev. Dis. Primers* **2017**, *3*, 17050.

15. WHO, Global malaria report 2021. World Health Organization Geneva: 2021. https://www.who.int/teams/global-malaria-programme/reports/world-malaria-report-2021 (accessed 10 December 2021).

16. White, N., Plasmodium knowlesi: the fifth human malaria parasite. *Clin Infect Dis.* **2008**, *46 (2)*, 172-173.

17. Millar, S.; Cox-Singh, J., Human infections with Plasmodium knowlesi—zoonotic malaria. *Clin. Microbiol. Infect.* **2015**, *21* (7), 640-648.

18. Campo, B.; Vandal, O.; Wesche, D. L.; Burrows, J. N., Killing the hypnozoite–drug discovery approaches to prevent relapse in Plasmodium vivax. *Pathog. Global Health* **2015**, *109* (3), 107-122.

19. Baird, J. K., Evidence and implications of mortality associated with acute Plasmodium vivax malaria. *Clin. Microbiol. Rev.* **2013**, *26* (1), 36-57.

20. Tilley, L.; Dixon, M. W.; Kirk, K., The Plasmodium falciparum-infected red blood cell. *Int. J. Biochem. Cell Biol.* **2011**, *43* (6), 839-842.

21. Okumu, F. O.; Moore, S. J., Combining indoor residual spraying and insecticide-treated nets for malaria control in Africa: a review of possible outcomes and an outline of suggestions for the future. *Malar. J.* **2011**, *10* (1), 208.

22. WHO, Global technical strategy for malaria 2016-2030. World Health Organization: Geneva, 2015. https://www.who.int/docs/default-source/documents/global-technical-strategy-for-malaria-2016-2030.pdf (accessed 11 October 2022).

23. Feachem, R.; Sabot, O., A new global malaria eradication strategy. *Lancet* **2008**, *371* (9624), 1633-1635.

24. Chanda, E.; Ameneshewa, B.; Bagayoko, M.; Govere, J. M.; Macdonald, M. B., Harnessing integrated vector management for enhanced disease prevention. *Trends Parasitol.* **2017**, *33* (1), 30-41.

25. Choi, L.; Pryce, J.; Garner, P., Indoor residual spraying for preventing malaria in communities using insecticide-treated nets. *Cochrane Database Syst Rev* **2019**, *5*, 1-62.

26. Consortium, I. O. I. R., Implications of insecticide resistance for malaria vector control with long-lasting insecticidal nets: trends in pyrethroid resistance during a WHO-coordinated multi-country prospective study. *Parasites Vectors* **2018**, *11* (1), 550.

27. Protopopoff, N.; Rowland, M., Accelerating the evidence for new classes of long-lasting insecticide-treated nets. *Lancet* **2018**, *391* (10138), 2415-2416.

28. Kamareddine, L., The biological control of the malaria vector. *Toxins* **2012**, *4* (9), 748-767.

29. Derua, Y. A.; Kweka, E. J.; Kisinza, W. N.; Githeko, A. K.; Mosha, F. W., Bacterial larvicides used for malaria vector control in sub-Saharan Africa: review of their effectiveness and operational feasibility. *Parasites Vectors* **2019**, *12* (1), 426.

30. WHO, WHO recommends groundbreaking malaria vaccine for children at risk. https://www.who.int/news/item/06-10-2021-who-recommends-groundbreaking-malaria-vaccine-for-children-at-risk (accessed 06 October 2021).

31. WHO, Background paper on the RTS, S/AS01 Malaria vaccine. Geneva, 2015.

32. King, A., The problematic parasite. *Nature* **2019**, *575* (7784), S51-S54.

33. van den Berg, M.; Ogutu, B.; Sewankambo, N. K.; Biller-Andorno, N.; Tanner, M., RTS, S malaria vaccine pilot studies: addressing the human realities in large-scale clinical trials. *Trials* **2019**, *20* (1), 1-4.

34. Duffy, P. E.; Patrick Gorres, J., Malaria vaccines since 2000: progress, priorities, products. *npj Vaccines* **2020**, *5* (1), 48.

35. Hoefnagel, J. G.; Massar, K.; Hautvast, J. L., Non-adherence to malaria prophylaxis: The influence of travel-related and psychosocial factors. *J. Infect. Public Health* **2020**, *13* (4), 532-537.

36. Berman, J. D., Approval of Tafenoquine for Malaria Chemoprophylaxis. *Am. J. Trop. Med. Hyg.* **2019**, *100* (6), 1301-1304.

37. Meltzer, E.; Schwartz, E., Utility of 8-Aminoquinolines in Malaria Prophylaxis in Travelers. *Curr. Infect. Dis. Rep.* **2019**, *21* (11), 43.

38. DeVos, E.; Dunn, N., Malaria Prophylaxis. In *StatPearls [Internet]*, StatPearls Publishing: 2021. https://www.ncbi.nlm.nih.gov/books/NBK551639/ (accessed 28 August 2021)

39. Hemingway, J.; Shretta, R.; Wells, T. N.; Bell, D.; Djimdé, A. A.; Achee, N.; Qi, G., Tools and strategies for malaria control and elimination: what do we need to achieve a grand convergence in malaria? *PLoS Biol.* **2016**, *14* (3), e1002380.

40. Eisele, T. P., Mass drug administration can be a valuable addition to the malaria elimination toolbox. *Malar. J.* **2019**, *18* (1), 1-5.

41. White, N. J., Does antimalarial mass drug administration increase or decrease the risk of resistance? *Lancet Infect. Dis.* **2017**, *17* (1), e15-e20.

42. Fang, C.-T.; Chang, H.-L.; Hsieh, W.-C., Malaria eradication on islands. *Lancet* **2001**, *357* (9255), 560.

43. Raphemot, R.; Posfai, D.; Derbyshire, E. R., Current therapies and future possibilities for drug development against liver-stage malaria. *The Journal of clinical investigation* **2016**, *126* (6), 2013-2020.

44. White, N. J.; Hien, T. T.; Nosten, F. H., A brief history of Qinghaosu. *Trends Parasitol.* **2015**, *31* (12), 607-610.

45. Liu, C-x., Discovery and development of artemisinin and related compounds. *Chin. Herb. Med.* **2017**, *9* (2), 101-114.

46. Youyou, T., The development of the antimalarial drugs with new type of chemical structure-qinghaosu and dihydroqinghaosu. *Southeast Asian J. Trop. Med. Public Health* **2004**, *35* (2), 250-251.

47. Tu, Y., The discovery of artemisinin (qinghaosu) and gifts from Chinese medicine. *Nat. Med.* **2011**, *17* (10), 1217-1220.

48. Davis, T. M.; Karunajeewa, H. A.; Ilett, K. F., Artemisinin-based combination therapies for uncomplicated malaria. *Med. J. Aust.* **2005**, *182* (4), 181-185.

49. Edwin, G. T.; Korsik, M.; Todd, M. H., The past, present and future of anti-malarial medicines. *Malar. J.* **2019**, *18* (1), 1-21.

50. Pukrittayakamee, S.; Chotivanich, K.; Chantra, A.; Clemens, R.; Looareesuwan, S.; White, N. J., Activities of artesunate and primaquine against asexual-and sexual-stage parasites in falciparum malaria. *Antimicrob. Agents Chemother.* **2004**, *48* (4), 1329-1334.

51. Price, R. N.; Nosten, F.; Luxemburger, C.; Ter Kuile, F. O.; Paiphun, L.; Chongsuphajaisiddhi, T.; White, N. J., Effects of artemisinin derivatives on malaria transmissibility. *Lancet* **1996**, *347* (9016), 1654-1658.

52. Andrews, K. A.; Wesche, D.; McCarthy, J.; Möhrle, J. J.; Tarning, J.; Phillips, L.; Kern, S.; Grasela, T., Model-informed drug development for malaria therapeutics. *Annu. Rev. Pharmacol. Toxicol.* **2018**, *58*, 567-582.

53. van Huijsduijnen, R. H.; Wells, T. N., The antimalarial pipeline. *Curr. Opin. Pharmacol.* **2018**, *42*, 1-6.

54. Dondorp, A. M.; Smithuis, F. M.; Woodrow, C.; von Seidlein, L., How to contain artemisinin-and multidrug-resistant falciparum malaria. *Trends Parasitol.* **2017**, *33* (5), 353-363.

55. Straimer, J.; Gnädig, N. F.; Witkowski, B.; Amaratunga, C.; Duru, V.; Ramadani, A. P.; Dacheux, M.; Khim, N.; Zhang, L.; Lam, S., K13-propeller mutations confer artemisinin resistance in Plasmodium falciparum clinical isolates. *Science* **2015**, *347* (6220), 428-431.

56. Ross, L. S.; Fidock, D. A., Elucidating mechanisms of drug-resistant Plasmodium falciparum. *Cell Host Microbe* **2019**, *26* (1), 35-47.

57. Paloque, L.; Ramadani, A. P.; Mercereau-Puijalon, O.; Augereau, J.-M.; Benoit-Vical, F., Plasmodium falciparum: multifaceted resistance to artemisinins. *Malar. J.* **2016**, *15* (1), 1-12.

58. Zaw, M. T.; Lin, Z.; Emran, N. A., Importance of kelch 13 C580Y mutation in the studies of artemisinin resistance in Plasmodium falciparum in Greater Mekong Subregion. *J. Microbiol., Immunol. Infect.* **2020**, *53* (5), 676-681.

59. Uwimana, A.; Legrand, E.; Stokes, B. H.; Ndikumana, J. M.; Warsame, M.; Umulisa, N.; Ngamije, D.; Munyaneza, T.; Mazarati, J. B.; Munguti, K.; Campagne, P.; Criscuolo, A.; Ariey, F.; Murindahabi, M.; Ringwald, P.; Fidock, D. A.; Mbituyumuremyi, A.; Menard, D., Emergence and clonal expansion of in vitro artemisinin-resistant Plasmodium falciparum kelch13 R561H mutant parasites in Rwanda. *Nat Med* **2020**, *26* (10), 1602-1608.

60. Uwimana, A.; Umulisa, N.; Venkatesan, M.; Svigel, S. S.; Zhou, Z.; Munyaneza, T.; Habimana, R. M.; Rucogoza, A.; Moriarty, L. F.; Sandford, R.; Piercefield, E.; Goldman, I.; Ezema, B.; Talundzic, E.; Pacheco, M. A.; Escalante, A. A.; Ngamije, D.; Mangala, J.-L. N.; Kabera, M.; Munguti, K.; Murindahabi, M.; Brieger, W.; Musanabaganwa, C.; Mutesa, L.; Udhayakumar, V.; Mbituyumuremyi, A.; Halsey, E. S.; Lucchi, N. W., Association of Plasmodium falciparum kelch13 R561H genotypes with delayed parasite clearance in Rwanda: an open-label, single-arm, multicentre, therapeutic efficacy study. *Lancet Infect. Dis.* **2021**, *21* (8), 1120-1128.

61. Rosenthal, P. J., Are Artemisinin-Based Combination Therapies For Malaria Beginning To Fail in Africa? *Am. J. Trop. Med.* **2021**, *105* (4), 857-858.

62. Duffey, M.; Blasco, B.; Burrows, J. N.; Wells, T. N. C.; Fidock, D. A.; Leroy, D., Assessing risks of Plasmodium falciparum resistance to select next-generation antimalarials. *Trends Parasitol.* **2021**, *37* (8), 709-721.

63. Achan, J.; Talisuna, A. O.; Erhart, A.; Yeka, A.; Tibenderana, J. K.; Baliraine, F. N.; Rosenthal, P. J.; D'Alessandro, U., Quinine, an old anti-malarial drug in a modern world: role in the treatment of malaria. *Malar. J.* **2011**, *10* (1), 144.

64. Hobbs, C.; Duffy, P., Drugs for malaria: something old, something new, something borrowed. *F1000 Biol. Rep.* **2011**, *3*.

65. Kumar, S.; Bawa, S.; Gupta, H., Biological activities of quinoline derivatives. *Mini-Rev. Med. Chem.* **2009**, *9* (14), 1648.

66. Veiga, M. I.; Dhingra, S. K.; Henrich, P. P.; Straimer, J.; Gnädig, N.; Uhlemann, A.-C.; Martin, R. E.; Lehane, A. M.; Fidock, D. A., Globally prevalent PfMDR1 mutations modulate Plasmodium falciparum susceptibility to artemisinin-based combination therapies. *Nat. Commun.* **2016**, *7* (1), 1-12.

67. Flannery, E. L.; Chatterjee, A. K.; Winzeler, E. A., Antimalarial drug discovery—approaches and progress towards new medicines. *Nat. Rev. Microbiol.* **2013**, *11* (12), 849-862.

68. Hyde, J. E., Exploring the folate pathway in Plasmodium falciparum. *Acta Trop.* **2005**, *94* (3), 191-206.

69. Nzila, A., The past, present and future of antifolates in the treatment of Plasmodium falciparum infection. *J. Antimicrob. Chemother.* **2006**, *57* (6), 1043-1054.

70. Heinberg, A.; Kirkman, L., The molecular basis of antifolate resistance in Plasmodium falciparum: looking beyond point mutations. *Ann. N. Y. Acad. Sci.* **2015**, *1342* (1), 10.

71. Ding, X. C.; Ubben, D.; Wells, T. N., A framework for assessing the risk of resistance for anti-malarials in development. *Malar. J.* **2012**, *11* (1), 292.

72. Savelkoel, J.; Binnendijk, K. H.; Spijker, R.; van Vugt, M.; Tan, K.; Hänscheid, T.; Schlagenhauf, P.; Grobusch, M. P., Abbreviated atovaquone-proguanil prophylaxis regimens in travellers after leaving malaria-endemic areas: A systematic review. *Travel Med. Infect. Dis.* **2018**, *21*, 3-20.

73. Briolant, S.; Fusaï, T.; Rogier, C.; Pradines, B., Tetracycline antibiotics in malaria. *Open Trop. Med. J.* **2008**, *1* (1).

74. Dahl, E. L.; Rosenthal, P. J., Apicoplast translation, transcription and genome replication: targets for antimalarial antibiotics. *Trends Parasitol.* **2008**, *24* (6), 279-284.

75. Friesen, J.; Silvie, O.; Putrianti, E. D.; Hafalla, J. C.; Matuschewski, K.; Borrmann, S., Natural immunization against malaria: causal prophylaxis with antibiotics. *Sci. Transl. Med.* **2010**, *2* (40), 40ra49.

76. Schwartz, E., Prophylaxis of malaria. *Mediterr J Hematol Infect Dis* **2012**, *4* (1), e2012045.

77. Mishra, M.; Mishra, V. K.; Kashaw, V.; Iyer, A. K.; Kashaw, S. K., Comprehensive review on various strategies for antimalarial drug discovery. *Eur. J. Med. Chem.* **2017**, *125*, 1300-1320.

78. Belete, T. M., Recent Progress in the Development of New Antimalarial Drugs with Novel Targets. *Drug Des Devel Ther.* **2020**, *14*, 3875-3889.

79. Wells, T. N.; Van Huijsduijnen, R. H.; Van Voorhis, W. C., Malaria medicines: a glass half full? *Nat. Rev. Drug Discov* **2015**, *14* (6), 424-442.

80. Taylor, W. R.; White, N. J., Antimalarial drug toxicity: a review. *Drug Saf* **2004**, *27* (1), 25-61.

81. Peters, P. J.; Thigpen, M. C.; Parise, M. E.; Newman, R. D., Safety and Toxicity of Sulfadoxine/Pyrimethamine. *Drug Saf* **2007**, *30* (6), 481-501.

82. Bitta, M. A.; Kariuki, S. M.; Mwita, C.; Gwer, S.; Mwai, L.; Newton, C., Antimalarial drugs and the prevalence of mental and neurological manifestations: A systematic review and meta-analysis. *Wellcome Open Res* **2017**, *2*, 13.

83. Jozefowicz-Korczynska, M.; Pajor, A.; Lucas Grzelczyk, W., The Ototoxicity of Antimalarial Drugs-A State of the Art Review. *Front Neurol* **2021**, *12*, 661740.

84. Travassos, M.; Laufer, M. K., Antimalarial drugs: An overview. UpToDate. **2021**.https://www.uptodate.com/contents/antimalarial-drugs-an-overview (accessed 05 Septermber 2021).

85. Antony, H. A.; Parija, S. C., Antimalarial drug resistance: An overview. *Trop Parasitol* **2016**, *6* (1), 30-41.

86. Price, R. N.; Uhlemann, A. C.; Brockman, A.; McGready, R.; Ashley, E.; Phaipun, L.; Patel, R.; Laing, K.; Looareesuwan, S.; White, N. J.; Nosten, F.; Krishna, S., Mefloquine resistance in Plasmodium falciparum and increased pfmdr1 gene copy number. *Lancet* **2004**, *364* (9432), 438-447.

87. van der Pluijm, R. W.; Amaratunga, C.; Dhorda, M.; Dondorp, A. M., Triple Artemisinin-Based Combination Therapies for Malaria – A New Paradigm? *Trends Parasitol.* **2021**, *37* (1), 15-24.

88. Nayyar, G. M.; Breman, J. G.; Newton, P. N.; Herrington, J., Poor-quality antimalarial drugs in southeast Asia and sub-Saharan Africa. *Lancet Infect Dis* **2012**, *12* (6), 488-96.

89. Ashley, E. A.; Phyo, A. P., Drugs in development for malaria. *Drugs* **2018**, *78* (9), 861-879.

90. Okombo, J.; Chibale, K., Recent updates in the discovery and development of novel antimalarial drug candidates. *MedChemComm* **2018**, *9* (3), 437-453.

91. Burrows, J. N.; Duparc, S.; Gutteridge, W. E.; van Huijsduijnen, R. H.; Kaszubska, W.; Macintyre, F.; Mazzuri, S.; Möhrle, J. J.; Wells, T. N., New developments in anti-malarial target candidate and product profiles. *Malar. J.* **2017**, *16* (1), 26.

92. Erhunse, N.; Sahal, D., Protecting future antimalarials from the trap of resistance: Lessons from artemisinin-based combination therapy (ACT) failures. *J. Pharm. Anal.* **2021**, *11* (5), 541-554.

93. Rasmussen, C.; Alonso, P.; Ringwald, P., Current and emerging strategies to combat antimalarial resistance. *Expert Rev. Anti-Infect. Ther.* **2021**, 1-20.

94. Smith, D. L.; Klein, E. Y.; McKenzie, F. E.; Laxminarayan, R., Prospective strategies to delay the evolution of anti-malarial drug resistance: weighing the uncertainty. *Malar. J.* **2010**, *9* (1), 1-10.

95. Thu, A. M.; Phyo, A. P.; Landier, J.; Parker, D. M.; Nosten, F. H., Combating multidrug-resistant Plasmodium falciparum malaria. *FEBS J.* **2017**, *284* (16), 2569-2578.

96. Chookajorn, T., How to combat emerging artemisinin resistance: Lessons from "The Three Little Pigs". *PLoS Pathog.* **2018**, *14* (4), e1006923.

97. Burrows, J. N.; van Huijsduijnen, R. H.; Möhrle, J. J.; Oeuvray, C.; Wells, T. N., Designing the next generation of medicines for malaria control and eradication. *Malar. J.* **2013**, *12* (1), 187.

98. Maxmen, A., Busting the billion-dollar myth: how to slash the cost of drug development. *Nature* **2016**, *536*, 388-390.

99. Chen, J.; Luo, X.; Qiu, H.; Mackey, V.; Sun, L.; Ouyang, X., Drug discovery and drug marketing with the critical roles of modern administration. *Am. J. Transl. Res.* **2018**, *10* (12), 4302.

100. MMV, MMV-supported projects. https://www.mmv.org/research-development/mmv-supported-projects (accessed 24 June 2021).

101. Yuthavong, Y.; Tarnchompoo, B.; Vilaivan, T.; Chitnumsub, P.; Kamchonwongpaisan, S.; Charman, S. A.; McLennan, D. N.; White, K. L.; Vivas, L.; Bongard, E., Malarial dihydrofolate reductase as a paradigm for drug development against a resistance-compromised target. *Proc. Natl. Acad. Sci. U. S. A.* **2012**, *109* (42), 16823-16828.

102. Rottmann, M.; Jonat, B.; Gumpp, C.; Dhingra, S. K.; Giddins, M. J.; Yin, X.; Badolo, L.; Greco, B.; Fidock, D. A.; Oeuvray, C.; Spangenberg, T., Preclinical Antimalarial Combination Study of M5717, a Plasmodium falciparum Elongation Factor 2 Inhibitor, and Pyronaridine, a Hemozoin Formation Inhibitor. *Antimicrob. Agents Chemother.* **2020**, *64* (4), e02181-19.

103. Solapure, S.; Patil, V.; Henrich, P. P.; Magistrado, P. A.; Bharath, S.; Murugan, K.; Viswanath, P.; Puttur, J.; Srivastava, A.; Bellale, E., Triaminopyrimidine is a fast-killing and long-acting antimalarial clinical candidate. *Nat. Commun.* **2015**, *6*, 6715.

104. Kamath, H. Ipca and Medicines for Malaria Venture. https://www.ipca.com/pdf/noticeOfBM/announcement-ipca-and-MMV.pdf (accessed 23 September 2021).

105. Collins, K. A.; Rückle, T.; Elliott, S.; Marquart, L.; Ballard, E.; Chalon, S.; Griffin, P.; Möhrle, J. J.; McCarthy, J. S., DSM265 at 400 milligrams clears asexual stage parasites but not mature gametocytes from the blood of healthy subjects experimentally infected with Plasmodium falciparum. *Antimicrob. Agents Chemother.* **2019**, *63* (4), e01837-18.

106. Llanos-Cuentas, A.; Casapia, M.; Chuquiyauri, R.; Hinojosa, J.-C.; Kerr, N.; Rosario, M.; Toovey, S.; Arch, R. H.; Phillips, M. A.; Rozenberg, F. D., Antimalarial activity of single-dose DSM265, a novel plasmodium dihydroorotate dehydrogenase inhibitor, in patients with uncomplicated Plasmodium falciparum or Plasmodium vivax malaria infection: a proof-of-concept, open-label, phase 2a study. *Lancet Infect. Dis.* **2018**, *18* (8), 874-883.

107. Paquet, T.; Le Manach, C.; Cabrera, D. G.; Younis, Y.; Henrich, P. P.; Abraham, T. S.; Lee, M. C.; Basak, R.; Ghidelli-Disse, S.; Lafuente-Monasterio, M. J., Antimalarial efficacy of MMV390048, an inhibitor of Plasmodium phosphatidylinositol 4-kinase. *Sci. Transl. Med.* **2017**, *9* (387), 1-14.

108. Sinxadi, P.; Donini, C.; Johnstone, H.; Langdon, G.; Wiesner, L.; Allen, E.; Duparc, S.; Chalon, S.; McCarthy, J. S.; Lorch, U., Safety, tolerability, pharmacokinetics, and antimalarial activity of the novel *Plasmodium* phosphatidylinositol 4-kinase inhibitor MMV390048 in healthy volunteers. *Antimicrob. Agents Chemother.* **2020**, *64* (4), e01896-19.

109. Kung, S. H.; Lund, S.; Murarka, A.; McPhee, D.; Paddon, C. J., Approaches and recent developments for the commercial production of semi-synthetic artemisinin. *Front. Plant Sci.* **2018**, *9*, 1-7.

110. Rosenthal, P. J., Artefenomel: a promising new antimalarial drug. *Lancet Infect. Dis.* **2016**, *16* (1), 6-8.

111. Baird, J. K., Tafenoquine for travelers' malaria: evidence, rationale and recommendations. *J. Travel Med.* **2018**, *25* (1), 1-13.

112. Commons, R. J.; McCarthy, J. S.; Price, R. N., Tafenoquine for the radical cure and prevention of malaria: the importance of testing for G6PD deficiency. *Med. J. Aust.* **2020**, *212* (4), 152.

113. Reed, M. D., The Rescue and Repurposing of Pharmaceuticals: Augmenting the Drug Development Paradigm. *J. Pediatr. Pharmacol. Ther* **2016**, *21* (1), 4-6.

114. Bala, M.; Lahiry, S.; Choudhury, S.; Mukherjee, A.; Bhunya, P. K.; Chowdhury, K.; Sinha, R., Antimalarials: Pre-clinical development update. *Asian J. Med. Sci.* **2017**, *8* (5), 1-3.

115. Shim, J. S.; Liu, J. O., Recent advances in drug repositioning for the discovery of new anticancer drugs. *Int. J. Biol. Sci.* **2014**, *10* (7), 654.

116. Chong, C. R.; Sullivan, D. J., New uses for old drugs. *Nature* **2007**, *448* (7154), 645-646.

117. Mignani, S.; Huber, S.; Tomas, H.; Rodrigues, J.; Majoral, J.-P., Why and how have drug discovery strategies in pharma changed? What are the new mindsets? *Drug Discov. Today* **2016**, *21* (2), 239-249.

118. Swinney, D. C.; Anthony, J., How were new medicines discovered? *Nat. Rev. Drug Discov* **2011**, *10* (7), 507-519.

119. Jhoti, H.; Rees, S.; Solari, R., High-throughput screening and structure-based approaches to hit discovery: is there a clear winner? *Expert Opin. Drug Discovery* **2013**, *8* (12), 1449-1453.

120. Mateus, A.; Gordon, L. J.; Wayne, G. J.; Almqvist, H.; Axelsson, H.; Seashore-Ludlow, B.; Treyer, A.; Matsson, P.; Lundbäck, T.; West, A., Prediction of intracellular exposure bridges the gap between target-and cell-based drug discovery. *Proc. Natl. Acad. Sci. U. S. A.* **2017**, *114* (30), E6231-E6239.

121. Aulner, N.; Danckaert, A.; Ihm, J.; Shum, D.; Shorte, S. L., Next-Generation Phenotypic Screening in Early Drug Discovery for Infectious Diseases. *Trends Parasitol.* **2019**.

122. Carolino, K.; Winzeler, E. A., The antimalarial resistome – finding new drug targets and their modes of action. *Current Opinion in Microbiology* **2020**, *57*, 49-55.

123. Yang, T.; Ottilie, S.; Istvan, E. S.; Godinez-Macias, K. P.; Lukens, A. K.; Baragaña, B.; Campo, B.; Walpole, C.; Niles, J. C.; Chibale, K.; Dechering, K. J.; Llinás, M.; Lee, M. C. S.; Kato, N.; Wyllie, S.; McNamara, C. W.; Gamo, F. J.;

Burrows, J.; Fidock, D. A.; Goldberg, D. E.; Gilbert, I. H.; Wirth, D. F.; Winzeler, E. A., MalDA, Accelerating Malaria Drug Discovery. *Trends Parasitol.* **2021**, *37* (6), 493-507.

124. Nalbantoglu, S. Metabolomics: Basic Principles and Strategies. https://www.intechopen.com/books/molecular-medicine/metabolomics-basic-principles-and-strategies (accessed 13 September 2021).

125. Gieger, C.; Geistlinger, L.; Altmaier, E.; De Angelis, M. H.; Kronenberg, F.; Meitinger, T.; Mewes, H.-W.; Wichmann, H.-E.; Weinberger, K. M.; Adamski, J., Genetics meets metabolomics: a genome-wide association study of metabolite profiles in human serum. *PLoS Genet* **2008**, *4* (11), e1000282.

126. Alonso, A.; Marsal, S.; Julià, A., Analytical methods in untargeted metabolomics: state of the art in 2015. *Front. Bioeng. Biotechnol.* **2015**, *3*, 23.

127. Allman, E. L.; Painter, H. J.; Samra, J.; Carrasquilla, M.; Llinás, M., Metabolomic profiling of the malaria box reveals antimalarial target pathways. *Antimicrob. Agents Chemother.* **2016**, *60* (11), 6635-6649.

128. Rath, C. M.; Benton, B. M.; de Vicente, J.; Drumm, J. E.; Geng, M.; Li, C.; Moreau, R. J.; Shen, X.; Skepper, C. K.; Steffek, M., Optimization of CoaD inhibitors against gram-negative organisms through targeted metabolomics. *ACS Infect. Dis.* **2017**, *4* (3), 391-402.

129. Puchades-Carrasco, L.; Pineda-Lucena, A., Metabolomics in pharmaceutical research and development. *Curr. Opin. Biotechnol.* **2015**, *35*, 73-77.

130. Xu, E. Y.; Schaefer, W. H.; Xu, Q., Metabolomics in pharmaceutical research and development: metabolites, mechanisms and pathways. *Curr. Opin. Drug Discovery Dev.* **2009**, *12* (1), 40-52.

131. Nalbantoglu, S. Metabolomics: Basic Principles and Strategies. https://www.intechopen.com/books/molecular-medicine/metabolomics-basic-principles-and-strategies (accessed 13 December 2021).

132. Cobbold, S. A.; Chua, H. H.; Nijagal, B.; Creek, D. J.; Ralph, S. A.; McConville, M. J., Metabolic dysregulation induced in Plasmodium falciparum by dihydroartemisinin and other front-line antimalarial drugs. *J. Infect. Dis.* **2016**, *213* (2), 276-286.

133. Spry, C.; Kirk, K.; Saliba, K. J., Coenzyme A biosynthesis: an antimicrobial drug target. *FEMS Microbiol. Rev.* **2008**, *32* (1), 56-106.

134. Grevengoed, T. J.; Klett, E. L.; Coleman, R. A., Acyl-CoA metabolism and partitioning. *Annu. Rev. Nutr.* **2014**, *34*, 1-30.

135. Saliba, K. J.; Ferru, I.; Kirk, K., Provitamin B5 (pantothenol) inhibits growth of the intraerythrocytic malaria parasite. *Antimicrob. Agents Chemother.* **2005**, *49* (2), 632-637.

136. Trager, W.; Jensen, J. B., Human malaria parasites in continuous culture. *Science* **1976**, *193* (4254), 673-675.

137. Saliba, K. J.; Kirk, K., H+-coupled pantothenate transport in the intracellular malaria parasite. *J. Biol. Chem.* **2001**, *276* (21), 18115-18121.

138. Ginsburg, H.; Stein, W., The new permeability pathways induced by the malaria parasite in the membrane of the infected erythrocyte: comparison of results using different experimental techniques. *J. Membr. Biol.* **2004**, *197* (2), 113-134.

139. Zhyvoloup, A.; Nemazanyy, I.; Panasyuk, G.; Valovka, T.; Fenton, T.; Rebholz, H.; Wang, M.-L.; Foxon, R.; Lyzogubov, V.; Usenko, V., Subcellular localization and regulation of coenzyme A synthase. *J. Biol. Chem.* **2003**, *278* (50), 50316-50321.

140. Hart, R. J.; Abraham, A.; Aly, A. S., Genetic characterization of coenzyme A biosynthesis reveals essential distinctive functions during malaria parasite development in blood and mosquito. *Front. Cell. Infect. Microbiol.* **2017**, *7*, 260.

141. Saliba, K.; Kirk, K., CJ-15,801, a fungal natural product, inhibits the intraerythrocytic stage of Plasmodium falciparum in vitro via an effect on pantothenic acid utilisation. *Mol. Biochem. Parasitol.* **2005**, *141* (1), 129-131.

142. Tjhin, E. T.; Spry, C.; Sewell, A. L.; Hoegl, A.; Barnard, L.; Sexton, A. E.; Howieson, V. M.; Maier, A. G.; Creek, D. J.; Strauss, E.; Marquez, R.; Auclair, K.; Saliba, K. J., Mutations in the pantothenate kinase of the malaria parasite confer resistance or hypersensitivity to diverse pantothenate analogues. *bioRxiv* **2017**, 137182.

143. de Villiers, M.; Macuamule, C.; Spry, C.; Hyun, Y.-M.; Strauss, E.; Saliba, K. J., Structural modification of pantothenamides counteracts degradation by pantetheinase and improves antiplasmodial activity. *ACS Med. Chem. Lett.* **2013**, *4* (8), 784-789.

144. Spry, C.; Macuamule, C.; Lin, Z.; Virga, K. G.; Lee, R. E.; Strauss, E.; Saliba, K. J., Pantothenamides are potent, on-target inhibitors of Plasmodium falciparum growth when serum pantetheinase is inactivated. *PLoS One* **2013**, *8* (2), e54974.

145. Macuamule, C. J.; Tjhin, E. T.; Jana, C. E.; Barnard, L.; Koekemoer, L.; de Villiers, M.; Saliba, K. J.; Strauss, E., A pantetheinase-resistant pantothenamide

with potent, on-target, and selective antiplasmodial activity. *Antimicrob. Agents Chemother.* **2015**, *59* (6), 3666-3668.

146. de Villiers, M.; Spry, C.; Macuamule, C. J.; Barnard, L.; Wells, G.; Saliba, K. J.; Strauss, E., Antiplasmodial mode of action of pantothenamides: pantothenate kinase serves as a metabolic activator not as a target. *ACS Infect. Dis.* **2017**, *3* (7), 527-541.

147. Schalkwijk, J.; Allman, E. L.; Jansen, P. A.; De Vries, L. E.; Verhoef, J. M.; Jackowski, S.; Botman, P. N.; Beuckens-Schortinghuis, C. A.; Koolen, K. M.; Bolscher, J. M., Antimalarial pantothenamide metabolites target acetyl–coenzyme A biosynthesis in Plasmodium falciparum. *Sci. Transl. Med.* **2019**, *11* (510), eaas9917.

148. Francklyn, C. S.; Mullen, P., Progress and challenges in aminoacyl-tRNA synthetase-based therapeutics. *J. Biol. Chem.* **2019**, *294* (14), 5365-5385.

149. Bruce Alberts, A. J., Julian Lewis, Martin Raff, Keith Roberts, and Peter Walter, Protein Function. *In Molecular Biology of the Cell.* , 4 ed.; Garland Science: New York, 2002.

150. Jain, V.; Kikuchi, H.; Oshima, Y.; Sharma, A.; Yogavel, M., Structural and functional analysis of the anti-malarial drug target prolyl-tRNA synthetase. *J. Struct. Funct. Genomics* **2014**, *15* (4), 181-190.

151. Khan, S., Recent advances in the biology and drug targeting of malaria parasite aminoacyl-tRNA synthetases. *Malar. J.* **2016**, *15* (1), 203.

152. Manickam, Y.; Chaturvedi, R.; Babbar, P.; Malhotra, N.; Jain, V.; Sharma, A., Drug targeting of one or more aminoacyl-tRNA synthetase in the malaria parasite Plasmodium falciparum. *Drug Discov. Today* **2018**, *23* (6), 1233-1240.

153. Nyamai, D. W.; Bishop, Ö. T., Aminoacyl tRNA synthetases as malarial drug targets: a comparative bioinformatics study. *Malar. J.* **2019**, *18* (1), 34.

154. Bhatt, T. K.; Kapil, C.; Khan, S.; Jairajpuri, M. A.; Sharma, V.; Santoni, D.; Silvestrini, F.; Pizzi, E.; Sharma, A., A genomic glimpse of aminoacyl-tRNA synthetases in malaria parasite Plasmodium falciparum. *BMC Genomics* **2009**, *10* (1), 644.

155. Pham, J. S.; Dawson, K. L.; Jackson, K. E.; Lim, E. E.; Pasaje, C. F. A.; Turner, K. E.; Ralph, S. A., Aminoacyl-tRNA synthetases as drug targets in eukaryotic parasites. *Int J Parasitol Drugs Drug Resist* **2014**, *4* (1), 1-13.

156. Coghi, P. S.; Zhu, Y.; Xie, H.; Hosmane, N. S.; Zhang, Y., Organoboron Compounds: Effective Antibacterial and Antiparasitic Agents. *Molecules* **2021**, *26* (11).

157. Zhang, P.; Ma, S., Recent development of leucyl-tRNA synthetase inhibitors as antimicrobial agents. *MedChemComm* **2019**, *10* (8), 1329-1341.

158. Khan, S.; Sharma, A.; Jamwal, A.; Sharma, V.; Pole, A. K.; Thakur, K. K.; Sharma, A., Uneven spread of cis-and trans-editing aminoacyl-tRNA synthetase domains within translational compartments of P. falciparum. *Sci. Rep.* **2011**, *1*, 188.

159. Mereddy, G. R.; Chakradhar, A.; Rutkoski, R. M.; Jonnalagadda, S. C., Benzoboroxoles: synthesis and applications in medicinal chemistry. *J. Organomet. Chem.* **2018**, *865*, 12-22.

160. Baker, S. J.; Tomsho, J. W.; Benkovic, S. J., Boron-containing inhibitors of synthetases. *Chem. Soc. Rev.* **2011**, *40* (8), 4279-4285.

161. Fernandes, G. F. S.; Denny, W. A.; Dos Santos, J. L., Boron in drug design: Recent advances in the development of new therapeutic agents. *Eur. J. Med. Chem.* **2019**.

162. Kitzen, J. M.; Pergolizzi Jr, J. V.; Taylor Jr, R.; Raffa, R. B., Crisaborole and apremilast: PDE4 inhibitors with similar mechanism of action, different indications for management of inflammatory skin conditions. *Pharmacol. Pharm.* **2018**, *9* (09), 357.

163. Rock, F. L.; Mao, W.; Yaremchuk, A.; Tukalo, M.; Crépin, T.; Zhou, H.; Zhang, Y.-K.; Hernandez, V.; Akama, T.; Baker, S. J., An antifungal agent inhibits an aminoacyl-tRNA synthetase by trapping tRNA in the editing site. *Science* **2007**, *316* (5832), 1759-1761.

164. Sharma, N.; Sharma, D., An upcoming drug for onychomycosis: Tavaborole. *J Pharmacol Pharmacother* **2015**, *6* (4), 236.

165. Dickie, E. A.; Giordani, F.; Gould, M. K.; Mäser, P.; Burri, C.; Mottram, J. C.; Rao, S. P.; Barrett, M. P., New drugs for human African trypanosomiasis: A twenty first century success story. *Trop. Med. Infect. Dis* **2020**, *5* (1), 29.

166. Wall, R. J.; Rico, E.; Lukac, I.; Zuccotto, F.; Elg, S.; Gilbert, I. H.; Freund, Y.; Alley, M. R.; Field, M. C.; Wyllie, S., Clinical and veterinary trypanocidal benzoxaboroles target CPSF3. *Proc. Natl. Acad. Sci. U. S. A.* **2018**, *115* (38), 9616-9621.

167. Si, Y.; Basak, S.; Li, Y.; Merino, J.; Iuliano, J. N.; Walker, S. G.; Tonge, P. J., Antibacterial Activity and Mode of Action of a Sulfonamide-Based Class of Oxaborole Leucyl-tRNA-Synthetase Inhibitors. *ACS Infect. Dis.* **2019**, *5* (7), 1231-1238.

168. O'Dwyer, K.; Spivak, A. T.; Ingraham, K.; Min, S.; Holmes, D. J.; Jakielaszek, C.; Rittenhouse, S.; Kwan, A. L.; Livi, G. P.; Sathe, G., Bacterial

resistance to leucyl-tRNA synthetase inhibitor GSK2251052 develops during treatment of complicated urinary tract infections. *Antimicrob. Agents Chemother.* **2015**, *59* (1), 289-298.

169. Zhang, Y.-K.; Plattner, J. J.; Freund, Y. R.; Easom, E. E.; Zhou, Y.; Gut, J.; Rosenthal, P. J.; Waterson, D.; Gamo, F.-J.; Angulo-Barturen, I., Synthesis and structure–activity relationships of novel benzoxaboroles as a new class of antimalarial agents. *Bioorg. Med. Chem. Lett.* **2011**, *21* (2), 644-651.

170. Sonoiki, E.; Palencia, A.; Guo, D.; Ahyong, V.; Dong, C.; Li, X.; Hernandez, V. S.; Zhang, Y.-K.; Choi, W.; Gut, J., Antimalarial benzoxaboroles target Plasmodium falciparum leucyl-tRNA synthetase. *Antimicrob. Agents Chemother.* **2016**, *60* (8), 4886-4895.

171. Sonoiki, E.; Ng, C. L.; Lee, M. C.; Guo, D.; Zhang, Y.-K.; Zhou, Y.; Alley, M.; Ahyong, V.; Sanz, L. M.; Lafuente-Monasterio, M. J., A potent antimalarial benzoxaborole targets a Plasmodium falciparum cleavage and polyadenylation specificity factor homologue. *Nat. Commun.* **2017**, *8* (1), 1-11.

172. Sindhe, K. M.; Wu, W.; Legac, J.; Zhang, Y.-K.; Easom, E. E.; Cooper, R. A.; Plattner, J. J.; Freund, Y. R.; DeRisi, J. L.; Rosenthal, P. J., Plasmodium falciparum Resistance to a Lead Benzoxaborole Due to Blocked Compound Activation and Altered Ubiquitination or Sumoylation. *mBio* **2020**, *11* (1).

173. Nsanzabana, C., Resistance to artemisinin combination therapies (ACTs): do not forget the partner drug! *Trop. Med. Infect. Dis* **2019**, *4* (1), 26.

174. Strauss, E., Coenzyme A biosynthesis and enzymology. *Chem. Biol.* **2010**, *7* (1), 351-410.

175. Skepper, C. K.; Moreau, R. J.; Appleton, B. A.; Benton, B. M.; Drumm III, J. E.; Feng, B. Y.; Geng, M.; Hu, C.; Li, C.; Lingel, A., Discovery and optimization of phosphopantetheine adenylyltransferase inhibitors with gram-negative antibacterial activity. *J. Med. Chem.* **2018**, *61* (8), 3325-3349.

176. Moreau, R. J.; Skepper, C. K.; Appleton, B. A.; Blechschmidt, A.; Balibar, C. J.; Benton, B. M.; Drumm III, J. E.; Feng, B. Y.; Geng, M.; Li, C., Fragment-based drug discovery of inhibitors of phosphopantetheine adenylyltransferase from gram-negative bacteria. *J. Med. Chem.* **2018**, *61* (8), 3309-3324.

177. de Jonge, B. L.; Walkup, G. K.; Lahiri, S. D.; Huynh, H.; Neckermann, G.; Utley, L.; Nash, T. J.; Brock, J.; San Martin, M.; Kutschke, A., Discovery of inhibitors of 4′-phosphopantetheine adenylyltransferase (PPAT) to validate PPAT as a target for antibacterial therapy. *Antimicrob. Agents Chemother.* **2013**, *57* (12), 6005-6015.

Chapter 2: Design, synthesis, and characterization

2.1. Chapter overview

The chapter begins with background information relating to 4′-phosphopantetheine adenylyltransferase (PPAT) inhibitors. This is followed by details of the synthesis of hit compounds, plans to develop structure-activity relationships (SARs) for PPAT inhibitors. Since the utilized chemical reactions and attendant mechanisms are all known and/or reported in literature, mechanistic details are purposely not included. The characterization of key intermediates and selected final compounds is also described. The same outline is followed for the benzoxaborole series.

2.2. PPAT inhibitors

2.2.1. General introduction

Drug repositioning refers to the use of approved drugs developed for different indications as templates for drug design for a new indication. This strategy can be used to identify new antimalarials in two ways: First, by using the approved drug as a template for the synthesis of new derivatives optimised for malaria; Second, by exploiting the known drug target (also known as target repurposing) of any origin in target-based malaria drug discovery.[178] Coenzyme A (CoA) is a central acyl carrier in many metabolic pathways and is essential for the survival of organisms.[133, 134] *Plasmodium falciparum (P. falciparum)* has an absolute requirement for CoA biosynthesis. Despite the importance of the CoA biosynthesis pathway, there are no clinical antimalarials known to target this pathway. Of the five enzymes involved in the CoA biosynthesis pathway, only the first enzyme (phosphopantetheine kinase, PanK) has been previously targeted for antimalarial drug discovery. There have been recent reports of a preclinical candidate that is metabolized by CoA biosynthesis pathway enzymes in *P. falciparum* and inhibits downstream metabolomic pathways (described in detail in **Chapter 1, section 1.10.2**).[144, 146, 147]

Antibacterial drug discovery campaigns at AstraZeneca (AZ) and Novartis have yielded compounds that target bacterial PPAT, the penultimate enzyme of the CoA biosynthesis pathway.[175-177] The Novartis work was initiated by biochemical screening involving a fragment-based drug discovery approach, which was followed by lead optimization. [175, 176] Lead optimization at AZ was guided by structure-based

drug design and led to the identification of compounds that inhibited cell growth of gram-positive bacteria. Mode-of-action (MoA) studies confirmed that PPAT was targeted by these compounds and *in vivo* efficacy studies in a mouse model concluded that further work was required to improve compound properties and optimize dose and administration before commencing clinical studies.[177] These bacterial programs have thus prompted work to reposition both PPAT as a target and reported inhibitors in antimalarial drug discovery program.

A 500-member compound library was obtained from AZ and subjected to medium-throughput screening (MTS) at H3D, UCT. This library comprised compounds belonging to two series designated as the cyclohexyl pyrimidine and the Ugi series. Four hits were identified during screening: two from the Ugi series (**Fig. 2.1**, **1** and **2**) and two from cyclohexyl pyrimidine series (**Fig. 2.1**, **3** and **4**). These displayed antiplasmodium activities between IC_{50}'s 1.04 μM and 2.9 μM and did not show cytotoxicity against Chinese Hamster Ovarian (CHO) cells at the maximum concentration tested (IC_{50} > 50 μM). Using the data from research publication on the Novartis PPAT inhibitors, the four most active compounds against bacterial PPAT (**Fig. 2.1**, **5**–**8**) were selected and proposed for evaluation as potential antiplasmodium activity. These eight compounds formed the basis of this study. Their antiplasmodium activity, physicochemical properties, and cytotoxicity were to be used to guide the design and selection of compounds for future hit-to-lead transitions, if warranted by the data.

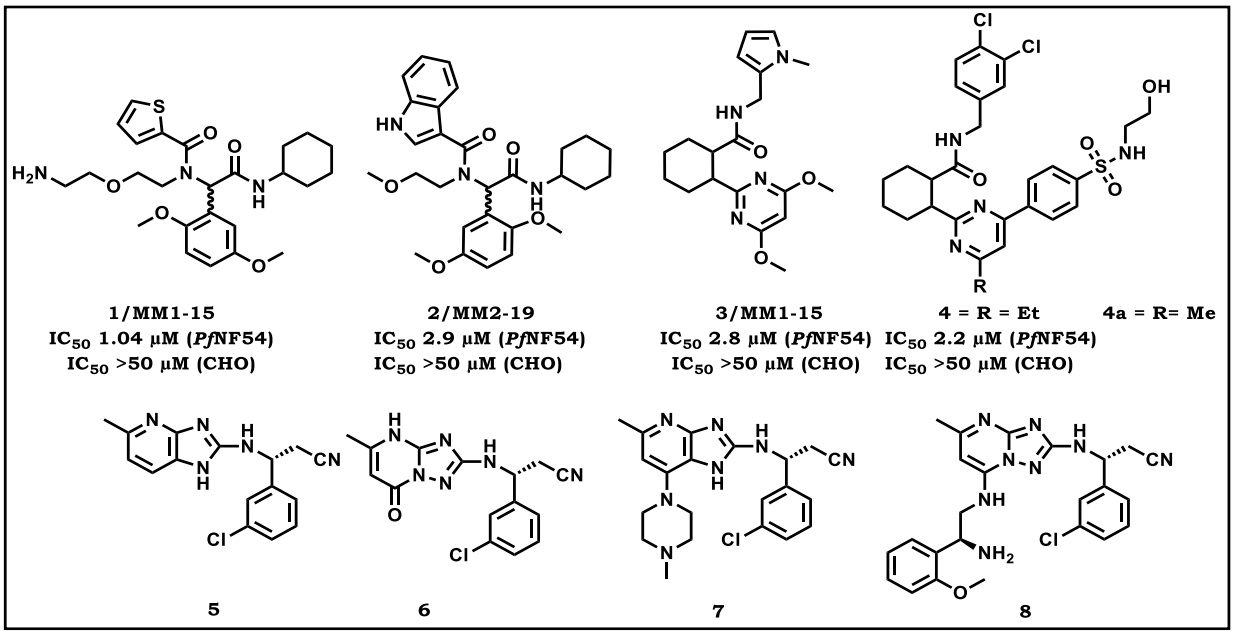

Figure 2.1 PPAT inhibitors from MTS screen against *P. falciparum* (**1**–**4**), synthesized analogue (**4a**), and reported Novartis bacterial PPAT inhibitors (**5**–**8**)

2.2.2. Rationale for SAR study of compounds

Rationale for the SAR study based on the AZ series compounds

A hit validation study involving resynthesis and retesting was conducted to confirm the activity of hits identified via the MTS campaign. All hits except compound **4** (**Fig. 2.1**) were successfully resynthesized. Purity was confirmed via liquid chromatography-mass spectrometry (LC-MS; >95% purity) and compounds were fully characterized via nuclear magnetic resonance (NMR). The compounds were then submitted for biological evaluation against the drug sensitive *Pf*NF54 strain. The compound was considered inactive if it had an IC_{50} greater than 6 µM (IC50 >6 µM) which is the highest concentration tested in this biological assay. The methyl analogue compound **4a/MM2-39** (**Fig. 2.1**) was produced instead of hit compound **4** because of synthetic challenges encountered in the reactions required to obtain the necessary intermediates. The hit validation study confirmed the antiplasmodium activity of compound **2/MM1-19** only and showed that its activity was lower than that reported in the MTS study (IC_{50} = 5.2 µM vs 2.9 µM). The compounds received from AZ had been stored as DMSO stock solutions, and the lack of activity observed suggests that non-validating hits may have been false positives perhaps due to compound decomposition in solution, a common observation in early drug discovery

phases.[179] However, as the IC_{50} of the newly synthetized compound **2/MM1-19** was within a two-fold difference of the IC_{50} obtained originally, this hit was taken forward to inform the design of compounds for a SAR exploration of this series (**Fig. 2.2**).

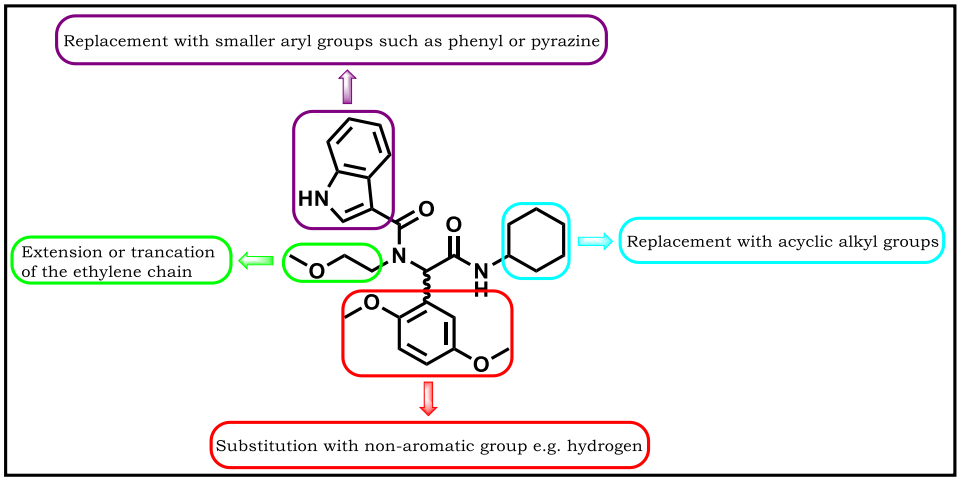

Figure 2.2: SAR study of the Ugi series-based hit compound **2/MM1-19**

The proposed target compounds were selected if they conformed with Lipinski's "rule of five" (Ro5) and depending on their property forecast index (PFI) value following the workflow summarized in **Fig. 2.3**. The Ro5 is based on the hypothesis that an ideal oral drug should have molecular weight < 500 g/mol, logP < 5, number of hydrogen-bond donors < 5, and number of hydrogen-bond acceptors < 10. At this juncture it is noteworthy that the Ro5 is only a guide and was used as such in this thesis work. The Ro5 parameters were calculated using ACD/Percepta and StarDrop software. The concept of the PFI value was devised by GSK and is calculated as the sum of aromatic rings and chromatographic $logD_{7.4}$ value of a molecule. A compound with PFI < 7 should meet multiple criteria for developability (e.g., high solubility and low albumin binding among others) whereas PFI > 7 is undesirable.[180] Compounds with PFI < 7 were selected for synthesis according to the proposed SAR exploration shown in **Fig. 2.2**.

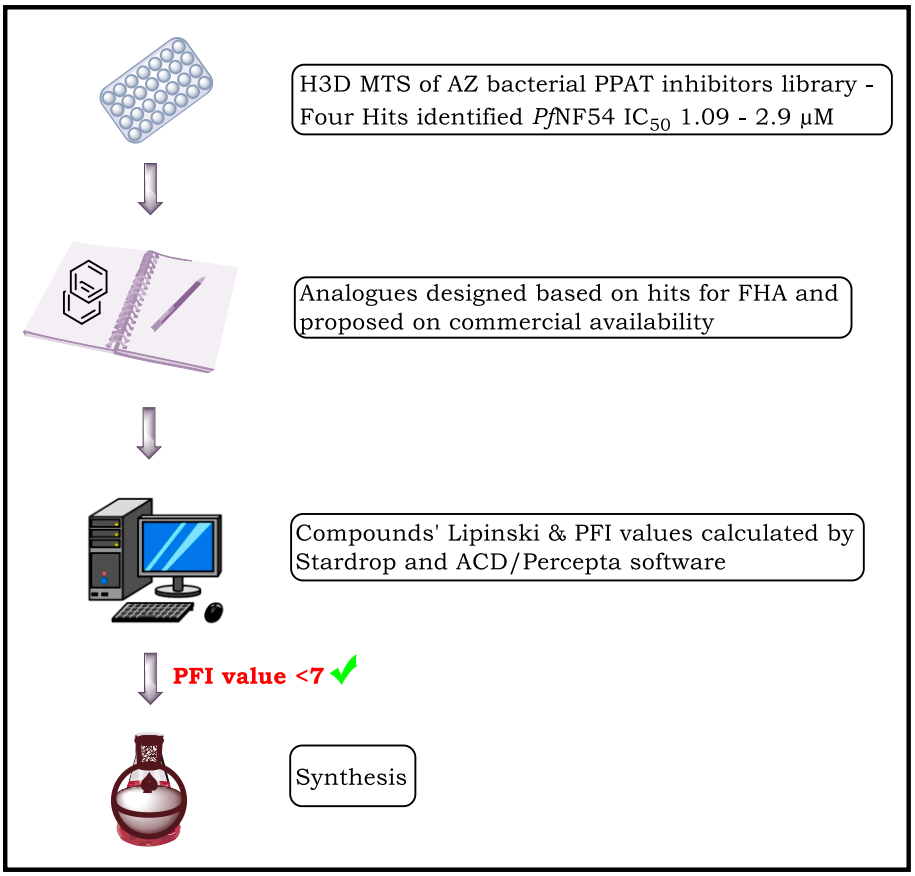

Figure 2.3: Workflow for the progression of compounds based on AZ bacterial PPAT inhibitors

MTS, medium-throughput screening; FHA, formal hit assessment; PFI, property forecast index

Rationale for the SAR study based on the Novartis series compounds

An attempt to synthesize the compounds reported by Novartis was unsuccessful. Synthetic challenges were encountered with (*R*)-3-amino-3-(3-chlorophenyl)propanenitrile substituent present in reported compounds (**Fig. 2.4**). Instead (3-chlorophenyl)methanamine substituent (example highlighted in purple on compound **9 Fig. 2.4**) was used in place of (*R*)-3-amino-3-(3-chlorophenyl)propanenitrile substituent (example highlighted in red on compound **5 Fig. 2.4**) to give minimum structure with core features of the reported compounds. The presence of the nitrile group likely interfered with one of the reaction steps run under acidic conditions, resulting in several side products. Therefore, compounds lacking the cyanomethyl group were synthesized. Commercial unavailability of (*S*)-1-

(2-methoxyphenyl)ethane-1,2-diamine also limited access to the pure enantiomer of compound **12** and rather racemic 1-(2-methoxyphenyl)ethane-1,2-diamine was used instead to prepare the compound as a racemate (**Fig. 2.4**). Respective compounds from the three series were obtained in high yield (azabenzimidazole (**9**), triazolopyrimidinone (**10**), and triazolopyrimidine (**12**) and were purified and characterized before submission for antiplasmodium activity evaluation. The synthesis of compound **11** was unsuccessful.

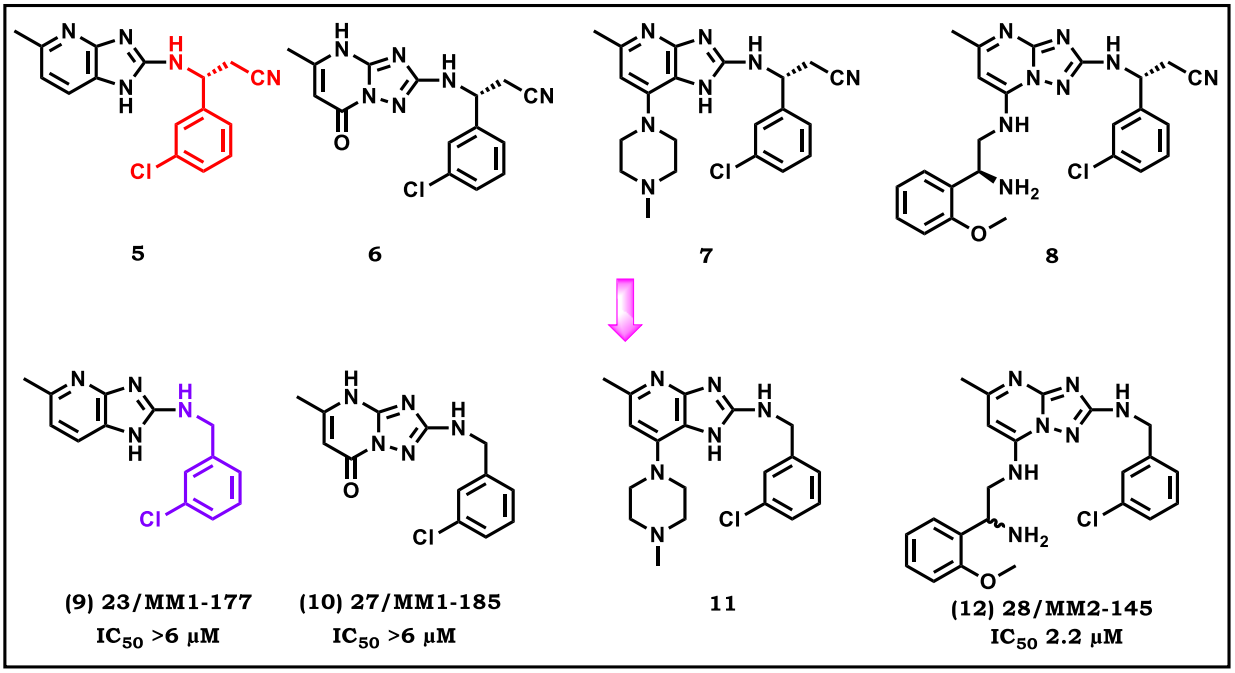

Figure 2.4: Proposed PPAT inhibitors

Compounds **9** (heretofore referred as **23/MM1-177**) and **10** (heretofore referred as **27/MM1-185**) showed no antiplasmodium activity (*Pf*NF54 IC_{50} > 6 µM, the highest concentration tested). However, the triazolopyrimidine compound **12** (**28/MM2-145**) displayed antiplasmodium activity (albeit weak) against *Pf*NF54 (IC_{50} = 2.2 µM). This compound informed the design of additional analogues for the triazolopyrimidine series for SAR evaluation. The design was guided by Craig plot substituents for **SAR 1** (**Fig. 2.5**) while maintaining 1-(2-methoxyphenyl)ethane-1,2-diamine. The Craig plot is used in rational drug design to guide the selection of substituents suitable to improve explore a range of physicochemical properties and how they impact bioactivity. Substituents are clustered by Hammett σ and Hansch π substituent constants displayed on a four-quadrant plot. This two-dimensional plot allows for

substituents to be selected based on their electron-withdrawing or -donating nature and influence on lipohphilicity.[181] Other changes included the removal of the halogen and addition of a chiral center on the methylene of the (3-chlorophenyl)methanamine to assess the importance of substituents on the phenyl and the influence of the stereocenter, respectively.

Changes for exploration of **SAR 2** using the Craig plot were limited by the commercial availability of the 1-(2-methoxyphenyl)ethane-1,2-diamine variants as the methoxy was intended to be replaced with various substituents, and various substituents were migrated to the *meta*- and *para*- positions (**Fig. 2.5**). **SAR 2** was also explored by assessing the importance of the amine.

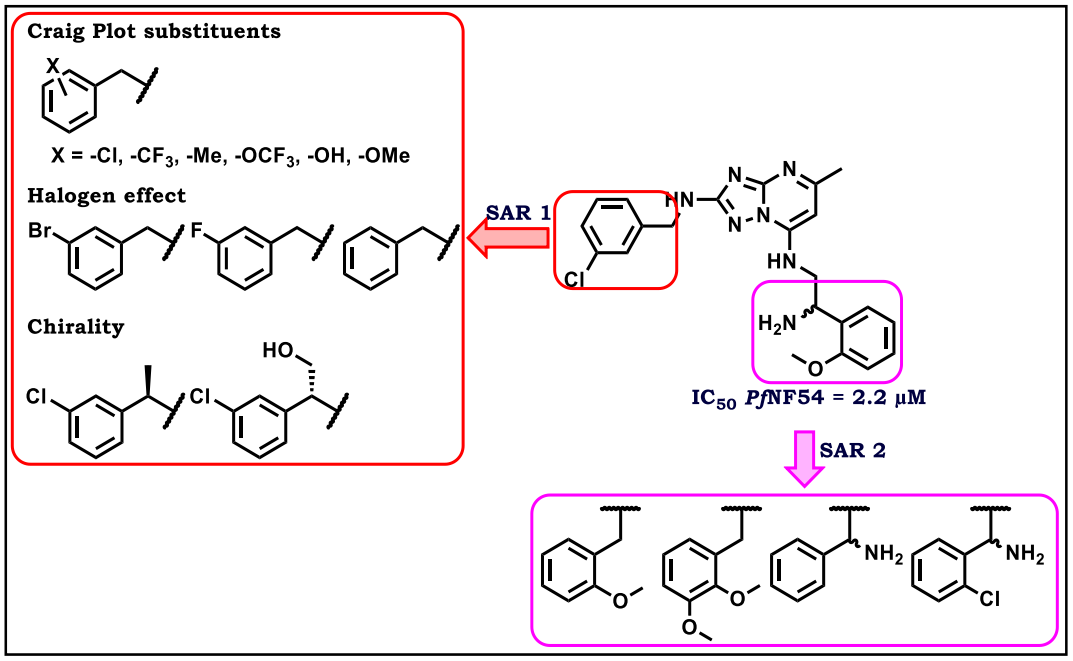

Figure 2.5: SAR design for the triazolopyrimidine series

2.3. Chemistry: synthesis of cyclohexyl pyrimidine and Ugi series compounds

2.3.1. Synthesis and characterization of the cyclohexyl pyrimidine series

General cyclohexyl pyrimidine series synthesis

Synthesis was performed according to the procedure reported by de Jonge *et al.* with slight modifications in the second step.[177] The compounds synthesized for this series are represented in **Table 2.1** and the reaction sequence is illustrated in **Scheme 2.1**.

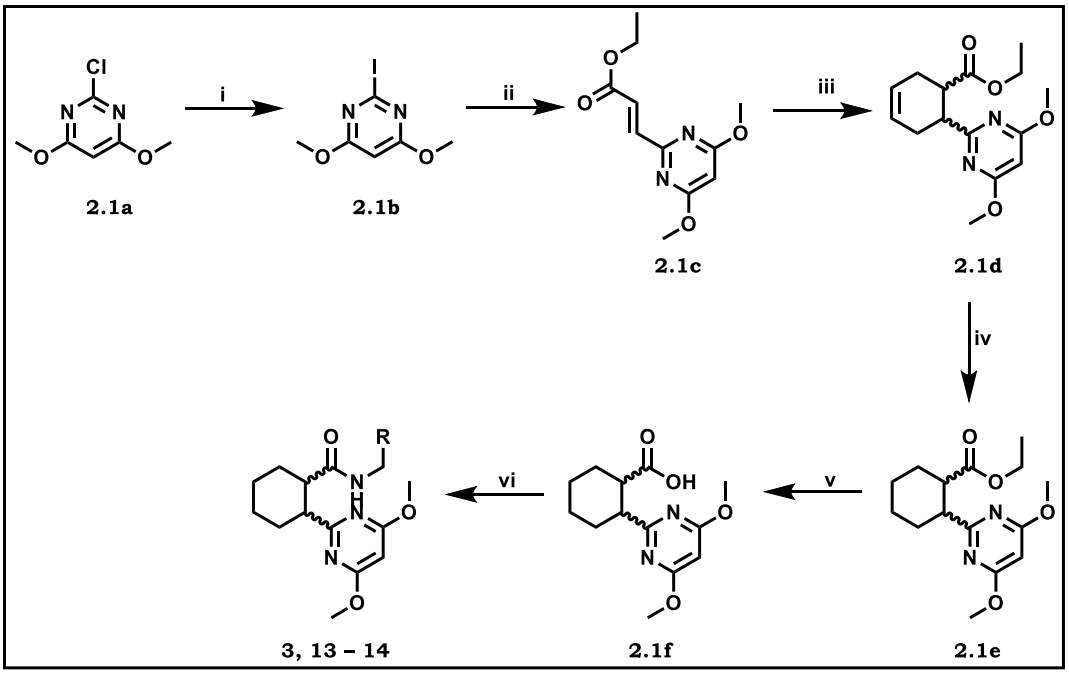

Scheme 2.1: Synthesis of the cyclohexane library

Reagents and conditions: (i) HI (57% wt. in H_2O), 0–24 °C, 4 h (quantitative); (ii) CH_2=$CHCOOC_2H_5$, $Pd(OAc)_2$, tri-*o*-tolylphosphine, Et_3N, 60 °C, 0.5 h, microwave (μW) (67%); (iii) $C_4H_6O_2S$, MePh, 155 °C, 24–72 h (28%); (iv) H_2, EtOH, 2 h, 0–24 °C (100%); (v) LiOH, MeOH/THF/H_2O (1:1:2, v/v), 70 °C, 12 h (66%); (vi) R–CH_2NH_2, EDCI, HOBt, DCM, 24 °C, 12 h (24 – 31%).

Table 2.1: Isolated yields of cyclohexyl pyrimidine compounds

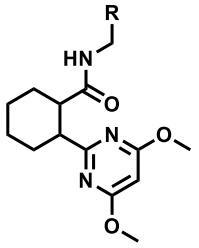

Compound code	R	Yield (%)
3/MM1-75		26
13/MM1-88	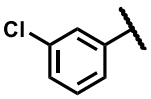	31
14/MM1-89	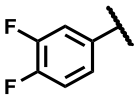	24

Synthesis started with the conversion of 2-chloro-4,6-dimethoxypyrimidine to 2-iodo-4,6-dimethoxypyrimidine (**Scheme 2.1(i)**). A commercially available 2-chloro-4,6-dimethoxypyrimidine **2.1a** was stirred at 24 °C in hydroiodic acid (57% wt. in H_2O) to facilitate the nucleophilic substitution of chloride to iodide to form the 2-iodo-4,6-dimethoxypyrimidine intermediate **2.1b**. This intermediate was subjected to Mizoroki-Heck coupling reaction (**Scheme 2.1: (ii)**). This carbon-carbon coupling reaction is widely used and is favored for its mild reaction conditions, low cost, low reagent toxicity, and high chemoselectivity. In addition, the palladium catalyst is advantageously recycled during the reaction.[13]

The Mizoroki-Heck coupling reaction (**Scheme 2.1(ii)**) was initially carried out neat in a sealed tube at 90 °C for 20 h using 10% palladium on carbon (Pd/C) as a catalyst, ethyl acrylate, and triethylamine. This resulted in moderate yield (67%) when following the procedure described by de Jonge *et al.*[177] When the reaction was carried out under microwave irradiation with the same conditions, no product was formed. However, when $Pd(OAc)_2$ was used instead of 10% Pd/C under microwave irradiation, the reaction was successful with an improved yield of 82% and a 30-min reaction

time compared to 20 h under conventional conditions. LC-MS analysis showed full conversion to **2.1c**, without any trace of starting material **2.1b**. These conditions have been investigated previously by Len *et al.*, but using water as a solvent.[182] The slight modification of these conditions (i.e., running the reaction neat) resulted in comparable yield (82% vs reported 90%). Improvement in yield with these conditions compared to those reported by de Jonge *et al.* may be attributed to the use of low amounts of Pd and microwave irradiation as a heat source, which reduces reaction times and thus side reactions.[182]

The acrylate **2.1c** was subjected to Diels-Alder cycloaddition. This is an ideal reaction for the formation of cyclic systems and is widely used in various applications. It involves a reaction between a diene (conjugated alkene) and dienophile (alkene).[183, 184] The Diels-Alder reaction used to convert the acrylate intermediate **2.1c** to a cyclohexene intermediate **2.1d** was achieved with the butadiene sulfone adduct in toluene in a sealed tube at high temperature (155 °C).

The cyclohexene obtained was reduced with hydrogen in the presence of 10% Pd/C in methanol to afford cyclohexane intermediate **2.1e**. Base-mediated hydrolysis with lithium hydroxide monohydrate ($LiOH{\cdot}H_2O$) produced the carboxylic acid intermediate **2.1f**. Amide coupling using hydroxybenzotriazole (HOBt) and 1-ethyl-3-(3-dimethylaminopropyl) carbodiimide (EDCI) resulted in the formation of the final compounds (**3/MM1-75**, **13/MM1-88**, and **14/MM1-89**).

Synthesis of the second cyclohexyl pyrimidine hit 4

This section covers the synthesis of the cyclohexyl pyrimidine hit **4**, which involved reactions other than those described in the preceding section. These are shown in **Scheme 2.2**. Synthesis was initiated by the formation of 4-bromo-*N*-(2-hydroxyethyl)benzenesulfonamide **2.2b** through nucleophilic substitution of ethanolamine on 4-bromobenzenesulfonyl chloride **2.2a** in high yield. This product was converted to the boronic ester **2.2c** through a Miyaura borylation reaction[185, 186] using bis(pinacolato)diboron. This reaction affords boronic acids or esters that are valuable intermediates for Suzuki-Miyaura carbon-carbon (C-C) bond formation reactions.

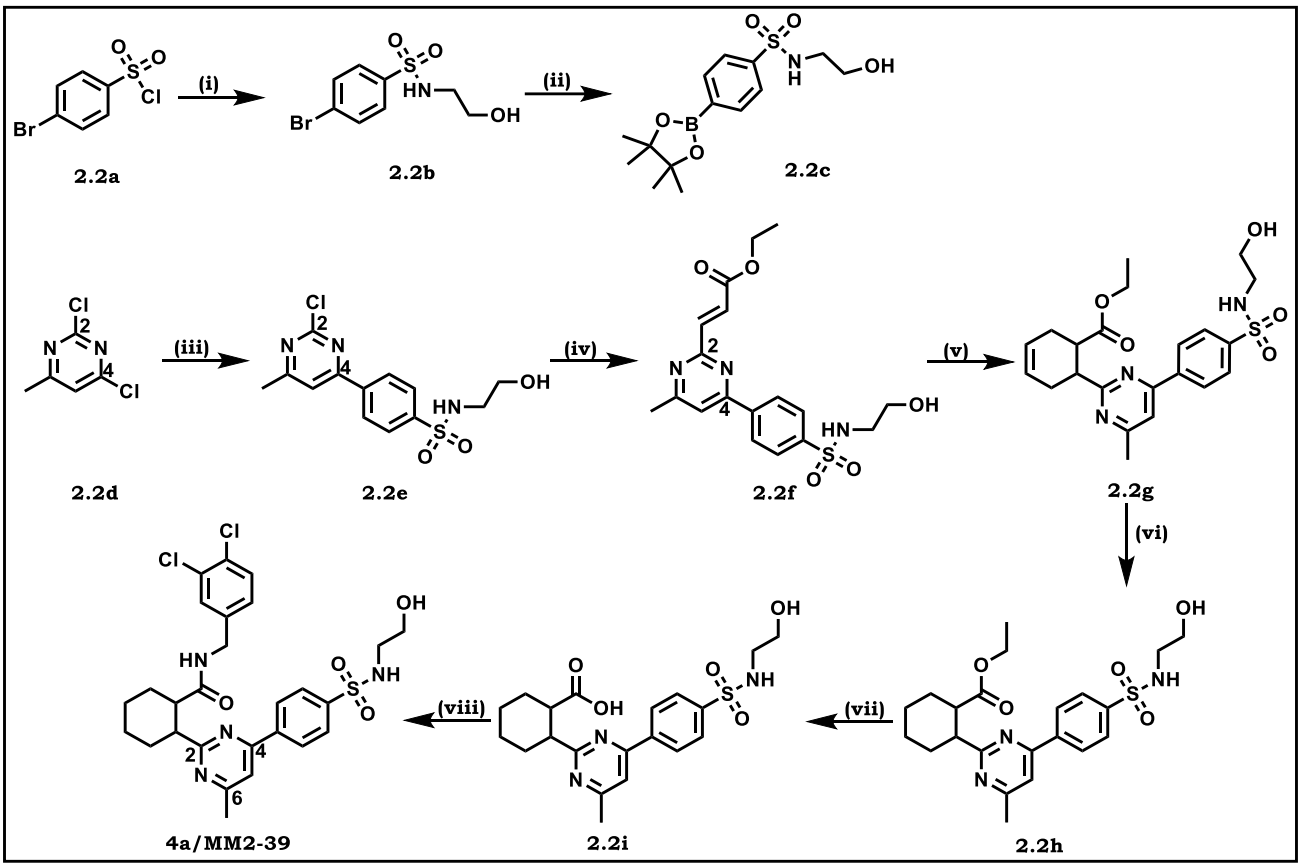

Scheme 2.2: Synthesis of cyclohexyl pyrimidine compound **4a/MM2-39**

Reagents and conditions: (i) $HOCH_2CH_2NH_2$, DIPEA, dioxane, 0–18 °C, 14 h (84%); (ii) B_2pin_2, Pd(dppf)Cl_2·DCM, KOAc, 80 °C, 20 h (52%); (iii) **2.2c**, Pd(dppf)Cl_2·DCM, Cs_2CO_3, dioxane:H_2O, μW, 70 °C, 0.5 h (40%); (iv) CH_2=$CHCOOC_2H_5$, DIPEA, tri-*o*-tolylphosphine, $Pd(OAc)_2$, MeCN, μW, 145 °C, 10 min (29%); (v) $C_4H_6O_2S$, MePh, 155 °C, 24–72 h; (vi) Pd/C (10%), H_2 (g), MeOH, 18 °C, 2 h; (vii) LiOH·H_2O, THF-MeOH, 50 °C, 18 h; (viii) 3,4-dichlorobenzylamine, EDCI, HOBt, DMF, 27 °C, 12 h (3%).

Intermediate **2.2c** was then used in a Suzuki-Miyaura cross-coupling reaction (**Scheme 2.2(iii)**). This reaction is important for C-C bond formation and is used in the synthesis of biaryls, which are oftentimes incorporated in important pharmaceutical compounds. Suzuki-Miyaura cross-coupling is a palladium-catalyzed reaction that facilitates C-C bond formation between an aryl halide and an aryl boronic species. This reaction is favored because of its ease in up-scaling, use of relatively cost-effective organoboron reagents, mild reaction conditions, and tolerance to diverse functional groups.[187]

The 2,4-dichloro-6-methylpyrimidine (**Scheme 2.2**: **2.2d**) and boronic ester **2.2c** reacted in the presence of a palladium catalyst (dppf) and base (Cs_2CO_3) in DMF to

form **2.2e**. This reaction, however, resulted in the formation of both the disubstituted and the desired mono-substituted compound **2.2e.** This was shown by LC-MS analysis as a mass of minor disubstituted product (*m/z* 391.44) and the desired product (*m/z* 327.78). The desired compound was successfully purified by flash column chromatography in moderate yield (40%). This implies that although cross-coupling occurred mainly at C4 of **2.2d**, the C2 chloride also reacted. Cross-coupling of polyhalogenated compounds has previously been studied.[188, 189] The C4 position is generally favored over C2 in polyhalogenated pyrimidine systems for Suzuki-Miyaura cross-coupling reactions, as noted by Montalban *et al.*[190] This regioselectivity is likely favored due to charge stabilization of the Meisenheimer salt, which occurs for reaction at C4.[188] Running the reaction at low temperature (70 °C) for a shorter period (30 min) with microwave irradiation reduced the formation of side products. In the next reaction, **2.2e** was subjected to Mizoroki-Heck coupling in the presence of $Pd(OAc)_2$, DIPEA as a base, and tri-*o*-tolylphosphine as a ligand under microwave irradiation. This reaction afforded the *E*-isomeric ethyl acrylate intermediate **2.2f**.

Isolation of subsequent intermediates (**Scheme 2.2g–i**) presented challenges and product mixtures were taken forward without further purification. The formation of each product in crude mixtures was confirmed via LC-MS. Mizoroki-Heck coupling was followed by Diels-Alder cyclization performed under reaction conditions previously described (**Scheme 2.2(v)**) to produce cyclohexene **2.2g** in the presence of butadiene sulfone at 155 °C. This cyclohexene was reduced to cyclohexane **2.2h** with hydrogen in the presence of 10% Pd/C (**Scheme 2.2(vi)**) and base-mediated $LiOH{\cdot}H_2O$ ester hydrolysis then afforded carboxylic acid **2.2i** (**Scheme 2.2(vii)**). Amide coupling of **2.2i** (**Scheme 2.2(viii)**) was successful in the presence of EDCI, HOBt, DIPEA, and an amine to produce **4a/MM2-39** in low yield (3% over four steps).

Characterization of target compound 3

Iodo intermediate 2.1b, acrylate intermediate 2.1c, and cyclohexene pyrimidine intermediate 2.1d

Intermediates **2.1b**–**2.1f** used in the synthesis of target compound **3** are shown here to illustrate characterization of compounds in this series. Iodination of 2-chloro-4,6-dimethoxypyrimidine **2.1a** with 57% hydroiodic acid (w/w in water) resulted in product **2.1b**. This was confirmed via LC-MS which revealed this compound displayed *m/z* 266.9 $[M+H]^+$ compared to *m/z* 175.0 $[M+H]^+$ and *m/z* 177.0 $[M+2]^+$ in the starting compound **2.1a**. Chloro-containing compounds display characteristic splitting patterns corresponding to molecular ion $[M+H]^+$ and $[M+2]^+$ peaks because of the presence of the ^{37}Cl heavy isotope.[191] The $[M+2]^+$ peak is approximately one third of the intensity of the molecular ion peak $[M+H]^+$. Comparison of the MS data for **2.1a** and **2.1b** showed that the latter had one intense peak and no additional peaks like the former, thus confirming the formation of **2.1b**.

^1H-NMR analysis of the Mizoroki–Heck coupling product **2.1c** revealed that the intermediate formed was an *E*-isomer (**Fig. 2.6A**). This was attributed to coupling of the double bond protons H4 and H5, resulting in a large coupling constant J = 15.7 Hz at δ 7.13 and 7.51 ppm, respectively. Formation of the Diels-Alder cyclohexene compound **2.1d** was confirmed via ^1H-NMR by the presence of the alkene protons H6 and H7 which appear at δ 5.73 ppm as a merged doublet of triplets (**Fig. 2.6B**). The doublet of triplets arises from the coupling of H6 to H7 and to chemically nonequivalent protons H5. Likewise, for H7 this is due to coupling to H6 and chemically nonequivalent H8 protons. In addition, the triplet of doublets was observed for H4 (δ 3.13 ppm, J = 10.9, 5.4 Hz) and H9 (δ 3.27 ppm, J = 10.9, 5.5 Hz; **Fig. 2.6B**). This implies that the trans-isomer formed, placing these protons in an axial position.

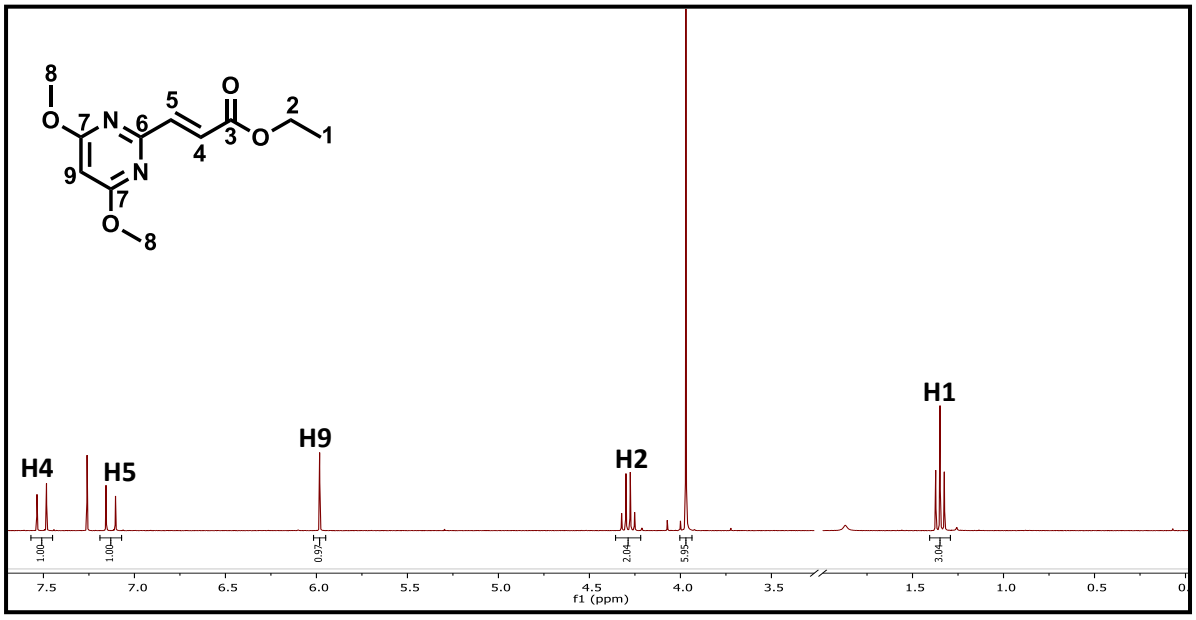

Figure 2.6A: ^{1}H-NMR spectrum of ethyl (E)-3-(4,6-dimethoxypyrimidin-2-yl)acrylate **2.1c** in $CDCl_3$ at 300 MHz

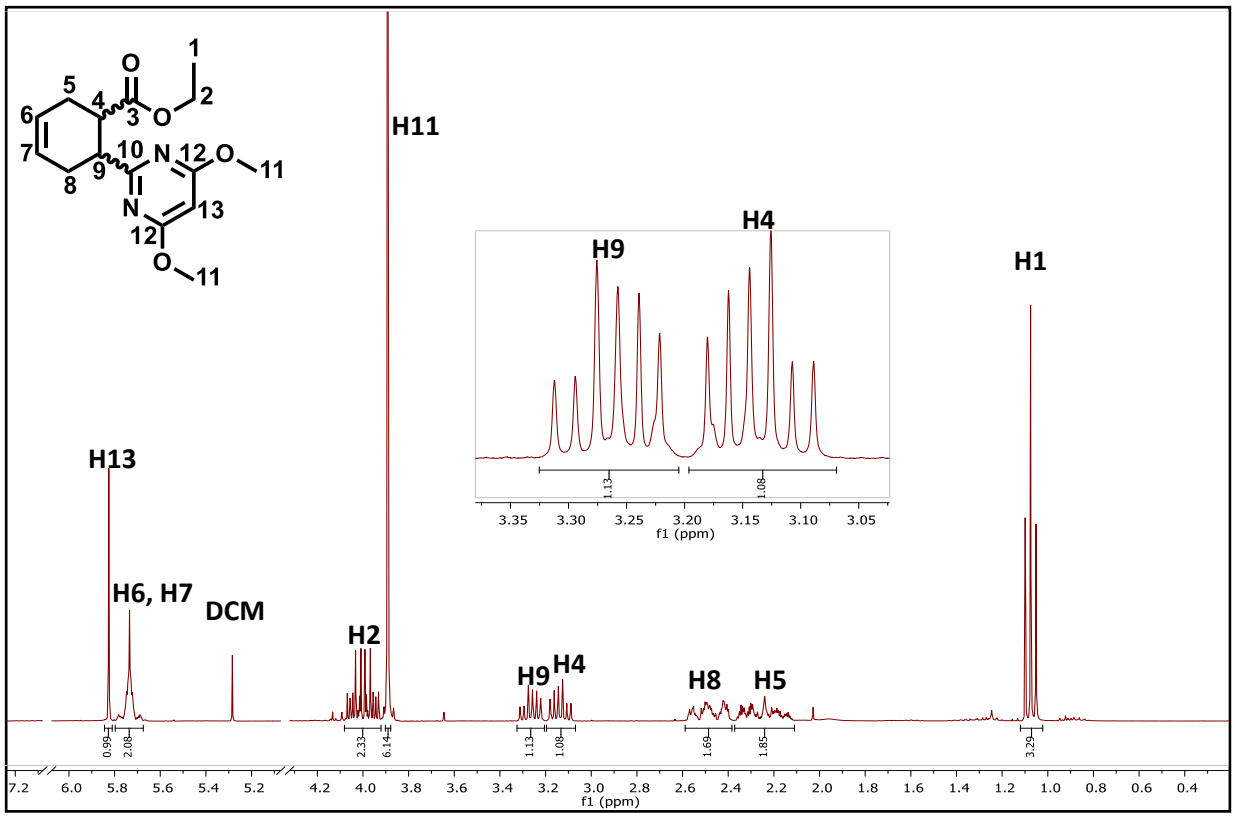

Figure 2.6B: 1H-NMR spectrum of ethyl 6-(4,6-dimethoxypyrimidin-2-yl)cyclohex-3-ene-1-carboxylate **2.1d** in $CDCl_3$ at 300 MHz

Cyclohexane pyrimidine intermediate 2.1e and carboxylic acid 2.1f

Reduction of **2.1d** with hydrogen in the presence of 10% Pd/C resulted in a cyclohexane intermediate **2.1e**. ^{1}H-NMR analysis revealed the disappearance of the double bond protons that had previously been observed at δ 5.73 ppm for **2.1d** (**Fig. 2.7A**). Four aliphatic protons are visible in **2.1e** as a multiplet integrating for four protons at δ 1.50–1.21 ppm. Base ester hydrolysis resulted in carboxylic acid **2.1f**, which was evidenced by the disappearance of the ethyl moiety observed for **2.1e** (-CH_3 δ 1.01 and -CH_2 δ 3.91 ppm; **Fig. 2.7B**).

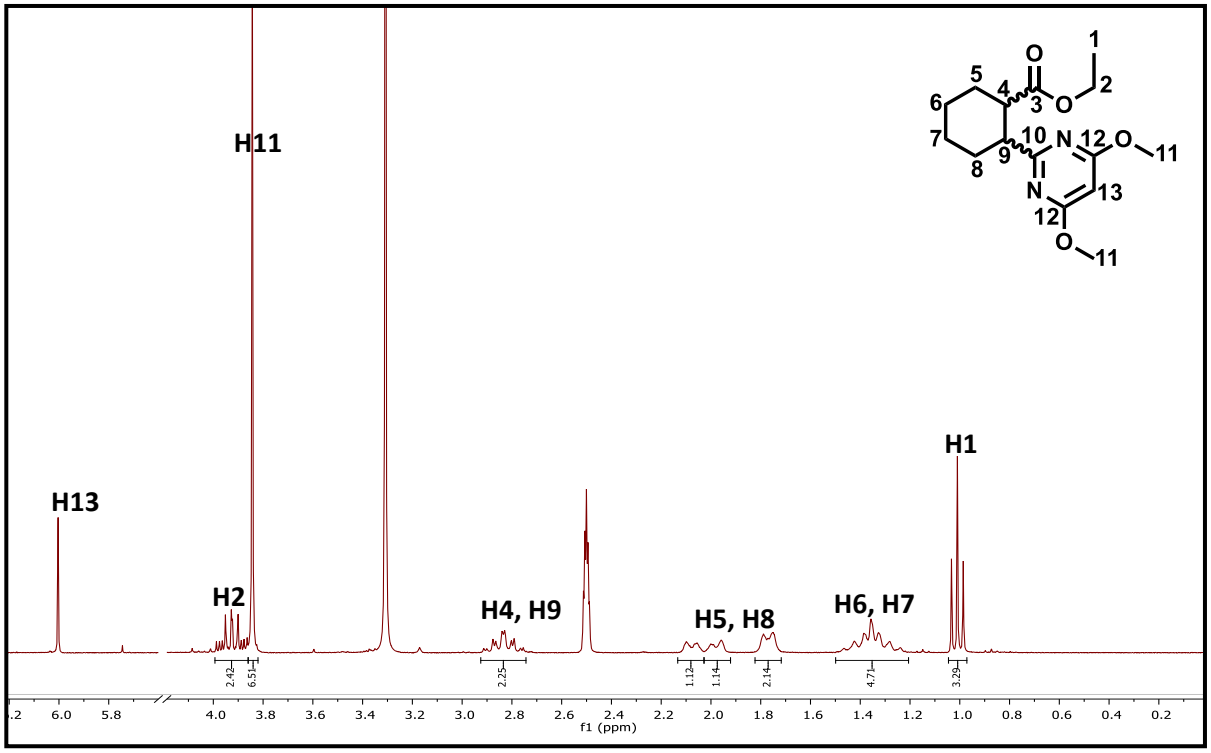

Figure 2.7A: ^{1}H-NMR spectrum of ethyl 2-(4,6-dimethoxypyrimidin-2-yl)cyclohexane-1-carboxylate **2.1e** in DMSO-d_6 at 300 MHz

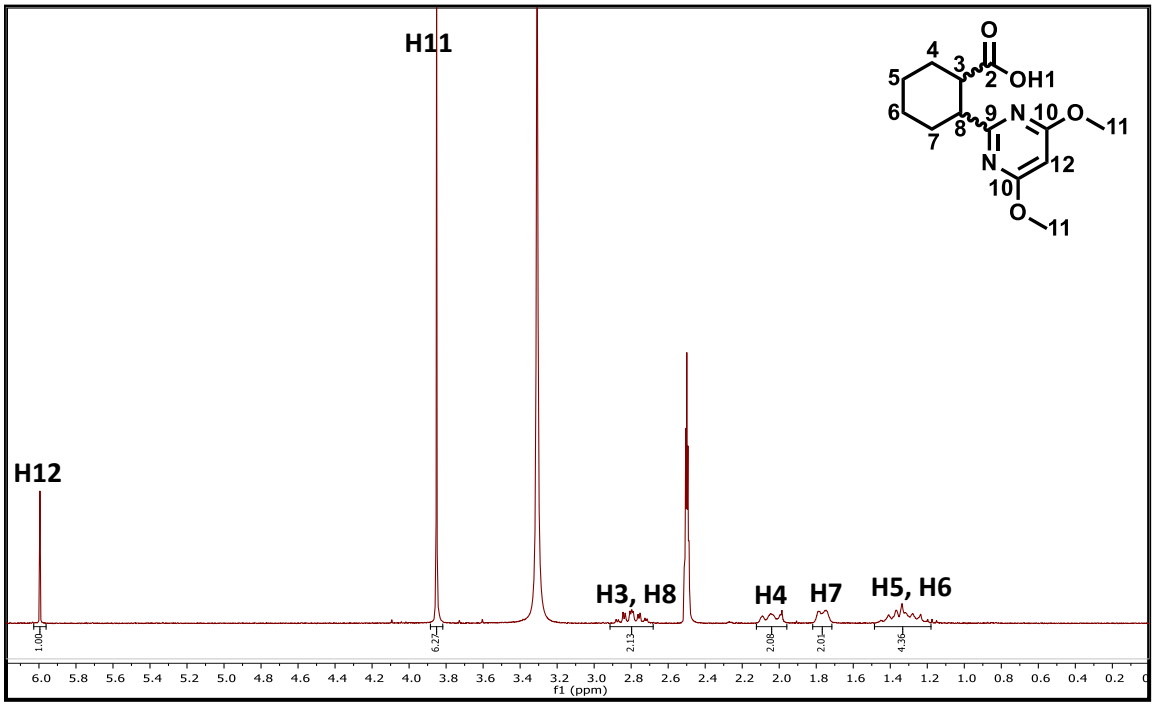

Figure 2.7B: ^{1}H-NMR spectrum of 2-(4,6-dimethoxypyrimidin-2-yl)cyclohexane-1-carboxylic acid **2.1f** in DMSO-d_6 at 300 MHz

N-(3-chlorobenzyl)-2-(4,6-dimethoxypyrimidin-2-yl)cyclohexane-1-carboxamide 3/MM1-75

Carboxylic acid **2.1f** was subjected to an amide coupling reaction under conditions previously described with 3-chlorobenzylamine to produce amide compound **3/MM1-75**. ^{1}H-NMR analysis of **3/MM1-75** revealed additional peaks: methylene protons H9 (δ 4.09–4.23 ppm), aromatic region protons H11, H13, H14, and H15 (δ 6.96–7.21 ppm), and an –NH (H8, δ 8.10 ppm; **Fig. 2.8**). The methylene protons (H9) appear separately as two doublets of doublets as they are diastereotopic and this effect is attributed to the presence of the stereogenic centers in the molecule. They experience germinal coupling (J = 15.48 and 15.50 Hz) and vicinal coupling to H8 (J = 5.77 and 6.39 Hz). The –NH (H8) shows a triplet (J = 6.14 Hz) coupling to H9. In the aromatic region, protons H13 and H14 appear as multiplet (δ 7.25–7.22 ppm) as is the case for H11 and H15. The cyclohexyl ring protons are well resolved where protons H2 and H5, and H3 and H4 are multiplets at δ 2.00–1.77 ppm and δ 1.45–1.29 ppm, respectively.

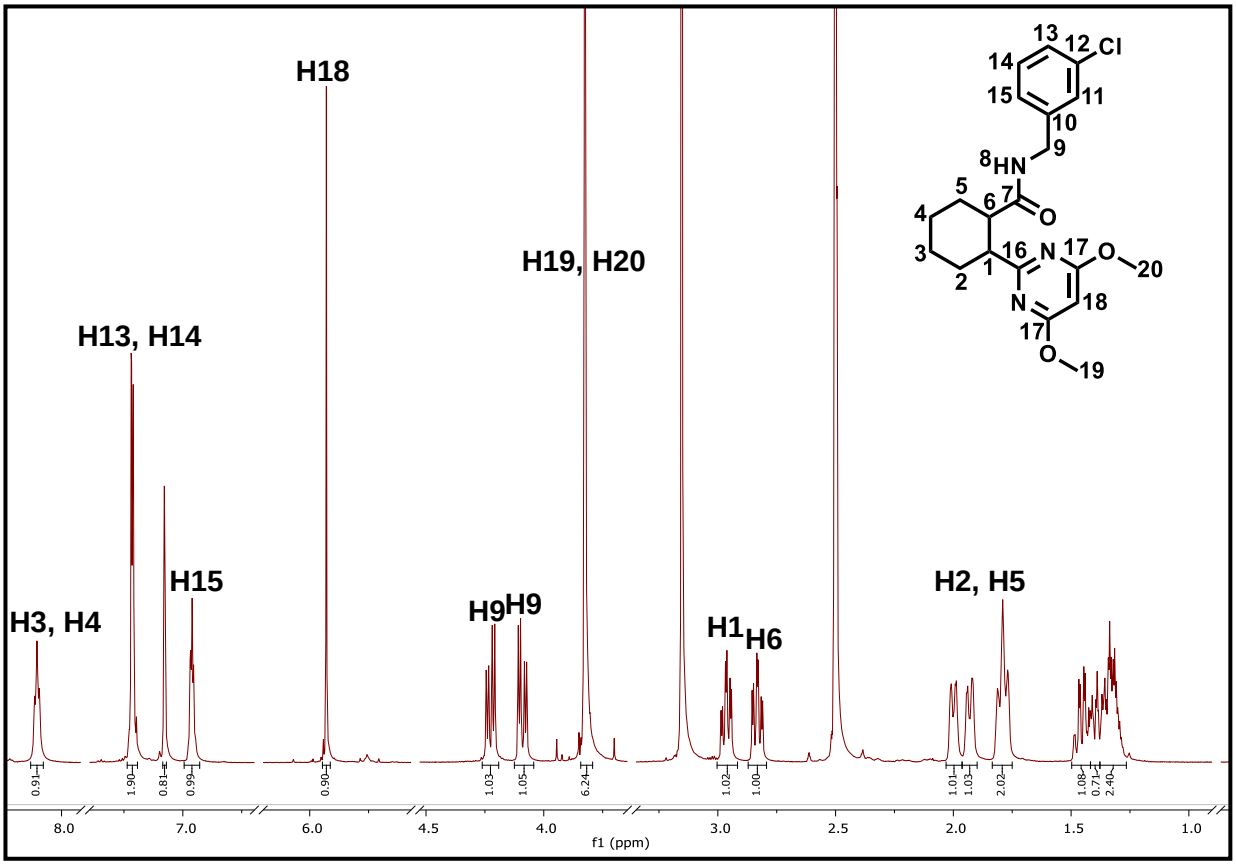

Figure 2.8: ^{1}H-NMR spectrum of N-(3-chlorobenzyl)-2-(4,6-dimethoxypyrimidin-2-yl)cyclohexane-1-carboxamide **3/MM1-75** in DMSO-d_6 at 300 MHz

Analysis of H1 and H6 confirmed that a pure diastereoisomer had been obtained. The cyclohexane ring system favors the chair conformation where the bulky groups are in the equatorial position. This conformation prevents the 1,3-diaxial interactions of bulky groups with other atoms in the axial position and is therefore favored. In the case of compound **3/MM1-75**, H1 and H6 both appear as triplets of doublets at δ 2.96 ppm (td, J = 12.0, 6 Hz, 1H, H1) and δ 2.83 ppm (td, J = 12.3, 6 Hz, 1H, H6), respectively. These protons experience two axial-axial couplings and one axial-equatorial coupling (**Fig. 2.9**). H1 forms axial-axial coupling with H6 and H2ax (J = 12 Hz) and equatorial-axial coupling with H2eq (J = 6 Hz). H6 formed axial-axial coupling with H1 and H5ax (J = 12.3 Hz) and equatorial-axial coupling with H5eq (J = 6 Hz). These coupling constants indicate that **3/MM1-75** was obtained as a trans-isomer. The same coupling pattern was observed for other analogues in this series.

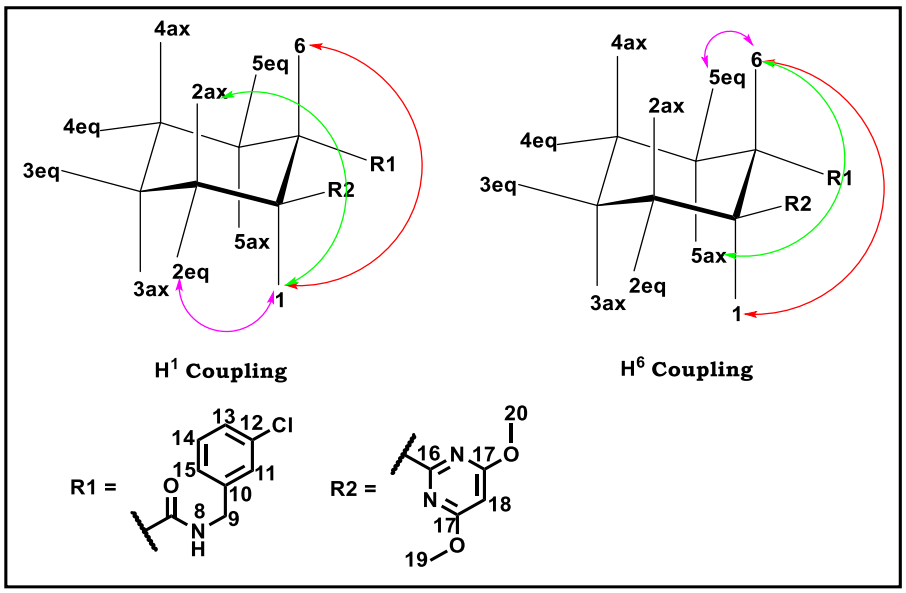

Figure 2.9: Illustration of the coupling patterns for H1 and H6 of *N*-(3-chlorobenzyl)-2-(4,6-dimethoxypyrimidin-2-yl)cyclohexane-1-carboxamide **3/MM1-75**
ax: axial; eq: equatorial.

Characterization of cyclohexyl pyrimidine 4a/MM2-39

Ethanolamine intermediate 2.2b and the boronic ester 2.2c

The structures of intermediates **2.2b** (**Fig. 2.10A**) and **2.2c** (**Fig. 2.10B**) were confirmed via ^{1}H-NMR spectroscopy. Formation of the ethanolamine moiety **2.2b** was confirmed by the appearance of two distinct triplets H1 and H2 (J = 6 Hz, **Fig. 2.10A**). Addition of the boron pinacol is illustrated in **2.2c** as a singlet resulting from the protons of four methyl groups integrating to twelve protons (δ 1.35 ppm; **Fig. 2.10B**).

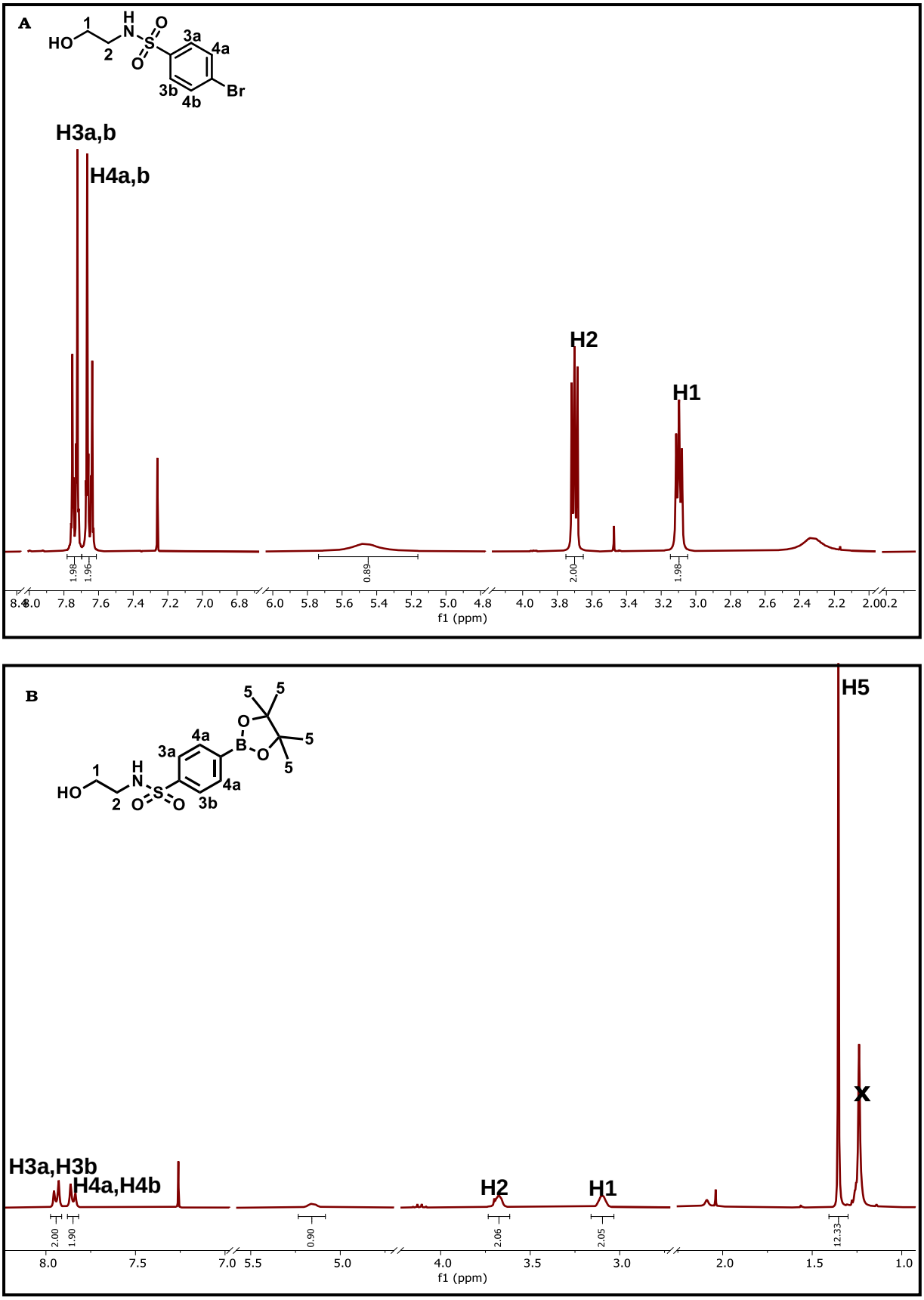

Figure 2.10: ^{1}H-NMR spectra of intermediates **2.4b** (**A**) and **2.4c** (**B**) in $CDCl_3$ at 300 MHz

Suzuki-Miyaura coupling intermediate 2.2e

The boronic ester **2.2c** reacted with 2,4-dichloro-6-methylpyrimidine (**2.2d**) under the Suzuki-Miyaura reaction conditions previously discussed. LC-MS analysis revealed the product mixture comprised both the disubstituted and monosubstituted products. The monosubstituted product **2.2e** was isolated and its structural characterization is covered in this section. The ^{1}H-NMR analysis of **2.2e** concurred with previous reports noting that the major product resulted from substitution at C4 of the polyhalogenated pyrimidine and confirmed that the desired product had been isolated.[190] This was verified via ^{1}H-NMR (**Fig. 2.11A**) and ^{13}C-NMR analysis in conjunction with heteronuclear multiple bond correlation (HMBC, **Fig. 2.11B**) of **2.2e**. ^{3}J coupling was observed via HMBC between H5 and C8 (arrow marked **X**, **Fig. 2.11B**), confirming that the C4 is the position at which substitution occurred.

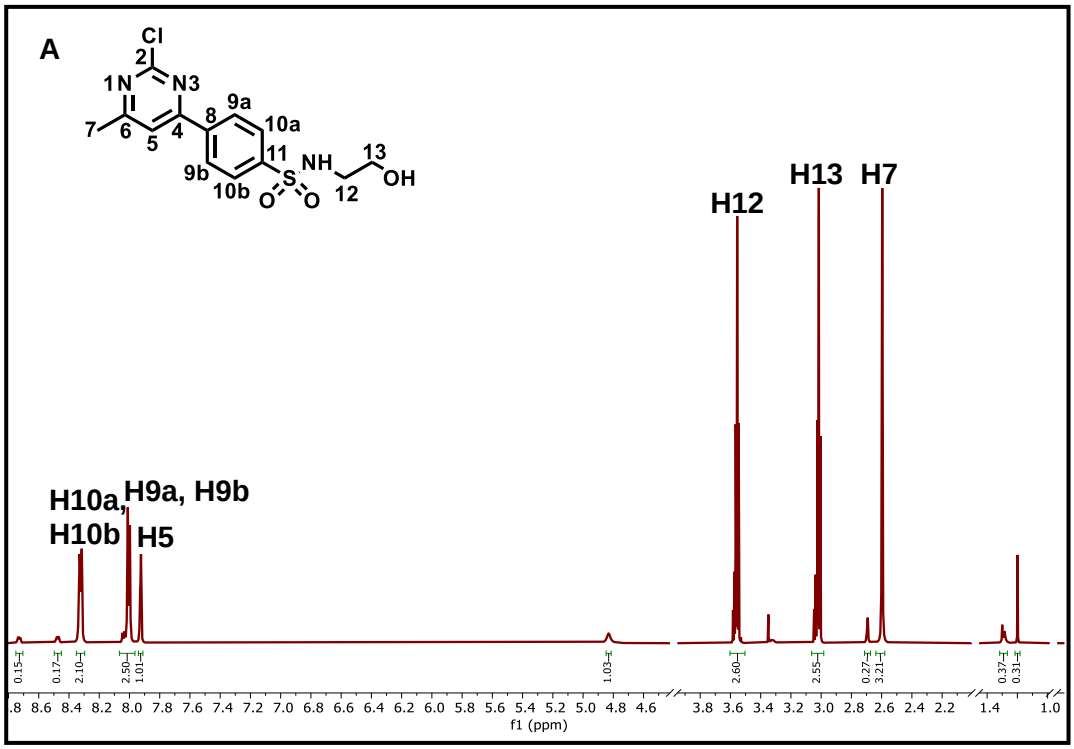

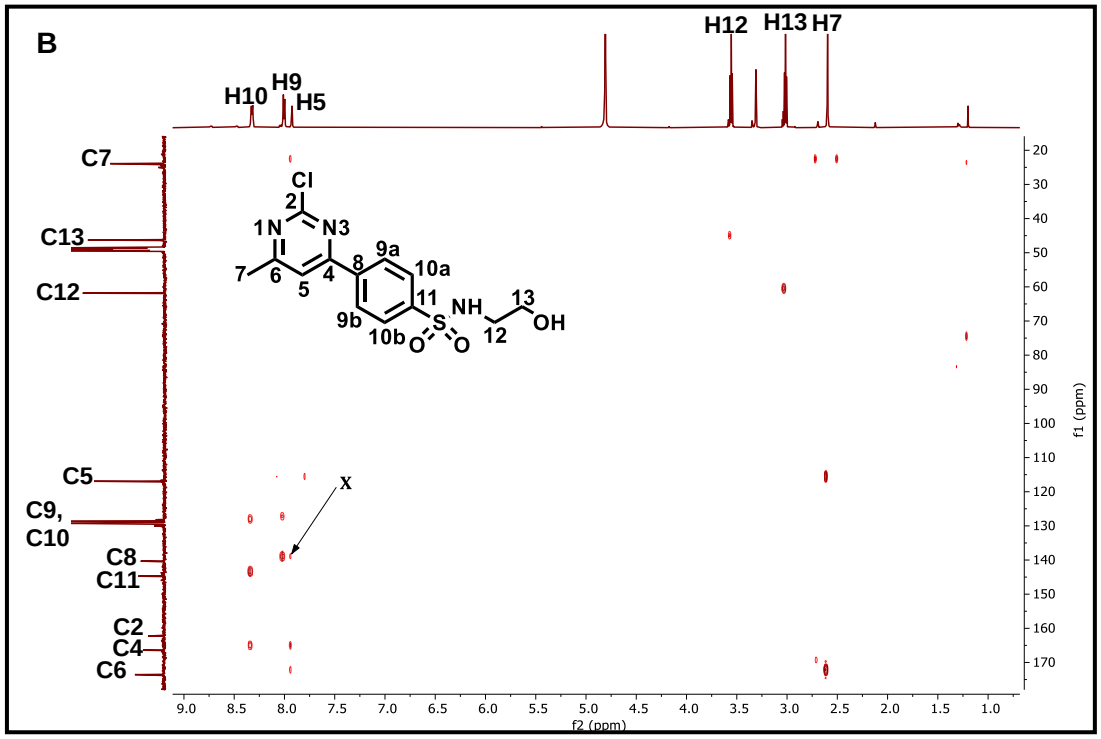

Figure 2.11: ^{1}H-NMR (**A**) and HMBC (**B**) spectra of intermediate **2.4e** in MeOD at 600 MHz

Mizoroki-Heck coupling intermediate 2.2f

The intermediate **2.2f** was obtained via Mizoroki-Heck coupling as previously described and its structure was confirmed via ^{1}H-NMR spectroscopy (**Fig. 2.12**). The evident change from the structure of **2.2e** was the addition of methyl H1' (δ 1.36 ppm) and two alkene protons H3' and H4' (δ 7.32 and 7.74 ppm, respectively). Vinyl protons revealed that the *E*-isomer was isolated as the coupling constant between H3' and H4' was J = 15.7 Hz.

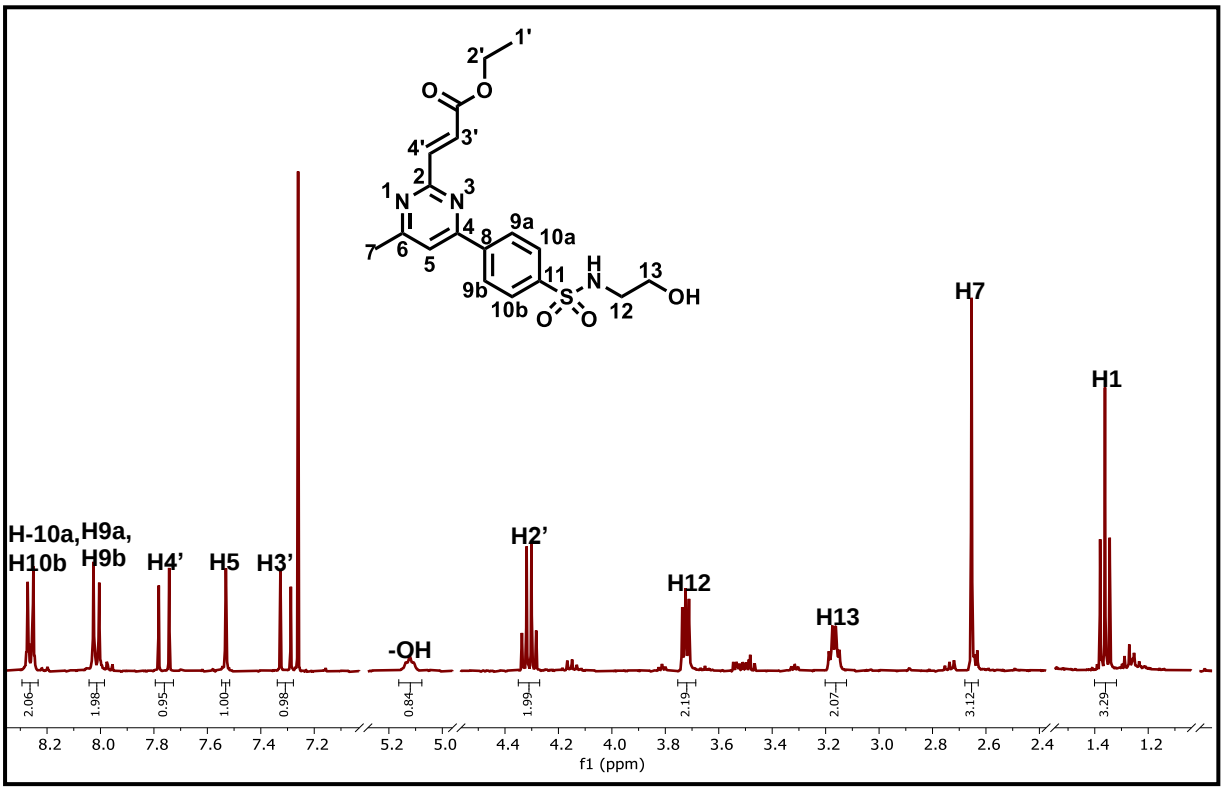

Figure 2.12: ^{1}H-NMR spectrum of **2.2f** in $CDCl_3$ at 300 MHz

Target compound 4a/MM2-39

Intermediates between **2.2f** and the target compound **4a/MM2-39** were not isolated and were taken forward without further purification. LC-MS analysis was used to confirm formation of the desired compound in the crude mixtures at each given step. The structure of amide coupling product **4a/MM2-39** was confirmed via ^{1}H-NMR spectroscopy (**Fig. 2.13**, CD_3CN), which revealed distinct protons from the cyclohexane and 3,4-dichlorobenzylamine. Methylene protons H7' from the latter were visible at δ 5.81 ppm as a broad singlet. Cyclohexane protons were also observed on the aliphatic region of the spectrum. In line with the previous observation regarding compounds in the cyclohexane series, trans-coupling (J = 15.1, 5.1 Hz) between the two stereoisomeric protons H1' and H2' was also observed. Each of these protons split into a doublet of doublets as a result of coupling with each other and one of the neighbouring protons (H6' for H1' and H3' for H2'). This is consistent with the fact that bulky groups are positioned in the equatorial position to reduce 1,3-diaxial interactions, as previously discussed for other compounds in

this series. ^{1}H-NMR analysis thus confirmed that the pure trans-diastereisomer was obtained for **4a/MM2-39**.

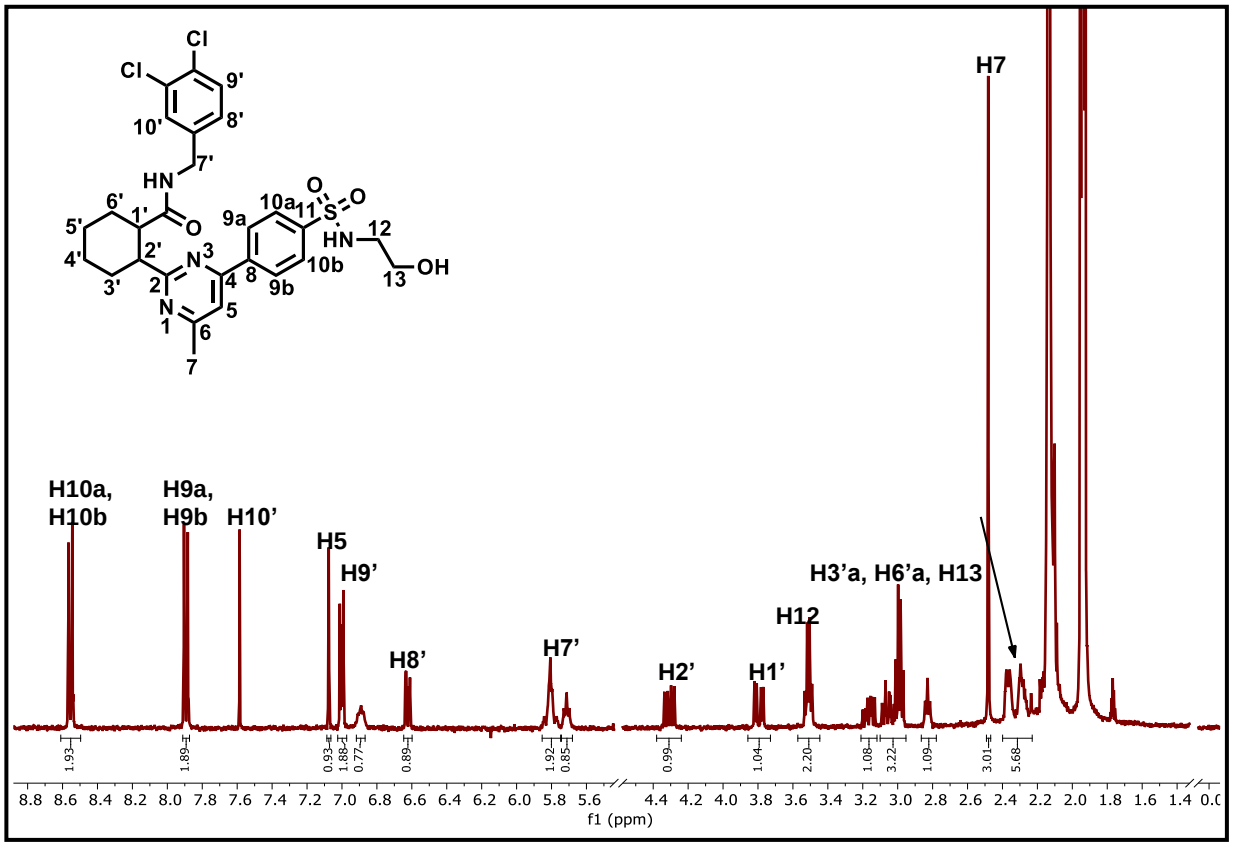

Figure 2.13: ^{1}H-NMR spectrum of **4a/MM2-39** in CD_3CN at 300 MHz

2.3.2. Synthesis and characterization of compounds in the Ugi series

Synthesis of compounds in the Ugi series

The Ugi four-component reaction (U-4CR) is a reaction between a carboxylic acid, amine, aldehyde, and isocyanide that forms an acetoamide carboxamide product with a stereocenter (**Scheme 2.3**). This is obtained as a racemate and enantioselective conditions for U-4CR are a subject of active research. In this regard, recent promising reports described the use of chiral phosphoric acids, which yielded Ugi products with high enantioselectivity.[192-194]

Scheme 2.3: Initial compounds used in the synthesis of Ugi series compounds

In the current study, the U-4CR was used to resynthesize two Ugi series hits, which were first identified via MTS. Additional analogues were synthesized for SAR exploration and were obtained in low to high yield (**Table 2.2**). The reaction was conducted according to methods previously described by adding an appropriate amine, aldehyde, and carboxylic acid in methanol in a reaction flask. Isocyanide was then added at 24 °C and the reaction stirred for 16-24 h. The yield improved when the U-4CR was performed under microwave irradiation.[195] The final compounds were obtained as racemic mixtures although compound **2/MM1-19** was subjected to preparative chiral HPLC to obtain pure enantiomers **2A/MM1-19** and **2B/MM1-19**.

Table 2.2: Isolated yields of compounds in the Ugi series

Code	Structure	Yield (%)
1/MM1-15	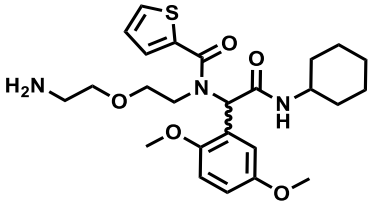	12
2A/MM1-19A	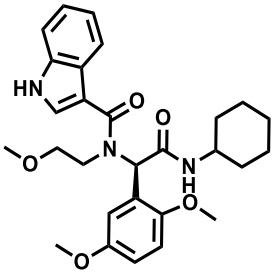	

2B/MM1-19

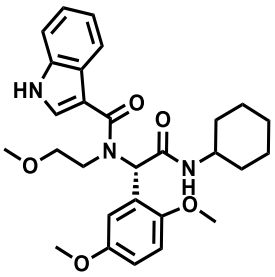

2/MM1-19

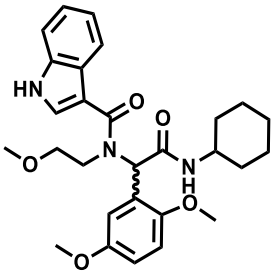

31

15/MM1-85

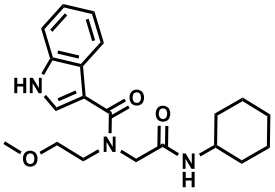

22

16/MM1-86

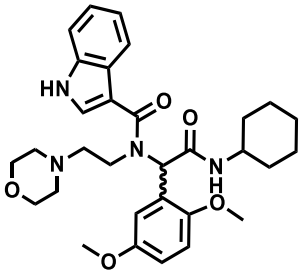

33

17/MM1-56

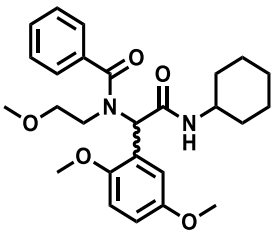

34

18/MM1-82

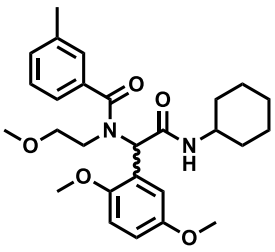

77

19/MM1-63	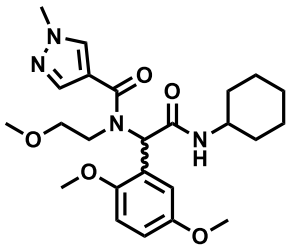	9
20/MM1-64	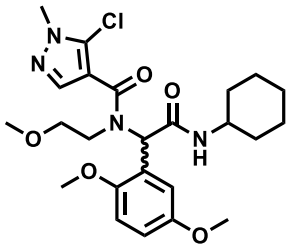	21
21/MM1-81	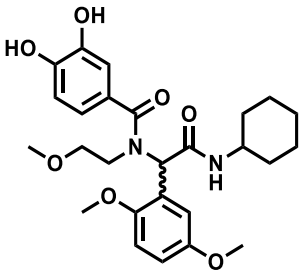	18
22/MM1-53	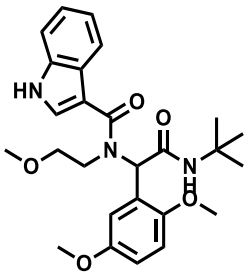	52

Characterization of compounds in the Ugi series

Compound **18/MM1-82** is used as an example for ^{1}H- and ^{13}C-NMR analysis. The ^{1}H-NMR spectrum did not show the expected triplet splitting pattern for the methylene protons H10 and H11 on the 2-methoxyethylamine substituent (**Fig. 2.14**). Instead, the observed pattern throughout the series was either a multiplet integrating for two protons, or broad singlets integrating for one proton. However, spectra were reconciled with the expected number of protons for all compounds. This pattern can be attributed to the stereocenter, in this case at C9, in the molecule rendering methylene protons diastereotopic.[191] The cyclohexane protons (H1, H2, H3, H4, and H5) were observed at δ 1.1–1.8 ppm as a multiplet. H6 was observed downfield at δ 2.75 ppm as a multiplet. The methyl protons H15 were observed at δ 2.34 ppm as a singlet integrating for three protons and the two methoxy protons H20

and H21 were observed at δ 3.15 ppm and δ 3.7 ppm, respectively. The methoxy of the 2-methoxyethylamine substituent appears within the multiplet at δ 3.78–3.62 ppm. All aromatic protons (H14, H16, H17, H18, H21, H22 and H24) were reconciled with the number of expected aromatic protons.

The structure was further confirmed by the ^{13}C-NMR spectrum obtained, which showed the two methoxy carbons C20 and C25, and methyl C15 at δ 48.34 ppm and δ 21.35 ppm, respectively (**Fig. 2.15**). Two carbonyl carbons corresponding to C8 and C12 were identified at δ 168.83 ppm. Carbons C13 and C15 appeared at δ 137.90 ppm and δ 137.60 ppm, respectively. All aromatic carbons were accounted for and appeared at δ 112.56–130.30 ppm, a region assigned to C14, C17, C18, C19, C22, C23, C26 and C27. The cyclohexyl, methylene, and C9 carbons were also assigned as they appear upfield, thus further confirming the structural assignment.

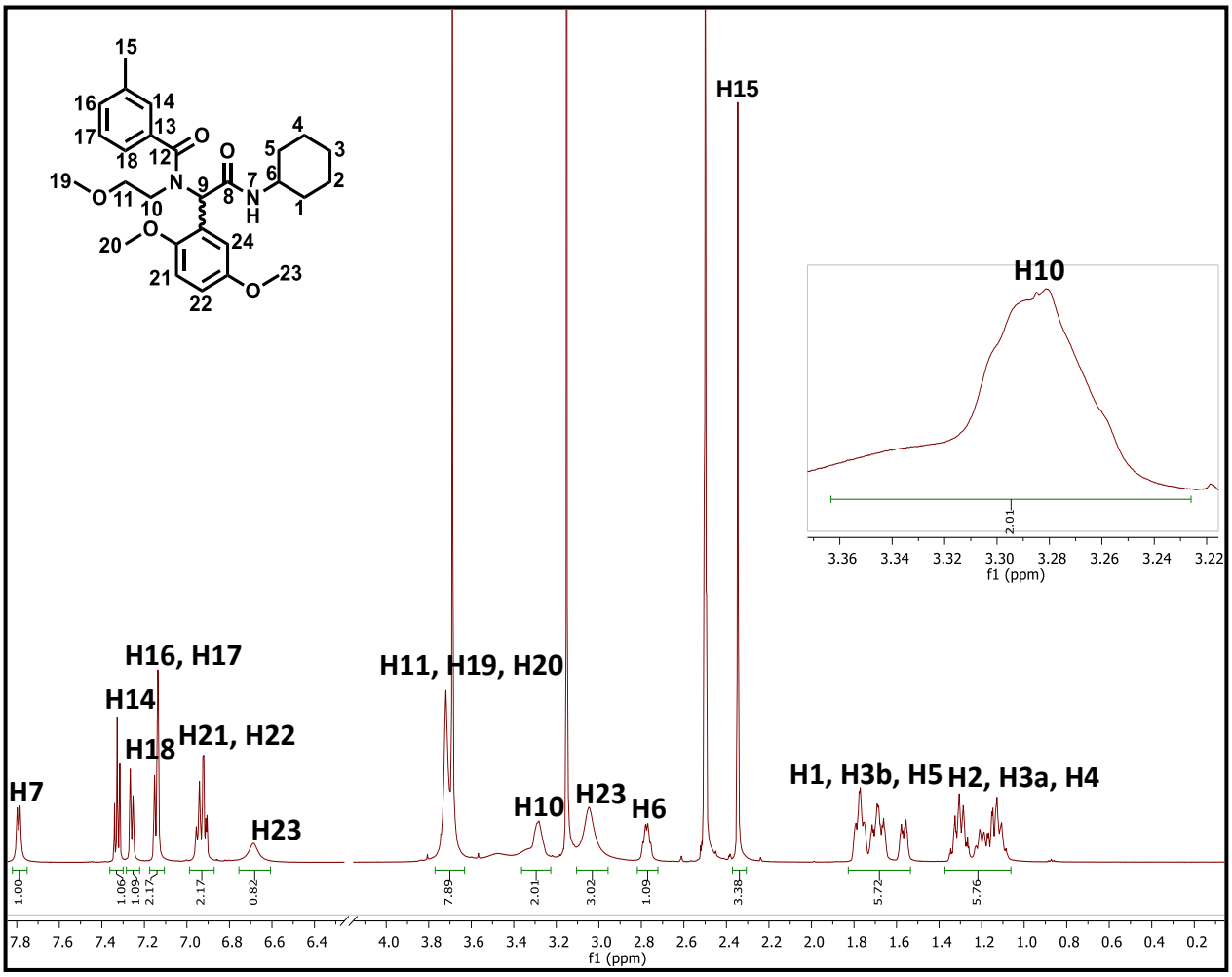

Figure 2.14: ^{1}H-NMR spectrum of *N*-(2-(cyclohexylamino)-1-(2,5-dimethoxyphenyl)-2-oxoethyl)-N-(2-methoxyethyl)-4-methylbenzamide **18/MM1-82** in DMSO-d_6 at 600 MHz

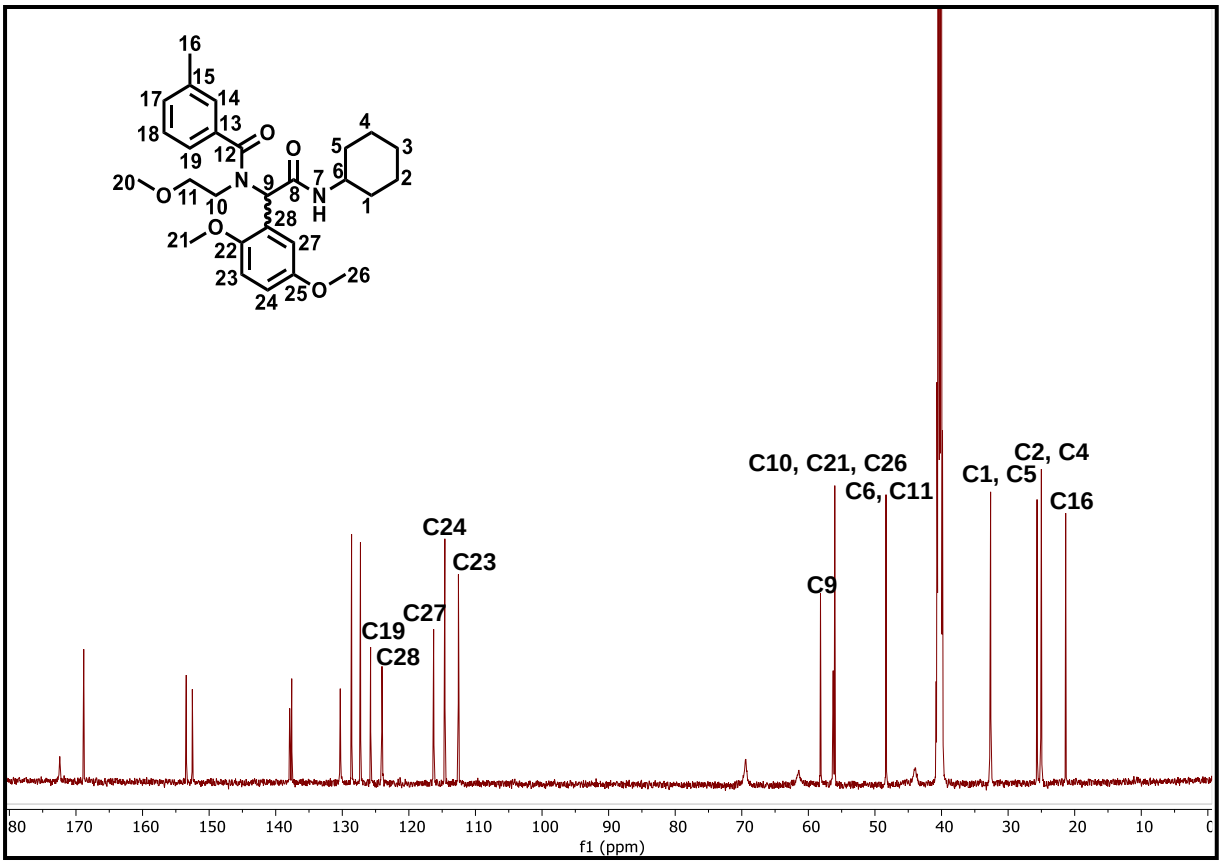

Figure 2.15: ^{13}C-NMR spectrum of *N*-(2-(cyclohexylamino)-1-(2,5-dimethoxyphenyl)-2-oxoethyl)-N-(2-methoxyethyl)-4-methylbenzamide **18/MM1-82** in DMSO-d_6 at 600 MHz

2.4. Novartis series

2.4.1. Synthesis of azabenzimidazole compounds

Azabenzimidazole compounds (**Table 2.3**) were produced in low yield via the synthetic route shown in **Scheme 2.4**.

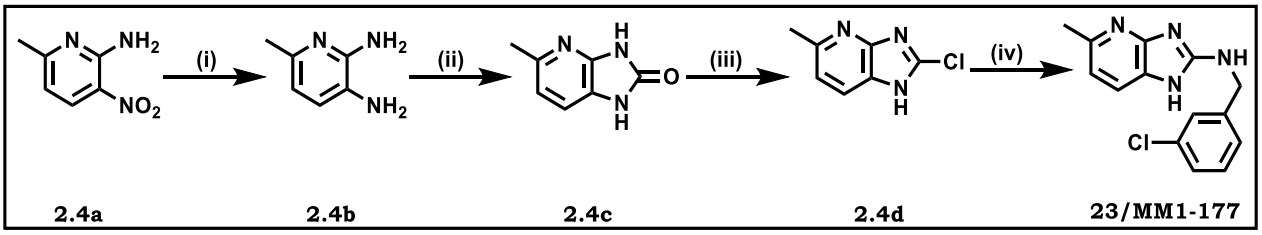

Scheme 2.4: General synthetic approach for azabenzimidazole

Reagents and conditions: (i) $N_2H_4.H_2O$, 10% Pd/C, MeOH, 4 h, reflux (100%); (ii) Urea, μW, 130 °C, 30 min (58%); (iii) $POCl_3$, 105 °C (18%), 14 h; (iv) (3-chlorophenyl)methanamine, EtOH, μW, 150 °C, 1 h (28%).

Table 2.3: Isolated yields of azabenzimidazole compounds

Code	Structure	Yield (%)
23/MM1-177	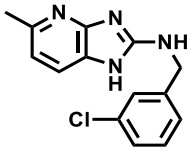	28
24/MM2-83	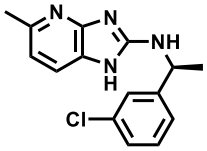	23
25/MM2-78	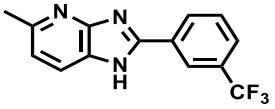	18
26/MM2-77	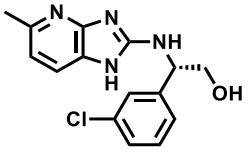	11

Commercially available 6-methyl-3-nitropyridin-2-amine **2.4a** was subjected to reduction with hydrazine monohydrate and 10% Pd/C in methanol to provide aryl diamine **2.4b**.[196, 197] Cyclization product **2.4c** proceeded through reaction of **2.4b** with urea under microwave conditions. This was followed by chlorination with phosphorus oxychloride ($POCl_3$) to afford intermediate **2.4d** from which analogues for this series were synthesized (**Table 2.3, 23–26**).

2.4.2. Characterization of azabenzimidazole compounds

The characterization of intermediates and target compound **23/MM1-177** as a representative example are described here. The reduction of 6-methyl-3-nitropyridin-2-amine **2.4a** with hydrazine monohydrate and 10% Pd/C produced the diamine intermediate **2.4b** (**Figure 2.16A**). Formation of the cyclization product **2.4c** (**Figure 2.16B**) was confirmed by the downfield appearance of two -NH protons at δ 10.75 ppm and δ 11.75 ppm corresponding to NH1 and NH2, respectively. Formation of the chloro intermediate **2.4d** (**Figure 2.16C**) was confirmed by the absence of the NH1 and NH2 protons observed in **2.4c**. In addition, the MS spectrum showed a

characteristic chloride splitting pattern with molecular ion *m/z* 168.0 [M+H] and 170.0 [M+2] (**Figure 2.17**).

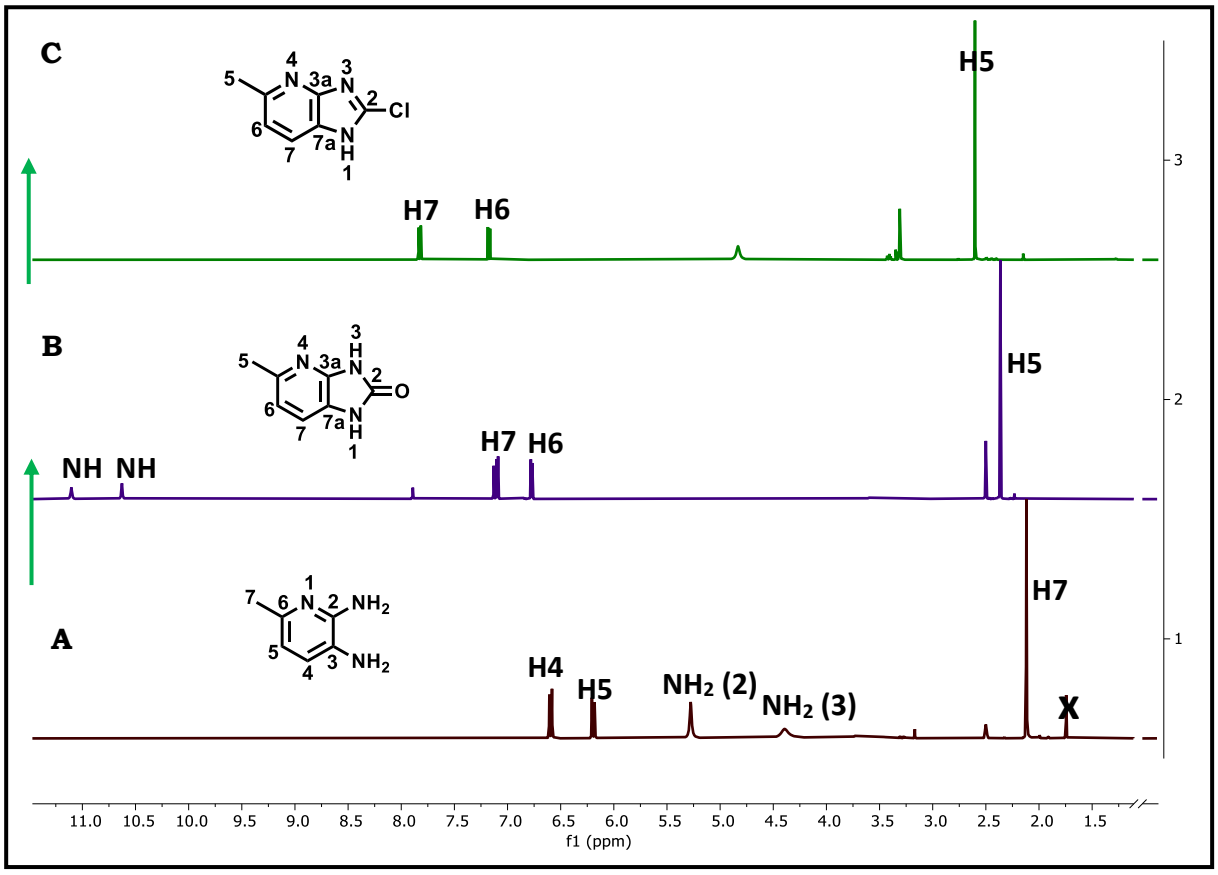

Figure 2.16: ^{1}H-NMR spectrum of intermediates **2.4b** (**A**) at 300 MHz in MeOD, **2.4c** (**B**) at 600 MHz in DMSO-d_6, and **2.4d** (**C**) at 600 MHz in DMSO-d_6

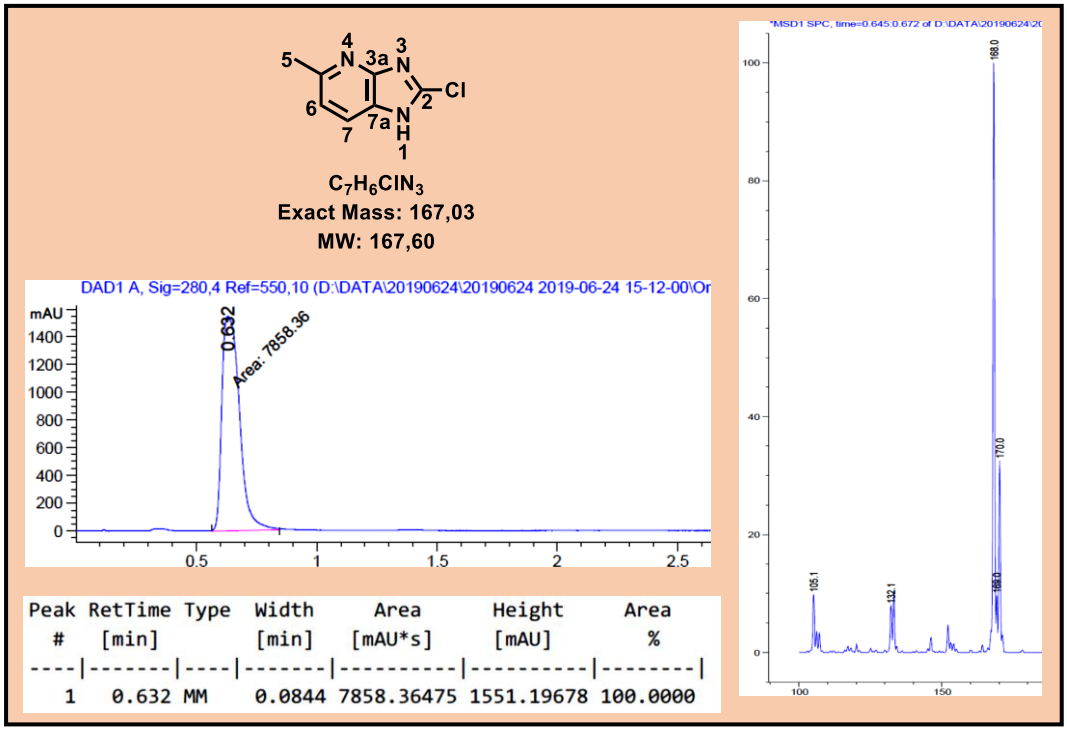

Figure 2.17: LC-MS chromatogram and spectrum of intermediate **2.4d**

Target compound **23/MM1-177** was obtained as previously described. ^{1}H-NMR analysis revealed a doublet at δ 4.51 ppm associated with the methylene protons (H1') coupling with the amine proton (**Fig. 2.18**). Methyl protons from H5 were observed at δ 2.39 ppm as a singlet and all corresponding aromatic protons were accounted for in the aromatic region as a multiplet integrating for six protons (H6, H7, H3', H5', H6', and H7'). The molecular ion of the compound was identified via LC-MS with *m/z* 273.1 [M+H] and showed the characteristic splitting pattern of chloride-containing compounds (**Fig. 2.19**). This concurred with the calculated exact mass of 272.03.

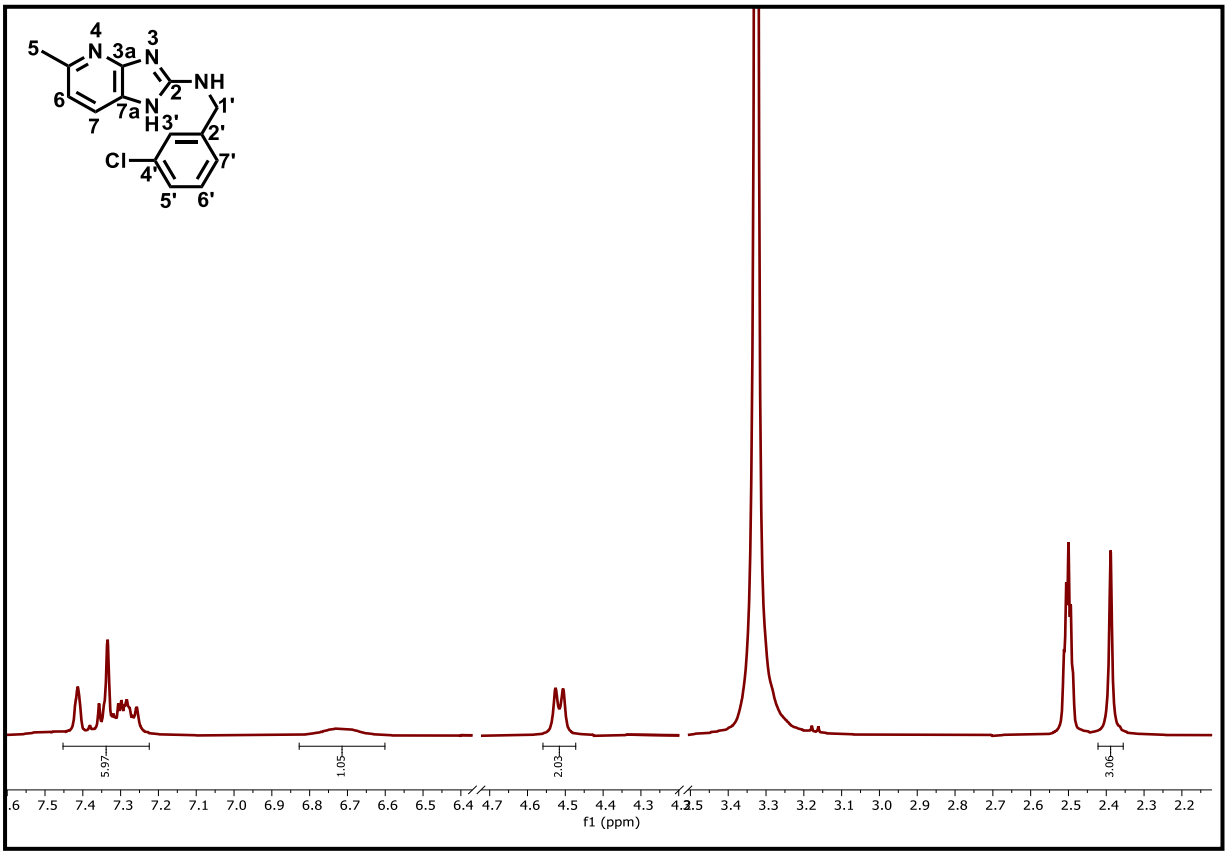

Figure 2.18: ^{1}H-NMR spectrum of **23/MM1-177** in DMSO-d_6 at 300 MHz

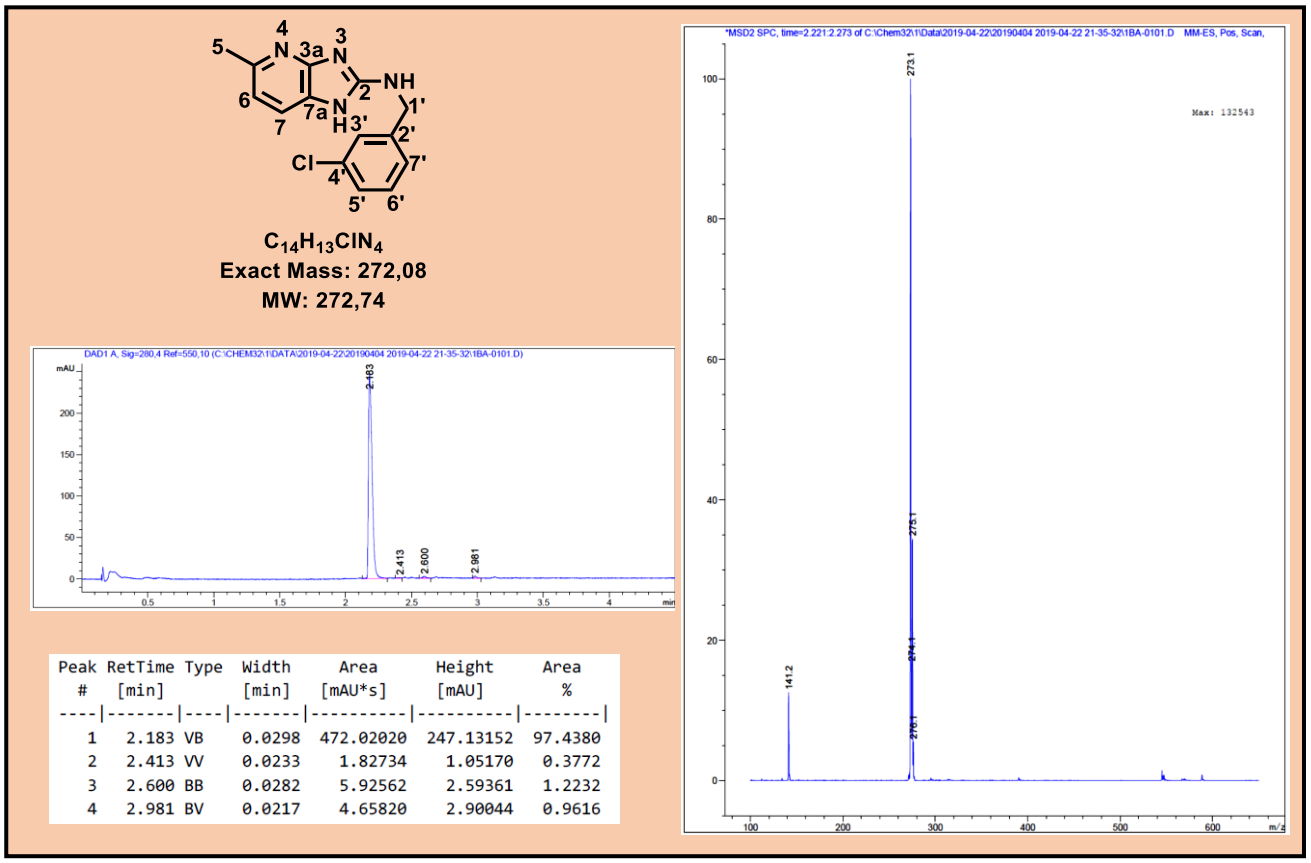

Peak #	RetTime [min]	Type	Width [min]	Area [mAU*s]	Height [mAU]	Area %
1	2.183	VB	0.0298	472.02020	247.13152	97.4380
2	2.413	VV	0.0233	1.82734	1.05170	0.3772
3	2.600	BB	0.0282	5.92562	2.59361	1.2232
4	2.981	BV	0.0217	4.65820	2.90044	0.9616

Figure 2.19: LC-MS chromatogram and spectrum of **23/MM1-177**

2.4.3. Synthesis of triazolopyrimidinones and triazolopyrimidines synthesis

Compounds **27–42** were synthesized following reported procedures (**Table 2.4**). Synthesis of compound **28** is used to illustrate the mechanism of reactions in this series and the characterization of these compounds (**Scheme 2.5**).

Table 2.4: Isolated yields of triazolopyrimidinone and triazolopyrimidine compounds

Code	Structure	Yield (%)
27/MM1-185	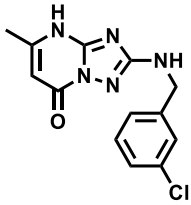	56

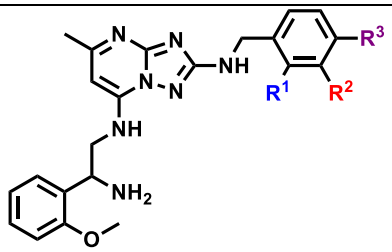

Code	R^1	R^2	R^3	Yield (%)
28/MM2-145	H	-Cl	H	40
29/MM3-144	H	H	-Cl	15
30/MM3-189	-Cl	H	H	67
31/MM3-205	H	$-CF_3$	H	62
32/MM3-159	H	H	$-CF_3$	30
33/MM3-167	$-CF_3$	H	H	64
34/MM4-75	H	-Me	H	22
35/MM4-19	H	H	-Me	39
36/MM4-34	-Me	H	H	46
37/MM3-140	H	H	H	82

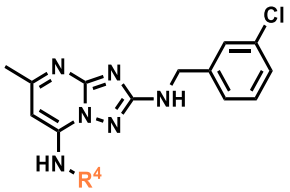

Code	R^4	Yield (%)
38/MM2-141	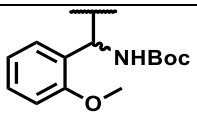	32
39/MM3-75	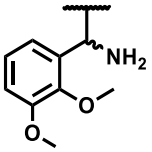	48
40/MM3-59	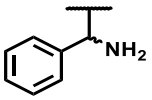	30
41/MM3-139	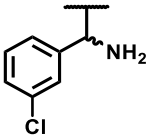	56
42/MM3-60	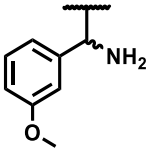	51

Synthesis of 1,2,4-triazole **2.5c** was achieved in two steps starting with the reaction of diphenyl *N*-cyanocarbonimidate **2.5a** and (3-chlorophenyl)methanamine in 2-propanol to produce intermediate **2.5b**. This intermediate was treated with hydrazine monohydrate and stirred at 50 °C in methanol to afford the 1,2,4-triazole **2.5c**. The triazolopyrimidinone **27/MM1-185** was synthesized via cyclization of the 1,2,4-triazole **2.5c** reacting with ethyl acetoacetate under microwave conditions. Chlorination of **27/MM1-185** to form **2.5d** was achieved in $POCl_3$ under reflux. The nucleophilic aromatic substitution (S_NAr) reaction of **2.5d** with an appropriate amine under microwave conditions in ethanol afforded compound **38/MM2-141**. Boc-deprotection of **38/MM2-141** in trifluoroacetic acid (TFA) afforded target compound **28**.

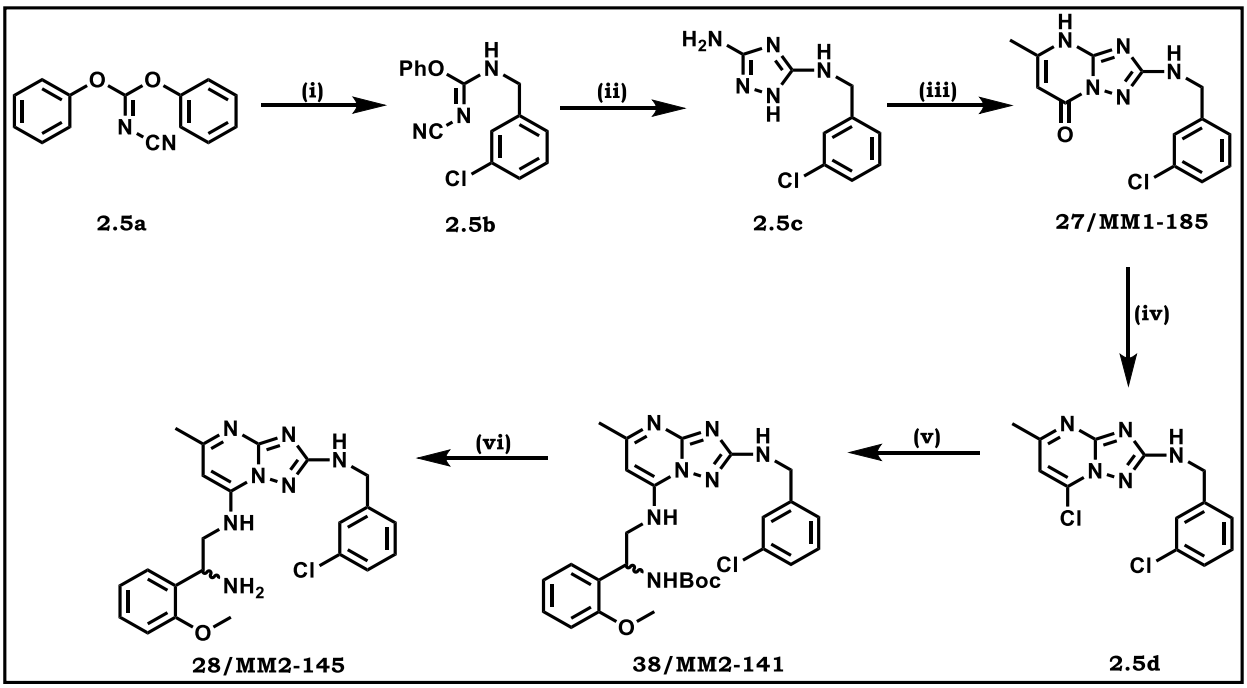

Scheme 2.5: Synthesis of triazolopyrimidines

Reagents and conditions: (a) (3-chlorophenyl)methenamine, *i*-PrOH, 60 °C, 2 h then 16 h at 23 °C (56%); (b) $NH_2NH_2.H_2O$, MeOH, 50 °C, 14 h (64%); (c) $CH_3COCH_2COOC_2H_5$, AcOH, 165 °C, μW, 10 min then 23 °C, 14 h (56%); (d) $POCl_3$, 95 °C, 14 h (78%); (e) EtOH, 150 °C, μW, 20 min (32%); (f) TFA, 23 °C, 4 h (40%).

2.4.4. Characterization of triazolopyrimidinone and triazolopyrimidine compounds

Characterization of intermediates 2.5b, 2.5c, 27/MM1-185, and 2.5d

The formation of intermediate **2.5b** was confirmed via ^{1}H-NMR spectroscopy by the appearance of the methylene protons H4 and the number of aromatic protons reconciling to expectations (**Fig. 2.20A**). The structure was further confirmed via LC-MS, which revealed the characteristic splitting pattern of chloro-containing compounds. In this case, the molecular ion identified had *m/z* 286.0 [M+H] and 288.0 [M+3] when compared to a calculated exact mass of 285.0. Formation of the 1,2,4-triazole **2.5c** was confirmed by the disappearance of aromatic protons observed in **2.5b**, which is associated with the loss of the phenol during cyclization (**Fig. 2.20B**). There were four aromatic protons for **2.5c**, which is consistent with the expected structure and molecular ion identified via LC-MS *m/z* 224.0 [M+H] and 226.0 [M+3], calculated exact mass of 223.0. Formation of the cyclization product

triazolopyrimidinone **27/MM1-185** was confirmed by the presence of the methyl protons H5 at δ 2.23 ppm as a singlet integrating for three protons and a vinyl proton H6 as a singlet at δ 5.64 ppm (**Fig. 2.21**). Four protons corresponding to H9, H10, H11, and H12 were identified in the aromatic region as well as a triplet corresponding to an exocyclic NH as it couples with the methylene protons H8. The H8 protons appear at δ 4.40 ppm as a doublet resulting from coupling with exocyclic NH. The LC-MS profile showed *m/z* 290.0 [M+1] and 291.0 [M+2], which is in agreement with the calculated exact mass of 289.07. Formation of the chlorination product compound **2.5d** was confirmed by a downfield shift of proton H6 from δ 5.64 ppm in **27/MM1-185** to δ 7.10 ppm in **2.5d** associated with the addition of the electron-withdrawing chloride atom to the ring (**Fig. 2.22**). The formation of this compound was also confirmed via LC-MS showing the molecular ion 308.0 [M+H] and 310.0 [M+3], which is associated with chloride splitting, in agreement with the calculated mass of 307.04.

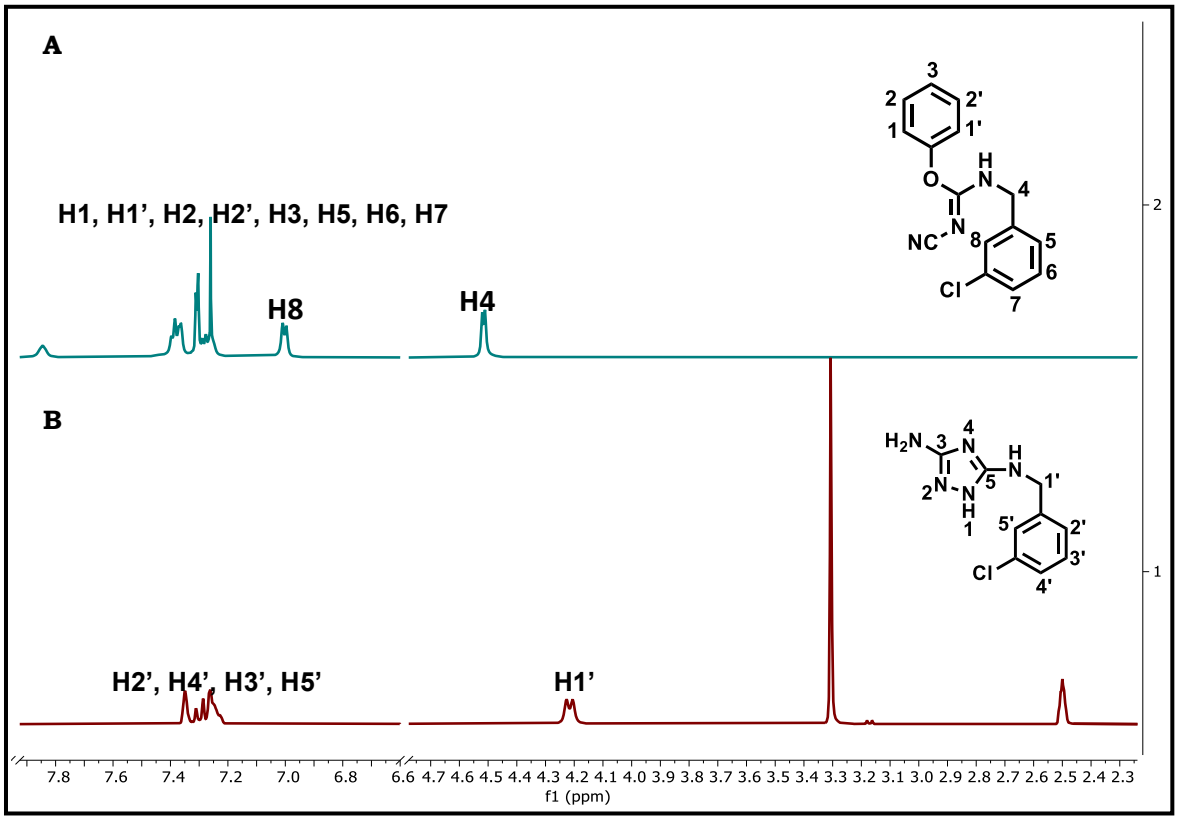

Figure 2.20: ^{1}H-NMR spectrum of **2.5b** in $CDCl_3$ and **2.5c** in DMSO-d_6 at 300 MHz

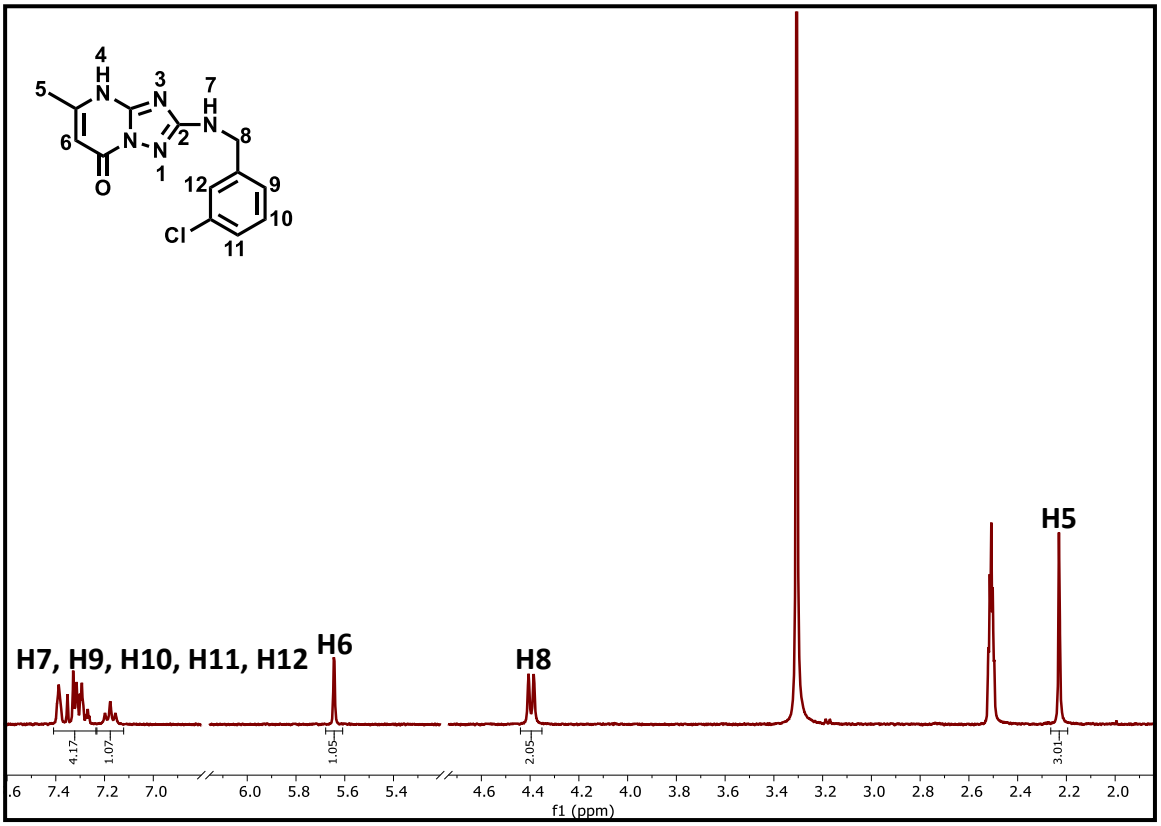

Figure 2.21: ^{1}H-NMR spectrum of **27/MM1-185** in DMSO-d_6 at 300 MHz

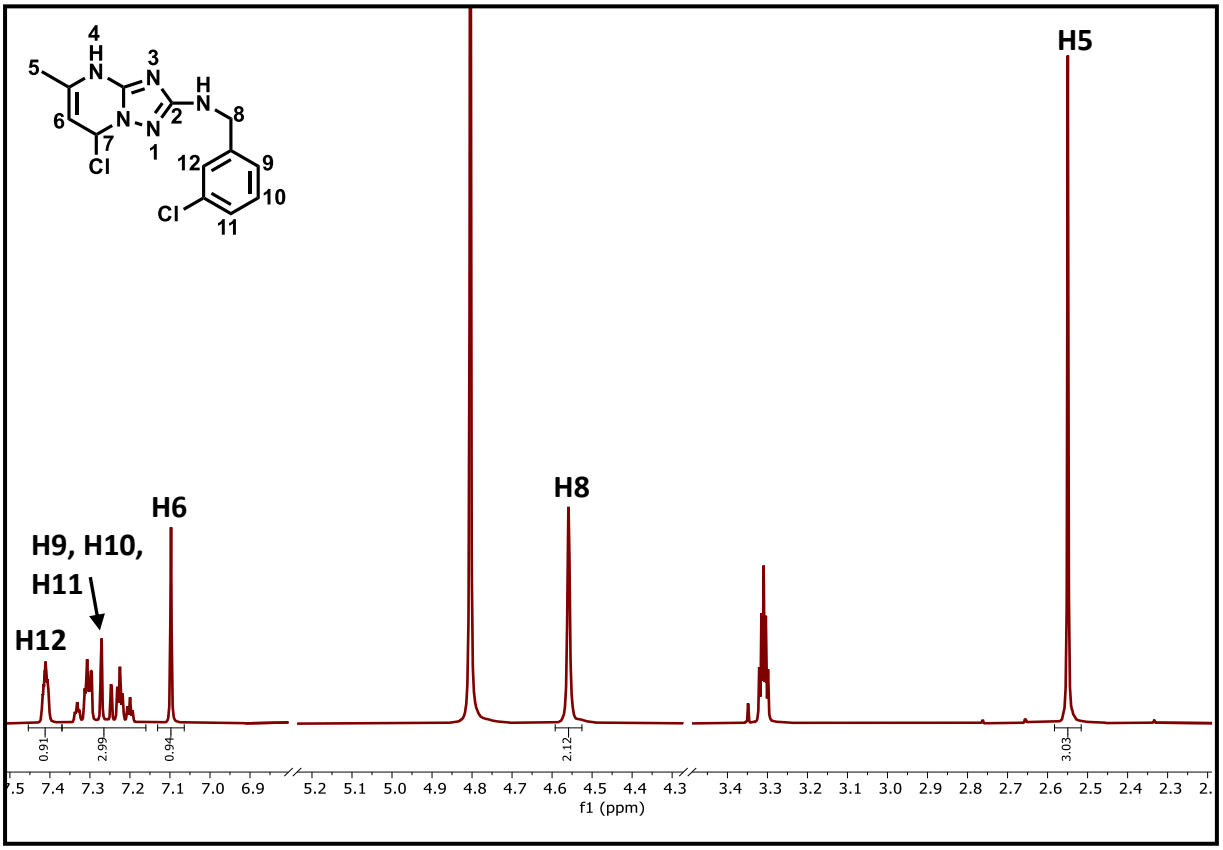

Figure 2.22: ^{1}H-NMR spectrum of **2.5d** in MeOD at 300 MHz

Characterization of intermediate 38/MM2-141 and target compound 28/MM2-145

The S_NAr reaction on intermediate **2.5d** resulted in intermediate **38/MM2-141**. The ^{1}H-NMR spectrum revealed two methylene protons corresponding to H13 at δ 3.50 ppm and δ 3.46 ppm integrating for one proton each resonating as a multiplet (**Fig. 2.23**). This is due to their proximity to the stereocenter on C14 making these protons diastereotopic. In addition, these protons couple to each other (H14 and NH, H20). The proton on chiral carbon H14 resonated downfield at δ 5.18 ppm as a multiplet as it coupled to two H13 protons and the NH_2 protons. The methoxy protons H19 resonated at δ 3.86 ppm and the methyl protons H5 are observed upfield at δ 2.36 ppm as singlets integrating for three protons each. A doublet at δ 4.49 ppm corresponds to methylene protons H8 coupled with NH. On the aromatic region (δ 7.41–7.25 ppm), eight protons (H9, H10, H11, H12, H15, H16, H17, and H18) were revealed and reconciled with the expected number of protons. The vinyl proton H6 integrating for a singlet appears at δ 6.11 ppm. Formation of the target compound **28/MM2-145** was confirmed by the disappearance of the singlet attributed to the *tert*-butyl of the Boc group at δ 1.28 ppm (**Fig. 2.24**).

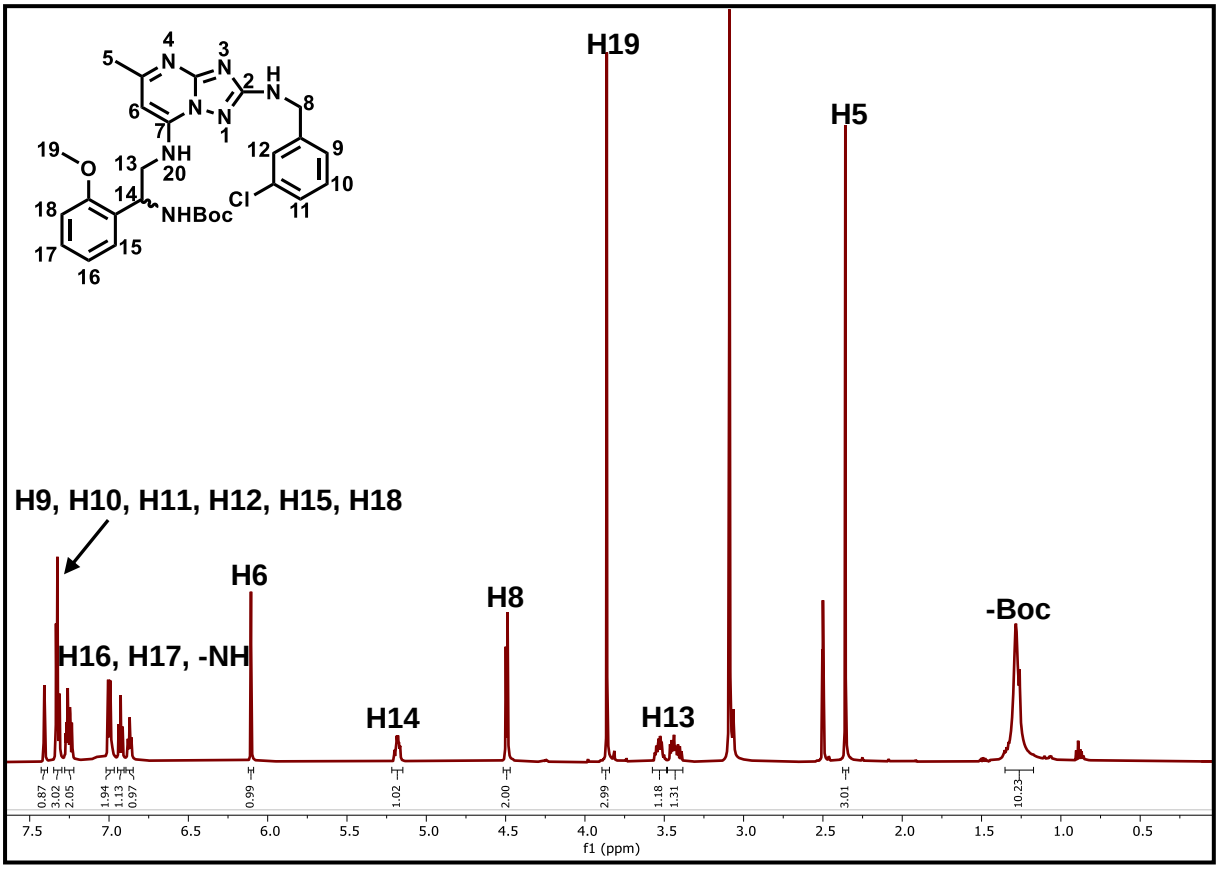

Figure 2.23: ^{1}H-NMR spectrum of **38/MM2-141** in DMSO-d_6 at 600 MHz

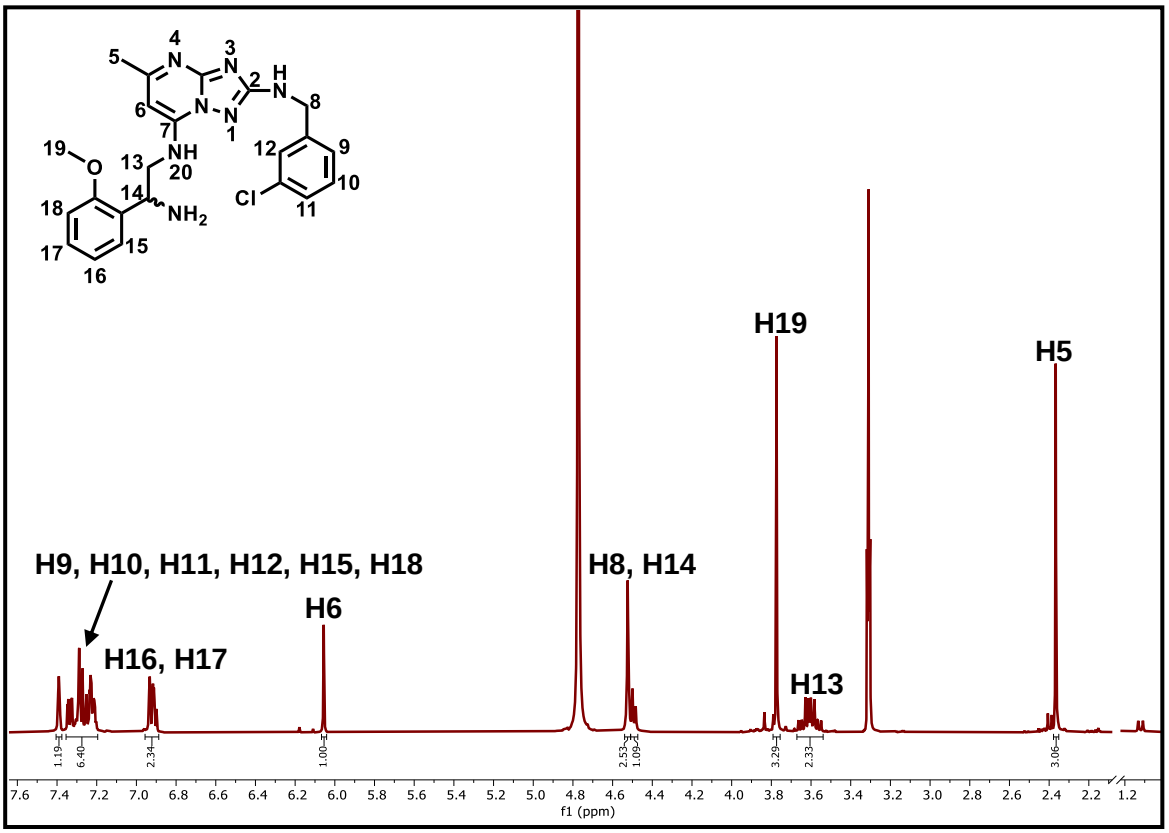

Figure 2.24: ^{1}H-NMR spectrum of **28/MM2-145** in MeOD at 600 MHz

The ^{13}C-NMR spectrum of **28/MM2-145** was also analyzed (**Fig. 2.25**). This spectrum confirmed the presence of upfield carbons corresponding to aliphatic carbons of methyl C5 (δ 24.51 ppm), methoxy C19 (δ 55.83 ppm), and two methylene carbons C8 (δ 46.70 ppm) and C13 (δ 51.11 ppm). The most deshielded triazolopyrimidyl core carbons attached to electronegative nitrogen atoms C2, C3a, and C7 appeared downfield between δ 148.09 and 166.98 ppm. Other deshielded carbons in the molecule *viz*. C4a, C8a, C11a, and C19 were also observed between δ 135.94 and 156.56 ppm. LC-MS data also confirmed the molecular ion as *m/z* 438.1 [M+H] and 439.1 [M+2], as the compound contains a chloride atom, which concurs with the calculated exact mass of 437.17 (**Fig. 2.26**).

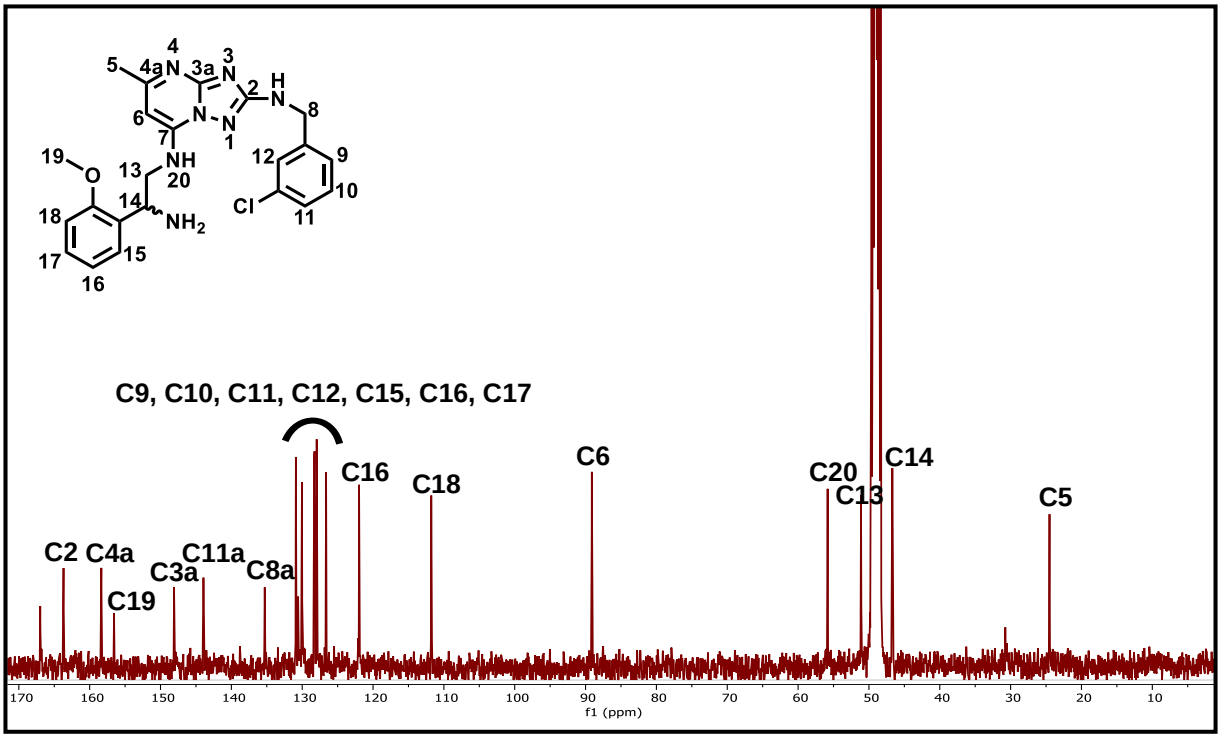

Figure 2.25: ^{1}H-NMR spectrum of **28/MM2-145** in MeOD at 600 MHz

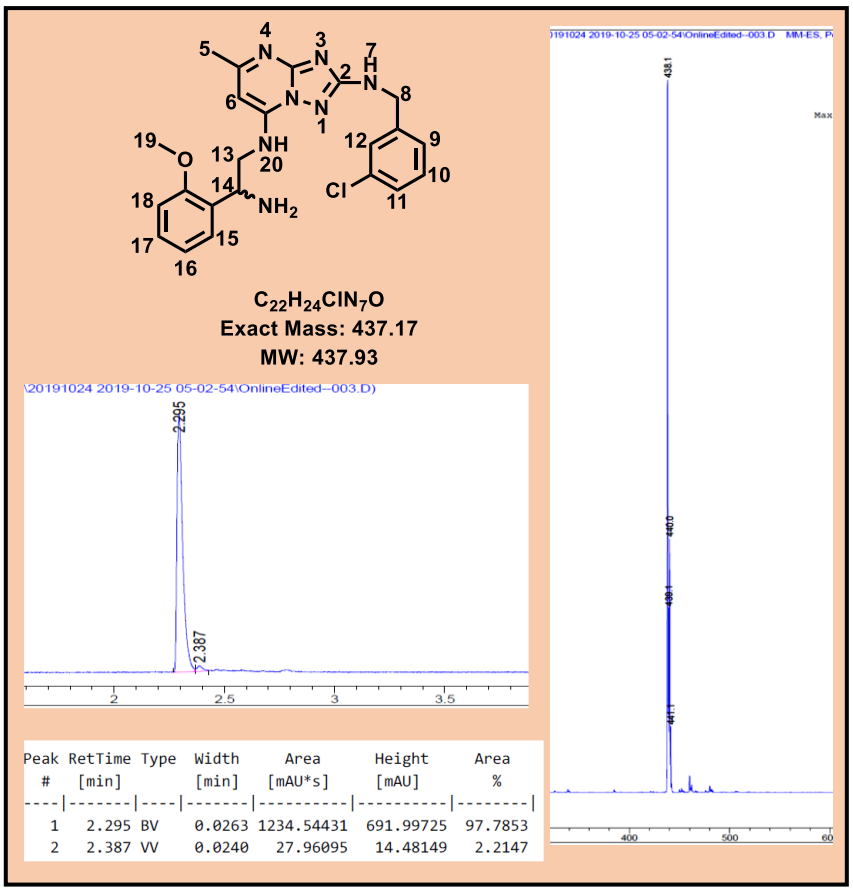

Figure 2.26: LC-MS chromatogram and spectrum of **28/MM2-145**

2.5. Benzoxaboroles series

2.5.1. Introduction

In a project aimed at identifying penicillin-binding protein-3 (PBP-3) inhibitors, benzoxaboroles were selected from a library of compounds screened against *Pseudomonas aeruginosa* PBP-3 using X-ray crystallography.[198] X-ray structures revealed that some benzoxaboroles were covalently bound to *P. aeruginosa* PBP-3. These compounds were also cross-screened for antiplasmodium activity wherein **H3D-006145 (43)** was identified as a hit (*Pf*NF54 IC_{50} = 1.06 μM; **Fig. 2.27**). This compound provided the basis for a formal hit assessment campaign to establish whether a tractable SAR against plasmodium can be established.

2.5.2. SAR plan

As part of hit validation **H3D-006145** (**43/MM2-92**) was resynthesized and retested. In addition, the opposite *R*-enantiomer (**83/MM2-90**) and racemic version (**45/MM2-91**) were synthesized and their antiplasmodium activities also evaluated. The activity of the hit compound was confirmed, and both the *R*-enantiomer (**83/MM2-90**) and racemic (**45/MM2-91**) analogue also showed antiplasmodium activity (0.85 and 0.64 μM, respectively). These results led to the proposal of the SAR evaluation summarized in **Fig. 2.27**. SAR1 explored variations on the phenylglycine methyl esters (**45–83** and **90–93**) guided by Craig plot substituents. The methyl and dimethyl amide matched-pairs of **45/MM2-91** were also proposed to assess the effect of stability differences between ester and amide. The effect of reversed amide was also evaluated through compound **44/MM4-26**. This SAR also evaluated the importance of chirality in the phenylglycine and in addition, alkyl amines (**84–89**) were also synthesized (**Fig. 2.27**).

SAR2 focused on the ethyl ester matched-pairs of the methyl esters explored in SAR1 and corresponding carboxylic acid analogues. The third SAR (SAR3) assessed the importance of the substituent on C7 as observed in various reported antiplasmodium benzoxaborole compounds.[156] Isolated yields of all compounds except those from SAR3 and SAR4 are presented in **Table 2.5**.

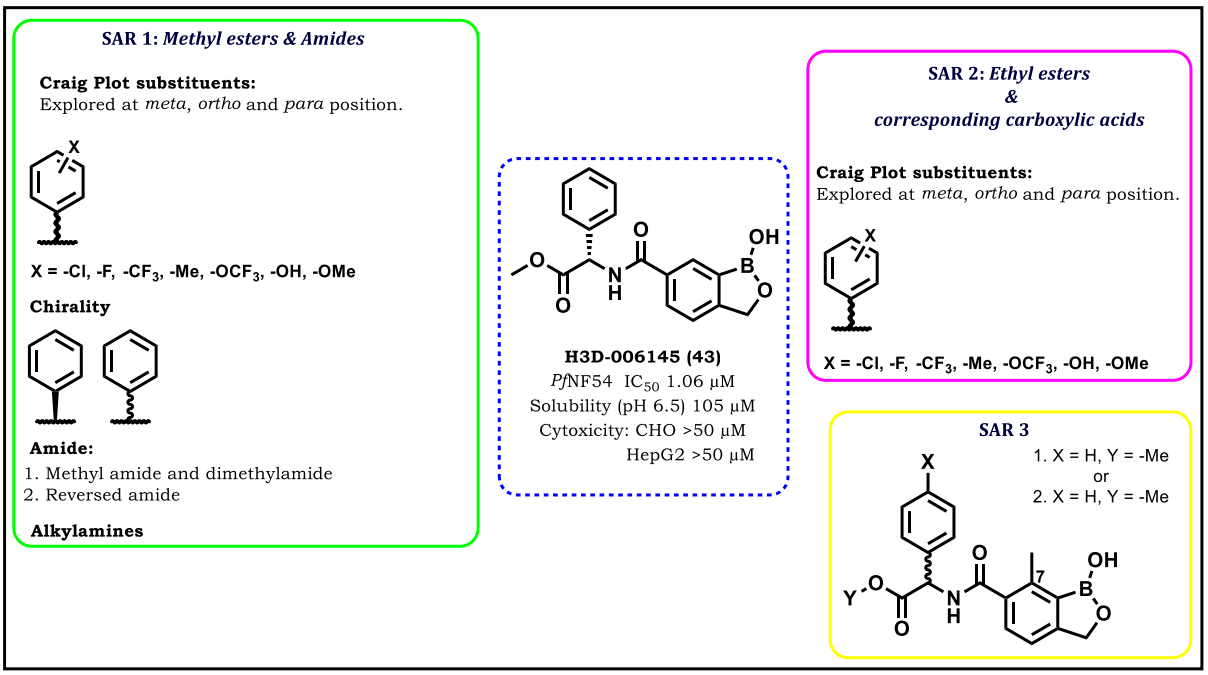

Figure 2.27: SAR design for the benzoxaboroles series

2.5.3. Chemistry

Phenylglycine and its unnatural amino acids derivatives

Phenylglycine derivatives and cyclohexyl amino acids were converted into methyl or ethyl esters by stirring in methanol or ethanol, respectively, and thionyl chloride under reflux for 14 h (**Scheme 2.14**).

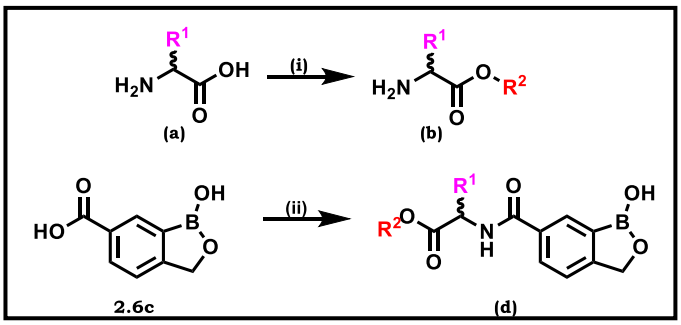

Scheme 2.6: Synthesis of benzoxaboroles

Reagents and conditions: (i) $SOCl_2$, MeOH, 70 °C, 16 h (quantitative); (ii) Alkylamine/phenylglycine/ unnatural phenyglycine/cyclohexyl amino acid, EDCI, HOBt, DMF, 27 °C, 14 h or HATU, DIPEA, DMF, 27 °C, 14 h or T3P®, triethylamine (Et_3N), DMF, 27 °C, 14 h. **R^1** = a substituent *viz.* phenyl, substituted phenyl or hydrogen for alkyl amine and **R^2** = -Me or -Et (6-77%).

Table 2.5: Isolated yields of benzoxaboroles series

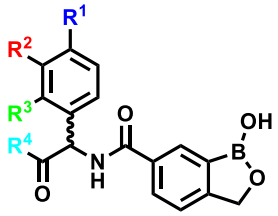

Number/Code	R^1	R^2	R^3	R^4	%Yield
45/MM2-91	H	H	H	-OMe	39
46/MM2-174	-Me	H	H	-OMe	33
47/MM2-196	H	-Me	H	-OMe	39
48/MM4-81	H	H	-Me	-OMe	26
49/MM2-201	-F	H	H	-OMe	22
50/MM4-44	H	-F	H	-OMe	61
51/MM4-64	H	H	-F	-OMe	34
52/MM3-160	-OMe	H	H	-OMe	48
53/MM4-15	H	-OMe	H	-OMe	24
54/MM4-46	H	H	-OMe	-OMe	35
55/MM3-8	-OH	H	H	-OMe	15
56/MM4-101	H	-OH	H	-OMe	35
57/MM4-108	H	H	-OH	-OMe	26
58/MM3-9	$-CF_3$	H	H	-OMe	68
59/MM4-14	H	$-CF_3$	H	-OMe	56
60/MM4-16	H	H	$-CF_3$	-OMe	22
61/MM3-175	-Cl	H	H	-OMe	41
62/MM4-12	H	-Cl	H	-OMe	77
63/MM4-07	H	H	-Cl	-OMe	38
64/MM3-57	H	H	H	-OEt	66
65/MM4-50	-Cl	H	H	-OEt	63
66/MM4-93	H	-Cl	H	-OEt	75
67/MM4-114	H	H	-Cl	-OEt	55
68/MM4-105	H	-Me	H	-OEt	59
69/MM4-100	H	H	-Me	-OEt	34
70/MM4-56	H	F	H	-OEt	47
71/MM4-55	H	H	F	-OEt	45
72/MM2-173	H	H	H	-OH	43
73/MM2-177	-Me	H	H	-OH	29

74/MM4-134	H	-Me	H	-OH	58
75/MM4-137	H	H	-Me	-OH	43
76/MM4-86	-Cl	H	H	-OH	71
77/MM4-127	H	-Cl	H	-OH	76
78/MM4-136	H	H	-Cl	-OH	43
79/MM4-89	H	-F	H	-OH	47
80/MM4-87	H	H	-F	-OH	70
81/MM3-136	H	H	H	-NMe	8
82/MM4-60	H	H	H	$-NMe_2$	22

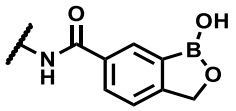

43/MM2-92	$-PhCHCOOCH_3$ (*S*)	28
83/MM2-90	$-PhCHCOOCH_3$ (*R*)	16
45A/MM2-224A	$-PhCHCOOCH_3$ (*S*) chiral col	
45B/MM2-224B	$-PhCHCOOCH_3$ (*R*) Chiral col	
84/MM2-124	$-CH_2CH_2C(CH_3)_2OH$	18
85/MM2-123	$-CH_2CH_2CH(CH_3)OH$	16
86/MM2-119	$-CH_2CH_2OCH_3$	15
87/MM2-44	$-CH_2CF_3$	4
88/MM2-130	$-PhCH_2OH$	11
89/MM2-165	$-CHC_6H_{11}COOCH_3$	18
90/MM3-85	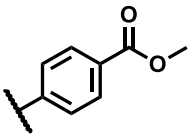	6
91/MM3-11	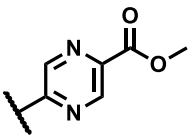	14
92/MM3-42	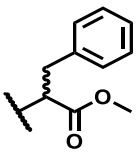	44

93/MM3-10	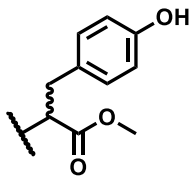	32
44/MM4-26	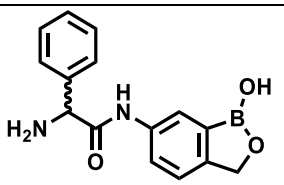	63

Amide coupling

Amide coupling was achieved using methyl esters and alkyl amines as nucleophiles with a commercially available 6-carboxybenzoboroxole with (i) EDCI and HOBt, (ii) HATU, or (iii) propylphosphonic anhydride (T3P®) amide coupling reactions (**Scheme 2.6(ii)**). The conditions used to obtain each compound are presented in detail in **Chapter 7**. In this study, amide coupling reactions were performed in *N*,*N*-dimethylmethanamide (DMF) with the addition of HOBt and EDCI in a mixture of 6-carboxybenzoxaborole **2.6c (Scheme 2.6)** and DIPEA, stirring for 14 h at 27 °C. This was also applied to the reactions in which T3P® was used. When HATU was used, carboxylic acid **2.15c**, DIPEA, and HATU were first stirred in DMF for 30 min followed by the addition of amine and the reaction was stirred for 14 h at 27 °C. The final amides were obtained in low to high yield (4–77%).

2.5.4. Chromatography and spectroscopic characterization of compounds in the benzoxaborole series

Compound **83/MM2-90** is used as an illustrative example for ^{1}H-NMR spectrum interpretation in this series (**Fig. 2.28**). The benzoxaborole moiety was confirmed by the presence of a singlet at δ 5.12 ppm integrating for two protons corresponding to the methylene protons H3. The doublet of doublets of H5 observed at δ 7.95 ppm indicates coupling with H4 (J = 8.2 Hz) and meta-coupling with H7 (J = 1.7 Hz). The phenyl protons H3'a, H3'b, H4'a, H4'b, and H5' appeared as a multiplet between δ 7.34 ppm and 7.48 ppm, and H7 appeared as a singlet integrating for one proton at δ 8.15 ppm. The singlet at δ 5.72 ppm integrating for one proton is indicative of the phenylglycine proton H2' and a singlet at δ 3.75 ppm integrating for three protons corresponds to the methyl ester protons H1'.

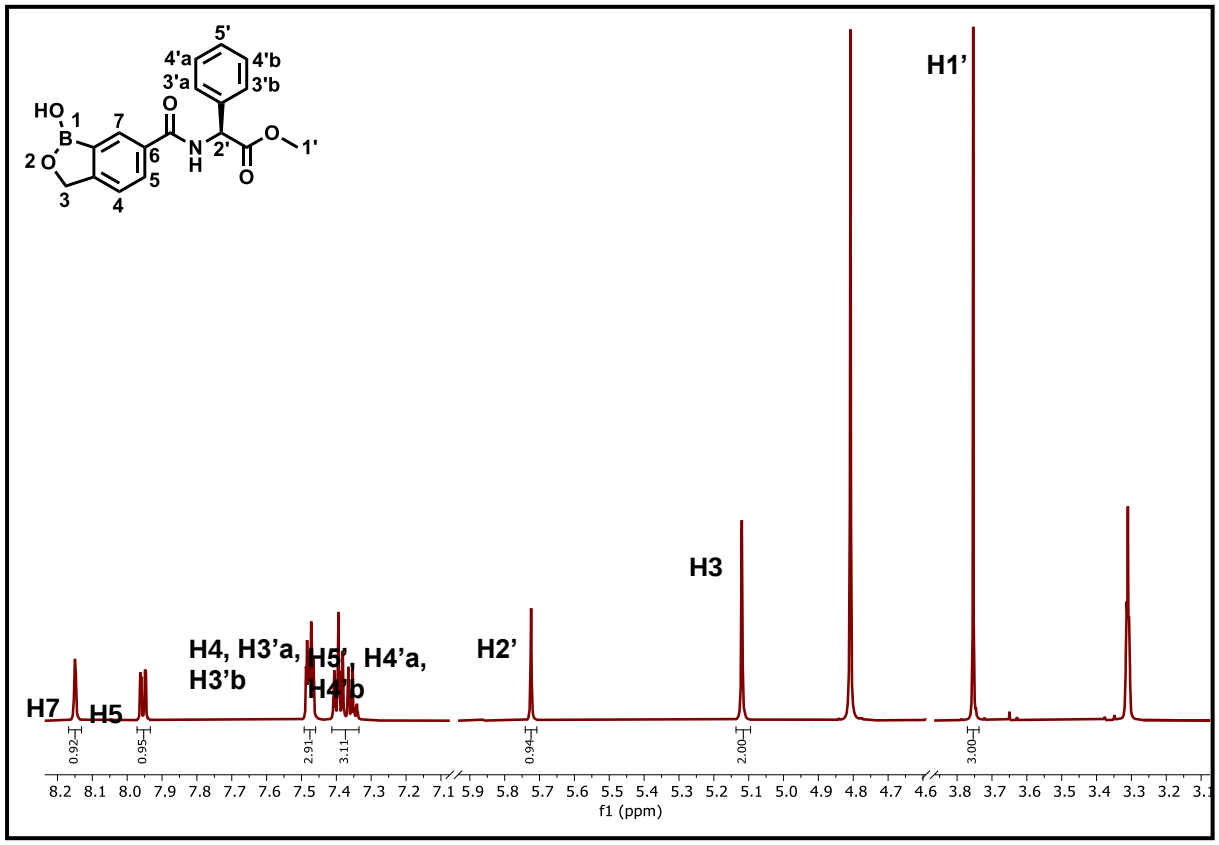

Figure 2.28: ^{1}H-NMR spectrum of **83/MM2-90** in MeOD at 600 MHz

^{13}C-NMR was also used for characterization of these compounds. The ^{13}C-NMR spectrum of **83/MM2-90** is used as a representative example for this series (**Fig. 2.29**). The two most downfield carbons C2' (δ 172.77 ppm) and C8 (δ 170.22 ppm) were attributed to ester and amide carbonyls, respectively. The methylene carbon C3 appeared downfield at δ 72.27 ppm and the methoxy carbon C1' was observed at δ 53.07 ppm. All aromatic carbons were reconciled with the expected number of carbons (12 carbons) and the two sets of symmetric carbons C5' and C6' appeared as two distinct carbons (two long peaks at δ 129.89 ppm and 129.08 ppm, respectively). In total, all 17 carbons for the compound were accounted for, thus confirming the structure. LC-MS data further confirmed the identity of the compound showing a molecular ion peak at *m/z* 326.1 [M+H] (**Fig. 30**) which corresponds to the calculated exact mass of 325.11.

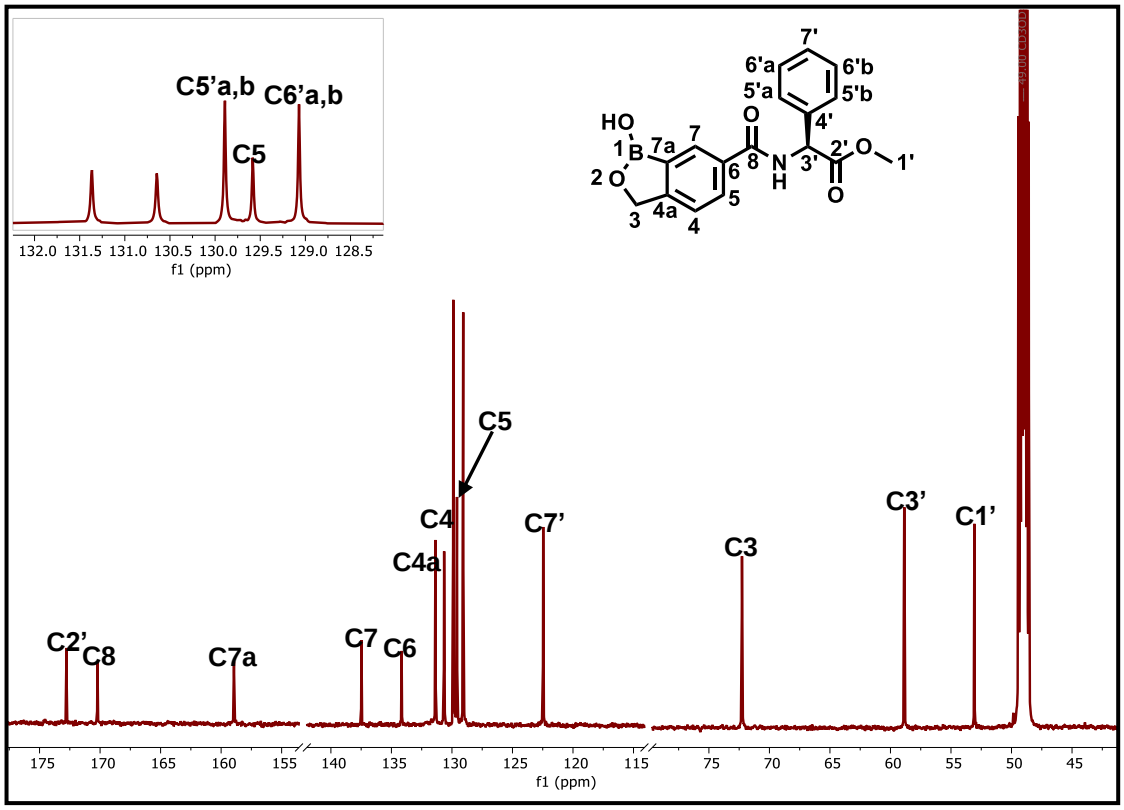

Figure 2.29: ^{13}C NMR spectrum of **83/MM2-90** in MeOD at 600 MHz

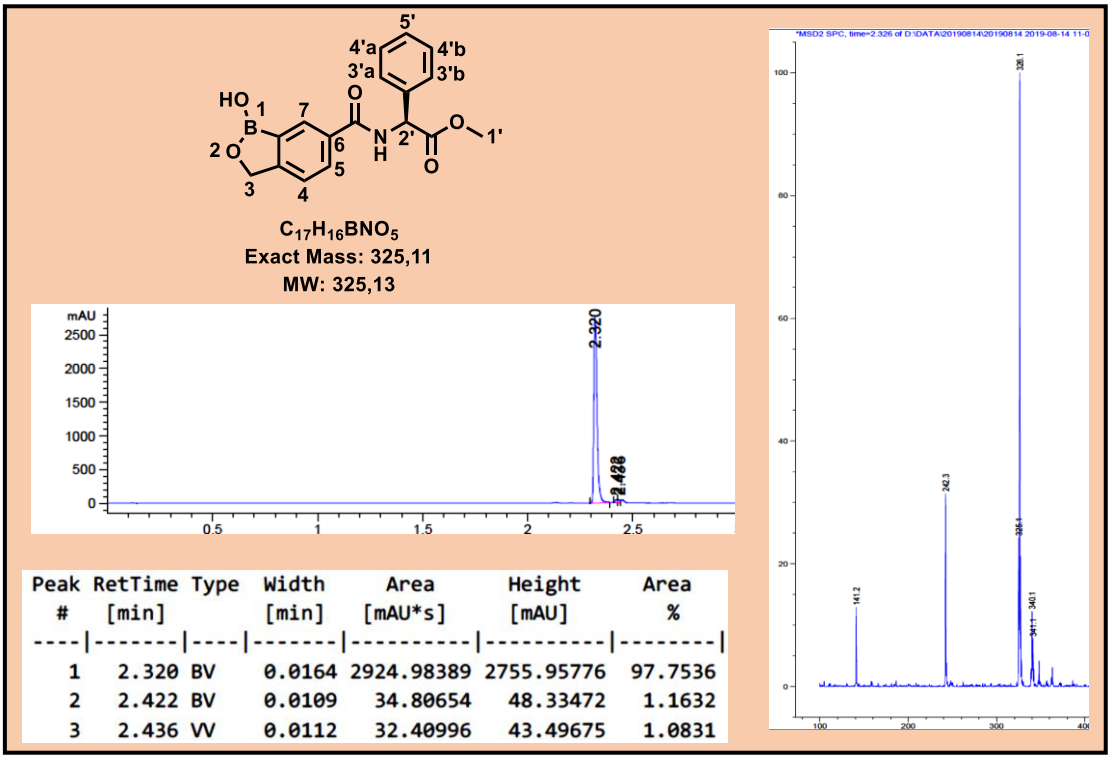

Figure 2.30: LC-MS chromatogram and spectrum of **83/MM2-90**

2.5.5. Synthesis, chromatography, and spectroscopic characterization of 7-methyl benzoxaborole

Synthesis of 6-carboxy-7-methylbenzoxaboroles followed the reported procedure (**Scheme 2.7**).[199] Target compounds and their isolated yields are presented in **Table 2.6**.

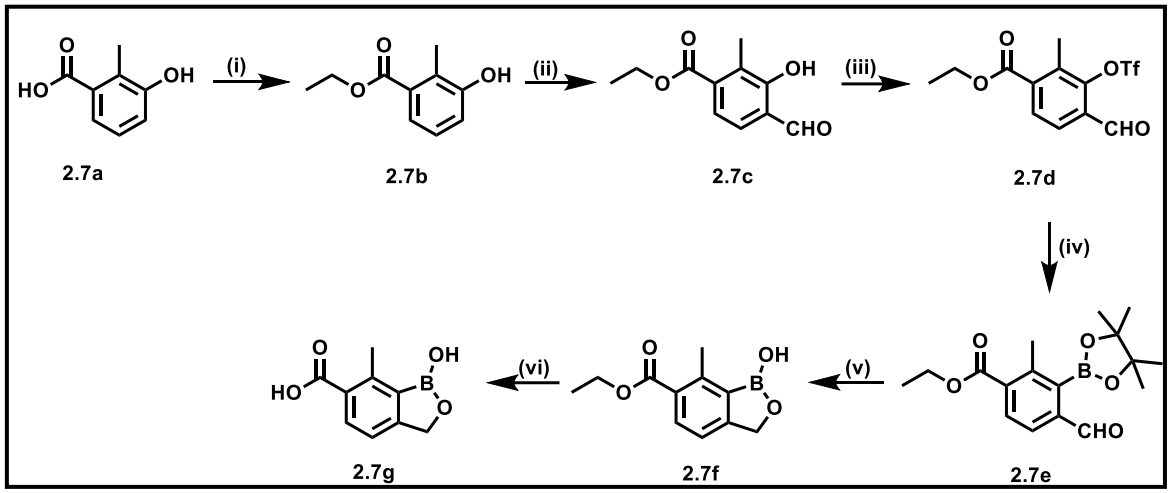

Scheme 2.7: Synthesis of 6-carboxy-7-methylbenzoxaborole

Reagents and conditions: (i) $SOCl_2$, EtOH, reflux, 4 h (100%); (ii) $MgCl_2$, $(CH_2O)_n$, Et_3N, THF, reflux, 14 h (64%); (iii) Tf_2O, pyridine, DMAP, DCM, 0–15 °C, 1 h (47%); (iv) Pin_2B_2, KOAc, Pd(dppf)Cl_2, 1,4-dioxane, N_2, 85 °C, 15 h; (v) $NaBH_4$, MeOH, THF, 0–15 °C, 1 h, then HCl, H_2O; (vi) NaOH, H_2O, 40 °C, 3 h, then 2M HCl (63%).

Table 2.6: Isolated yields of 6-carboxy-7-methylbenzoxaboroles

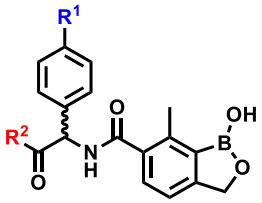

Number/Code	R^1	R^2	%Yield
94/MM4-141	H	-OMe	65
95/MM4-144	-Me	-OEt	32
96/MM4-150	-Me	-Me	70
97/MM4-148	-Me	-OH	73

The commercially available 3-hydroxy-2-methylbenzoic acid (**2.7a**) was converted into the corresponding ethyl ester via heating under reflux in ethanol with a catalytic

amount of thionyl chloride. The ethyl ester intermediate **2.7b** was subjected to modified Reimer-Tiemann formylation in the presence of magnesium chloride and paraformaldehyde. Aldehyde **2.7c** was reacted with triflic anhydride to afford intermediate **2.7d**. This intermediate was subjected Miyauro borylation to give boronic ester **2.7e** which was treated with sodium borohydride in methanol to afford intermediate **2.7f**. The base mediated hydrolysis with lithium hydroxide gave the desired carboxylic acid **2.7g**.

2.5.6. Chromatography and spectroscopic characterization of 6-carboxy-7-methylbenzoxaborole

The starting carboxylic acid **2.7a** was converted to an ethyl ester **2.7b**, and formation was confirmed via ^{1}H-NMR spectroscopy by the presence of the methyl (H1) integrating for three protons appearing as a triplet (J = 7.1 Hz) and the methylene protons (H2) integrating for two protons appearing as a quartet (J = 7.1 Hz) at δ 1.29 ppm and δ 4.25 ppm, respectively (**Fig. 2.31A**). The aromatic protons H7 (δ 7.16 ppm) and H5 (δ 6.98 ppm) integrate for one proton each as a doublet of doublets (J = 7.7 Hz and J = 7.9 Hz, respectively) and H5 (J = 9 Hz) at δ 6.98 ppm. Formation of the Reimer-Tiemann formylation product **2.7c** was confirmed by the presence of the aldehyde proton H4 as a singlet at δ 10.11 ppm (**Fig. 2.31B**). This product was reacted with triflic anhydride to afford triflate **2.7d**, and this was confirmed via LC-MS (molecular ion m/z 341.0). This was subjected to Miyaura borylation to afford intermediate **2.7e**. This intermediate was taken forward without further purification and thin-layer chromatography (TLC) analysis confirmed that **2.7d** had been consumed. Formation of the cyclized product **2.7f** was confirmed by the presence of the methylene protons H3, which integrated for two protons appearing as a singlet at δ 4.99 ppm and the hydroxyl H1 resonating as a singlet at δ 9.20 ppm (**Fig. 2.31C**). Formation of carboxylic acid **2.7g** was confirmed by the loss of the ethyl moiety with the absence of the methyl and methylene protons observed for **2.7f** (**Fig. 2.31D**).

The product was then used in the next step to synthesize analogues bearing the 7-methyl group. The ^{1}H-NMR spectrum from compound **94/MM4-141** is used as a representative example (**Fig. 2.32**). A singlet observed at δ 2.51 ppm integrating for three protons corresponds to methyl H7 and a singlet observed at δ 3.75 ppm corresponds to the methoxy H1'. The methylene protons H3 appear as a singlet at δ 5.04 ppm and the singlet at δ 5.68 ppm is H2'. The aromatic protons H4 (δ 7.22 ppm) appear as a doublet (J = 7.22 Hz) coupled with H5. The other aromatic protons (6H,

H5, H3'a,b, H4'a,b, and H5') are a multiplet between δ 7.51 and 7.30 ppm integrating for six protons. ^{13}C-NMR spectroscopy confirmed the presence of the methyl C7 at δ 17.8 ppm (**Fig. 2.33**).

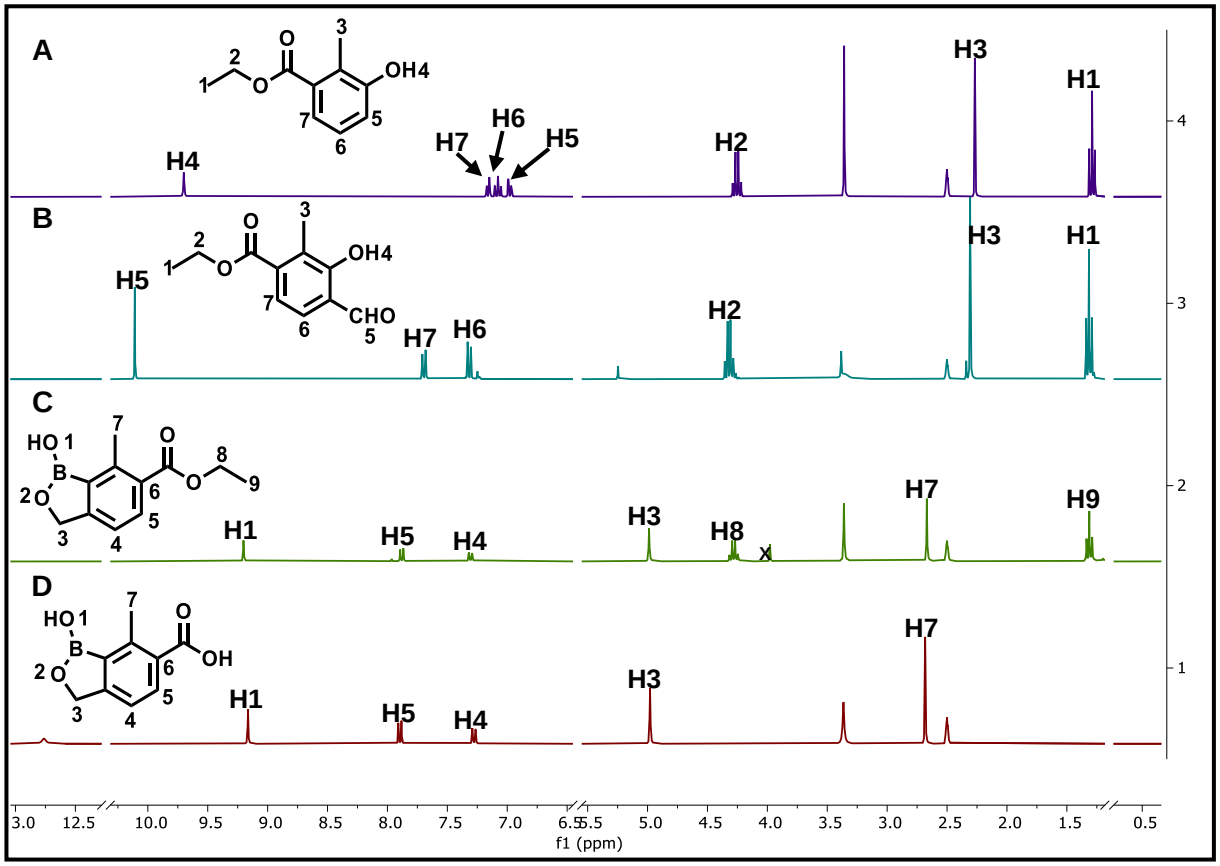

Figure 2.31: ^{1}H-NMR spectrum of **2.15b** (**A**), **2.15c** (**B**), **2.15d** (**C**) and **2.15g** (**D**) in DMSO-d_6 at 300 MHz

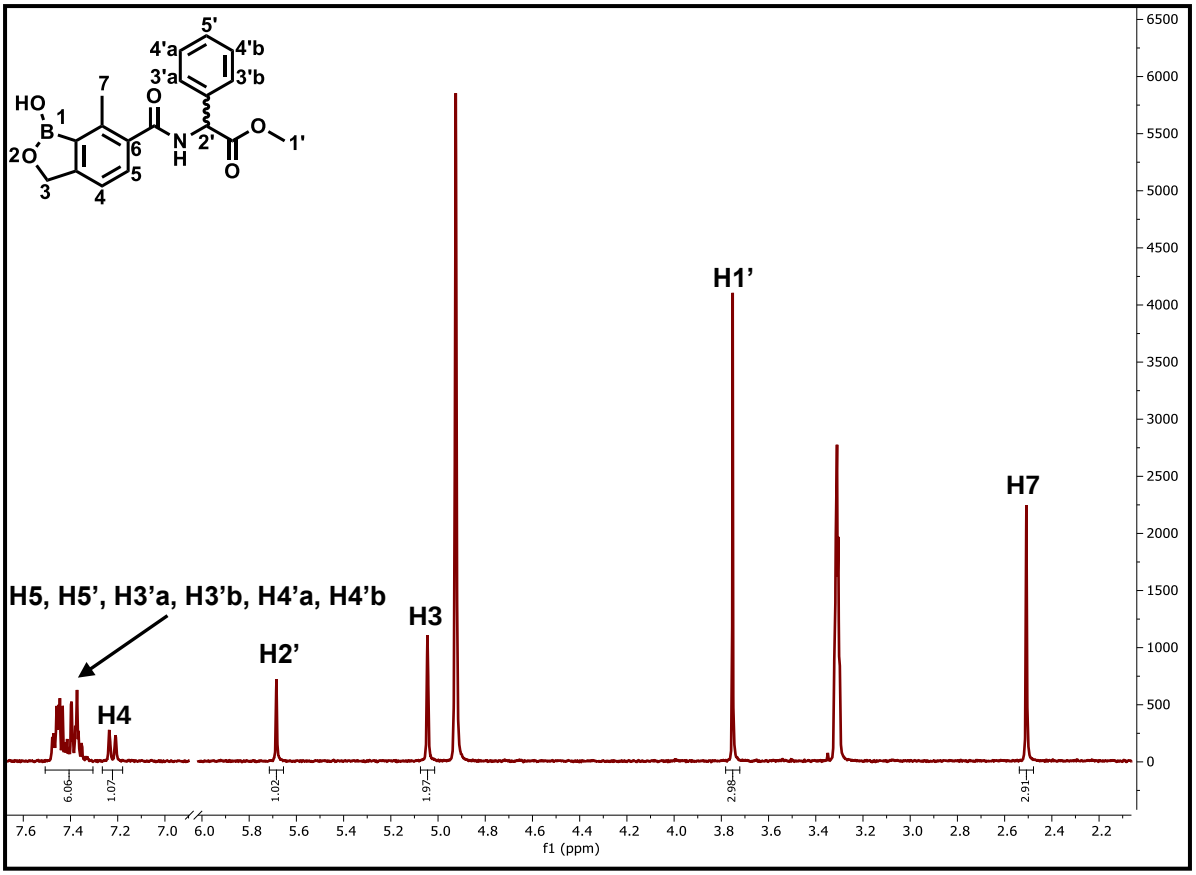

Figure 2.32: ^{1}H-NMR spectrum of **94/MM4-141** in MeOD at 600 MHz

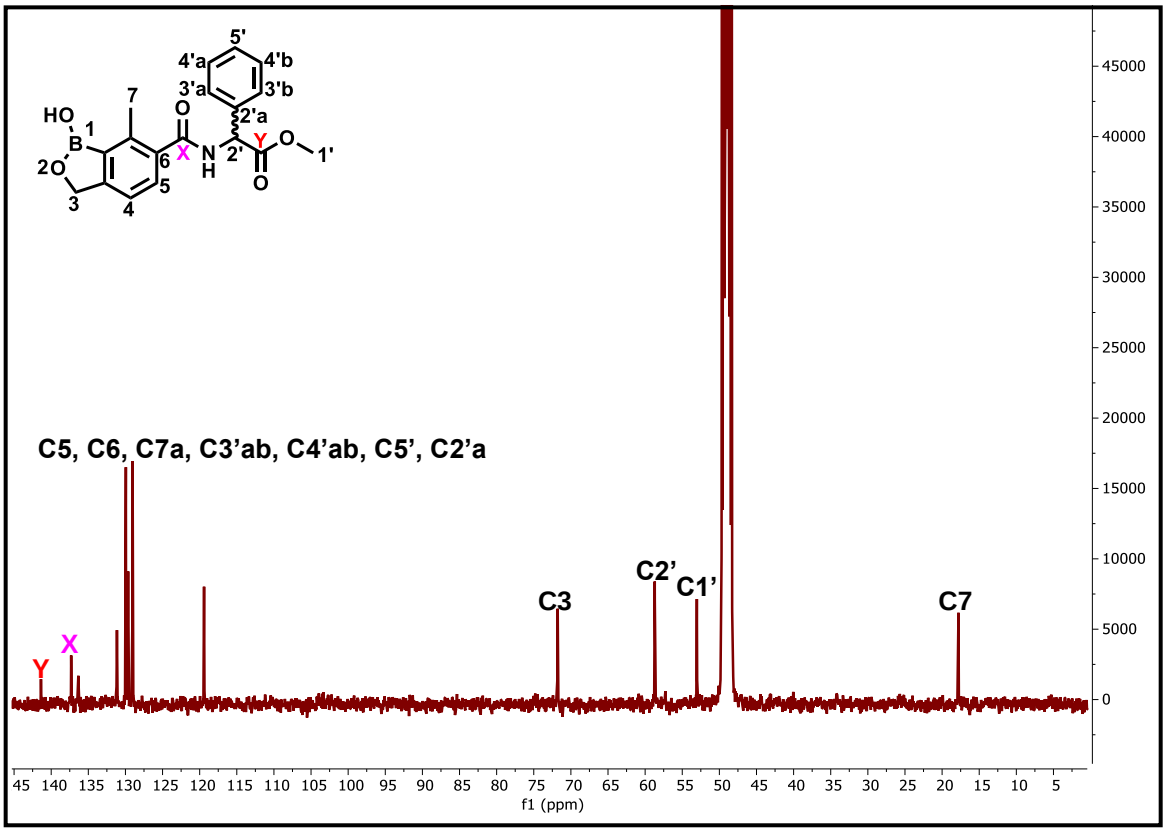

Figure 2.33: ^{13}C-NMR spectrum of **94/MM4-141** in MeOD at 600 MHz

2.7. Conclusion

This chapter expounded the rationale for the design of compounds synthesized here and described medicinal chemistry strategies employed to select compounds for synthesis. The five compound series (cyclohexyl pyrimidines, Ugi, azabenzimidazoles, triazolopyrimidines, and benzoxaboroles) were described and key intermediates as well as a selection of target compounds were highlighted to illustrate reactions and their mechanisms. Intermediates and target compounds were characterized using ^{1}H-NMR, ^{13}C-NMR, and LC-MS. Although only key intermediates and selected target compounds were characterized in this chapter, detailed characterization of all compounds is provided in **Chapter 7**. The compounds were obtained in low to high yield across all series and the LC-MS data showed that all final compounds were obtained with the purity required for biological screening (>95%). The biological and physicochemical studies are described in **Chapters 3**, **4** and **5**.

2.8. References

1. Nzila, A.; Ma, Z.; Chibale, K., Drug repositioning in the treatment of malaria and TB. *Future Med. Chem* **2011**, *3* (11), 1413-1426.

2. Spry, C.; Kirk, K.; Saliba, K. J., Coenzyme A biosynthesis: an antimicrobial drug target. *FEMS Microbiol. Rev.* **2008**, *32* (1), 56-106.

3. Grevengoed, T. J.; Klett, E. L.; Coleman, R. A., Acyl-CoA metabolism and partitioning. *Annu. Rev. Nutr.* **2014**, *34*, 1-30.

4. de Villiers, M.; Spry, C.; Macuamule, C. J.; Barnard, L.; Wells, G.; Saliba, K. J.; Strauss, E., Antiplasmodial mode of action of Pantothenamides: pantothenate kinase serves as a Metabolic activator not as a target. *ACS Infect. Dis.* **2017**, *3* (7), 527-541.

5. Spry, C.; Macuamule, C.; Lin, Z.; Virga, K. G.; Lee, R. E.; Strauss, E.; Saliba, K. J., Pantothenamides are potent, on-target inhibitors of Plasmodium falciparum growth when serum pantetheinase is inactivated. *PLoS One* **2013**, *8* (2), e54974.

6. Schalkwijk, J.; Allman, E. L.; Jansen, P. A.; De Vries, L. E.; Verhoef, J. M.; Jackowski, S.; Botman, P. N.; Beuckens-Schortinghuis, C. A.; Koolen, K. M.; Bolscher, J. M., Antimalarial pantothenamide metabolites target acetyl–coenzyme A biosynthesis in Plasmodium falciparum. *Sci. Transl. Med.* **2019**, *11* (510), eaas9917.

7. de Jonge, B. L.; Walkup, G. K.; Lahiri, S. D.; Huynh, H.; Neckermann, G.; Utley, L.; Nash, T. J.; Brock, J.; San Martin, M.; Kutschke, A., Discovery of inhibitors of 4′-phosphopantetheine adenylyltransferase (PPAT) to validate PPAT as a target for antibacterial therapy. *Antimicrob. Agents Chemother.* **2013**, *57* (12), 6005-6015.

8. Skepper, C. K.; Moreau, R. J.; Appleton, B. A.; Benton, B. M.; Drumm III, J. E.; Feng, B. Y.; Geng, M.; Hu, C.; Li, C.; Lingel, A., Discovery and Optimization of Phosphopantetheine Adenylyltransferase Inhibitors with Gram-Negative Antibacterial Activity. *J. Med. Chem.* **2018**, *61* (8), 3325-3349.

9. Moreau, R. J.; Skepper, C. K.; Appleton, B. A.; Blechschmidt, A.; Balibar, C. J.; Benton, B. M.; Drumm III, J. E.; Feng, B. Y.; Geng, M.; Li, C., Fragment-based drug discovery of inhibitors of phosphopantetheine adenylyltransferase from gram-negative bacteria. *J. Med. Chem.* **2018**, *61* (8), 3309-3324.

10. Hughes, J. P.; Rees, S.; Kalindjian, S. B.; Philpott, K. L., Principles of early drug discovery. *Br. J. Pharmacol.* **2011**, *162* (6), 1239-1249.

11. Young, R. J.; Green, D. V.; Luscombe, C. N.; Hill, A. P., Getting physical in drug discovery II: the impact of chromatographic hydrophobicity measurements and aromaticity. *Drug Discov. Today* **2011**, *16* (17-18), 822-830.

12. Ertl, P., Craig plot 2.0: an interactive navigation in the substituent bioisosteric space. *J. Cheminf.* **2020**, *12* (1), 1-8.

13. Herve, G.; Len, C., First ligand-free, microwave-assisted, Heck cross-coupling reaction in pure water on a nucleoside–Application to the synthesis of antiviral BVDU. *RSC Advances* **2014**, *4* (87), 46926-46929.

14. Diels-Alder Reaction. https://www.chemistrylearner.com/diels-alder-reaction.html (accessed 23 August 2021).

15. The Diels-Alder Reaction https://www.masterorganicchemistry.com/2017/08/30/the-diels-alder-reaction/ (accessed 23 August 2021).

16. Nyamai, D. W.; Tastan Bishop, Ö., Aminoacyl tRNA synthetases as malarial drug targets: a comparative bioinformatics study. *Malar J* **2019**, *18* (1), 34-61.

17. Chow, W. K.; Yuen, O. Y.; Choy, P. Y.; So, C. M.; Lau, C. P.; Wong, W. T.; Kwong, F. Y., A decade advancement of transition metal-catalyzed borylation of aryl halides and sulfonates. *RSC advances* **2013,** *3* (31), 12518-12539.

18. Lennox, A. J.; Lloyd-Jones, G. C., Selection of boron reagents for Suzuki–Miyaura coupling. *Chem. Soc. Rev.* **2014**, *43* (1), 412-443.

19. Almond-Thynne, J.; Blakemore, D. C.; Pryde, D. C.; Spivey, A. C., Site-selective Suzuki–Miyaura coupling of heteroaryl halides–understanding the trends for pharmaceutically important classes. *Chemical science* **2017**, *8* (1), 40-62.

20. Manabe, K.; Yamaguchi, M., Catalyst-controlled site-selectivity switching in Pd-catalyzed cross-coupling of dihaloarenes. *Catalysts* **2014**, *4* (3), 307-320.

21. Ceide, S. C.; Montalban, A. G., Microwave-assisted, efficient and regioselective Pd-catalyzed C-phenylation of halopyrimidines. *Tetrahedron letters* **2006**, *47* (26), 4415-4418.

22. Silverstein, R. M.; Webster, F. X.; Kiemle, D. J., *Spectrometric identification of organic compounds*. John wiley & sons: United States of America, 2005.

23. Rocha, R. O.; Rodrigues, M. O.; Neto, B. A. D., Review on the Ugi Multicomponent Reaction Mechanism and the Use of Fluorescent Derivatives as Functional Chromophores. *ACS Omega* **2020**, *5* (2), 972-979.

24. Zhang, Y.; Ao, Y. F.; Huang, Z. T.; Wang, D. X.; Wang, M. X.; Zhu, J., Chiral phosphoric acid catalyzed asymmetric Ugi reaction by dynamic kinetic resolution of

the primary multicomponent adduct. *Angew. Chem., Int. Ed. Engl.* **2016**, *55* (17), 5282-5285.

25. Jian Zhang, P. Y., Shao-Yu Li, He Sun, Shao-Hua Xiang, Jun (Joelle) Wang, Kendall N. Houk, Bin Tan, Asymmetric phosphoric acid–catalyzed four-component Ugi reaction. *Science* **2018**, *361* (6407), eaas8707.

26. Ingold, M.; Colella, L.; Dapueto, R.; López, G. V.; Porcal, W., Ugi Four-component Reaction (U-4CR) Under Green Conditions Designed for Undergraduate Organic Chemistry Laboratories. *World* **2017**, *5* (5), 153-157.

27. Diez-Cecilia, E.; Kelly, B.; Rozas, I., One-step double reduction of aryl nitro and carbonyl groups using hydrazine. *Tetrahedron letters* **2011**, *52* (50), 6702-6704.

28. El-Hout, S.; El-Sheikh, S.; Hassan, H. M.; Harraz, F. A.; Ibrahim, I.; El-Sharkawy, E., A green chemical route for synthesis of graphene supported palladium nanoparticles: A highly active and recyclable catalyst for reduction of nitrobenzene. *Applied Catalysis A: General* **2015**, *503*, 176-185.

29. Newman, H.; Krajnc, A.; Bellini, D.; Eyermann, C. J.; Boyle, G. A.; Paterson, N. G.; McAuley, K. E.; Lesniak, R.; Gangar, M.; von Delft, F.; Brem, J.; Chibale, K.; Schofield, C. J.; Dowson, C. G., High-Throughput Crystallography Reveals Boron-Containing Inhibitors of a Penicillin-Binding Protein with Di- and Tricovalent Binding Modes. *J. Med. Chem.* **2021**, *64* (15), 11379-11394.

30. Coghi, P. S.; Zhu, Y.; Xie, H.; Hosmane, N. S.; Zhang, Y., Organoboron Compounds: Effective Antibacterial and Antiparasitic Agents. *Molecules* **2021**, *26* (11), 1-26.

31. Akama, T.; Zhang, Y. K.; Freund, Y. R.; Berry, P.; Lee, J.; Easom, E. E.; Jacobs, R. T.; Plattner, J. J.; Witty, M. J.; Peter, R.; Rowan, T. G.; Gillingwater, K.; Brun, R.; Nare, B.; Mercer, L.; Xu, M.; Wang, J.; Liang, H., Identification of a 4-fluorobenzyl l-valinate amide benzoxaborole (AN11736) as a potential development candidate for the treatment of Animal African Trypanosomiasis (AAT). *Bioorg Med Chem Lett* **2018**, *28* (1), 6-10.

Chapter 3: Bacterial *4′-Phosphopantetheine Adenylyltransferase (PPAT)* inhibitors as potential antimalarial agents

3.1. Chapter Overview

A series of bacterial 4′-Phosphopantetheine Adenylyltransferase (PPAT) inhibitors and derivatives evaluated as antiplasmodium agents are discussed in this chapter. In addition to the *in vitro* asexual blood stage antiplasmodium activity, the solubility of the Ugi, cyclohexyl pyrimidine, azabenzimidazole, triazolopyrimidinone and triazolopyrimidine series was also measured and the results are presented below. The chemical rescue experiments related to the coenzyme A biosynthesis pathway on selected Ugi and triazolopyrimidine series compounds as well as the metabolomics data of selected compounds are also reported.

3.2. *In vitro* antiplasmodium profiling of proposed PPAT inhibitors and solubility data

The *in vitro* antiplasmodium activity was evaluated against the drug sensitive *Pf*NF54 strain. Compounds were tested for cytotoxicity against the hepatocellular carcinoma cells (HepG2) at 2 μM (reported as percentage inhibition). The HepG2 assay measures the ability of the test compound to inhibit the proliferation of the HepG2 cells after 48 h monitoring absorbance measured at 450 nM using CytoSelect™.[200]

The *in vitro* antiplasmodium activity screening was carried out at the Holistic Drug Discovery and Development (H3D) Centre, University of Cape Town (UCT), using an assay that measures the activity of the parasite's lactate dehydrogenase (LDH) for parasite viability. *Plasmodium* relies on anaerobic glycolysis which requires a continuous regeneration of the nicotinamide adenine dinucleotide (NAD^+).[201] LDH reduces NAD^+ to NADH during anaerobic carbohydrate metabolism.[202] The parasite LDH (pLDH) has the ability to use the 3-acetylpyridine adenine dinucleotide (APAD), an analogue of NAD^+, at a faster rate than the human LDH isoform for lactate to pyruvate conversion. This conversion is detected and quantified spectrophotometrically upon reacting with the probe substrate, and the measurements are converted into logarithmic values for plotting in dose-response curves and determining the half-maximum inhibitory concentrations (IC_{50}'s).

The approximated solubility of the compounds was determined using the turbidimetric (kinetic) solubility assay in which test compounds' solutions in DMSO are added to a buffered solution (pH 7.4).[203] This method is a cheap method used in order to quickly attain solubility of the compound and, it has limitations including the estimation of solubility over a concentration range (0-200 μM) and often overestimates solubility. This assay detects the turbidity that results from test compound's precipitation and measures its absorbance on UV-VIS at the wavelength where the compound is not expected to absorb (620 nm). The concentration value above which turbidity occurs is approximated to solubility of a given compound. Compounds with the concentration 40 - <5 μM were considered poor solubility, compounds with concentration between 50 and 120 are classified as moderate solubility and those with >120 μM have high solubility.

The antiplasmodium data of the compounds from the screens described above is presented in **Tables 3.1**-**3.3** and relevant SAR trends are elaborated.

3.2.1. Asexual blood stage antiplasmodium activity and solubility evaluation of the cyclohexyl pyrimidine and Ugi series compounds

The antiplasmodium activity assessment of these series commenced with the hit validation study. Hit compounds **1**-**4** which were identified in medium-throughput screening (MTS) with *Pf*NF54 IC_{50} 1.04, 2.9, 2.8 and 2.2 μM, respectively, were reprepared and re-evaluated for antiplasmodium activity. Compound **4** could not be resynthesized, however, a closely related analogue **4a/MM2-39** with a methyl group was synthesized. Following the hit validation, the structure-activity relationship (SAR) was investigated based on compound **2/MM1-19** (**Table 3.1**) which showed the highest antiplasmodium activity (IC_{50} = 5.2 μM), albeit slightly lower than that reported from the MTS. The design of additional analogues was guided by the principles described in **Chapter 2 section 2.2.1.1**. A summary of modifications made for the Ugi series is shown in **Fig. 3.1**.

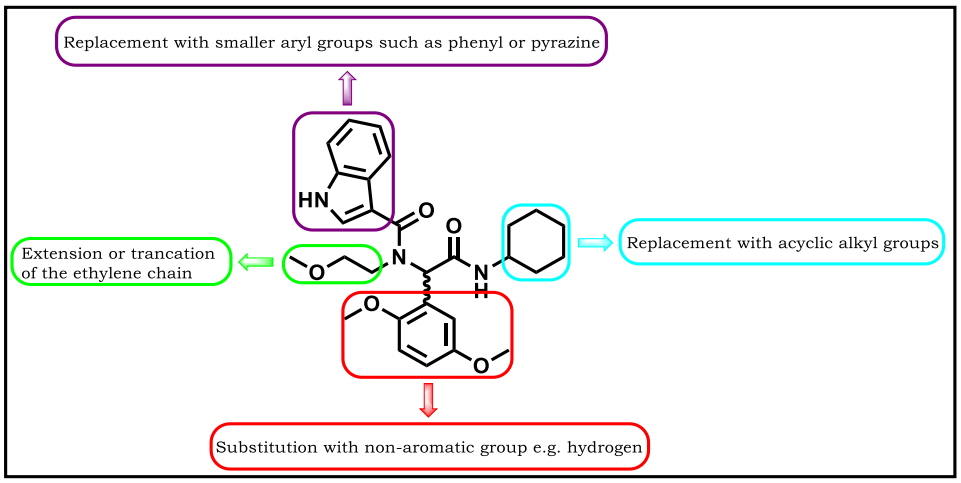

Figure 3.1. The SAR modifications for the Ugi series hit **2/MM1-19**

The absence of antiplasmodium activity for the resynthesized Ugi hit compound **1/MM1-15** (IC_{50} >6 μM, i.e., the highest concentration tested) did not compare to that of the MTS (IC_{50} 1.04 μM). On the other hand, the resynthesized Ugi hit **2/MM1-19** showed a lower antiplasmodium activity (IC_{50} 5.2 μM) compared to that reported from the MTS (IC_{50} 2.9 μM). Pure enantiomers of this compound were also obtained following separation via preparative chiral HPLC. The profile of the racemic mixture showed two peaks at different retention times, 7.83 and 10.08 min (**Fig. 3.2 C**) and that of each of the two enantiomers (**Fig 3.2 A** and **B**) demonstrated >95% purity. These pure enantiomers were then assessed for antiplasmodium activity with enantiomer **2A/MM1-19A** showing IC_{50} 5.4 μM and **2B/MM1-19B** showing IC_{50} >6 μM. This result showed that **2A/MM1-19A** as opposed to **2A/MM1-19B** has the same activity as the racemic mixture and implies that it may be responsible for the activity observed for **2**. This phenomenon is common, and some clinical drugs are used as racemic mixtures though only one enantiomer is the active component.[204-207]

The SAR evaluation (**Table 3.1**) with the substitution of the indole in the active Ugi hit **2/MM1-19** with smaller aromatic rings phenyl (**17/MM1-56**), tolyl (**18/MM1-82**), 1-methyl-1*H*-4,3-pyrazole (**19/MM1-63**), 5-chloro-1-methyl-1*H*-4,3-pyrazole (**20/MM1-64**) and 3,4-dihydroxyphenyl (**21/MM1-81**) resulted in lower antiplasmodium activity with all compounds showing IC_{50} >6 μM. Replacement of the cyclohexane of **2/MM1-19** with the acyclic alkyl *tert*-butyl group (**22/MM1-53**),

removal of the 1,5-dimethoxyphenyl with non-aromatic group, in this case hydrogen (**15/MM1-85**), and substitution of 2-morpholinoethan-1-amine for 2-methoxyethan-1-amine (**16/MM1-86**) also led to lower antiplasmodium activity, IC_{50} >6 µM relative to **2/MM1-19**. Solubility within this series varied from 20-160 µM. Most compounds with an indole ring had high solubility except compound **2B/MM1-19B** likely due to the nitrogen or -NH in the indole encouraging hydrogen bonding.

Table 3.1: *In vitro Pf*NF54 antiplasmodium activity, solubility and cytotoxicity of the Ugi series analogues.

Number/Code	Structure	[a]*Pf*NF54 IC_{50}, µM	[b]Solubility, µM, pH 6.5	[c]Cytotoxicity (% inhibition)
1/ MM1-15	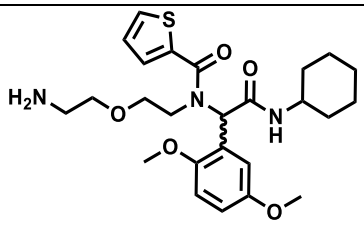	>6	110	
2A/ MM1-19A	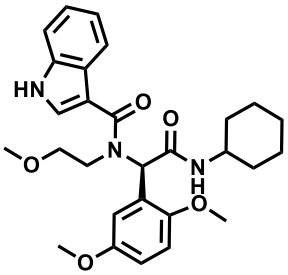	5.4	*160	2.1
2B/ MM1-19A	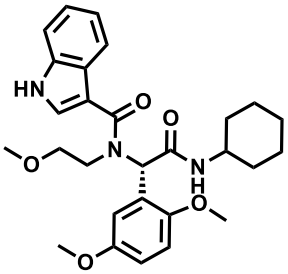	>6	20	0
2/MM1-19	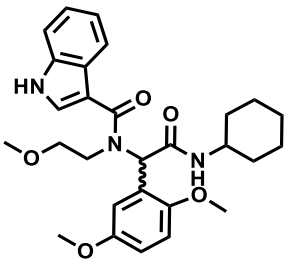	5.2	*160	3.4

15/MM1-85	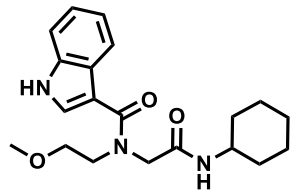	>6	155
16/MM1-86	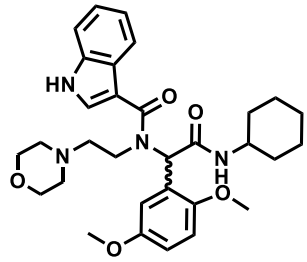	>6	*160
17/MM1-56	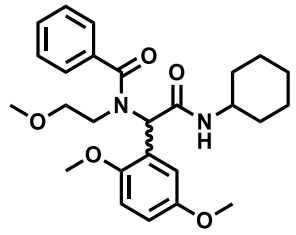	>6	*40
18/MM1-82	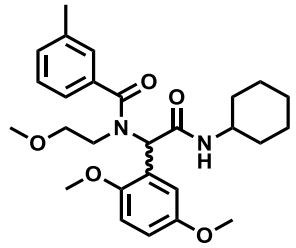	>6	95
19/MM1-63	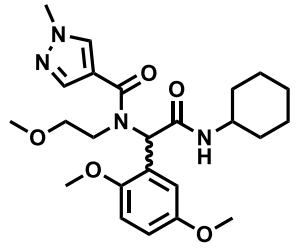	>6	*80
20/MM1-64	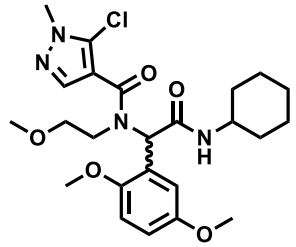	>6	145
21/MM1-81	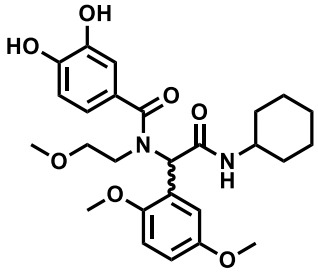	>6	*120

22/MM1-53	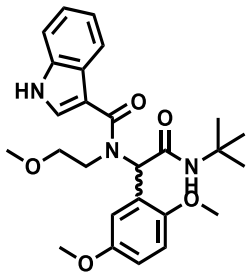	>6	85

[a]Mean values from n = 2 determinations. [b]Chloroquine and artesunate were used as controls with the standard *Pf*NF54 IC_{50} values of 0.016 µM and 0.004 µM, respectively. [c]Cytotoxicity was evaluated in mammalian HepG2 cells at 2 µM concentration of the compound for one biological replicate of technical duplicates and is reported as percentage inhibition. *Turbidimetric solubility

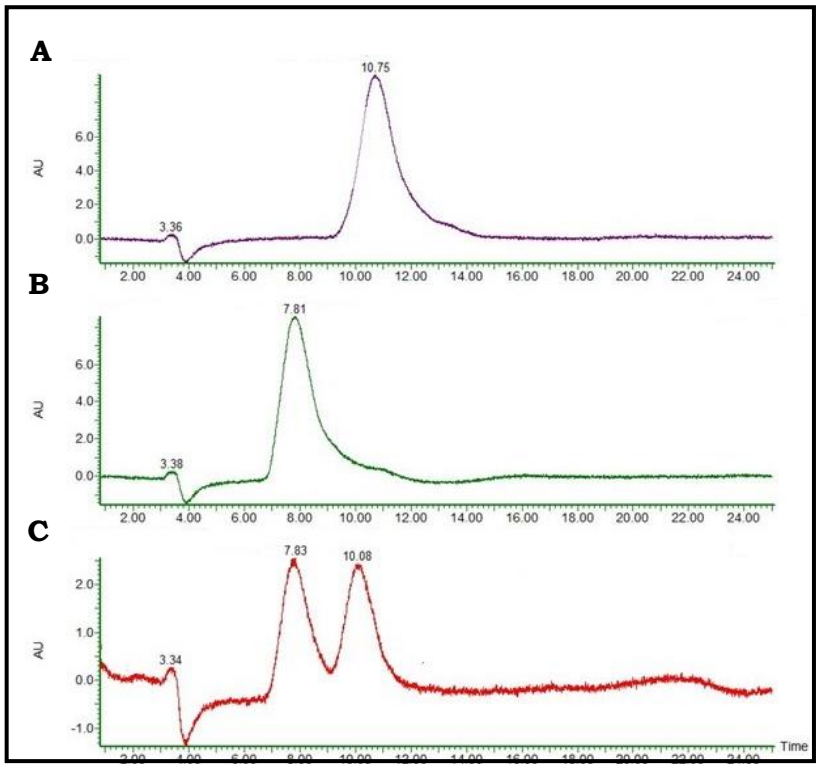

Figure 3.2: The chiral prep-HPLC analytical profile for the separation of pure enantiomers of **2/MM1-19**

The antiplasmodium activity of cyclohexyl pyrimidine series as indicated in **Table 3.2** revealed that the resynthesized hit **3/MM1-75** has lower activity than the same hit from MTS (IC_{50} >6 µM vs 2.8 µM). Compound **4a/MM2-39** activity (IC_{50} 2.2 µM), on the other hand, compared well with hit **4** from the MTS (IC_{50} 2.2 µM). Replacement of pyrrole ring with chloro- and difluoro- substituted groups (**13/MM1-88** and **14/MM1-89**) led to lower activity (IC_{50} >6 µM) and lower solubility (both 40 µM) compared to **3/MM1-75** (>200 µM). This is expected as the group like phenyl will encourage pi-pi interactions and the halogens introduce lipophilicity which then

lower solubility. Although compound **4a/MM2-39** showed high antiplasmodium activity, synthetic accessibility was challenging in that it involved seven synthesis steps towards the final compound with low yields on key intermediates as described in **Chapter 2 section 2.3.1** and as such SAR evaluation based on this compound was not pursued.

Table 3.2: *In vitro Pf*NF54 antiplasmodium activity and solubility of the cyclohexyl pyrimidine series analogues

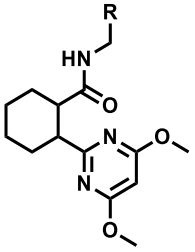

Number/Code	R	[a,b]*Pf* NF54 IC_{50}, µM	Solubility, µM, pH 6.5
3/MM1-75	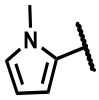	>6	*>200
13/MM1-88	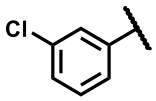	>6	*40
14/MM1-89	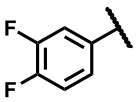	>6	*40
4a/MM2-39	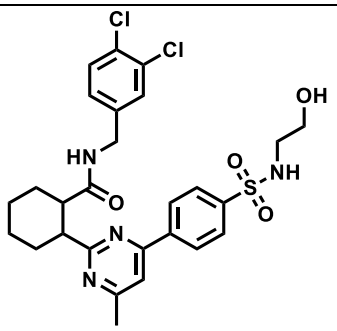	2.2	<5

[a]Mean values from n = 2 determinations. [b]Chloroquine and artesunate were used as controls with the standard *Pf*NF54 IC_{50} values of 0.016 µM and 0.004 µM, respectively. *Turbidimetric solubility

It is not uncommon in the early drug discovery phase to find compounds that had activity in high throughput screenings to not validate upon re-evaluation.[208] The loss of activity can be due to several factors and among them is that compounds for throughput screening platforms often degrade during storage in DMSO solvent over a prolonged period of time, and the activity may be the result of impurities or of interference with biochemical assay spectrophotometric recording.[179, 209] Lower antiplasmodium activity for the analogues of hit **2/MM1-19** during SAR evaluation may be due to these compounds having a different interaction with the putative target. This has been observed previously for the compounds derived from the phenotypic screening without knowledge of the target.[210] The loss in antiplasmodium activity of the freshly prepared hit samples and the lack of activity for analogues imply that the Ugi and cyclohexyl pyrimidine compounds may not be acting on the *P. falciparum* PPAT as seen for the bacterial PPAT in the work reported by AstraZeneca.[177] In order to understand whether the lack of antiplasmodium activity may have been due to compounds not acting on the same pathway or target as in bacteria, selected compounds were investigated for relevance on CoA biosynthesis pathway by conducting chemical rescue and targeted metabolomics experiments presented in the following sections of this chapter.

3.2.2. Asexual blood stage antiplasmodium activity and solubility evaluation of the azabenzimidazole, triazolopyrimidinone and triazolopyrimidine series

The antiplasmodium activity of the azabenzimidazole, triazolopyrimidinone and triazolopyrimidine series was investigated against *Pf*NF54 at UCT under conditions previously described. The four azabenzimidazole compounds (**Table 3.3**) were designed based on the substitution with (3-chlorophenyl)methanamine (**23**), the removal of the amine linker (**25**) to assess the importance of the spacer and introduction of chirality on the methylene of the (3-chlorophenyl)methanamine substituent (**24** and **25**) to mimic the chiral compounds reported by Novartis.[175, 176] The use of (3-chlorophenyl)methanamine instead of the (*R*)-3-amino-3-(3-chlorophenyl)propanenitrile was because synthesis with substitution of the latter was unsuccessful. Therefore, **23** was synthesized as an analogue of the azabenzimidazole lead reported by Novartis. For the triazolopyrimidine, two SAR points were explored (**Fig. 3.3**). SAR1 analogues were designed guided by selection of Craig plot substituents onto the phenyl ring of the phenylmethanamine appendage

while keeping the 1-(2-methoxyphenyl)ethane-1,2-diamine constant. SAR2 explored the effect of changes on the 1-(2-methoxyphenyl)ethane-1,2-diamine appendage while maintaining the (3-chlorophenyl)methanamine. Within the context of repositioning, triazolopyrimidinone compound **27** was assessed for antiplasmodium activity because triazolopyrimidinones were also reported as bacterial PPAT inhibitors in the study conducted by Novartis.[176]

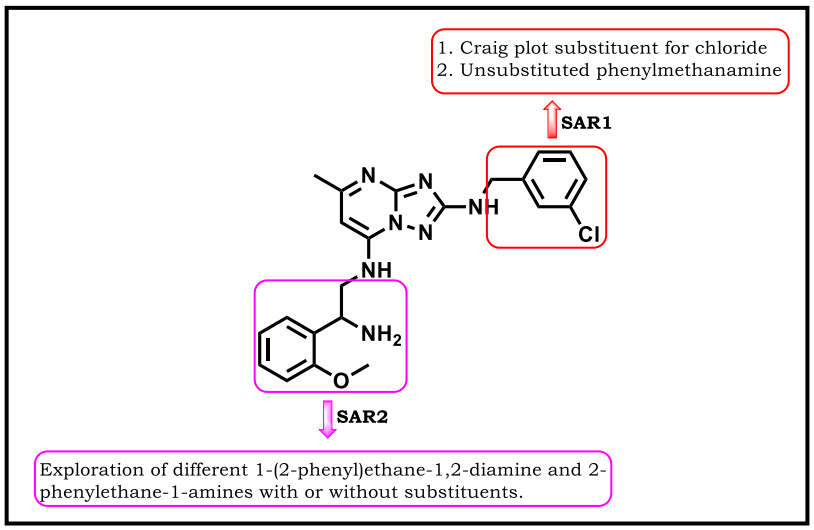

Figure 3.3. The SAR plan for the triazolopyrimidine series

Azabenzimidazole series (**23/MM1-177** – **26/MM2-77**) showed low antiplasmodium activity with IC_{50}'s >6 μM (**Table 3.3**). This was also the case for triazolopyrimidinone intermediate **27** with an IC_{50} >6 μM (**Table 3.4**). The boc-protected triazolopyrimidinine compound **38** (**Table 3.5**) had an IC_{50} of 4.6 μM, which upon boc-deprotection resulted in two-fold gain in activity for free amine **28** (IC_{50} = 2.2 μM) (**Table 3.4**). In light of this result, and as indicated in **Figure 3.4**, SAR1 based on triazolopyrimidine **28** was explored. Compound **29** with the *para* chloro-substituent and compound **30** with the *ortho* chloro-substituent led to 2- to 3-fold lower antiplasmodium activity with IC_{50}'s = 4.5 and 4.8 μM, respectively. Replacement of the chloro with a trifluoro methane substituent on the *meta*, *para* and *ortho* position to give compounds **31**, **32** and **33**, respectively, also led to loss of activity (IC_{50}'s >6 μM, = 5.3 μM and >6 μM, respectively). The same was observed for compounds **34**, **35** and **36** bearing the electron-donating lipophilic methyl substituent on the *meta*, *para* and *ortho* positions, respectively, as IC_{50}'s were >6 μM. Phenylmethanamine analogue **37** was also less active (IC_{50} > 6 μM). These results suggest that the chloro

substituent at the *meta* position is optimal for activity. Compounds within the series showed improved solubility (40 to >200 µM) relative to **28** (20 µM). Notably, compound **35** with the *para*-methyl substituent and **37** with an unsubstituted phenyl showed higher solubility of 160 µM and >200 µM, respectively.

Table 3.3: *In vitro Pf*NF54 antiplasmodium activity and solubility of the cyclohexyl pyrimidine series analogues

Number/Code	Structure	[a,b]*Pf* NF54 IC_{50}, µM	Solubility, µM, pH 6.5
23/MM1-177	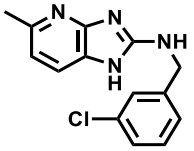	>6	20
24/MM2-83	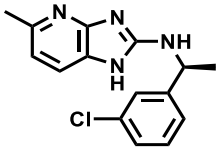	>6	110
25/MM2-78	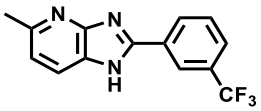	>6	<5
26/MM2-77	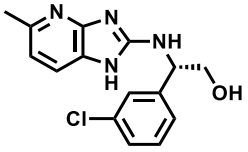	>6	[c]N.D

[a]Mean values from n = 2 determinations. [b]Chloroquine and artesunate were used as controls with the standard *Pf*NF54 IC_{50} values of 0.016 µM and 0.004 µM, respectively. [c]N.D = not determined.

Table 3.4: *In vitro* antiplasmodium activity against *P. falciparum* (NF54) and solubility of the triazolopyrimidinone and triazolopyrimidine series SAR1

Number/Code	Structure	[a,b]*Pf* NF54 IC_{50}, µM	[c]Solubility, µM, pH 6.5
27/MM1-185	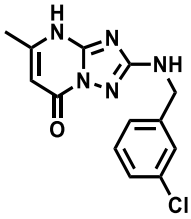	>6	30

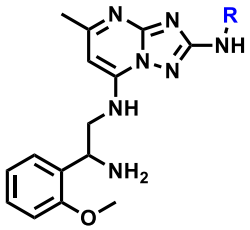

Number/Code	R	[a,b]*Pf* NF54 IC_{50}, µM	Solubility, µM, pH 6.5
28/MM2-145	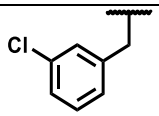	2.2	20
29/MM3-144	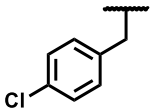	4.5	90
30/MM3-189	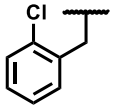	4.8	*40
31/MM3-205	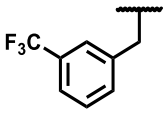	5.8	*20
32/MM3-159	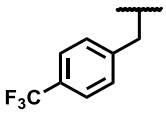	5.3	*120
33/MM3-167	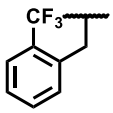	>6	*40
34/MM4-75	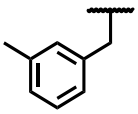	>6	110

35/MM4-19	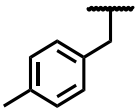	>6	*160
36/MM4-34	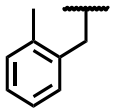	>6	*60
37/MM3-140	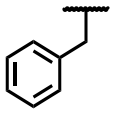	>6	*>200

[a]Mean values from n = 2 determinations. [b]Chloroquine and artesunate were used as controls with the standard *Pf*NF54 IC_{50} values of 0.016 µM and 0.004 µM, respectively. *****Not determined. *Turbidimetric Solubility

Synthesis of compounds for SAR2 evaluation (**Table 3.5**) was limited by commercial availability of the 1-(2-phenyl)ethane-1,2-diamine and 2-phenylethane-1-amine inputs. The antiplasmodium activity and solubility of the compounds are discussed relative to compound **28/MM2-145** (IC_{50} = 2.2 µM). Removal of the methoxy group as shown by **40/MM3-59** led to loss of antiplasmodium activity (IC_{50} >6 µM). Addition of the *meta* methoxy, as for the dimethoxy compound **39/MM3-75** without the benzylamine, and removal of the amino group while retaining the methoxy in the same position for compound **42/MM3-60** both resulted in loss of activity (IC_{50} >6 µM). Marginal activity (IC_{50} = 5.1 µM) was obtained for the *ortho* chloro-substituted compound **41/MM3-139** suggesting the importance of the amino group to antiplasmodium activity as is the substituent on the phenyl ring, as observed by the loss of activity for compound **40/MM3-59**.

Table 3.5: *In vitro* antiplasmodium activity against *P. falciparum* (NF54) and solubility of the azabenzimidazole, triazolopyrimidinone and triazolopyrimidine series SAR2

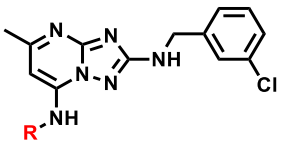

Number/Code	R	[a,b]*Pf* NF54 IC_{50}, µM	Solubility, µM, pH 6.5
38/MM2-141	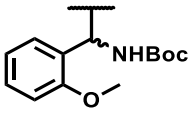	4.6	[c]ND
39/MM3-75	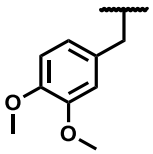	>6	<5
40/MM3-59	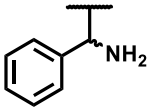	>6	20
41/MM3-139	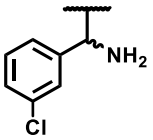	5.1	*80
42/MM3-60	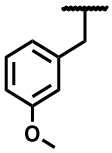	>6	*20

[a]Mean values from n = 2 determinations. [b]Chloroquine and artesunate were used as controls with the standard *Pf*NF54 IC_{50} values of 0.016 µM and 0.004 µM, respectively. [c]ND = not determined. *Turbidimetric Solubility

3.2.3. *In vitro* gametocytocidal activity

Currently, only primaquine shows gametocytocidal activity in the clinic though other compounds, including artemisinins, have *in vitro* activity against early-stage gametocytes.[211, 212] One of the desirable traits of novel antimalarials is that they should be transmission-blocking (Target Candidate Profile 5) by acting against gametocytes which are the transmissible forms of *Plasmodium*.[91] Compounds with

this feature will interrupt the *Plasmodium* life cycle by disrupting the interhost transfer. Recently, CoA biosynthesis has been shown to be essential for the development of gametocytes. Developing molecules that inhibit CoA biosynthesis can therefore potentially lead to promising transmission blocking agents.[213] Within this context, the Ugi compound **2/MM1-19** and its pure enantiomers **2A/MM1-19A** and **2B/MM1-19B** were selected for gametocytocidal activity screening based on their *in vitro* asexual blood stage antiplasmodium activity and availability of the compounds at the time of the assay.

A reported luciferase reporter assay was used to assess *in vitro* gametocytocidal activity of the test compounds.[214, 215] This assay uses the transgenic *Pf*NF54 parasite line NF54-*Pf*S16-GFP-Luc to assess stage-specific activity of test compounds on day 5 and 10 (representing >90% of either early stage II/III or mature stage IV/V gametocytes, respectively). Luciferase activity is determined from the parasite lysate and the bioluminescence is quantified to give percentage inhibition of the gametocytes' development (this method is described in detail in Chapter 6). This dual-point assay assesses activity at 1 μM and 5 μM compound concentrations and is used to prioritize compounds for full IC_{50} determination.

At 1 μM **2/MM1-19**, **2A/MM1-19A** and **2B/MM1-19B** were not active against both early stage gametocytes (EG) and late stage gametocytes (LG) (**Fig. 3.4**). When these compounds were tested at 5 μM, the racemic compound **2/MM1-19** showed 15% inhibition and the pure enantiomer **2B/MM1-19B** showed 38% inhibition against the EG (**Fig. 3.4**). At 5 μM, these compounds did not show inhibition of LG. Enantiomer **2A/MM1-19A** did not inhibit either EG or LG at 5 μM (**Fig. 3.4**). Overall, the data indicate that **2/MM1-19, 2A/MM1-19A** and **2B/MM1-19B** have minimal or no activity against gametocytes at 5 μM.

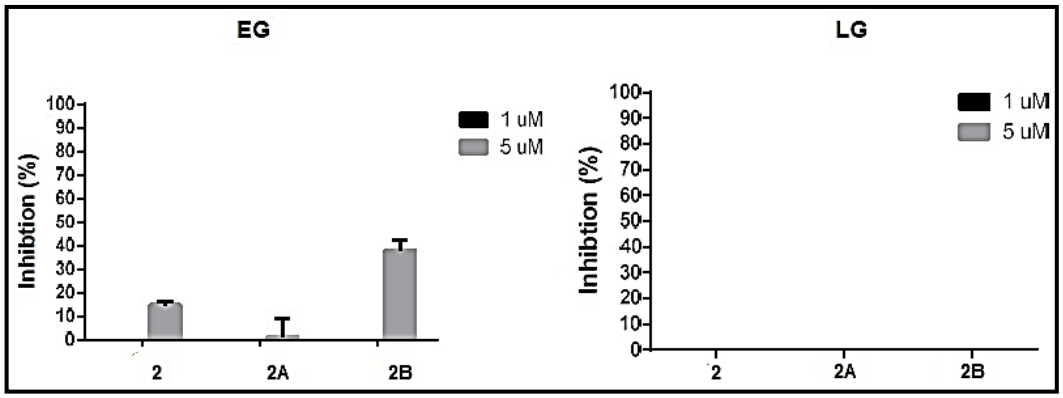

Figure 3.4: The percentage inhibition of the early and late-stage gametocytes following compound treatment at 1 μM and 5 μM for compounds **2/MM1-19**, **2A/MM1-19A** and **2B/MM1-19B**

3.3. Chemical Rescue experiments

Chemical rescue, which is the supplementation of the assay media with the end-product or the intermediate of a targeted pathway, can be used to validate the inhibitory effect of the compound in culture. The rationale for this approach is that supplementation will reverse the effects of the compound and thus implicate that the compound acts along the pathway. The rescue experiments have been studied for *P. falciparum* in recent years and have demonstrated the potential for uncovering the targeted pathways.[216, 217] In a recent report by Avery *et al.* chemical rescue experiments for diverse antiplasmodium hits operating in the CoA biosynthesis pathway [213, 218] showed that supplementation with CoA negated the inhibitory effect, supporting inhibition of the CoA biosynthesis pathway as the mode of action. In the subsequent study these authors also showed that supplementation with the metabolites of the pathway were also able to reverse the pharmacological effect.[213]

CoA is particularly important in this experiment in that it is the end-product of the pathway and thus its supplementation will rescue the parasite from inhibitors of its biosynthesis pathway.[218] Pantothenate is the precursor of CoA, and it is metabolized through this pathway to CoA and has successfully been used in chemical rescue experiments of *P. falciparum* to identify molecules relevant to the CoA biosynthesis pathway.[219, 220] Lastly, PPAT and dephospho-Coenzyme A (DeCoA) kinase have been shown to be essential for the survival of the blood stage malaria parasite even when the preceding enzymes are bypassed for CoA biosynthesis.[140, 221] The substrate of PPAT, pantetheine, has been proposed to be able to complete CoA biosynthesis

without the need for preceding enzymes or intermediates.[140, 222] The intermediate DeCoA is therefore crucial for the completion of CoA biosynthesis and thus its supplementation to the media will rescue the parasite. As it is the product of PPAT, it is also essential for assessing the specificity of the inhibition of this enzyme.

Herewith, the chemical rescue experiment was performed to assess if the proposed bacterial PPAT inhibitors act through inhibition of *Pf*PPAT and/or along the CoA biosynthesis pathway. The selected compounds **2/MM1-19**, **28/MM2-145** and **38/ MM2-141** were used as they showed some weak to moderate antiplasmodium activity (*Pf*NF54 IC_{50} 5.2, 2.2 and 4.6 μM, respectively) in initial screen. The concentrations of CoA, DeCoA and calcium pantothenate (CaP) were set at 2 μM and 20 μM (**Table 3.6**), and these were confirmed not to be toxic to the parasite.

For the chemical rescue following treatment with **2/MM1-19**, there was no shift in IC_{50} values when the medium was supplemented with either 2 μM or 20 μM of CoA, DeCoA or CaP (IC_{50} >6 μM for all experiments) (**Fig. 3.3**). The triazolopyrimidine compound **28/MM2-145** drug alone inhibited the parasite with IC_{50} 2.6 μM and the supplementation with 2 μM CoA, DeCoA and CaP did not show any significant shift in IC_{50} (= 3.3, = 2.9 and = 3.0 μM, respectively) (**Fig. 3.3**). When the concentration of each supplement was increased to 20 μM, there was still no obvious shift in the IC_{50} for **28/MM2-145** (CoA: IC_{50} = 2.7 μM, DeCoA: IC_{50} = 2.6 μM and CaP: IC_{50} = 3.1 μM). The same observation was made for the boc-protected analogue **38/MM2-141** (IC_{50} = 3.6 μM drug alone) when the chemical rescue was conducted with CoA (IC_{50} = 3.5 μM), DeCoA (IC_{50} = 3.7 μM) and CaP (IC_{50} = 3.4 μM) at 2 μM. At the 20 μM CoA, DeCoA and CaP there was no shift with the IC_{50} = 3.7 μM, = 3.3 μM and = 3.7 μM, respectively.

Table 3.6: The antiplasmodium activity of the test compounds in the chemical rescue experiment

		Concentration [2 μM]			Concentration [20 μM]		
Number/Code	**Drug alone**	**CoA**	**DeCoA**	**CaP**	**CoA**	**DeCoA**	**CaP**
2/MM1-19	[a,b]>6	>6	>6	>6	>6	>6	>6
28/MM2-145	2.8	3.3	2.9	3.0	2.7	2.6	3.1
38/MM2-141	3.6	3.5	3.7	3.4	3.7	3.3	3.7

[a]*Pf*NF54 IC_{50} in μM Parasite: 2% rings, 72h pLDH; [b]Mean values from n = 2 determinations.

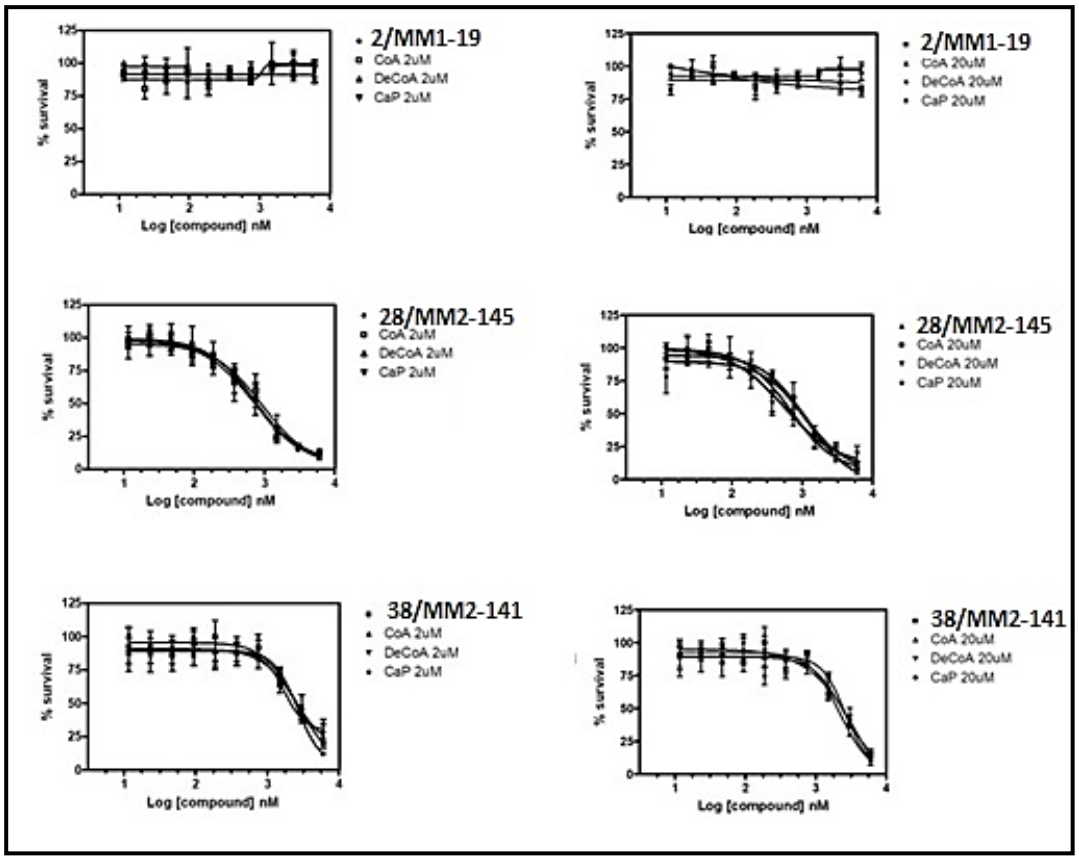

Figure 3.5: The chemical rescue assay with supplementation of 2 μM CoA for compounds **2/MM1-19, 28/MM2-145** and **38/MM2-141**

As the high concentrations of CoA, pantothenate and DeCoA have previously been used to successfully rescue the parasite from compounds inhibitory effects, the failure to negate the effects of the test compounds implies that they do not act along the CoA biosynthesis pathway.[213, 218, 219] As DeCoA was intended to further ascertain

that *Pf*PPAT and/or DeCoA kinase are possible targets, its inability to rescue the parasite implies that *Pf*PPAT is not the target of these compounds.

The bacterial and the *P. falciparum* PPAT are divergent at the sequence level and while the described chemotypes showed activity against bacterial PPAT, it is possible that they do not bind to *Pf*PPAT.[175-177] The putative *Pf*PPAT sequence found on the PlasmoDB (the database of *Plasmodium* genome) was insufficiently homologous with bacterial PPAT to build a homology model and thus guide the design of the inhibitors. This was observed during an attempt to build a homology model with the Schrodinger suite with many gaps in modelled protein. This highlighted the key differences that exist and meant that the homology model generated would not have given an adequate prediction of the secondary structures such as the helices and the loops will not be feasible. Furthermore, there are no established assays that can be used to study the *Plasmodium* enzymes along the CoA biosynthesis pathway except the first enzyme PanK. This makes the study of specific CoA biosynthesis pathway enzymes targeted by novel antimalarials challenging. The failure to rescue the parasite from inhibition effect with the CoA biosynthesis pathway metabolites prompted an investigation of the possible target pathways. This was accomplished by the use of targeted hydrophilic metabolomics described in the next section.

3.4. Metabolomics studies

Metabolomics has recently been used in antimalarial drug discovery to study the target pathways upon which novel antimalarials with unknown mechanisms act.[132, 223, 224] The metabolomics profile resulting from treatment with antimalarials can provide a comprehensive analysis of potential pathways targeted by a compound of interest. This is presented as a metaprint that can be a unique metabolite phenotype for the test compound.[127] This has helped reveal pathways targeted by different antimalarial compounds. This metabolomics approach was therefore used to investigate the pathway/s targeted by compounds **2/MM1-19**, **28/MM2-145** and **38/MM2-141** (**Fig. 3.6**).

Separate treatment of the *Pf*3D7 parasites with the Ugi compound **2/MM1-19** and triazolopyrimidine boc-protected compound **38/MM2-141** caused an increase in the pyrimidine biosynthesis precursors *N*-carbamoyl-L-aspartate (*N*-Carb-Asp) and dihydroorotate (DHO) (**Fig. 3.6**). These compounds also caused a marked decrease in peptides, suggesting that they also act in the peptide catabolism pathway. This

phenotype implies that the compounds have another target that is not involved in pyrimidine biosynthesis. Disruption of haemoglobin catabolism was observed to be indicative of a decrease in peptides, and this suggests that the compounds affect haemoglobin metabolism.[127, 223] The breakdown of peptides is important to provide the parasite with amino acids. The decrease in peptides prompted an investigation into the potential of these compounds as beta-hematin inhibitors. The beta-hematin inhibition assay is based on the use of beta-hematin (synthetic hemozoin) to mimic the inhibition of hemozoin formation in the parasite. Hemozoin formation, a validated target for *P. falciparum*, can be disrupted by compounds such as chloroquine.[225] The data showed the IC_{50}'s for **2/MM1-19** and **38/MM2-141** were 1541 and 194 μM, respectively, for beta-hematin inhibition compared to 15 μM for chloroquine (**Fig. 3.7**). This suggests that **2/MM1-19** is not a beta-hematin inhibitor whereas **38/MM2-141** is a weak inhibitor. Thus, the inhibition of beta-hematin formation by **38/MM2-141** may be a contributing mechanism amongst other possible modes of action.

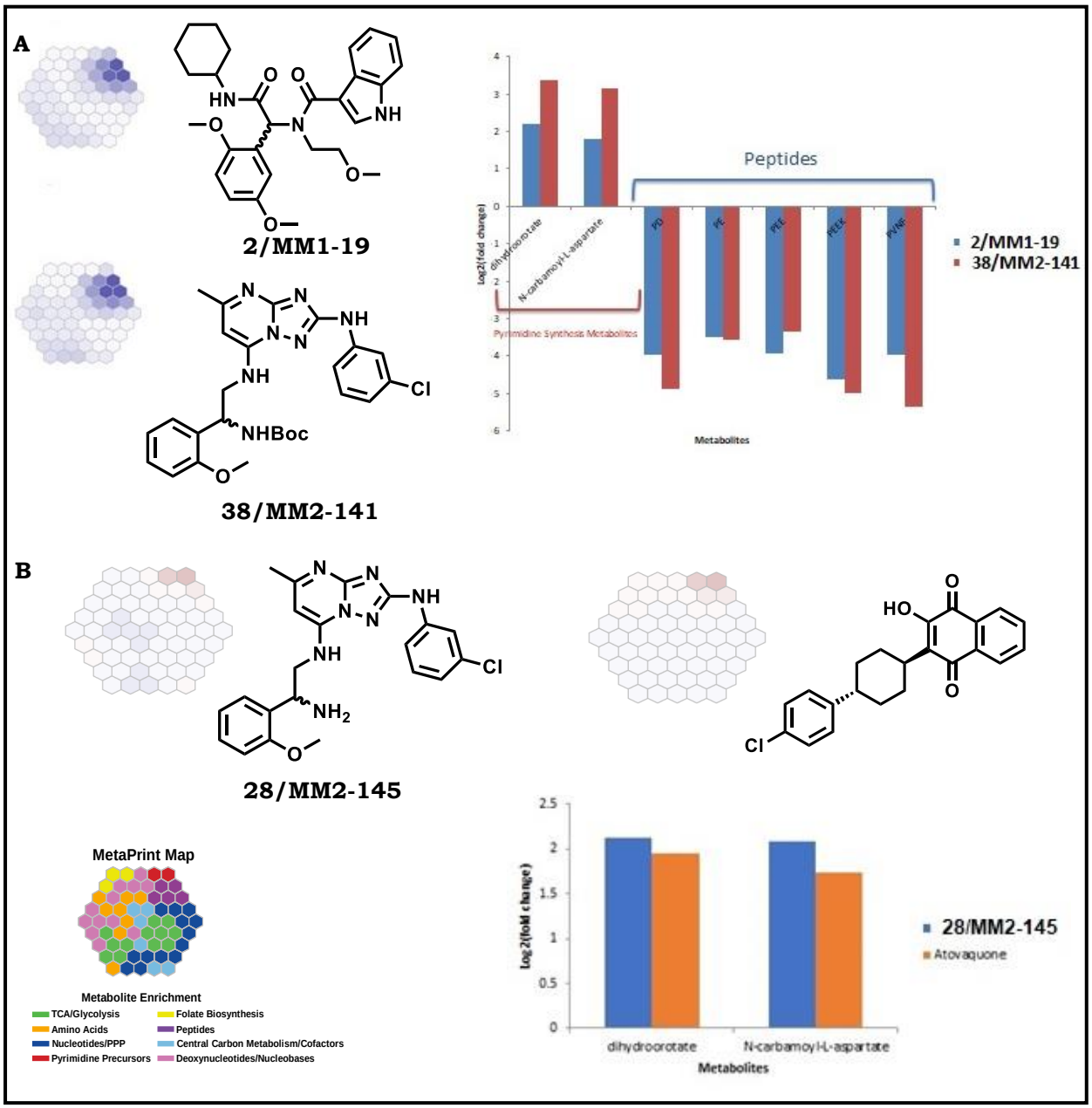

Figure 3.6: Metabolomics data of 4′-phosphopantetheine adenylyltransferase (PPAT) inhibitors **2/MM1-19**, **38/MM2-141** (**A**), and **28/MM2-145** (**B**)

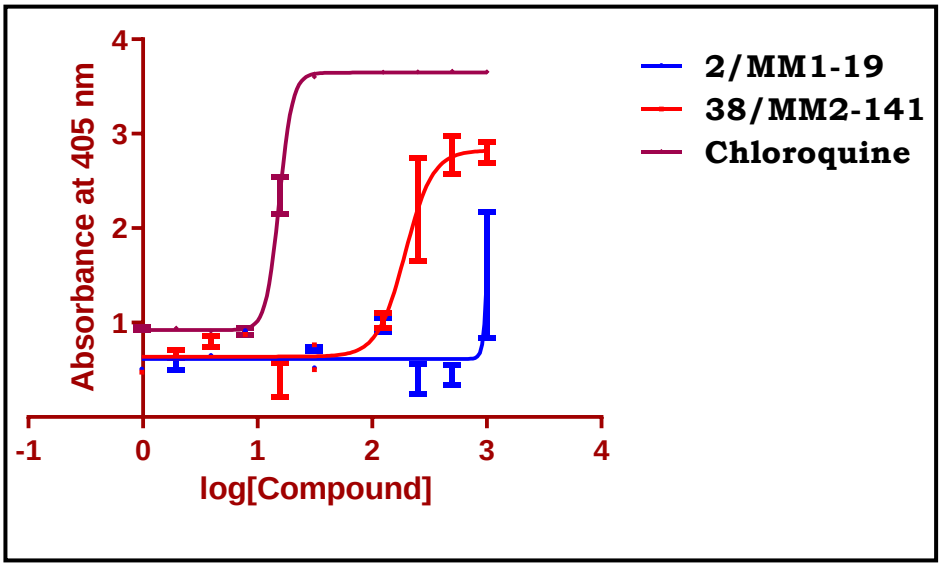

Figure 3.7: Beta-hematin inhibition assay results

The metabolomic profile of triazolopyrimidine amine **28/MM2-145** showed similar metabolic perturbation associated with atovaquone which involves an increase in metabolites *N*-Carb-Asp and DHO, and the latter disrupts the mitochondrial electron transport chain (mtETC) by inhibiting the *Plasmodium* bc_1 complex.[226] Furthermore, atovaquone previously showed an increase in the pyrimidine biosynthesis precursors *N*-Carb-Asp and DHO as a result of indirect inhibition of dihydroorotate dehydrogenase following its action on the bc_1 complex.[127] Although the metabolic signature of compound **28/MM2-145** matches that of atovaquone and the exact target remains unknown, this metabolomic profile implicates also the pyrimidine biosynthesis pathway. Unlike compound **38/MM2-141**, compound **28/MM2-145** did not appear to act on the peptide catabolism pathway. The log2-fold changes of the pyrimidine precursors resulting from **28/MM2-145** and **38/MM2-141** were comparable.

These data support the chemical rescue findings that showed that the compounds do not act along CoA biosynthesis pathway nor any of its metabolizing pathways. The metabolomic signatures suggest the two main targeted pathways involve pyrimidine biosynthesis and peptide catabolism. The triazolopyrimidine compounds **28/MM2-145** and **38/MM2-141** bear a similar core scaffold as the advanced triazolopyrimidine clinical candidate **DSM265**. The latter has a similar metaprint as atovaquone and is associated with large increases in *N*-Carb-Asp and DHO, implying that it also targets the pyrimidine biosynthesis pathway.[127] **DSM265**, on the other

hand, is a direct inhibitor of *Pf* mitochondrial dihydroorotate dehydrogenase (*Pf*DHODH) (**Fig. 3.8**) and its metaprint shows an interlink between mtETC and pyrimidine biosynthesis.[227, 228] *Pf*DHODH has demonstrated potential as an antimalarial target following its significance in the binding of the developmental antimalarials with the triazolopyrimidine core. This enzyme is essential in that it cannot be bypassed during the pyrimidine biosynthesis. Pyrimidine is important in that it is an essential precursor for DNA and RNA biosynthesis. Thus, the inhibition of this *Pf*DHODH will incapacitate the parasite and lead to its death. Furthermore, given that DNA and RNA are required throughout stages of parasite development, this enzyme can lead to multi-stage activity of the potential *Pf*DHODH inhibitors. This implies that the target of **28/MM2-145** is likely along the pyrimidine biosynthesis pathway and/or mtETC. To reconcile this result with the hypothesis that the triazolopyrimidine compounds may be repositioned as *Pf*PPAT inhibitors requires target identification to be undertaken on more potent compounds. Docking studies of **28/MM2-145** failed to have it fit into *Pf*DHODH binding pocket, though it does not rule out that the increase in pyrimidine biosynthesis precursors would be a potential mechanism of action.

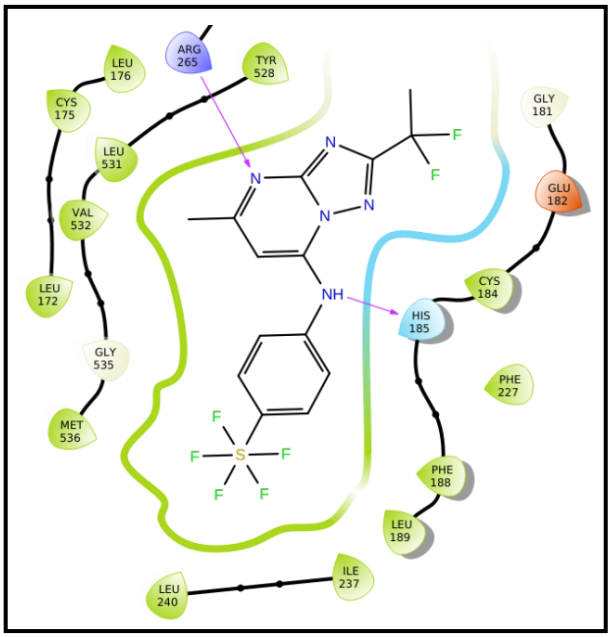

Figure 3.8: 2-D representation of **DSM265** in *Pf*DHODH (PDB: 4RX0) and key interactions

A recent study of pantothenamides proposed to target the CoA biosynthesis pathway through inhibition of PanK revealed that other CoA antimetabolites are formed acting

downstream. Metabolomic data revealed that the pathway forms pantothenamide-CoA-conjugates that block acetyl-CoA synthetase.[147] Contrary to the initial proposal, the lack of direct inhibition of the enzymes along the CoA biosynthesis pathway by pantothenamides prompts a detailed investigation into the target of the current triazolopyrimidine series. This will delineate whether or not the metabolic perturbations observed are a likely consequence of indirect effects and future work on more potent compounds should focus on the *in vitro* selection of resistance to identify genetic changes that will implicate target proteins.

3.5. Conclusion

This study showed that only one hit from the Ugi series of the four hits from the Ugi and cyclohexyl pyrimidine series MTS was validated with respect to antiplasmodium activity, albeit with lower activity than initially found (IC_{50} = 2.8 μM vs 5.2 μM). The SAR exploration based on this hit resulted in compounds with loss of antiplasmodium activity at the maximum concentration tested, IC_{50} >6 μM. One of the enantiomers of this compound showed similar antiplasmodium activity (IC_{50} 5.4 μM vs 5.2 μM). From the azabenzimidazole, triazolopyrimidinone and triazolopyrimidine compounds structurally related to those reported by Novartis, a triazolopyrimidine hit with an IC_{50} = 2.2 μM was identified, and SAR was derived based on this hit, which resulted in compounds with low to complete loss of antiplasmodium activity (IC_{50}'s = 4.5 to >6 μM). The chemical rescue experiment for the Ugi series hit and two triazolopyrimidine compounds did not support the compounds acting along the CoA biosynthesis pathway. Support was also not provided by metabolomics studies that showed that the compounds effected an increase in pyrimidine biosynthesis precursors and a decrease in peptides. Overall, the study presented in this chapter shows that the Ugi, cyclohexyl pyrimidine, azabenzimidazole, triazolopryimidinone and triazolopyrimidine series of compounds are not acting along the CoA biosynthesis pathway in *P. falciparum* like in bacteria.

3.7. References

1. Verlinden, B. K.; Niemand, J.; Snyman, J.; Sharma, S. K.; Beattie, R. J.; Woster, P. M.; Birkholtz, L.-M., Discovery of Novel Alkylated (bis)Urea and (bis)Thiourea Polyamine Analogues with Potent Antimalarial Activities. *J. Med. Chem.* **2011**, *54* (19), 6624-6633.

2. Sinha, S.; Sarma, P.; Sehgal, R.; Medhi, B., Development in Assay Methods for In Vitro Antimalarial Drug Efficacy Testing: A Systematic Review. *Front. Pharmacol.* **2017**, *8* (754), 1-14.

3. Lappin, A. F. S. L. Biochemistry, Lactate Dehydrogenase. https://www.ncbi.nlm.nih.gov/books/NBK557536/ (accessed 28 October 2021).

4. Bevan, C. D.; Lloyd, R. S., A High-Throughput Screening Method for the Determination of Aqueous Drug Solubility Using Laser Nephelometry in Microtiter Plates. *Anal. Chem.* **2000**, *72* (8), 1781-1787.

5. Andrew Somogyi, F. B., David Foster, Inside the isomers: the tale of chiral switches. *Aust. Prescr.* **2004**, *27* (2), 109-113.

6. Mwamwitwa, K. W.; Kaibere, R. M.; Fimbo, A. M.; Sabitii, W.; Ntinginya, N. E.; Mmbaga, B. T.; Shewiyo, D. H.; Shearer, M. C.; Smith, A. D.; Kaale, E. A., A retrospective cross-sectional study to determine chirality status of registered medicines in Tanzania. *Sci. Rep.* **2020**, *10* (1), 17834.

7. Long, A. S.; Zhang, A. D.; Meyer, C. E.; Egilman, A. C.; Ross, J. S.; Wallach, J. D., Evaluation of Trials Comparing Single-Enantiomer Drugs to Their Racemic Precursors: A Systematic Review. *JAMA Netw. Open* **2021**, *4* (5), e215731.

8. Mannschreck, A.; Kiesswetter, R.; von Angerer, E., Unequal Activities of Enantiomers via Biological Receptors: Examples of Chiral Drug, Pesticide, and Fragrance Molecules. *J. Chem. Educ.* **2007**, *84* (12), 2012.

9. Lipinski, C. A., Overview of Hit to Lead: The Medicinal Chemist's Role from HTS Retest to Lead Optimization Hand Off. In *Topics in Medicinal Chemistry* M.M., H., Ed. Springer: Berlin, 2009; Vol. 5, pp 1-24.

10. Hughes, J. P.; Rees, S.; Kalindjian, S. B.; Philpott, K. L., Principles of early drug discovery. *Br. J. Pharmacol.* **2011**, *162* (6), 1239-1249.

11. Roy, A., Early Probe and Drug Discovery in Academia: A Minireview. *High-Throughput* **2018**, *7* (1), 4.

12. Moffat, J. G.; Vincent, F.; Lee, J. A.; Eder, J.; Prunotto, M., Opportunities and challenges in phenotypic drug discovery: an industry perspective. *Nat. Rev. Drug Discov* **2017**, *16* (8), 531-543.

13. de Jonge, B. L.; Walkup, G. K.; Lahiri, S. D.; Huynh, H.; Neckermann, G.; Utley, L.; Nash, T. J.; Brock, J.; San Martin, M.; Kutschke, A., Discovery of inhibitors of 4′-phosphopantetheine adenylyltransferase (PPAT) to validate PPAT as a target for antibacterial therapy. *Antimicrob. Agents Chemother.* **2013**, *57* (12), 6005-6015.

14. Moreau, R. J.; Skepper, C. K.; Appleton, B. A.; Blechschmidt, A.; Balibar, C. J.; Benton, B. M.; Drumm III, J. E.; Feng, B. Y.; Geng, M.; Li, C., Fragment-based drug discovery of inhibitors of phosphopantetheine adenylyltransferase from gram-negative bacteria. *J. Med. Chem.* **2018**, *61* (8), 3309-3324.

15. Skepper, C. K.; Moreau, R. J.; Appleton, B. A.; Benton, B. M.; Drumm III, J. E.; Feng, B. Y.; Geng, M.; Hu, C.; Li, C.; Lingel, A., Discovery and Optimization of Phosphopantetheine Adenylyltransferase Inhibitors with Gram-Negative Antibacterial Activity. *J. Med. Chem.* **2018**, *61* (8), 3325-3349.

16. Butterworth, A. S.; Skinner-Adams, T. S.; Gardiner, D. L.; Trenholme, K. R., Plasmodium falciparum gametocytes: with a view to a kill. *Parasitology* **2013**, *140* (14), 1718-1734.

17. Lucantoni, L.; Avery, V., Whole-cell in vitro screening for gametocytocidal compounds. *Future Med. Chem.* **2012**, *4* (18), 2337-2360.

18. Burrows, J. N.; Duparc, S.; Gutteridge, W. E.; van Huijsduijnen, R. H.; Kaszubska, W.; Macintyre, F.; Mazzuri, S.; Möhrle, J. J.; Wells, T. N., New developments in anti-malarial target candidate and product profiles. *Malar. J.* **2017**, *16* (1), 26.

19. Fletcher, S.; Lucantoni, L.; Sykes, M. L.; Jones, A. J.; Holleran, J. P.; Saliba, K. J.; Avery, V. M., Biological characterization of chemically diverse compounds targeting the Plasmodium falciparum coenzyme A synthesis pathway. *Parasites Vectors* **2016**, *9* (1), 589.

20. van der Watt, M. E.; Reader, J.; Churchyard, A.; Nondaba, S. H.; Lauterbach, S. B.; Niemand, J.; Abayomi, S.; van Biljon, R. A.; Connacher, J. I.; van Wyk, R. D. J.; Le Manach, C.; Paquet, T.; González Cabrera, D.; Brunschwig, C.; Theron, A.; Lozano-Arias, S.; Rodrigues, J. F. I.; Herreros, E.; Leroy, D.; Duffy, J.; Street, L. J.; Chibale, K.; Mancama, D.; Coetzer, T. L.; Birkholtz, L.-M., Potent Plasmodium falciparum gametocytocidal compounds identified by exploring the kinase inhibitor chemical space for dual active antimalarials. *J. Antimicrob. Chemother.* **2018**, *73* (5), 1279-1290.

21. Reader, J.; Botha, M.; Theron, A.; Lauterbach, S. B.; Rossouw, C.; Engelbrecht, D.; Wepener, M.; Smit, A.; Leroy, D.; Mancama, D.; Coetzer, T. L.;

Birkholtz, L.-M., Nowhere to hide: interrogating different metabolic parameters of Plasmodium falciparum gametocytes in a transmission blocking drug discovery pipeline towards malaria elimination. *Malar. J.* **2015**, *14* (1), 213.

22. Yeh, E.; DeRisi, J. L., Chemical rescue of malaria parasites lacking an apicoplast defines organelle function in blood-stage Plasmodium falciparum. *PLoS Biol* **2011**, *9* (8), e1001138.

23. Wu, W.; Herrera, Z.; Ebert, D.; Baska, K.; Cho Seok, H.; DeRisi Joseph, L.; Yeh, E., A Chemical Rescue Screen Identifies a Plasmodium falciparum Apicoplast Inhibitor Targeting MEP Isoprenoid Precursor Biosynthesis. *Antimicrob. Agents Chemother.* **2015**, *59* (1), 356-364.

24. Fletcher, S.; Avery, V. M., A novel approach for the discovery of chemically diverse anti-malarial compounds targeting the Plasmodium falciparum Coenzyme A synthesis pathway. *Malar. J.* **2014**, *13* (1), 343.

25. Spry, C.; Chai, C. L.; Kirk, K.; Saliba, K. J., A class of pantothenic acid analogs inhibits Plasmodium falciparum pantothenate kinase and represses the proliferation of malaria parasites. *Antimicrob. Agents Chemother.* **2005**, *49* (11), 4649-4657.

26. Guan, J.; Spry, C.; Tjhin, E. T.; Yang, P.; Kittikool, T.; Howieson, V. M.; Ling, H.; Starrs, L.; Duncan, D.; Burgio, G.; Saliba, K. J.; Auclair, K., Exploring Heteroaromatic Rings as a Replacement for the Labile Amide of Antiplasmodial Pantothenamides. *J. Med. Chem.* **2021**, *64* (8), 4478-4497.

27. Hart, R. J.; Abraham, A.; Aly, A. S., Genetic characterization of coenzyme A biosynthesis reveals essential distinctive functions during malaria parasite development in blood and mosquito. *Front. Cell. Infect. Microbiol.* **2017**, *7*, 260.

28. Swift, R. P.; Rajaram, K.; Liu, H. B.; Prigge, S. T., Dephospho-CoA kinase, a nuclear-encoded apicoplast protein, remains active and essential after Plasmodium falciparum apicoplast disruption. *Embo j* **2021**, *40* (16), e107247.

29. De Villiers, M.; Strauss, E., Metabolism: jump-starting CoA biosynthesis. *Nat. Chem. Biol.* **2015**, *11* (10), 757-758.

30. Murithi, J. M.; Owen, E. S.; Istvan, E. S.; Lee, M. C. S.; Ottilie, S.; Chibale, K.; Goldberg, D. E.; Winzeler, E. A.; Llinás, M.; Fidock, D. A.; Vanaerschot, M., Combining Stage Specificity and Metabolomic Profiling to Advance Antimalarial Drug Discovery. *Cell Chem Biol* **2020**, *27* (2), 158-171.

31. Yu, X.; Feng, G.; Zhang, Q.; Cao, J., From Metabolite to Metabolome: Metabolomics Applications in Plasmodium Research. *Front. Microbiol.* **2021**, *11* (3375), 1-13.

32. Cobbold, S. A.; Chua, H. H.; Nijagal, B.; Creek, D. J.; Ralph, S. A.; McConville, M. J., Metabolic dysregulation induced in Plasmodium falciparum by dihydroartemisinin and other front-line antimalarial drugs. *J. Infect. Dis.* **2016**, *213* (2), 276-286.

33. Allman, E. L.; Painter, H. J.; Samra, J.; Carrasquilla, M.; Llinás, M., Metabolomic profiling of the malaria box reveals antimalarial target pathways. *Antimicrob. Agents Chemother.* **2016**, *60* (11), 6635-6649.

34. Sandlin, R. D.; Fong, K. Y.; Wicht, K. J.; Carrell, H. M.; Egan, T. J.; Wright, D. W., Identification of β-hematin inhibitors in a high-throughput screening effort reveals scaffolds with in vitro antimalarial activity. *Int J Parasitol Drugs Drug Resist* **2014**, *4* (3), 316-325.

35. Birth, D.; Kao, W.-C.; Hunte, C., Structural analysis of atovaquone-inhibited cytochrome bc1 complex reveals the molecular basis of antimalarial drug action. *Nat. Commun.* **2014**, *5* (1), 4029.

36. A Phillips, M.; K Rathod, P., Plasmodium dihydroorotate dehydrogenase: a promising target for novel anti-malarial chemotherapy. *Infect. Disord.: Drug Targets* **2010**, *10* (3), 226-239.

37. Phillips, M. A.; Lotharius, J.; Marsh, K.; White, J.; Dayan, A.; White, K. L.; Njoroge, J. W.; El Mazouni, F.; Lao, Y.; Kokkonda, S., A long-duration dihydroorotate dehydrogenase inhibitor (DSM265) for prevention and treatment of malaria. *Sci. Transl. Med.* **2015**, *7* (296), 296ra111.

38. Schalkwijk, J.; Allman, E. L.; Jansen, P. A.; De Vries, L. E.; Verhoef, J. M.; Jackowski, S.; Botman, P. N.; Beuckens-Schortinghuis, C. A.; Koolen, K. M.; Bolscher, J. M., Antimalarial pantothenamide metabolites target acetyl–coenzyme A biosynthesis in Plasmodium falciparum. *Sci. Transl. Med.* **2019**, *11* (510), eaas9917.

Chapter 4: Benzoxaboroles as antimalarial agents

4.1. Chapter overview

This chapter describes the *in vitro* antiplasmodium activity and solubility of benzoxaborole compounds, including details of the SAR analysis and cytotoxicity of selected compounds. Results from *in vitro* microsomal metabolic stability, metabolomics and cross resistance studies are also presented. The chapter also provides a retrospective analysis in an attempt to rationalize binding of the compounds in LeuRS based on molecular docking data.

4.2. *In vitro* antiplasmodium activity, solubility and cytotoxicity of benzoxaborole compounds designed as penicillin-binding protein-3 (PBP-3) inhibitors

In vitro antiplasmodium activity screening was carried out at UCT in H3D, the University of Pretoria (UP), and the Swiss Tropical and Public Health Institute (STPH; University of Basel, Switzerland). The assay performed at H3D is described in **Chapter 3**, **section 3.2**. Screening performed at UP made use of SYBR Green DNA binding dye.[200] This assay exploits the fact that proliferating parasites containing DNA can be distinguished from mature erythrocytes that do not have DNA or RNA.[201] The DNA-bound SYBR Green emits light, and the fluorescence count can be plotted against the logarithm of a drug concentration to generate a dose-response curve from which the drug's IC_{50} can be calculated.[229] STPH uses the incorporation of [^{3}H]hypoxanthine into the parasite as a measure of parasite proliferation in blood culture. Malaria parasites are incapable of *de novo* synthesis of purines including hypoxanthine and rely exclusively on an exogenous supply.[201] As infected erythrocytes from the blood are incapable of synthesizing DNA, RNA, or peptides, only live parasites that continuously divide take up and incorporate [^{3}H]hypoxanthine. [^{3}H]Hypoxanthine incorporation measured using a liquid scintillation counter[201, 230] thus directly reflects the amount of parasite-infected erythrocytes.

As already stated in **Chapter 2 section 2.5.1**, **H3D-006145** (**43/MM2-92**) was identified from a series of antibacterial compounds designed as PBP-3 inhibitors. This compound also showed antiplasmodium activity against *P. falciparum* (IC_{50} =

1.06 µM) but showed no cytotoxicity against CHO or HepG2 mammalian cell lines at the maximum concentration tested (IC_{50} >50 µM). This compound became the basis of a formal hit assessment using the proposed SAR strategy depicted in **Fig. 4.1**.

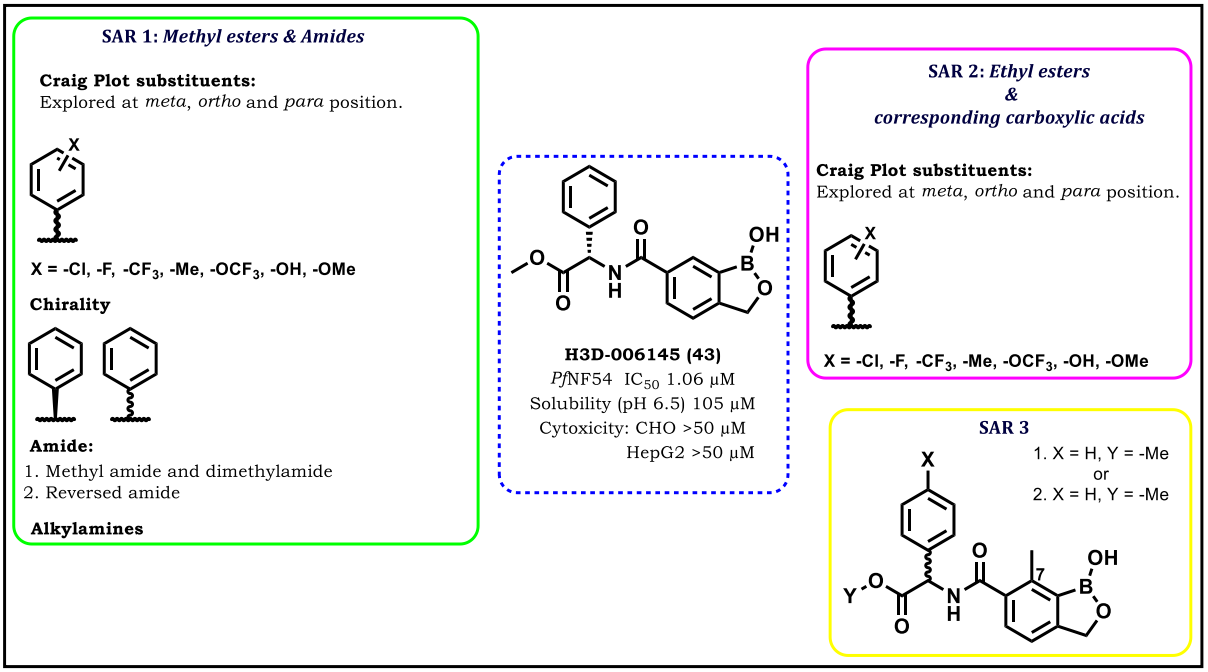

Figure 4.1: SAR design for compounds in the benzoxaboroles series

4.2.1 SAR1

SAR1 explores the effects of Craig plot substituents on the phenylglycine appendage (**Table 4.1**) and enantiomers (versus racemates) and the removal of the phenyl to produce alkylamine compounds (**Table 4.2**). The reversed amide (**Table 4.1**) was also synthesized to understand the effect of this change on activity relative to the racemate **45/MM2-91**. The methyl ester compounds **45/MM2-91**–**63/MM4-07** (**Table 4.1**) displayed low to high antiplasmodium activity against the chloroquine (CQ)-sensitive strain *Pf*NF54 (IC_{50} = 0.64–2.29 µM), except for **54/MM4-46**, **60/MM4-16**, and **62/MM4-12** which showed no activity (IC_{50} >6 µM) at the highest concentration tested. The *R*-enantiomer **83/MM2-90** (**Table 4.1**) and the racemate **45/MM2-91** displayed higher activity than **43/MM2-92** with *Pf*NF54 IC_{50} = 0.64 and 0.85 µM, respectively. This suggests that the putative target is enantioselective and the activity of the racemate may result from that of **83/MM2-90**. The racemic mixture **45/MM2-91** was further subjected to preparative chiral HPLC to obtain pure enantiomers **45A/MM2-224A** and **45B/MM2-224B**. Compounds **45A/MM2-224A** and **45B/MM2-224B** (**Table 4.2**) showed activities similar to those of **83/MM2-90**

and **43/MM2-92**, with IC_{50} = 0.86 and 1.12 μM, respectively. The reversal of the amide in compound **44/MM4-26** was detrimental to activity with *Pf*NF54 IC_{50} = 4.5 μM.

In terms of solubility, compounds **43/MM2-92**, **45/MM2-91**, and **83/MM2-90** displayed high solubility (164, 150, and 200 μM, respectively). The compounds bearing *ortho*-trifluoromethyl (**60/MM4-16**) and -chloride (**63/MM4-07**) groups were also more soluble than the *meta* and *para* regioisomers. Benzoxaboroles have previously been reported to exist in equilibrium at physiological pH between boron-hydrated sp^3 and non-hydrated sp^2 forms, with pKa = 7.[231, 232] This suggests that benzoxaboroles are water-soluble. However, the solubility of these compounds in aqueous media is likely to be influenced by the phenylglycine substituent. In this regard and as expected, lipophilic substituents such as trifluoromethyl in **60/MM4-16** and chloride in **63/MM4-07** are likely responsible for the low aqueous solubility observed. Removal of the phenylglycine in the alkyl series of compounds **84/MM2-124**–**87/MM2-44** (**Table 4.2**) was detrimental to activity (IC_{50} > 6 μM) and compound **88/MM2-130** comprising phenylglycinol was also inactive with IC_{50} > 6 μM. This suggests that the phenylglycine appendage with the carboxylic acid or the ester, the latter seen for **88/MM2-130**, is essential for this series of benzoxaboroles. Replacement with phenyl (**90/MM3-85**) or pyrazine (**91/MM3-11**), and addition of the spacer in phenylalanine (**92/MM3-42**) and tyrosine (**93/MM3-10**) did not result in compounds with greater activity (all IC_{50} > 6 μM) (**Table 4.2**). Compounds **91/MM3-11** and **93/MM3-10** showed high antiplasmodium activity when screened at STPH with IC_{50} = 0.52 and 0.93 μM, respectively. This difference may be due to different screening conditions as already indicated the assay conducted at UCT is based on LDH measurement while that at STPH is based on the quantification of [^{3}H]hypoxanthine incorporation.

Table 4.1: *In vitro Pf*NF54 and *Pf*K1 antiplasmodium activity, solubility and cytotoxicity of the benzoxaboroles series (SAR1)

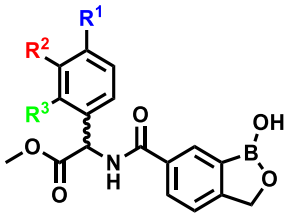

				[a]IC50 (µM) vs *Pf*NF54/K1 (in parentheses)	Solubility at pH 6.5 (µM)*	[b]Cytotoxicity in CHO (µM) and HepG2 (%)	[c]Selectivity index
Number/Code	**R1**	**R2**	**R3**				
45/MM2-91	H	H	H	0.85 [d](0.206)	150	>50	59
46/MM2-174	-Me	H	H	2.41 [d](1.13)	90	>50	
47/MM2-196	H	-Me	H	1.47	[e]N.D	>50	
48/MM4-81	H	H	-Me	2.83	60	13	
49/MM2-201	-F	H	H	0.72 [d](0.215)	120	>50	69
50/MM4-44	H	-F	H	1.39	130	>50	
51/MM4-64	H	H	-F	1.74		>50	
52/MM3-160	-OMe	H	H	1.19 [d](0.820)	*80	>50	
53/MM4-15	H	-OMe	H	2.38	75	>50	
54/MM4-46	H	H	-OMe	>6	125	>50	
55/MM3-8	-OH	H	H	2.22 [d](0.411)	*120	>50	
56/MM4-101	H	-OH	H	0.598/1.28	*160	12	
57/MM4-108	H	H	-OH	5.32	N.D	>50	
58/MM3-9	$-CF_3$	H	H	2.29 [d](0.910)	30	>50	
59/MM4-14	H	$-CF_3$	H	>6	*40	>50	
60/MM4-16	H	H	$-CF_3$	>6 [d](0.934)	160	>50	
61/MM3-175	-Cl	H	H	1.28/2.27	125	>50	
62/MM4-12	H	-Cl	H	>6	70	>50	
63/MM4-07	H	H	-Cl	2.07	140	>50	

44/MM4-26	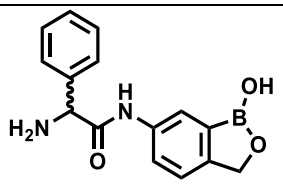	4.5/>6	140	>50	

[a]Mean values from n = 2 determinations. Chloroquine and artesunate were used as controls with the standard *Pf*NF54 IC_{50} values of 0.016 µM and 0.004 µM, respectively. [b]Cytotoxicity was evaluated in mammalian CHO as IC_{50} values in µM and HepG2 cells at a concentration of 2 µM for one biological replicate and technical duplicates and is reported as percentage inhibition. [c]Selectivity index is the ratio of CHO IC_{50} to *Pf*NF54 IC_{50}. [d]Data from STPH. [e]N.D, not determined. *Turbidimetric solubility.

Table 4.2: *In vitro Pf*NF54 and *Pf*K1 antiplasmodium activity, solubility and cytotoxicity of the benzoxaboroles series (SAR1)

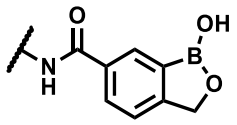

Number/Code		**[a]IC_{50} (µM) vs *Pf*NF54/K1 (in parentheses)**	**Solubility at pH 6.5 (µM)***	**[b]Cytotoxicity in CHO (µM) and HepG2 (%)**	**[c]Selectivity index**
43/MM2-92	-PhCHCOOCH$_3$ (*S*)	1.06	164	>50	>47
83/MM2-90	-PhCHCOOCH$_3$ (*R*)	0.64/3.88	200	>50	>50
45A/ MM2-224A	-PhCHCOOCH$_3$ (*S*) chiral col	0.864 [d](0.207)/ 1.89	[e]N.D	>50	>78
45B/ MM2-224B	-PhCHCOOCH$_3$ (*R*) Chiral col	1.12 [d](0.266)/ 2.67	N.D	>50	>45
84/MM2-124	-$CH_2CH_2C(CH_3)_2OH$	>6	20	>50	
85/MM2-123	-$CH_2CH_2CH(CH_3)OH$	>6	<5	N.D	
86/MM2-119	-$CH_2CH_2OCH_3$	>6	<5	N.D	
87/MM2-44	-CH_2CF_3	>6	<5	N.D	
88/MM2-130	-$PhCH_2OH$	>6	<5	N.D	
89/MM2-165	-$CHC_6H_{11}COOCH_3$	>6	20	N.D	
90/MM3-85	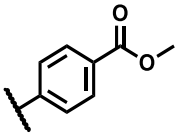	>6 [d](>10)	80	>50	

91/MM3-11	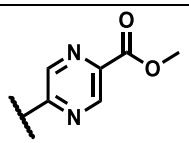	>6 [d](0.519)	160	>50	
92/MM3-42	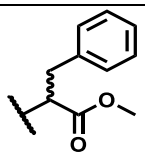	5.52	190	>50	
93/MM3-10	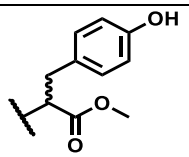	>6 [d](0.934)	>200	>50	

[a]Mean values from n = 2 determinations. Chloroquine and artesunate were used as controls with the standard *Pf*NF54 IC_{50} values of 0.016 µM and 0.004 µM, respectively. [b]Cytotoxicity was evaluated in mammalian CHO as IC_{50} values in µM and HepG2 cells at a concentration of 2 µM for one biological replicate and technical duplicates and is reported as percentage inhibition. [c]Selectivity index is the ratio of CHO IC_{50} to *Pf*NF54 IC_{50}. [d]Data from STPH. [e]N.D, not determined. *Turbidimetric solubility.

4.2.2 SAR2

SAR2 assesses corresponding ethyl esters from the Craig plot substituents series and their carboxylic acid matched-pairs from SAR1 (**Table 4.3**). Ethyl esters **64/MM3-57** – **71/MM4-55** showed lower antiplasmodium activity (*Pf*NF54 IC_{50} = 1.21–3.97 µM) than their methyl ester counterparts. Selected compounds (**66/MM4-93** – **68/MM4-105**) were also screened against the CQ-resistant *Pf*K1 strain and displayed lower activities (IC_{50} = 1.47–8.73 µM). The carboxylic acid matched-pairs showed the highest activity out of the compounds explored in this series (*Pf*NF54 IC_{50} = 0.121–2.86 µM). Compound **73/MM2-177** was the most active with the *para* methyl substituent showing the greatest activity against the CQ-sensitive strain *Pf*NF54 (IC_{50} = 0.121 µM). However, the *meta*- and *ortho*-methyl regioisomers (**74/MM4-134** and **75/MM4-137**, respectively) showed loss of activity (IC_{50} = 2.58 and 3.25 µM, respectively). In addition, these compounds were not active at the highest concentration tested against the CQ-resistant *Pf*K1 strain with IC_{50} >6 and 3.06 µM for **73/MM2-177** and **74/MM4-134**, respectively. The *meta*- chloro and fluoro compounds **77/MM4-127** and **79/MM4-89** also displayed high activity (*Pf*NF54 IC_{50}'s = 0.39 and 0.34 µM, respectively). These were also equipotent against CQ-resistant *Pf*K1 strain (IC_{50} = 0.39 and 0.48 µM, respectively). The benzoxaborole compounds comprising an amide were proposed to be hydrolyzed in *P. falciparum* by a putative esterase/amidase identified as prodrug activation and resistance esterase (*Pf*PARE).[172] *Pf*PARE cleaved the amide bond of the preclinical candidate **AN13762**

to the corresponding carboxylic acid **AN10248**, which was equipotent (**Fig. 4.2**). The data for the current series show that the carboxylic acid group confers activity that is two- and four-fold higher than that associated with a methyl and ethyl ester, respectively. Future work on this series should investigate whether esters are slowly hydrolyzed into corresponding carboxylic acids over time in a metabolite identification study. This will provide an understanding on whether a similar esterase/amidase activation effect previously reported also occurs for this series.

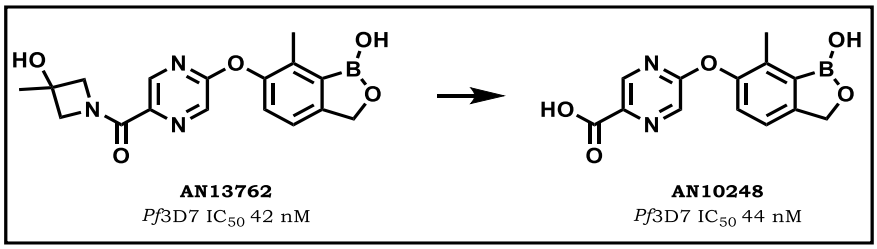

Figure 4.2: The structures and antiplasmodium activity of benzoxaboroles **AN13762** and **AN10248**

Table 4.3: *In vitro Pf*NF54 and *Pf*K1 antiplasmodium activity, solubility and cytotoxicity of the benzoxaboroles series (SAR2)

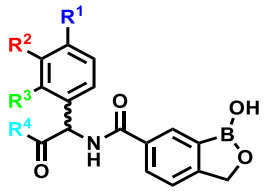

Number/Code	R^1	R^2	R^3	R^4	IC_{50} (µM) vs *Pf*NF54/K1 (in parentheses)[a]	Solubility at pH 6.5 (µM)*	[b]Cytotoxicity in CHO (µM) and HepG2 (%)	[c]Selectivity index
64/MM3-57	H	H	H	-OEt	1.21	60	>50	41
65/MM4-50	-Cl	H	H	-OEt	[e]3.34	*140	10	
66/MM4-93	H	-Cl	H	-OEt	[e]1.90/1.47	*80	9.3	
67/MM4-114	H	H	-Cl	-OEt	[e]3.97/8.73	*40	11	
68/MM4-105	H	-Me	H	-OEt	[e]1.65/2.12	120	14	
69/MM4-100	H	H	-Me	-OEt	>6	*80	18	
70/MM4-56	H	F	H	-OEt	[e]1.65	*40	8.6	
71/MM4-55	H	H	F	-OEt	[e]2.91	*160	9.3	
72/MM2-173	H	H	H	-OH	0.674	150	>50	74
73/MM2-177	-Me	H	H	-OH	0.121/>6 [d](0.199/0.253)	130	>50	>413
74/MM4-134	H	-Me	H	-OH	[e]2.575/3.057	140	14	

75/MM4-137	H	H	-Me	-OH	[e]3.25	120	[f]N.D	
76/MM4-86	-Cl	H	H	-OH	[e]0.931/2.135	*80	9	
77/MM4-127	H	-Cl	H	-OH	[e]0.399/0.385	*160	24	
78/MM4-136	H	H	-Cl	-OH	[e]1.74/2.858	*80	15	
79/MM4-89	H	-F	H	-OH	[e]0.344/0.475	*160	15	
80/MM4-87	H	H	-F	-OH	[e]1.97/2.77	N.D	20	
81/MM3-136	H	H	H	-NMe	[e]0.559/0.595	150	>50	
82/MM4-60	H	H	H	$-NMe_2$	>6/>6	135	N.D	

[a]Mean values from n = 2 determinations. Chloroquine and artesunate were used as controls with the standard *Pf*NF54 IC_{50} values of 0.016 µM and 0.004 µM, respectively. [b]Cytotoxicity was evaluated in mammalian CHO as IC_{50} values in µM and HepG2 cells at a concentration of 2 µM for one biological replicate and technical duplicates and it is reported as percentage inhibition. [c]Selectivity index = IC_{50} (CHO)/IC_{50} (*Pf*NF54). [d]Data from STPH. [e]Data from UP. [f]N.D, not determined. *Turbidimetric solubility.

4.2.3 SAR3

SAR3 interrogated the installation of the substituent on position-7 of the benzoxaborole core in line with other benzoxaboroles that show high antiplasmodium activity, including the recent preclinical candidate **AN13762** (**Fig. 4.2**).[156] The installation of the 7-methyl group resulted in abrogated activity relative to that of the methyl and ethyl esters and the corresponding carboxylic acids (**Table 4.4**). IC_{50} values against the CQ-sensitive strain *Pf*NF54 were between 1.33 and 4.03 µM, and between 1.97 and 2.86 µM in the drug-resistant strain *Pf*K1. The compounds in the series also showed high aqueous solubility (>160 µM) except for compound **95/MM4-144** (80 µM) likely due the lipophilicity imposed by the ethyl substituent. The overall good solubility observed for other compounds may result from the sp^3 hybridized 7-methyl substituent disrupting molecular planarity by twisting the carboxamide out of the plane from the benzoxaborole in addition to the effect resulting intrinsically from boron-hydration in aqueous media.[233]

Table 4.4: *In vitro* *Pf*NF54 and *Pf*K1 antiplasmodium activity, solubility and cytotoxicity of the 6-carboxy-7-methylbenzoxaboroles (SAR3)

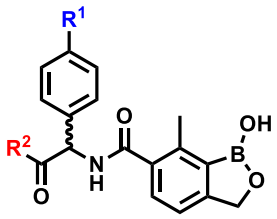

Number/Code	R^1	R^2	IC_{50} in *Pf*NF54 and *Pf*K1 (µM)[a]	[b]Solubility at pH 6.5 (µM)	[c]Cytotoxicity in HepG2 cells (%)
94/MM4-141	H	-OMe	1.33/2.86	160	22
95/MM4-144	-Me	-OEt	4.03/2.14	80	25
96/MM4-150	-Me	-OMe	3.72/1.97	160	22
97/MM4-148	-Me	-OH	>5/>5	140	19

[a]Mean values from n = 2 determinations from UP. Chloroquine and artesunate were used as controls with the standard *Pf*NF54 IC_{50} values of 0.016 µM and 0.004 µM, respectively. [b]Turbidimetric solubility. [c]Cytotoxicity was evaluated in mammalian HepG2 cells at a concentration of 2 µM for one biological replicate and technical duplicates and is reported as percentage inhibition.

4.3. *In vitro* gametocytocidal activity

The *in vitro* gametocytocidal assay employed in this study is described in **Chapter 3**, **section 3.2.3**. The series of benzoxaborole compounds in this study did not show inhibition of either early- nor late-stage gametocyte development at both 1 μM or 5 μM.

4.4. Cytotoxicity evaluation

Cytotoxicity was assessed in HepG2 (described in **Chapter 3**, **section 3.2**) and CHO cells assay. The latter is a gold-standard calorimetric cytotoxicity assay that correlates cell viability with the reduction of MTT salt (3-(4, 5-dimethylthiazolyl-2)-2, 5-diphenyltetrazolium bromide) to insoluble purple formazan crystals by oxidoreductases.[234] Using commercial solubilizing reagents for the assay (details provided in **Chapter 7**), formazan crystals are dissolved and absorbance is measured via spectrophotometry to provide data from which the IC_{50} of each compound can be determined.

The cytotoxicity (percentage inhibition) for the compounds assessed in HepG2 cells was between 9 and 11.3% (**Tables 4.1**–**4.4**). Compounds tested against CHO cells all showed IC_{50}'s >50 μM. Selectivity index (SI) was determined only for compounds where both the activity against the CQ-sensitive *Pf*NF54 IC_{50} and the IC_{50} value from CHO cytotoxicity assay are reported. SI was not determined for the compounds whose cytotoxicity values were reported from the HepG2 cytotoxicity assay as these are given in percentage inhibition. Compounds showed high SI ratios overall and this suggest this series of benzoxaboroles is selective for the parasite over mammalian cells.

4.4. Microsomal metabolic stability

Most drugs are metabolized after administration influencing the therapeutic level of the drug in the body. The liver is the primary organ of drug metabolism for the majority of drugs as it contains a variety of enzymes that induce biotransformations.[235] This impacts a drug's PK parameters such as its bioavailability, half-life, and clearance. Therefore, understanding drug metabolism and elimination pathways otherwise from the body is essential during the early drug discovery phase. To this end, the metabolic stability of a compound can be investigated using liver microsomes in an *in vitro* system to predict drug clearance *in*

vivo.[179] Liver microsomes are endoplasmic reticulum fractions that also contain ribosomes and are rich in CYP450 enzymes and esterases that are largely involved in drug metabolism.[236, 237] Microsomal stability studies were conducted at H3D for a selection of benzoxaboroles compounds, and the resulting data were used to determine projected half-life and *in vitro* intrinsic clearance (**Table 4.5**). These compounds were selected according to the following criteria: antiplasmodium activity in *Pf*NF54 IC_{50} <1 µM, CHO IC_{50} >50 µM or <50% inhibition of HepG2 at 2 µM, and solubility >50 µM.

Table 4.5: *In vitro* microsomal stability data of selected benzoxaborole compounds

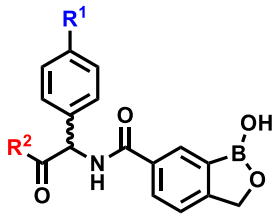

			Metabolic stability (% remaining after 30 min)	Projected $t_{1/2}$ (min)	Intrinsic clearance (CL_{int}, µL/min/mg)
Number/Code	**R¹**	**R²**	**H/R/M**	**H/R/M**	**H/R/M**
83/MM2-90	(*R*) H	-OMe	>99/90.3/89.1	>150/>150/>150	<11.6/<11.6/<11.6
45/MM2-91	H	-OMe	92.3/98.9/86.7	>150/145/>150	<11.6/<11.6/11.9
49/MM2-201	F	-OMe	97.2/94/86.9	>150/>150/>150	<11.6/<11.6/<11.6
72/MM2-173	H	-OH	90.5/89.8/90.1	>150/>150/>150	<11.6/<11.6/<11.6
73/MM2-177	-Me	-OH	90.6/91.8/96.5	148/>150/>150	<11.6/<11.6/11.7

H, Human; R, rat; M, mouse.

The methyl esters **45/MM2-91** and **49/MM2-201** showed similar microsomal stability to the carboxylic acids **72/MM2-173** and **73/MM2-177** in human microsomes. The *R*-enantiomer **83/MM2-90** showed excellent metabolic stability in human microsomes with >99% of the compound remaining after 30 min, which was higher than all other tested compounds. It also had a long projected half-life ($t_{1/2}$ > 150 min) and low intrinsic clearance (CL_{int} < 11.6 µL/min/mg) across all species. Conversely, carboxylic acids **72/MM2-173** and **73/MM2-177** were less stable in human microsomes with 90% of the compound remaining after 30 min. However, the differences were small, and all the compounds had high projected half-lives ($t_{1/2}$

≥ 148 and $t_{1/2}$ > 150 min) and intrinsic clearance (CL_{int} < 11.6 µL/min/mg) similar to those of the methyl ester series.

Methyl esters were less stable in mouse microsomes (87–89%) than the carboxylic acids (97–90%), suggesting that there are species differences with regard to microsomal metabolic stability.

4.5. Metabolomic studies

Compounds **45/MM2-91**, **49/MM2-201**, and **83/MM2-90** were selected for targeted metabolomic analysis of hydrophilic metabolites described in **Chapter 3 section 3.4** in order to understand the possible pathway(s) upon which benzoxaboroles act. The metaprints of compounds **45/MM2-91** and **83/MM2-90** showed weak signals of pyrimidine precursors and peptides, and folate biosynthesis, respectively (**Fig. 4.3**). Compound **49/MM2-201** showed weak signals of pyrimidine precursors, which is seen by the action of atovaquone in line with its MoA involving inhibition of electron transport that ultimately leads to pyrimidine biosynthesis.

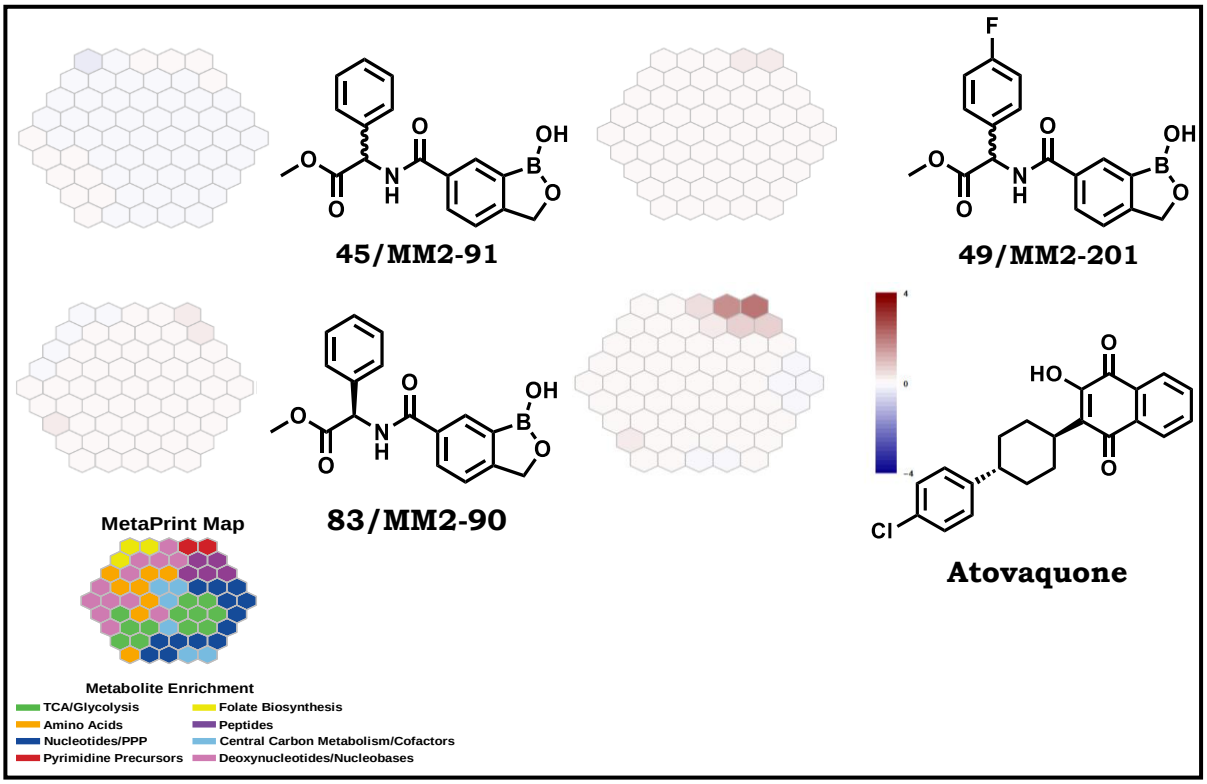

Figure 4.3: Metaprints of compounds **45/MM2-91**, **49/MM2-201**, **83/MM2-90**, and atovaquone

Benzoxaboroles act via a new MoA in the parasite by targeting multiple proteins, including the editing domain of LeuRS and the homolog of mammalian endonuclease CPSF3 which have previously been identified.[170, 172, 238] The former is involved in protein translation[153] while the latter carries out mRNA processing prior to exit from the nucleus.[239] These two processes are unlikely to yield specific metabolites and may result in broad signatures or low signals as observed in the compounds investigated here. Previous studies have revealed that compounds including antimalarials in clinical use (e.g., dihydroartemisinin) give low signals, resulting in ambiguous metabolic profiles and metaprints. These compounds are referred to as affecting an "unclassified" pathway because they do not cluster with known or defined pathways. They are thought to perturb broad biological processes such as translation and redox homeostasis, which do not result in definite metabolic changes recorded in the Metaprint assessments.

The benzoxaboroles under study potentially target a broad range of parasite metabolic processes and thus do not result in specific metabolic perturbations. Moreover, a limitation is that the metabolomic approach used in this study targets a dataset of known hydrophilic metabolites,[127] and benzoxaboroles may be inducing changes otherwise. As an alternative, the use of unbiased, untargeted metabolomics may provide more valuable insight into metabolites induced by benzoxaborole treatment.

4.6. Antiplasmodium activity against DNA-barcoded resistant mutant parasites

In vitro cross-resistance studies against DNA-barcoded *P. falciparum* resistant strains were conducted at the Wellcome Sanger Institute (United Kingdom). This newly developed assay can aid in identifying the target(s) or resistance mechanism(s) of novel antimalarials from the competitive growth of a pool of DNA-barcoded mutant *P. falciparum* lines derived from *in vitro* resistance selections or CRISPR editing. In this study, the pool comprised forty-two *Pf*3D7 or Dd2 mutant lines that were generated by inserting a 101-base pair barcode cassette into the non-essential *Pf*PARE locus using CRISPR/Cas9 gene editing technology. Treatment of this pool with the test compound at 3 × IC_{50} inhibits the growth of parasites in the pool, except for those with a resistant phenotype. At the end of the assay, barcoded lines that out-grow others in the pool relative to the untreated control are submitted for next-generation sequencing to identify the parasite line. The particular gene mutated in the resulting sequenced parasites is suggestive of the target.

Compound **45/MM2-91** showed no significant change (log-fold) in the count of barcodes for either *Pf*3D7 or Dd2 strains as the barcode proportions of the treated and untreated parasites were similar at day 14 of the assay (**Fig. 4.4**). These data suggest that this compound may be acting through a novel MoA and that the mechanism of action and/or resistance was not identified or not represented in the pool interrogated. The *P. falciparum* mRNA endonuclease cleavage and polyadenylation specificity factor 3 (*Pf*CPSF3) homolog has previously been suggested to be the target of benzoxaboroles, in addition to multiple proteins.[172, 238] However, the data show that the compound did not induce any significant log-fold change in the barcoded mutant line with the *Pf*CPSF3 mutation Y408S. The *Pf*CPSF3 mutations previously reported are T406I, Y408S, T409A, and D470N, raised from a benzoxaborole preclinical candidate **AN13762**.[172] There was no resistance to **45/MM2-91** in the presence of the mutant lines carrying the Y408S mutation and this suggests that there is no cross-resistance with **AN13762**, though it is possible that **45/MM2-91** inhibits *Pf*CPSF3 differently. That the pool did not show any resistant mutant lines resistant to compound **45/MM2-91** suggests that there is no cross-resistance with the current antimalarials and preclinical candidates represented by the pool.

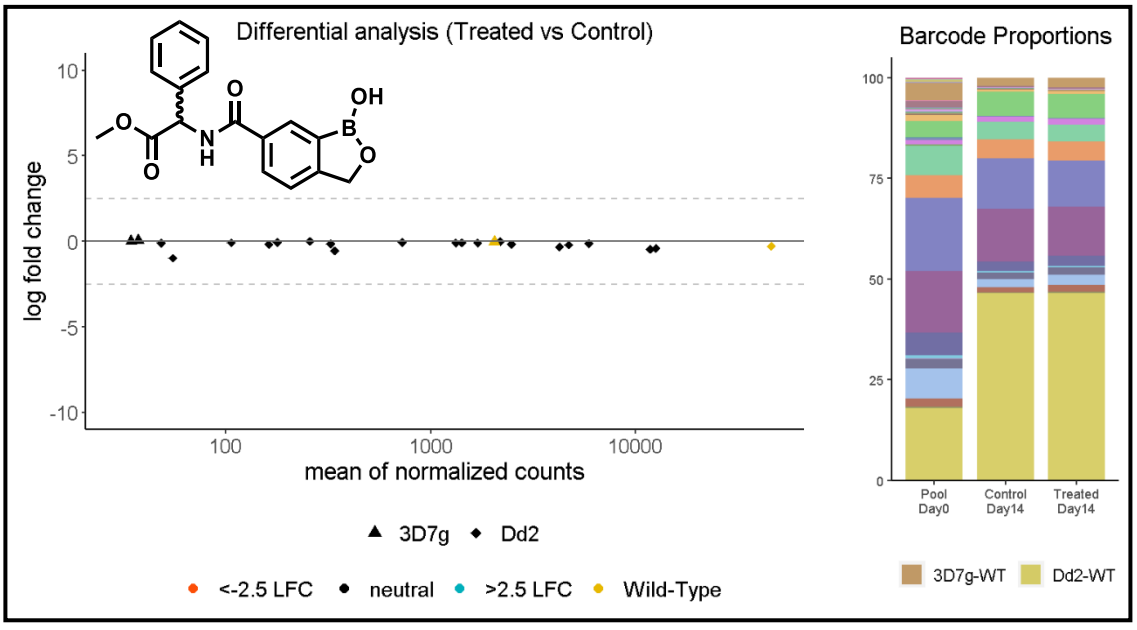

Figure 4.4: Barcoded library profile of **45/MM2-91**

4.7. Docking of benzoxaboroles in the *Pf*LeuRS editing domain

In addition to biological data, an attempt was made to rationalize the binding interactions of the compounds with the use of molecular docking in the *Pf*LeuRS editing domain. Sonoiki *et al.* reported the model of the benzoxaborole **AN6426**-adenosine monophosphate (AMP) adduct, which showed binding in the editing domain of *Pf*LeuRS.[170] The proposed mechanism showed that **AN6426** forms reversible covalent bond with the hydroxyls of the ribose ring of the AMP resulting in spiro-adduct about the boron atom on the benzoxaborole core (**Fig. 4.5**). The model was built using the crystal structure of the *Cryptosporidium muris* LeuRS which had been crystallized with **AN6426-AMP** (PDB 5FOM). This structure was aligned with that of the *Pf*LeuRS derived model to understand the **AN6426-AMP** binding interactions (PDB 5FO4). The homology model was derived based on the fact that the editing domain of the LeuRS for both species share 38.4% sequence similarity and this was enough for studying interactions in the *P. falciparum* model.[170] This model was used in the current study to rationalize the binding of **77/MM4-127** and **79/MM4-89**, both of which showed high antiplasmodium activity.

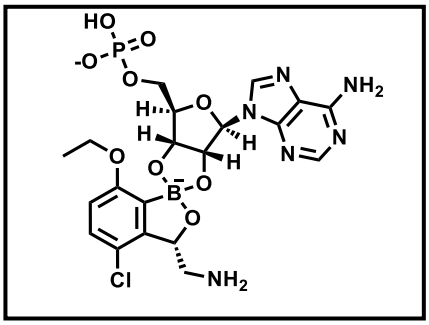

Figure 4.5: The AN6426-AMP adduct

Molecular docking was conducted with Maestro 13.0 of the Schrodinger suite using the imported *Pf*LeuRS (PDB 5FO4) with the **AN6426-AMP** bound in the editing domain. Ligands for the study were prepared as AMP covalent adducts as reported by Sonoiki *et al.* for **AN6426**.[170] All the structures were imported as SMILES (Simplified Molecular Input Line Entry Specification) entries and prepared using LigPrep to give the 3D structures of possible states generated at pH 7±2. Protein preparation was performed with the Protein Preparation tool with the default settings keeping the pH = 7. Following this, the receptor grid was generated with the Glide receptor grid generator to define the binding site. Ligand docking as the AMP adducts

was then conducted with Glide docking to give binding scores which were used to rationalize the binding of the series of benzoxaborole compounds under study. Docked compounds were visually inspected to select the compound poses showing stronger binding with the *Pf*LeuRS relative to the **AN6426-AMP**. The binding models (**Fig. 4.6 A**, **C** and **E**) as well as the 2D representations (**Fig. 4.6 B**, **D** and **F**) to show possible interactions were derived using the PyMoL software. **77/MM4-127** and **79/MM4-89**

Docking of the **AN6426-AMP** (**Fig 4.6 A** and **B**) showed polar hydrogen bonding of Lys 560 with the OH of the phosphate group of the AMP. Other hydrogen bonding interactions were observed resulting from the backbone NH_2 of the AMP with both Asp 635 and Tyr 633. Lys 642 interacts with the oxygen on the spiro-adduct of the complex and the arene-H interaction was observed for Gln639 with the pyrimidine ring of the AMP. For the compounds **77/MM4-127-AMP** (**Fig 4.6 C** and **D**) and **79/MM4-89-AMP** (**Fig 4.6 E** and **F**), the AMP NH_2 interactions present with **AN6426-AMP** Asp 635 and Tyr 633 were conserved. In addition, the imidazole N of the AMP for these adducts acted as the proton acceptor from Val 636. An arene-H interaction of the benzisoxazole observed with Gln639 for **AN6426-AMP** shifted to the imidazole ring of the AMP for **77/MM4-127-AMP** and **79/MM4-89-AMP**. The phosphate of the AMP was found to form three hydrogen bonding interactions with Ile 559 and Lys 590. The phenylglycine appendage appeared to be beneficial to the binding as it accepted a hydrogen bond or salt bridge from the carboxylic acid to Lys 642. Lys 642 also donated a hydrogen bond to the carbonyl oxygen of the benzoxaborole core. The compounds also displayed metal or ion contact through the carbonyl oxygen. These compounds show additional interactions absent in the **AN6426-AMP** adduct, which likely contribute to their predicted strong binding in the *Pf*LeuRS. The limitation with the best comparison in terms of the activities for these compounds and **AN6426-AMP** is that the former were investigated in the *Pf*NF54 strain while the latter was reported in the *Pf*3D7. However, the docking results of **77/MM4-127-AMP** and **79/MM4-89-AMP** suggest that the compounds show better binding than **AN6426-AMP**. This molecular docking data is in line with the hypothesis that benzoxaborole **77/MM4-127** and **79/MM4-89** adducts potentially bind in the editing domain of *Pf*LeuRS.

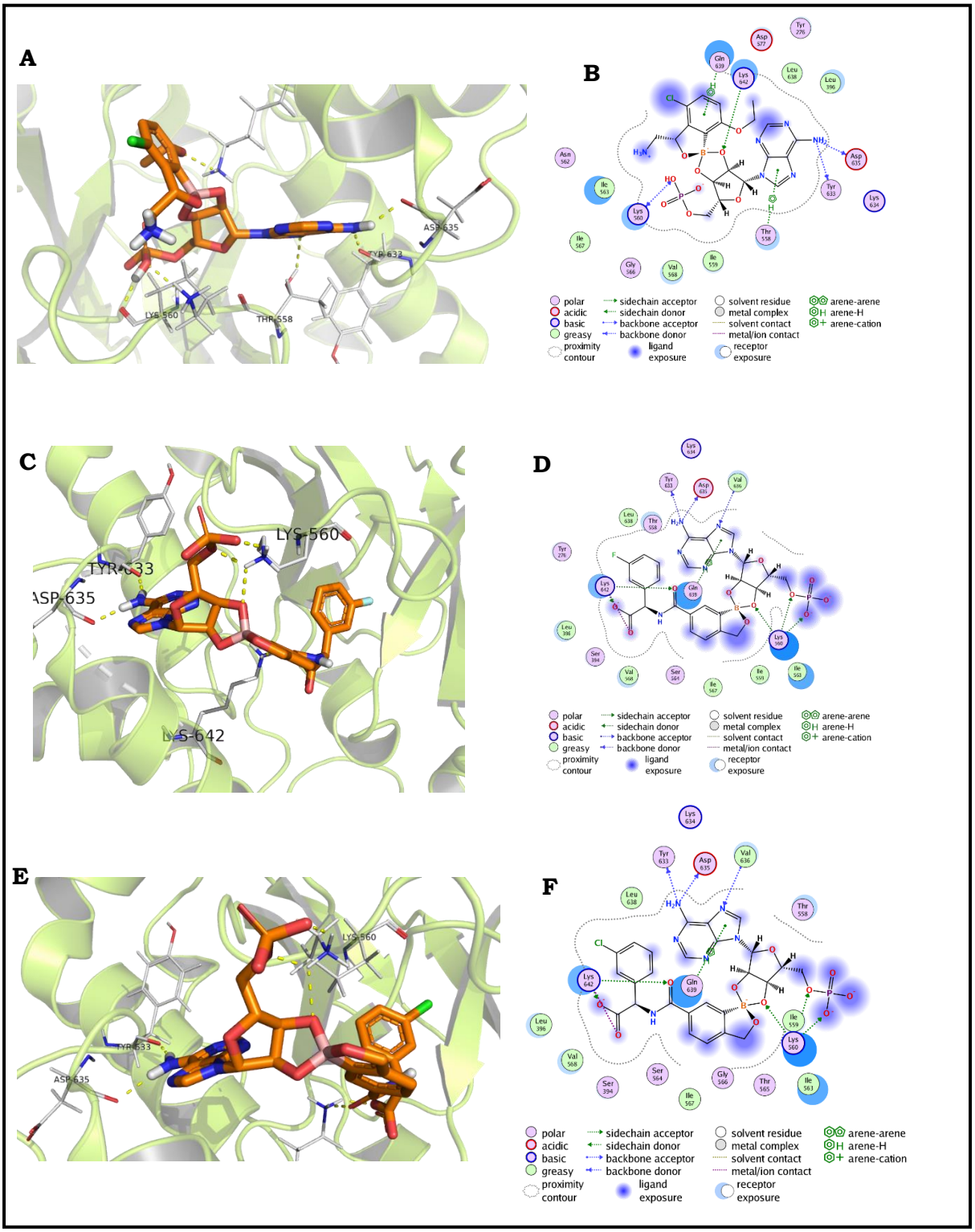

Figure 4.6: The binding model in the editing domain of LeuRS (**A**), (**C**) and (**E**) for compounds **AN6426-AMP**, **77/MM4-127-AMP** and **79/MM4-89-AMP** adducts respectively and, 2D representations of possible binding interactions (**B**), (**D**) and (**F**), respectively.

4.8. Summary and Conclusion

A series of benzoxaborole compounds was synthesized, with some showing high antiplasmodium activity against both drug sensitive *Pf*NF54 and the drug resistant *Pf*K1 strains. Ethyl ester analogues about the phenylglycine appendage were less active than the methyl ester analogues, which were also less active than the carboxylic acid match pairs. The latter showed high antiplasmodium activity and high solubility as determined via a turbidimetric solubility assay. The selected benzoxaborole compounds subjected to metabolomic studies showed weak signals and thus ambiguous metaprints. This suggests that these compounds act on pathways involving metabolites other than those covered in the assay and that they target other cellular processes. The compounds were also found to be metabolically stable *in vitro* in liver microsomes. The DNA-barcoded mutant line studies performed with a representative benzoxaborole revealed that these compounds are not cross-resistant with current clinical antimalarials, which suggests a novel MoA for this class of compounds. Lastly, the compounds are proposed to bind to the *Pf*LeuRS with additional interactions conferred by the polar groups of the phenylglycine appendage. In conclusion, this study identified a new class of benzoxaboroles with high antiplasmodium activity and microsomal stability without toxicity against mammalian cells and further revealed that these compounds may act by inhibiting novel targets.

4.9. References

1. Verlinden, B. K.; Niemand, J.; Snyman, J.; Sharma, S. K.; Beattie, R. J.; Woster, P. M.; Birkholtz, L.-M., Discovery of Novel Alkylated (bis)Urea and (bis)Thiourea Polyamine Analogues with Potent Antimalarial Activities. *J. Med. Chem.* **2011**, *54* (19), 6624-6633.

2. Sinha, S.; Sarma, P.; Sehgal, R.; Medhi, B., Development in Assay Methods for In Vitro Antimalarial Drug Efficacy Testing: A Systematic Review. *Front. Pharmacol.* **2017**, *8* (754), 1-14.

3. Smilkstein, M.; Sriwilaijaroen, N.; Kelly, J. X.; Wilairat, P.; Riscoe, M., Simple and inexpensive fluorescence-based technique for high-throughput antimalarial drug screening. *Antimicrob Agents Chemother* **2004**, *48* (5), 1803-1806.

4. de Cózar, C.; Caballero, I.; Colmenarejo, G.; Sanz, L. M.; Álvarez-Ruiz, E.; Gamo, F. J.; Cid, C., Development of a Novel High-Density [3H]Hypoxanthine Scintillation Proximity Assay To Assess Plasmodium falciparum Growth. *Antimicrob Agents Chemother* **2016**, *60* (10), 5949-5956.

5. Baker, S. J.; Tomsho, J. W.; Benkovic, S. J., Boron-containing inhibitors of synthetases. *Chem. Soc. Rev.* **2011**, *40* (8), 4279-4285.

6. Kusano, S.; Konishi, S.; Yamada, Y.; Hayashida, O., Synthesis of water-soluble anthracene-appended benzoxaboroles and evaluation of their cis-1,2-diol recognition properties. *Org. Biomol. Chem.* **2018**, *16* (25), 4619-4622.

7. Sindhe, K. M.; Wu, W.; Legac, J.; Zhang, Y.-K.; Easom, E. E.; Cooper, R. A.; Plattner, J. J.; Freund, Y. R.; DeRisi, J. L.; Rosenthal, P. J., Plasmodium falciparum Resistance to a Lead Benzoxaborole Due to Blocked Compound Activation and Altered Ubiquitination or Sumoylation. *mBio* **2020**, *11* (1), e02640-19.

8. Coghi, P. S.; Zhu, Y.; Xie, H.; Hosmane, N. S.; Zhang, Y., Organoboron Compounds: Effective Antibacterial and Antiparasitic Agents. *Molecules* **2021**, *26* (11), 3309.

9. Ishikawa, M.; Hashimoto, Y., Improving the Water-Solubility of Compounds by Molecular Modification to Disrupt Crystal Packing. In *The Practice of Medicinal Chemistry (Fourth Edition)*, Elsevier: 2015; pp 747-765.

10. Kumar, P.; Nagarajan, A.; Uchil, P. D., Analysis of cell viability by the MTT assay. *Cold spring harbor protocols* **2018**, https://pubmed.ncbi.nlm.nih.gov/29858338/. (accessed 23 November 2021).

11. Almazroo, O. A.; Miah, M. K.; Venkataramanan, R., Drug Metabolism in the Liver. *Clin Liver Dis* **2017**, *21* (1), 1-20.

12. Hughes, J. P.; Rees, S.; Kalindjian, S. B.; Philpott, K. L., Principles of early drug discovery. *Br. J. Pharmacol.* **2011**, *162* (6), 1239-1249.

13. Gajula, S. N. R.; Nadimpalli, N.; Sonti, R., Drug metabolic stability in early drug discovery to develop potential lead compounds. *Drug Metab Rev* **2021**, *53* (3), 459-477.

14. Liederer, B. M.; Borchardt, R. T., Enzymes involved in the bioconversion of ester-based prodrugs. *J Pharm Sci.* **2006**, *95* (6), 1177-1195.

15. Sonoiki, E.; Ng, C. L.; Lee, M. C.; Guo, D.; Zhang, Y.-K.; Zhou, Y.; Alley, M.; Ahyong, V.; Sanz, L. M.; Lafuente-Monasterio, M. J., A potent antimalarial benzoxaborole targets a Plasmodium falciparum cleavage and polyadenylation specificity factor homologue. *Nat. Commun.* **2017**, *8*, 14574.

16. Sonoiki, E.; Palencia, A.; Guo, D.; Ahyong, V.; Dong, C.; Li, X.; Hernandez, V. S.; Zhang, Y.-K.; Choi, W.; Gut, J., Antimalarial benzoxaboroles target Plasmodium falciparum leucyl-tRNA synthetase. *Antimicrob. Agents Chemother.* **2016**, *60* (8), 4886-4895.

17. Nyamai, D. W.; Bishop, Ö. T., Aminoacyl tRNA synthetases as malarial drug targets: a comparative bioinformatics study. *Malar. J.* **2019**, *18* (1), 34-61.

18. Mandel, C. R.; Bai, Y.; Tong, L., Protein factors in pre-mRNA 3'-end processing. *Cell Mol Life Sci* **2008**, *65* (7-8), 1099-1122.

19. Allman, E. L.; Painter, H. J.; Samra, J.; Carrasquilla, M.; Llinás, M., Metabolomic profiling of the malaria box reveals antimalarial target pathways. *Antimicrob. Agents Chemother.* **2016**, *60* (11), 6635-6649.

Chapter 5: Physicochemical evaluation and analysis

5.1. Chapter Overview

This chapter focuses on the physicochemical properties that influence the drug-likeness of the compounds designed and reported in this thesis. The chapter begins with a brief introduction on the literature covering factors that affect drug-likeness with an emphasis on the guidelines such as the Lipinski rule of five and Veber's rules. The methods used to derive the physicochemical properties are briefly described followed by the report of the results. This is followed by an analysis of the drug-likeness of different series in this study. The last section covers experimentally determined physicochemical properties and their effect on solubility.

5.2. The effects of physicochemical properties on compounds' drug-likeness and developability

The physicochemical properties of a drug have an impact on its trajectory from the point of administration to the point of action. The features of this trajectory include what the body does to a drug or pharmacokinetics (PK), which has impact on the amount of the administered drug that reach the target tissue or body compartment. The parameters such absorption, distribution, metabolism, and excretion (ADME) play an important role in understanding the properties of the drug that are affected and these have become an integral part of the early drug discovery phase.[240-242] Understanding of these parameters ensures that quality molecules are selected for advancement in order to mitigate the failure in clinical phases.[243] The optimization of these properties will inevitably affect the physicochemical properties of the drug and thus its drug-likeness. In the past two decades guidelines such as the Lipinski rule of five (Ro5), Veber rule of 3 (Ro3) and the property forecast index (PFI) profile have been proposed in guiding the design of new molecules.[180, 244-246] In addition to these, software such as Stardrop and ACDLabs have played a role in predicting the physicochemical properties in the design of new molecules.

Lipisnki and co-workers studied the features that most oral drugs possess and reported the Ro5 which they proposed that drugs meeting this will have good permeation and absorption *in vivo*.[244, 245, 247] In the case of a disease like malaria, an oral drug is beneficial on many levels including the ease of dissemination, delivery of

single-dose administration and compliance in resource-limited endemic areas.[248, 249] The Ro5 study found that the compounds which make good oral drugs generally have: molecular weight (MW) <500 Da, cLogP <5, hydrogen bond acceptors (HBA) <10 and hydrogen bond donors (HBD) <5. Veber Ro3, defined for the fragment-based drug discovery, suggested MW <300 Da, cLogP <3 and the HBD <3.[246] The extension of the Veber guidelines also define that a good oral drug has less than 10 rotatable bonds and the topological polar surface area (TPSA) is less than 140 Å, this correlating with the number of oxygen and nitrogen atoms.[246, 250] Care should be taken in the application of these rules as they are guidelines, and some of the drugs with activity can be found beyond the chemical spaces covered by these rules and are in use in clinic.[250, 251] In addition to these, GSK published the PFI value metrics which also guides in the selection of the molecules which possess good properties to meet multiple criteria for developability such as good solubility, permeability, low intrinsic clearance and low toxicity. The PFI value is the sum of chromatographic logD and number of aromatic rings in the molecule, and compounds with the PFI value less than 7 are likely to meet the multiple parameter criteria.[180, 252]

The compounds designed in this thesis were evaluated for drug-likeness with the assessment of their compliance to Lipinski Ro5, Veber's parameters and PFI value. These compounds were further evaluated experimentally for physicochemical properties, and these were assessed for their influence on solubility.

5.3. Calculated and experimental physicochemical properties

5.3.1. Physicochemical Properties Determination Methods: Computational and Experimental

Stardrop software was used to determine computational physicochemical properties viz. MW, calculated logP (clogP), TPSA, HBA and HBD. Percepta ACDLabs software was used to determine logD at pH 7.4 and number of aromatic rings in the compound that were used to calculate the PFI value. The experimental melting point values were obtained with the observation from a hot stage microscope and reported uncorrected. Kinetic HPLC and turbidimetric solubility measures were determined in line with the methods outlined in Chapter 7 of this thesis. The latter reports the solubility of the compounds at the concentration above which turbidity ensues and details are provided in **chapter 3 section 3.2** of this thesis. The assay determines solubility

within a concentration range from 0, 5, 10, 20, 40, 80, 160 and 200 μM. The HPLC retention time (t_R) in min was obtained from the LC-MS with the conditions described in chapter 7 of the thesis. The t_R values were an indication of the polarity of the compounds as it traverses through the reversed phased column chromatography used for the LC-MS. All the graphs were generated from Microsoft Excel. The data is presented and discussed in the next sections.

5.3.2. Results: Characterization of physicochemical properties

Table 5.1: Physicochemical properties of the Ugi and cyclohexyl pyrimidine series

		[a]Calculated physicochemical properties						Experimental physicochemical properties		
Number/Code	**Structure**	**MW, in g/mol**	**cLogP**	**TPSA, Å²**	**HBA**	**HBD**	**PFI value**	**t_R, min**	**[b]m.p., °C**	**Solubility, µM**
1/ MM1-15	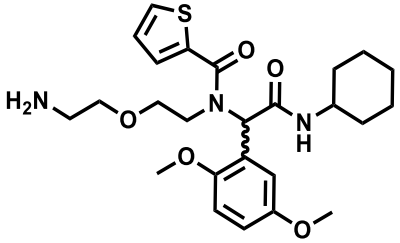	489.23	3.476	103.12	8	3	3.14	2.343	[c]N.D	110
2A/ MM1-19A	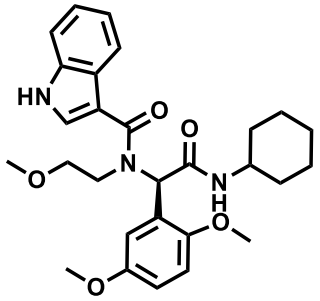	493.6	3.827	92.89	8	2	6.15	2.866	N.D	*160

2B/ MM1-19A	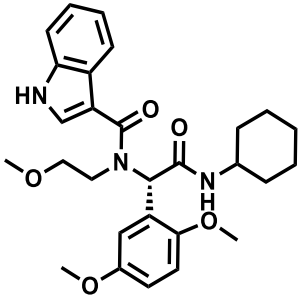	493.6	3.827	92.89	8	2	6.15	2.576	N.D	20
2/MM1-19	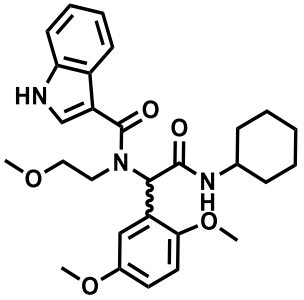	493.6	3.827	92.89	8	2	6.15	2.866	156	*160
15/MM1-85	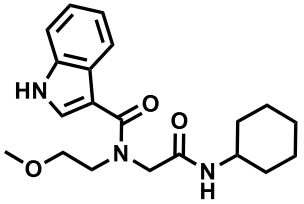	357.4	2.779	74.43	6	2	3.92	2.411	N.D	155

16/MM1-86	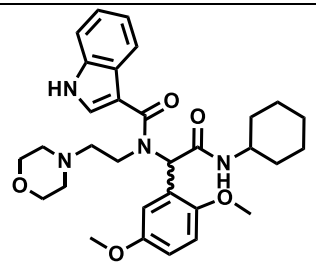	548.70	3.80	96.13	9	2	5.8	0.884	182	*160
17/MM1-56	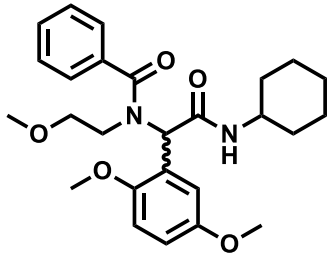	454.6	3.515	77.1	7	1	5.32	2.268	159	*40
18/MM1-82	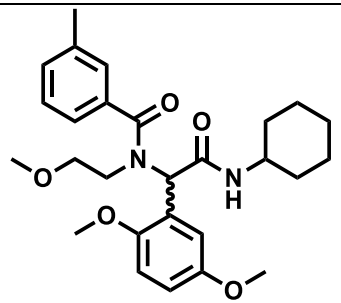	468.6	3.933	77.1	7	1	5.62	2.610	108	95
19/MM1-63	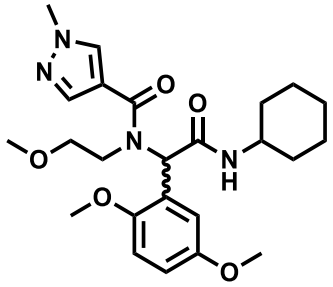	458.6	2.669	94.92	9	1	3.93	2.461	N.D	*80

20/MM1-64	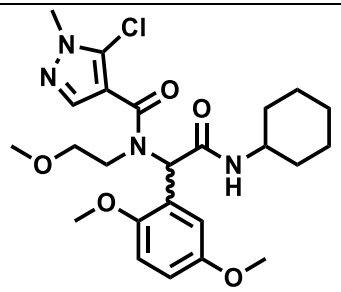	493	3.179	94.92	9	1	4.85	2.487	113	145

		Calculated physicochemical properties						**Experimental physicochemical properties**		
Number/Code	**Structure**	**MW, in g/mol**	**cLogP**	**TPSA, Å²**	**HBA**	**HBD**	**PFI value**	**t_R, min**	**m.p., °C**	**Solubility, µM**

21/MM1-81	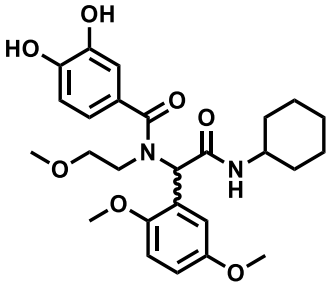	486.6	2.29	117.6	9	3	4.43	2.493	174	*120
22/MM1-53	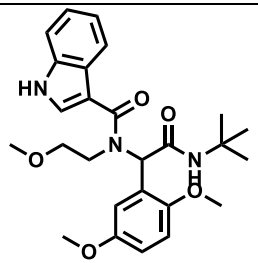	467.6	3.062	92.89	8	2	5.76	2.517	131	85
3/MM1-75	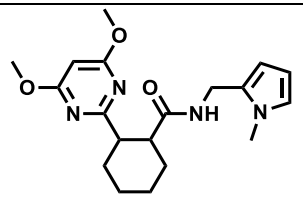	358.4	3.028	78.27	7	1	4.42	2.514	161	200
13/MM1-88	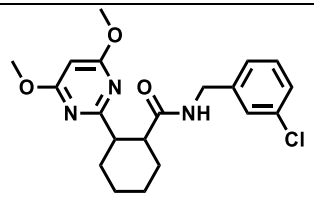	389.9	4.233	73.34	6	1	5.5	2.586	121	40

14/MM-88	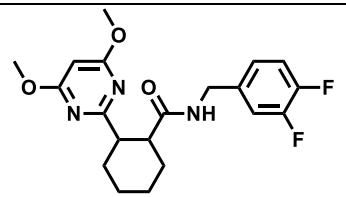	391.4	3.382	73.34	6	1	4.75	1.119	144	40
4a/MM2-39	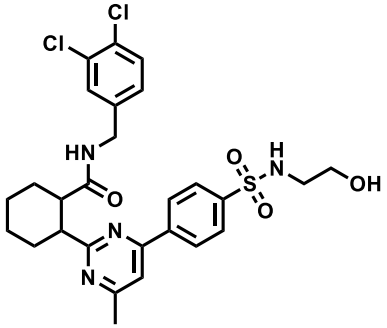	577.52	4.46	120.22	8	3	7.31	1.198	N.D	5

[a]Calculated with Stardrop v6.3. [b]m.p is the average of the upper and lower limit values of the experimental melting point. [c]N.D, not determined as the compound was obtained either oily or as a wax. *Turbidimetric solubility.

Table 5.2: Physicochemical properties of the triazolopyrimidine series

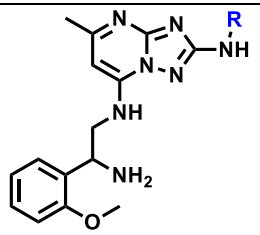

		[a]Calculated physicochemical properties						Experimental physicochemical properties		
Number/ Code	**R**	**MW, in g/mol**	**cLogP**	**TPSA, Å²**	**HBA**	**HBD**	**PFI value**	**t_R, min**	**[b]m.p., °C**	**Solubility, µM**
28/ MM2-145	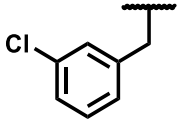	437.9	3.107	102.4	8	3	6.25	2.301	81	20
29/ MM3-144	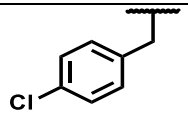	437.9	3.107	102.4	8	3	6.25	2.336	109	90
30/ MM3-189	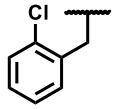	437.9	3.107	102.4	8	3	6.25	2.287	96	*40
31/ MM3-205	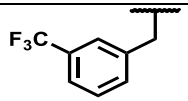	471.5	3.523	102.4	8	3	6.3	2.358	204	*20
32/ MM3-159	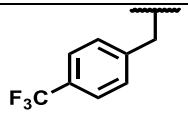	471.5	3.523	102.4	8	3	6.3	2.305	[c]N.D	*120

[a]Calculated with Stardrop v6.3. [b]m.p is the average of the upper and lower limit values of the experimental melting point. [c]N.D, not determined as the compound was obtained either oily or as a wax. *Turbidimetric solubility.

Table 5.2: Physicochemical properties of the triazolopyrimidine series

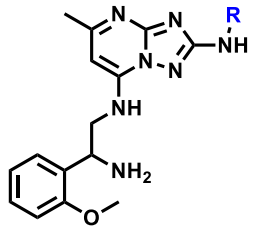

Number/ Code	R	[a]Calculated physicochemical properties						Experimental physicochemical properties		
		MW, in g/mol	cLogP	TPSA, Å^2	HBA	HBD	PFI value	t_R, min	[b]m.p., °C	Solubility, µM
33/ MM3-167	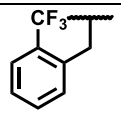	471.5	3.523	102.4	8	3	6.3	2.320	154	*40
34/ MM4-19	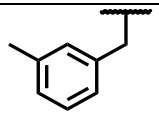	417.5	3.075	102.4	8	3	5.81	0.784	133	110
35/ MM4-75	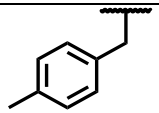	417.5	3.075	102.4	8	3	5.81	2.309	85	*160
36/ MM4-19	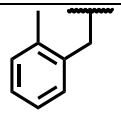	417.5	3.075	102.4	8	3	5.81	0.699	147	*60

37/ MM3-140	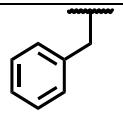	403.5	2.72	102.4	8	3	5.54	2.233	194	*>200

[a]Calculated with Stardrop v6.3. [b]m.p is the average of the upper and lower limit values of the experimental melting point. *Turbidimetric solubility.

Table 5.2: Physicochemical properties of the triazolopyrimidine series

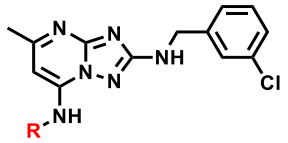

Number/ Code	R	[a]Calculated physicochemical properties						Experimental physicochemical properties		
		MW, in g/mol	cLogP	TPSA, Å²	HBA	HBD	PFI value	t_R, min	[b]m.p., °C	Solubility, µM
38/ MM2-141	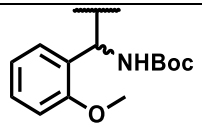	538	4.616	114.7	10	3	9.28	1.158	197	[c]N.D
39/ MM3-75	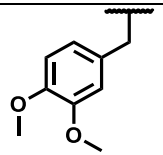	452.9	4.286	85.6	8	2	8.11	1.184	156	<5
40/ MM3-59	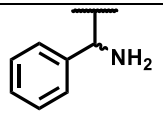	407.9	3.042	93.16	7	3	6.44	1.307	80	20
41/ MM3-139	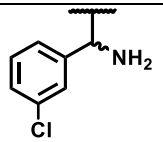	442.3	3.413	93.16	7	3	7.15	2.416	102	*80

42/ MM3-60	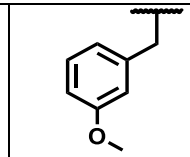	422.9	4.399	76.37	7	2	8.83	1.191	153	*20

[a]Calculated with Stardrop v6.3. [b]m.p is the average of the upper and lower limit values of the experimental melting point. [c]N.D, not determined as the compound was obtained either oily or as a wax. *Turbidimetric solubility.

Table 5.3: Physicochemical properties of the benzoxaborole series

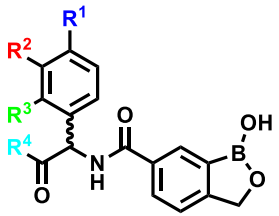

					[a]Calculated physicochemical properties						Experimental physicochemical properties		
Number/Code	**R^1**	**R^2**	**R^3**	**R^4**	**MW, in g/mol**	**cLogP**	**TPSA, Å²**	**HBA**	**HBD**	**PFI value**	**t_R, min**	**[b]m.p., °C**	**Solubility, µM**
45/MM2-91	H	H	H	-OMe	325.1	1.28	84.86	6	2	4.18	2.309	164	103
46/MM2-174	-Me	H	H	-OMe	339.2	1.73	84.86	6	2	4.29	2.369	161	90
47/MM2-196	H	-Me	H	-OMe	339.2	1.73	84.86	6	2	4.29	2.391	142	[d]N.D
48/MM4-81	H	H	-Me	-OMe	339.2	1.73	84.86	6	2	4.29	2.376	111	60
49/MM2-201	-F	H	H	-OMe	343.1	1.50	84.86	6	2	4.25	2.370	142	120
50/MM4-44	H	-F	H	-OMe	343.1	1.50	84.86	6	2	4.25	2.356	149	130
51/MM4-64	H	H	-F	-OMe	343.1	1.50	84.86	6	2	4.25	2.330	[c]N.D	*40
52/MM3-160	-OMe	H	H	-OMe	355.1	1.40	94.09	7	2	4.33	2.351	168	*80
53/MM4-15	H	-OMe	H	-OMe	355.1	1.40	94.09	7	2	4.33	0.919	151	75
54/MM4-46	H	H	-OMe	-OMe	355.1	1.40	94.09	7	2	4.33	2.330	96	125
55/MM3-8	-OH	H	H	-OMe	341.1	0.70	105.1	7	3	3.93	2.114	166	*120

56/MM4-101	H	-OH	H	-OMe	341.1	0.70	105.1	7	3	3.93	2.183	101	*160
57/MM4-108	H	H	-OH	-OMe	341.1	0.70	105.1	7	3	3.93	2.128	N.D	N.D
58/MM3-9	$-CF_3$	H	H	-OMe	393.1	2.43	84.86	6	2	4.68	2.489	135	30
59/MM4-14	H	$-CF_3$	H	-OMe	393.1	2.43	84.86	6	2	4.68	2.417	151	*40
60/MM4-16	H	H	$-CF_3$	-OMe	393.1	2.43	84.86	6	2	4.68	2.438	131	160
61/MM3-175	-Cl	H	H	-OMe	359.6	1.91	84.86	6	2	4.67	2.416	152	125
62/MM4-12	H	-Cl	H	-OMe	359.6	1.91	84.86	6	2	4.67	2.402	144	70
63/MM4-07	H	H	-Cl	-OMe	359.6	1.91	84.86	6	2	4.67	2.350	91	140

[a]Calculated with Stardrop v6.3. [b]m.p is the average of the upper and lower limit values of the experimental melting point. [c]N.D for m.p it is because the compound was obtained either oily or as a wax. [d]N.D, not determined. *Turbidimetric solubility.

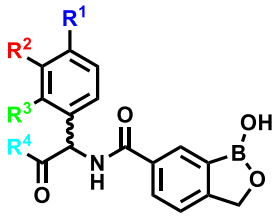

					[a]Calculated physicochemical properties						Experimental physicochemical properties		
Number/Code	**R^1**	**R^2**	**R^3**	**R^4**	**MW, in g/mol**	**cLogP**	**TPSA, Å²**	**HBA**	**HBD**	**PFI value**	**t_R, min**	**[b]m.p., °C**	**Solubility, µM**
64/MM3-57	H	H	H	-OEt	339.2	1.76	84.86	6	2	4.4	2.440	[c]N.D.	60
65/MM4-50	-Cl	H	H	-OEt	373.6	2.37	84.86	6	2	4.99	2.479	104	*140
66/MM4-93	H	-Cl	H	-OEt	373.6	2.37	84.86	6	2	4.99	2.474	150	*80
67/MM4-114	H	H	-Cl	-OEt	373.6	2.37	84.86	6	2	4.99	2.430	N.D	*40
68/MM4-105	H	-Me	H	-OEt	353.2	2.2	84.86	6	2	4.52	2.449	97	120
69/MM4-100	H	H	-Me	-OEt	353.2	2.2	84.86	6	2	4.52	2.435	100	*80
70/MM4-56	H	-F	H	-OEt	357.1	1.94	84.86	6	2	4.3	2.413	149	*40
71/MM4-55	H	H	-F	-OEt	357.1	1.94	84.86	6	2	4.3	2.389	144	*160
72/MM2-173	H	H	H	-OH	311.1	0.86	95.86	6	3	0.01	1.021	156	150
73/MM2-177	-Me	H	H	-OH	325.1	1.32	95.86	6	3	0.28	2.206	211	130
74/MM4-134	H	-Me	H	-OH	325.1	1.32	95.86	6	3	0.28	2.236	197	140

75/MM4-137	H	H	-Me	-OH	325.1	1.32	95.86	6	3	0.28	2.221	N.D	120
76/MM4-86	-Cl	H	H	-OH	345.5	1.48	95.86	6	3	0.48	2.233	139	*80
77/MM4-127	H	-Cl	H	-OH	345.5	1.48	95.86	6	3	0.48	2.227	144	*160
78/MM4-136	H	H	-Cl	-OH	345.5	1.48	95.86	6	3	0.48	2.102	162	*80
79/MM4-89	H	-F	H	-OH	329.1	1.10	95.86	6	3	0.11	1.950	134	*160
80/MM4-87	H	H	-F	-OH	329.1	1.10	95.86	6	3	0.11	1.913	N.D	[d]N.D
81/MM4-136	H	H	H	-NMe	324.1	0.64	87.66	6	3	3.68	2.317	217	150
82/MM4-60	H	H	H	$-NMe_2$	338.2	0.85	78.87	6	2	3.9	2.295	180	135

[a]Calculated with Stardrop v6.3. [b]m.p is the average of the upper and lower limit values of the experimental melting point. [c]N.D for m.p it is because the compound was obtained either oily or as a wax. [d]N.D, not determined. *Turbidimetric solubility.

Table 5.3: Physicochemical properties of the benzoxaborole series

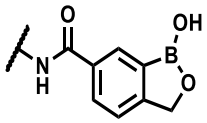

Number/Code	Substituent	[a]Calculated physicochemical properties						Experimental physicochemical properties		
		MW, in g/mol	cLogP	TPSA, Å^2	HBA	HBD	PFI value	t_R, min	[b]m.p., °C	Solubility, µM
43/MM2-92	-PhCHCOOCH$_3$ (*S*)	325.1	1.28	84.86	6	2	4.18	2.309	143	164
83/MM2-90	-PhCHCOOCH$_3$ (*R*)	325.1	1.28	84.86	6	2	4.18	2.321	131	200
45A/MM2-224A	-PhCHCOOCH$_3$ (*S*) chiral col	325.1	1.28	84.86	6	2	4.18	2.309	182	[d]N.D
45B/MM2-224B	-PhCHCOOCH$_3$ (*R*) Chiral col	325.1	1.28	84.86	6	2	4.18	2.321	131	N.D
84/MM2-120	-CH$_2$CH$_2$C(CH$_3$)$_2$OH	249.1	-0.01	78.79	5	3	2.6	0.308	[c]N.D	20
85/MM2-125	-CH$_2$CH$_2$CH(CH$_3$)OH	235	-0.46	78.79	5	3	2.04	0.253	177	<5
86/MM2-119	-CH$_2$CH$_2$OCH$_3$	235	0.23	67.79	5	2	2.43	0.469	N.D	<5
87/MM2-44	-CH$_2$CF$_3$	259	0.58	58.56	4	2	2.74	0.218	N.D	<5
88/MM2-130	-PhCH$_2$OH	297.1	0.75	78.79	5	3	3.89	2.044	N.D	<5
89/MM2-165	-CHC$_6$H$_{11}$COOCH$_3$	331.2	1.87	84.86	6	2	3.8	2.469	101	20

90/MM3-85	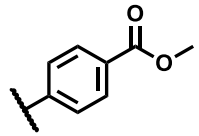	311.1	1.57	84.86	6	2	4.32	1.182	233	*80
91/MM3-11	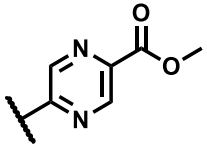	313.1	0.76	110.6	8	2	3.72	2.317	181	*160

[a]Calculated with Stardrop v6.3. [b]m.p is the average of the upper and lower limit values of the experimental melting point. [c]N.D for m.p it is because the compound was obtained either oily or as a wax. [d]N.D, not determined. *Turbidimetric solubility.

Table 5.3: Physicochemical properties of the benzoxaborole series

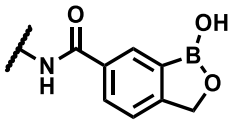

Number/Code	Substituent	[a]Calculated physicochemical properties						Experimental physicochemical properties		
		MW, in g/mol	cLogP	TPSA, Å^2	HBA	HBD	PFI value	t_R, min	[b]m.p., °C	Solubility, µM
92/MM3-42	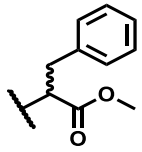	339.2	1.62	84.86	6	2	4.71	2.381	69	190
93/MM3-10	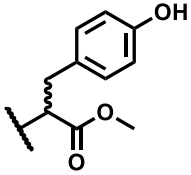	355.1	1.04	105.1	7	3	4.15	2.160	189	200
44/MM4-26	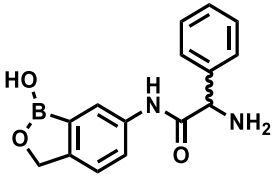	282.12	0.66	84.58	4	3	3.16	1.206	197	140

[a]Calculated with Stardrop v6.3. [b]m.p is the average of the upper and lower limit values of the experimental melting point.

Table 5.4: Physicochemical properties of the 7-methyl benzoxaborole series

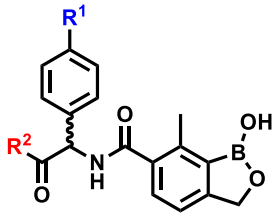

		Calculated physicochemical properties							Experimental physicochemical properties		
Number/Code	**R^1**	**R^2**	**MW, in g/mol**	**cLogP**	**TPSA, Å²**	**HBA**	**HBD**	**PFI value**	**t_R, min**	**m.p., °C**	**Solubility, µM**
94/MM4-141	H	-OMe	339.2	1.73	84.86	6	2	4.29	2.352	153	160
95/MM4-144	-Me	-OEt	367.2	2.63	84.86	6	2	4.95	2.486	119	80
96/MM4-150	-Me	-OMe	353.2	2.17	84.86	6	2	4.89	2.476	138	160
97/MM4-148	-Me	-OH	339.2	1.78	95.86	6	3	0.52	2.237	228	140

Table 5.5: A summary of the physicochemical properties and the targeted values

Series	MW, in g/mol	cLogP	TPSA, Å²	HBA	HBD	PFI value
Target value	500	<5	<10	<10	<5	<7
Ugi and cyclohexyl pyrimidine	357.4-577.5	2.29-4.46	73.3-120.22	6-9	1-3	3.14-7.31
Triazolopyrimidine	403.5-538	2.72-4.62	76.37-114.7	7-10	2-3	5.54-8.83
Benzoxaboroles	249.1 – 373.6	-0.46-2.63	58.86–110.6	4-8	2-4	0.01-4.99

5.3. Drug-likeness: Compliance to Lipinski's Ro5 and PFI

Ugi and cyclohexyl pyrimidines

The compounds in these series had molecular weights compliant with Lipinski guidelines ranging between 357.4-493.6 g/mol (**Fig. 5.1 A**) with the exception of compound **4a/MM2-39** and **16/MM1-86** with molecular weight 577.5 and 548.7 g/mol, respectively. The series met the criteria for other properties with the ranges of clogP 2.29-4.46 (**Fig. 5.1 B**), TPSA 77.1-120.22 (**Fig. 5.1 C**), HBA 6-9 and HBD 1-3. In addition, the developability of the compounds in these series as represented by PFI value showed that while the majority had PFI values <7 (**Fig. 5.1 D**) only **4a/MM2-39** was an exception with PFI = 7.31. Hence, the majority of compounds in the series demonstrated drug-likeness (**Table 5.5**).

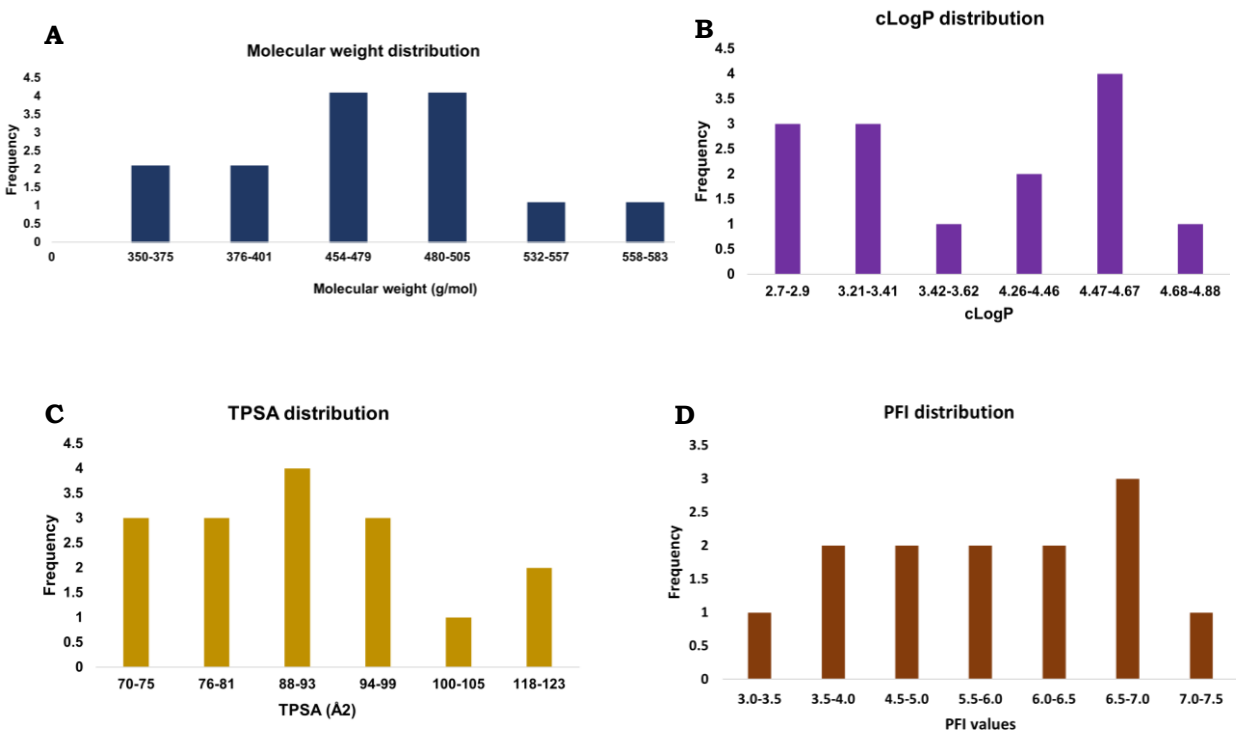

Figure 5.1: The frequency distribution of (**A**) molecular weight, (**B**) clogP, (**C**) TPSA and (**D**) PFI values for the Ugi and cyclohexyl pyrimidine series

Triazolopyrimidines

The compounds in this series complied with the Lipisnki Ro5 guidelines (**Table 5.5**) with molecular weight 403.5-471.5 g/mol with the exception being compound **38/MM2-141** which has a molecular weight of 538 g/mol (**Fig. 5.2 A**). Other Ro5 physicochemical parameters and the PFI value targets were met: clogP 2.72-4.62 (**Fig. 5.2 B**), TPSA 76.37-114.7 (**Fig. 5.2 C**), HBA 7-10, HBD 2-3. The majority of the compounds in this series had PFI values <7 with the exception of compounds **34-38** (**Fig. 5.2D**).

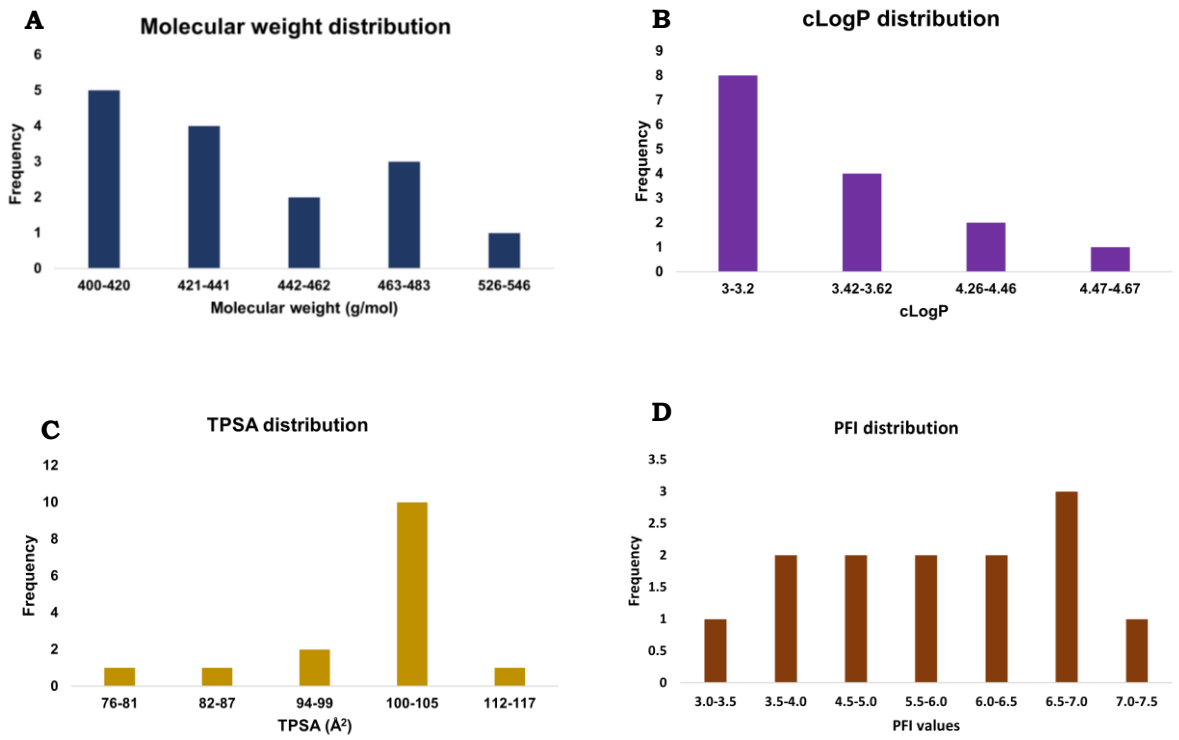

Figure 5.2: The frequency distribution of (**A**) molecular weight, (**B**) clogP, (**C**) TPSA and (**D**) PFI values for the triazolopyrimidine series

Benzoxaboroles

The compounds in this series were compliant to all Lipinski's Ro5 criteria: molecular weight 249.1 – 373.6 g/mol (**Fig. 5.3 A**), clogP -0.46 to 2.63 (**Fig. 5.3 B**), HBA 4-8 and the HBD 2-4 (**Table 5.4**) and Veber's guideline with TPSA 58.86–110.6 (**Fig. 5.3 C**). The PFI values for this series were within the target value as 0.01-4.99 (**Fig. 5.3 D**). These values show that the series possess drug-likeness and can meet the multiple criteria required for drug development (**Table 5.5**).

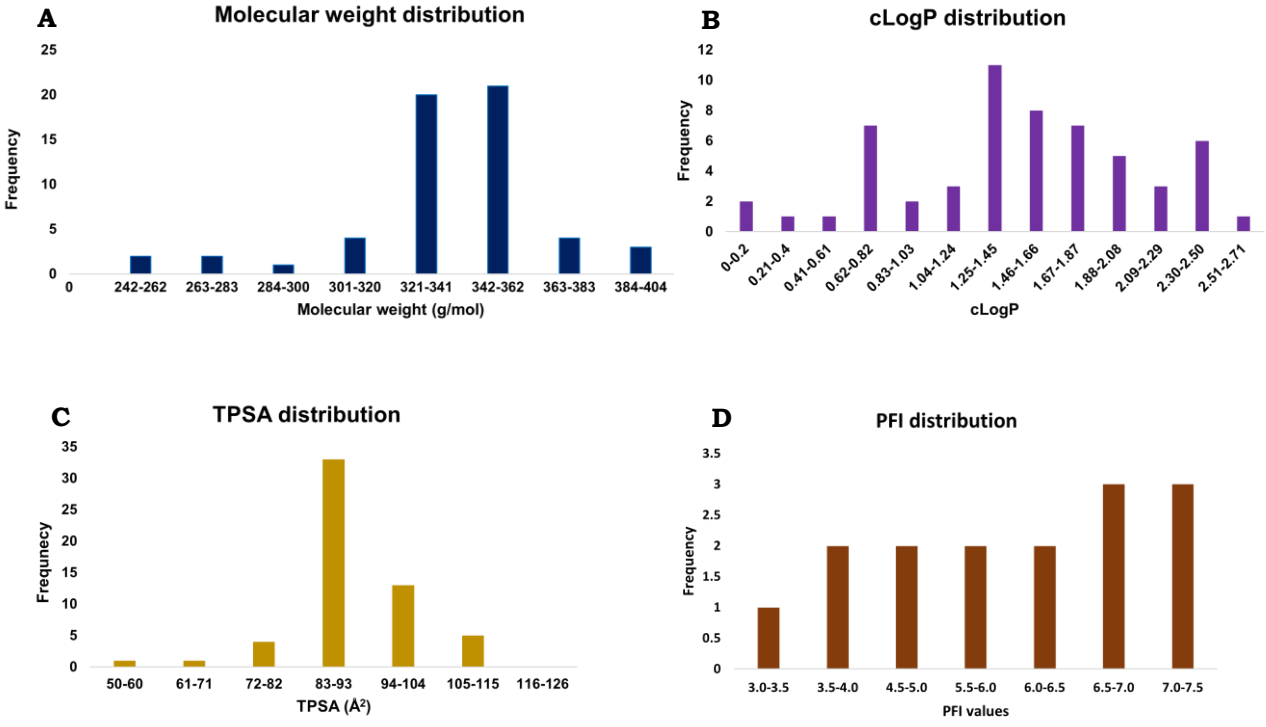

Figure 5.3: The frequency distribution of (**A**) molecular weight, (**B**) clogP, (**C**) TPSA and (**D**) PFI values for the benzoxaboroles series

5.4. Structure property effects on solubility

Solubility is an important parameter for oral drugs to enable absorption and permeation across different tissues and thus affect bioavailability.[253] To that end, factors influencing solubility for the series under study were analysed and are presented in this section and depicted in **Figure 5.4 A-L**. The melting point of the compound is linked to solubility since the crystal packing of compounds, oftentimes due to the presence of the aromatic rings that encourage π-π interactions and thus discourage dissolution.[254, 255] This will have an impact on the dissolution of the compound in the aqueous media. The clogP is the calculated value of the octanol: water partition coefficient of the neutral form of a compound and is an indicator of the lipophilicity of the compound.[256] This has impact on the absorption of the compounds, and it is an important parameter to assess in the early discovery phase. Also influencing absorption is the TPSA which factors in the polarity of the molecule with respect to the nitrogen and oxygen atoms.[246] Lastly, the retention time on the LC-MS resulting from the passage of the compound through the reversed-phase column chromatography, measured in min, as it is flushed by the polar aqueous phase was used as a proxy of the compound in the aqueous media and was studied

here to measure the polarity of the compounds. In this case, the most polar compounds will have retention time closer to 0 min while the lipophilic compounds will elute more slowly and will be retained longer resulting in longer retention times.

Discussion

There was weak correlation between solubility and melting point for the three series of compounds under study (**Fig. 5.4 A-C**). This may be due to the factors such as, for example, the turbidimetric method used to obtain solubility being limited in that it measures solubility in the presence of DMSO. The limitation with the measurement of solubility is also that the turbidimetric method only focused on a range of values as mentioned in section 5.3.1 above and it oftentimes overestimates solubility. Furthermore, solubility values which were reported as less than 5 μM, for instance, were assumed to be finite values (i.e., 5 μM) for the purposes of generating the correlation plots. This is also the case for the compounds reported to have solubility >200 μM. Therefore, these factors affect the correlation observed. The clogP had weak correlation with solubility for the Ugi and cyclohexyl pyrimidine series and, the triazolopyrimidine series (**Fig. 5.4 D-E**). There was no correlation for the benzoxaborole series (**Fig. 5.4 F**). However, all the compounds in this series had clogP <3 and overall better solubility likely as a result of high aqueous solubility of the benzoxaboroles.[231] Taken together, these data suggest that melting point and clogP do not influence solubility as measured and that other parameters or factors play a role. The HPLC retention time and TPSA showed weak correlation with solubility across the series. The compounds met the target value of TPSA <140 Å^2, proposed to be a good indicator that compounds will have acceptable permeability across membranes[246, 257], suggesting that those compounds with higher solubility would be orally bioavailable.

The three series studied in this section each covered a narrow chemical space. This may also be the reason for the lack of correlation between the physicochemical properties presented and solubility. For instance, the benzoxaboroles series retention time and TPSA were within narrow margins and thus appeared to be almost the same for most compounds (**Fig. 5.4 I** and **L**, respectively). This may have affected the distribution of the values and consequently correlation. Thus, solubility is not affected by the physicochemical properties investigated.

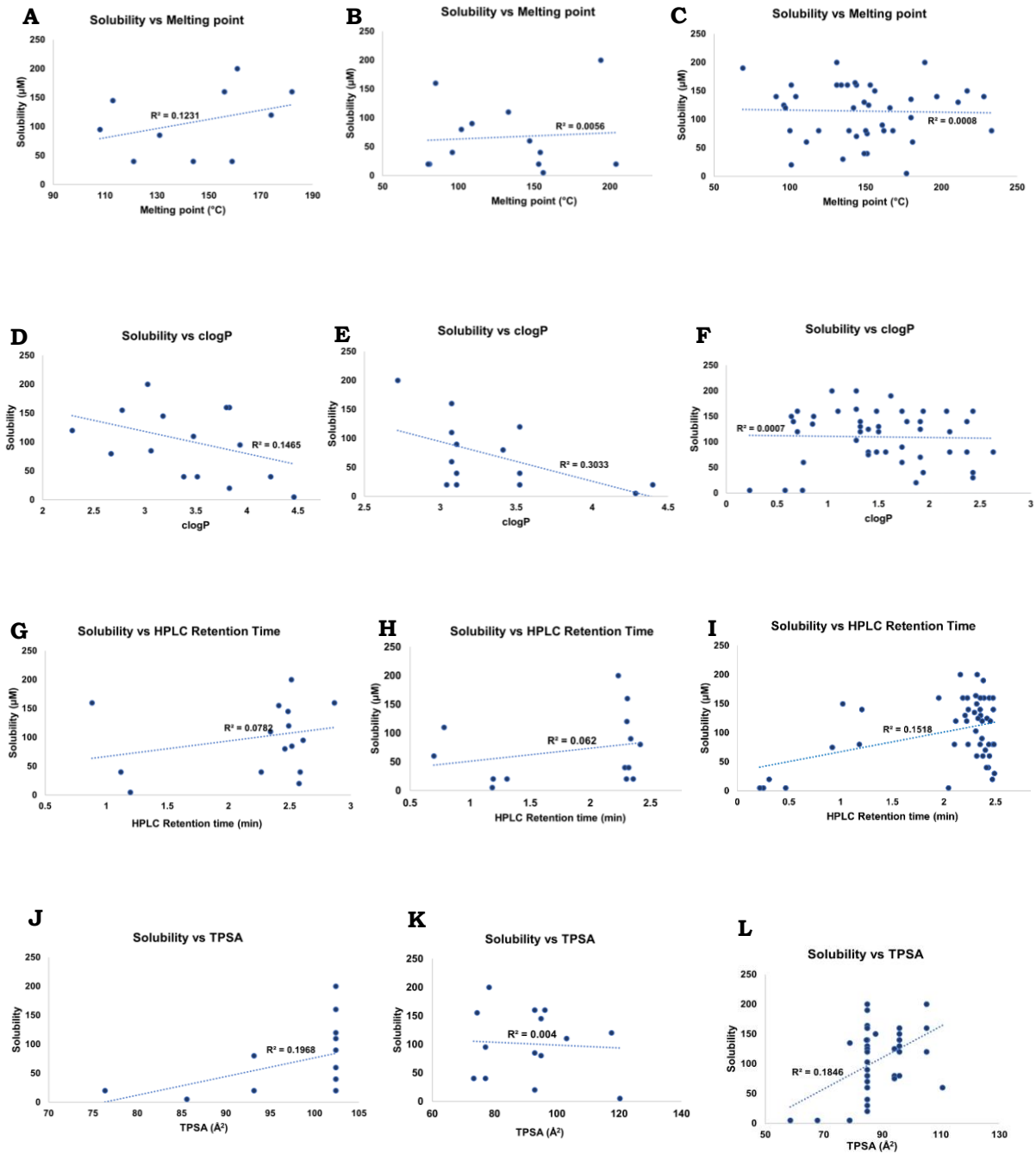

Figure 5.4: The correlation plots of solubility with (**A-C**) molecular weight for Ugi and cyclohexyl pyrimidine, Triazolopyrimidine and benzoxaboroles series, respectively; (**D-F**) clogP for Ugi and cyclohexyl pyrimidine, Triazolopyrimidine and benzoxaboroles series, respectively; (**G-I**) HPLC retention time for Ugi and cyclohexyl pyrimidine, Triazolopyrimidine and benzoxaboroles series, respectively; and (**J-L**) TPSA for Ugi and cyclohexyl pyrimidine, Triazolopyrimidine and benzoxaboroles series, respectively

5.5. Conclusion

This chapter presented the physicochemical properties for the Ugi and the cyclohexyl pyrimidine, triazolopyrimidine and the benzoxaborole series. The results showed that most of the Ugi and the cyclohexyl pyrimidine series met Lipinski Ro5. Most of the triazolopyrimidine compounds were also compliant with the Ro5 criteria. The benzoxaboroles showed total compliance to the stipulated Ro5 guidelines and were also more soluble overall. This series also had the PFI value <7 across the compounds in contrast to the triazolopyrimidine series. Therefore it is predicted that the oral bioavailability of these compounds will be favorable. There was no correlation observed between solubility and the physicochemical properties evaluated viz. melting point, clogP, HPLC retention time and TPSA.

5.6. References

1. Katherine Dunnington, N. B., Christine Brandquist, Nadia Cardillo-Marricco, Mike Di Spirito, Julie Grenier, Application of Pharmacokinetics in Early Drug Development. In *Pharmacokinetics and Adverse Effects of Drugs - Mechanisms and Risks Factors*, Malangu, N., Ed. Intechopen: 2017; pp 58-75.

2. Hong, W., What ADME Tests Should Be Conducted for Preclinical Studies? *Admet & Dmpk* **2013**, *1* (3), 19-28.

3. Wang, J.; Urban, L., The impact of early ADME profiling on drug discovery and development strategy. *Drug Discov. World* **2004**, *5* (4), 73-86.

4. Bickerton, G. R.; Paolini, G. V.; Besnard, J.; Muresan, S.; Hopkins, A. L., Quantifying the chemical beauty of drugs. *Nat Chem* **2012**, *4* (2), 90-98.

5. Lipinski, C. A.; Lombardo, F.; Dominy, B. W.; Feeney, P. J., Experimental and computational approaches to estimate solubility and permeability in drug discovery and development settings. *Adv Drug Deliv Rev* **2001**, *46* (1-3), 3-26.

6. Lipinski, C. A.; Lombardo, F.; Dominy, B. W.; Feeney, P. J., Experimental and computational approaches to estimate solubility and permeability in drug discovery and development settings. *Adv. Drug Delivery Rev.* **1997**, *23* (1), 3-25.

7. Veber, D. F.; Johnson, S. R.; Cheng, H.-Y.; Smith, B. R.; Ward, K. W.; Kopple, K. D., Molecular Properties That Influence the Oral Bioavailability of Drug Candidates. *J. Med. Chem.* **2002**, *45* (12), 2615-2623.

8. Young, R. J.; Green, D. V.; Luscombe, C. N.; Hill, A. P., Getting physical in drug discovery II: the impact of chromatographic hydrophobicity measurements and aromaticity. *Drug Discov. Today* **2011**, *16* (17-18), 822-830.

9. Leeson, P. D.; Springthorpe, B., The influence of drug-like concepts on decision-making in medicinal chemistry. *Nat. Rev. Drug Discovery* **2007**, *6* (11), 881-890.

10. Basore, K.; Cheng, Y.; Kushwaha, A. K.; Nguyen, S. T.; Desai, S. A., How do antimalarial drugs reach their intracellular targets? *Front. Pharmacol.* **2015**, *6* (91), 1-7.

11. Lu, H. D.; Ristroph, K. D.; Dobrijevic, E. L. K.; Feng, J.; McManus, S. A.; Zhang, Y.; Mulhearn, W. D.; Ramachandruni, H.; Patel, A.; Prud'homme, R. K., Encapsulation of OZ439 into Nanoparticles for Supersaturated Drug Release in Oral Malaria Therapy. *ACS Infect. Dis.* **2018**, *4* (6), 970-979.

12. Leeson, P. D., Molecular inflation, attrition and the rule of five. *Adv. Drug Delivery Rev.* **2016**, *101*, 22-33.

13. Doak, B. C.; Over, B.; Giordanetto, F.; Kihlberg, J., Oral druggable space beyond the rule of 5: insights from drugs and clinical candidates. *Chem Biol* **2014**, *21* (9), 1115-1142.

14. Leeson, P. D.; Young, R. J., Molecular property design: does everyone get it? *ACS Med. Chem. Lett.* **2015**, *6*, 722–725.

15. Savjani, K. T.; Gajjar, A. K.; Savjani, J. K., Drug solubility: importance and enhancement techniques. *ISRN Pharm.* **2012**, *2012* (2012), 1-10.

16. Docherty, R.; Pencheva, K.; Abramov, Y. A., Low solubility in drug development: de-convoluting the relative importance of solvation and crystal packing. *J. Pharm. Pharmacol.* **2015**, *67* (6), 847-856.

17. Ozaki, S.; Nakagawa, Y.; Shirai, O.; Kano, K., Substituent effect on the thermodynamic solubility of structural analogs: relative contribution of crystal packing and hydration. *J Pharm Sci.* **2014**, *103* (11), 3524-3531.

18. Young, R. J.; Green, D. V. S.; Luscombe, C. N.; Hill, A. P., Getting physical in drug discovery II: the impact of chromatographic hydrophobicity measurements and aromaticity. *Drug Discov. Today* **2011**, *16* (17), 822-830.

19. Baker, S. J.; Tomsho, J. W.; Benkovic, S. J., Boron-containing inhibitors of synthetases. *Chem. Soc. Rev.* **2011**, *40* (8), 4279-4285.

20. Ibrahim, Z. Y. u.; Uzairu, A.; Shallangwa, G. A.; Abechi, S. E., Pharmacokinetic predictions and docking studies of substituted aryl amine-based triazolopyrimidine designed inhibitors of Plasmodium falciparum dihydroorotate dehydrogenase (*Pf*DHODH). *Future J. Pharm. Sci.* **2021**, *7* (1), 133-143.

Chapter 6: Summary and future work

6.1. Chapter overview

This chapter provides a summary of the work covered in this project and makes future recommendations based on the key outcomes of this study. Firstly, a review of the antiplasmodium screening outcomes of the PPAT inhibitors covered under different series is discussed. This is followed by a summary of findings from other biological assays that supported the central hypothesis. The second part focuses on the benzoxaborole series, highlighting the key findings of the biological studies conducted. The chapter concludes with future recommendations for follow-up work to be undertaken based on different aspects of the current project.

6.2. Summary and conclusions

6.2.1. Bacterial PPAT inhibitors as antimalarial agents

Recent antibacterial campaigns at AZ and Novartis have produced a series of bacterial PPAT inhibitors.[175-177] The objective of the PhD project was therefore to reposition these series of compounds as potential antimalarial PPAT inhibitors. A 500-member compound library comprising both the cyclohexyl pyrimidine and Ugi series compounds was acquired from AZ and subjected to MTS screening at H3D. Four hits showing moderate antiplasmodium activity (*Pf*NF54 IC_{50} = 1.04 μM and 2.9 μM) and no cytotoxicity (IC_{50} > 50 μM in CHO cells) were identified.

Three of the four hits (**1-3**) were successfully re-synthesized and characterized and a close analogue of hit compound **4** (**4a/MM2-39**) was obtained. These compounds were re-tested against the blood-stage CQ-sensitive *Pf*NF54 strain in a hit validation study, and activity did not reproduce, likely invalidating the original hits. Additional analogues synthesized for the cyclohexyl pyrimidine series did not show any antiplasmodium activity (IC_{50} > 6 μM). However, compound **2/MM1-19** from the Ugi series showed antiplasmodium activity that was within two-fold of the original screening activity (IC_{50} = 5.2 μM vs 2.9 μM). SAR exploration based on this compound was then undertaken to identify compounds with greater antiplasmodium activity (**Fig. 6.1**). The series of compounds made resulted in abrogated antiplasmodium activity relative to compound **2/MM1-19** (IC_{50} 5.2 μM) as all compounds had IC_{50} > 6 μM (the highest concentration tested). Separation of the pure enantiomers of compound **2/MM1-19** revealed that one of the enantiomers (**2A/MM1-19A**) was

equipotent (IC_{50} = 5.4 μM) to the parent compound. These compounds did not show any gametocytocidal activity against either early- or late-stage gametocytes. However, they were not cytotoxic to mammalian cells when screened against Hep2G cells (compound concentration = 2 μM; percentage inhibition = 0–3.4%).

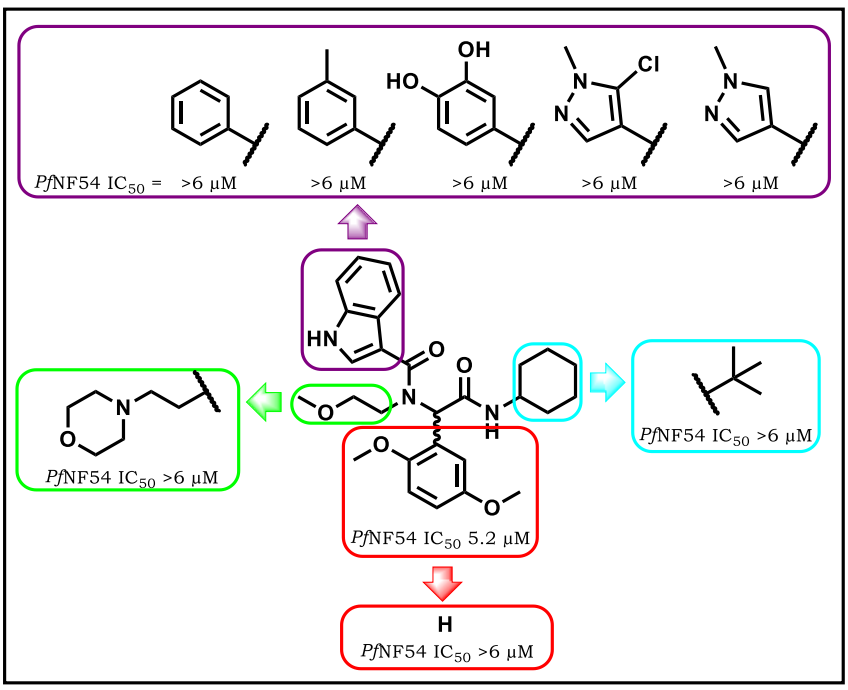

Figure 6.1: SAR derived from compound 2 and antiplasmodium activity of resulting analogues

The effects of Ugi series compounds on CoA biosynthesis and potential inhibition of *Pf*PPAT were interrogated via a chemical rescue experiment and metabolomic studies. The chemical rescue assay showed no shift in the IC_{50} of compound **2/MM1-19** upon supplementation of the assay media with the relevant CoA biosynthesis metabolites or the end-product CoA. Metabolomic data showed that treatment of the parasite with **2/MM1-19** resulted in an increase in pyrimidine biosynthesis precursors *N*-carbamoyl-L-aspartate (*N*-Carb-Asp) and dihydroorotate (DHO), and a marked decrease in the number of peptides. The latter was assessed in terms of whether it could be ascribed to peptide catabolism resulting from haemoglobin breakdown via a beta-hematin inhibition assay, which showed that **2/MM1-19** was not an inhibitor (IC_{50} = 1541 μM). Taken together, the chemical rescue experiment and metabolomics data suggest that Ugi series compounds target a different pathway in the parasite and not the PPAT or CoA biosynthesis pathways.

The triazolopyrimidine series is similar to that reported by Novartis.[175] Compound **28/MM2-145** showed moderate antiplasmodium activity with *Pf*NF54 IC_{50} = 2.2 μM.

Two SAR exploration points, SAR1 and SAR2, were proposed based on this compound (**Fig. 6.2**). The former mainly explored Craig plot substituents and the latter assessed the importance of amine and changes on the 1-(2-methoxyphenyl)ethane-1,2-diamine appendage. None of the compounds synthesized showed greater antiplasmodium activity than **28/MM2-145** (IC_{50} between 4.8 and >6 μM). Assessment of **28/MM2-145** via chemical rescue and metabolomic assays suggested that this compound is not a direct inhibitor of the CoA biosynthesis pathway but exerts its activity through other pathways. The former assay did not show any rescue of the parasite following supplementation of the assay medium with CoA and/or CoA biosynthesis metabolites. The metabolomic outcomes revealed that **28/MM2-145** shows a similar metaprint as atovaquone,[127] resulting in increased levels of *N*-Carb-Asp and DHO. This implies that this compound inhibits cellular processes other than CoA biosynthesis, and these are involved in the mitochondrial electron transport chain. In conclusion, the triazolopyrimidine series showed weak antiplasmodium activity and data suggest that these compounds do not act on the *Pf*PPAT or the CoA biosynthetic pathway. These findings suggest that the repositioning of both the target and the bacterial *Pf*PPAT inhibitors was not successful as shown by weak or lack of antiplasmodium activity of the compounds presented in this thesis.

The drug-likeness of proposed PPAT inhibitors was then assessed by investigating compliance of their physicochemical properties with the Lipinski rule-of-five (Ro5) and Veber's guidelines.[244, 246] All compounds in the Ugi series complied with the Lipinski Ro5 and Veber's TPSA guidelines, except for compound **16/MM1-86** which violated these guidelines (molecular weight = 548 g/mol vs recommended <500 g/mol). All cyclohexyl pyrimidine compounds met these criteria, with the exception of **4a/MM2-39** (molecular weight = 577.5 g/mol). Compounds in the triazolopyrimidine series were compliant with the guidelines with the exception of compound **38/MM2-141** which had a high molecular weight (538 g/mol). Assessment of compound properties thought to affect solubility showed no correlation between melting point, clogP, HPLC retention time (representing the polarity of the compounds in aqueous media), and TPSA. In conclusion, the majority of the compounds complied with the guidelines and displayed the desired drug-like properties associated with oral drugs.

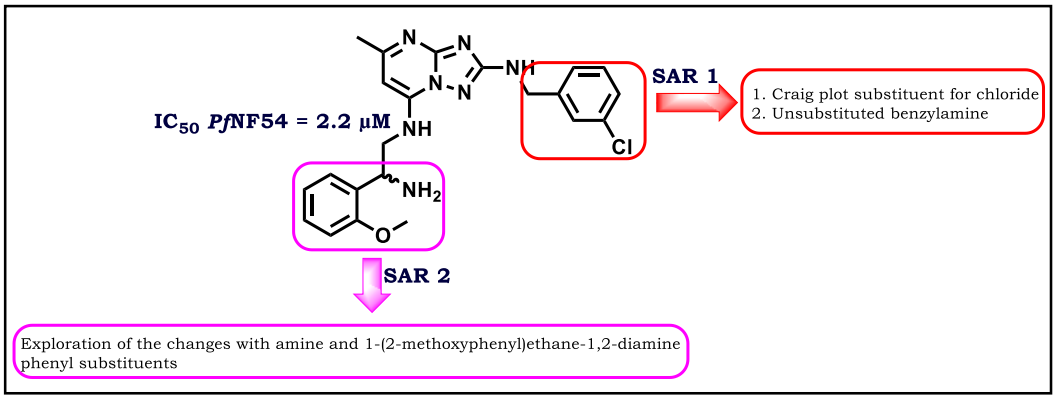

Figure 6.2: SAR exploration of the triazolopyrimidine series based on **28/MM2-145**

6.2.2. Benzoxaboroles

A series of benzoxaborole compounds acting as penicillin-binding protein (PBP) inhibitors were designed at H3D, and their binding hypothesis was retrospectively elaborated guided by the X-ray structure of bacterial PBP.[198] These compounds were co-screened to investigate their asexual blood-stage antiplasmodium activity against *P. falciparum*. One hit was thus identified (**H3D006145**, *Pf*NF54 IC_{50} = 1.06 µM). This compound was not cytotoxic against mammalian CHO or HepG2 cell lines (IC_{50} > 50 µM) and showed high solubility (105 µM) as determined from miniaturised shake flask method with HPLC. The re-synthesis of this compound (**43/MM2-92**) confirmed its antiplasmodium activity and SAR exploration was thus derived from it (**Fig. 6.3**). This figure also shows asexual blood-stage antiplasmodium activity. Ethyl esters (*Pf*NF54 IC_{50} between 1.21 and >6 µM) were less active than methyl esters (*Pf*NF54 IC_{50} between 0.4 and >6 µM), which were in turn less active than carboxylic acid derivatives (*Pf*NF54 IC_{50} = 0.12–2.6 µM). Three carboxylic acid derivatives (**73/MM2-177**, **77/MM4-127**, and **79/MM4-89**) exhibited higher antiplasmodium activity than all other compounds in this series. They also displayed favorable cytotoxicity profiles against mammalian cell lines and high aqueous solubility (**Table 6.1**).

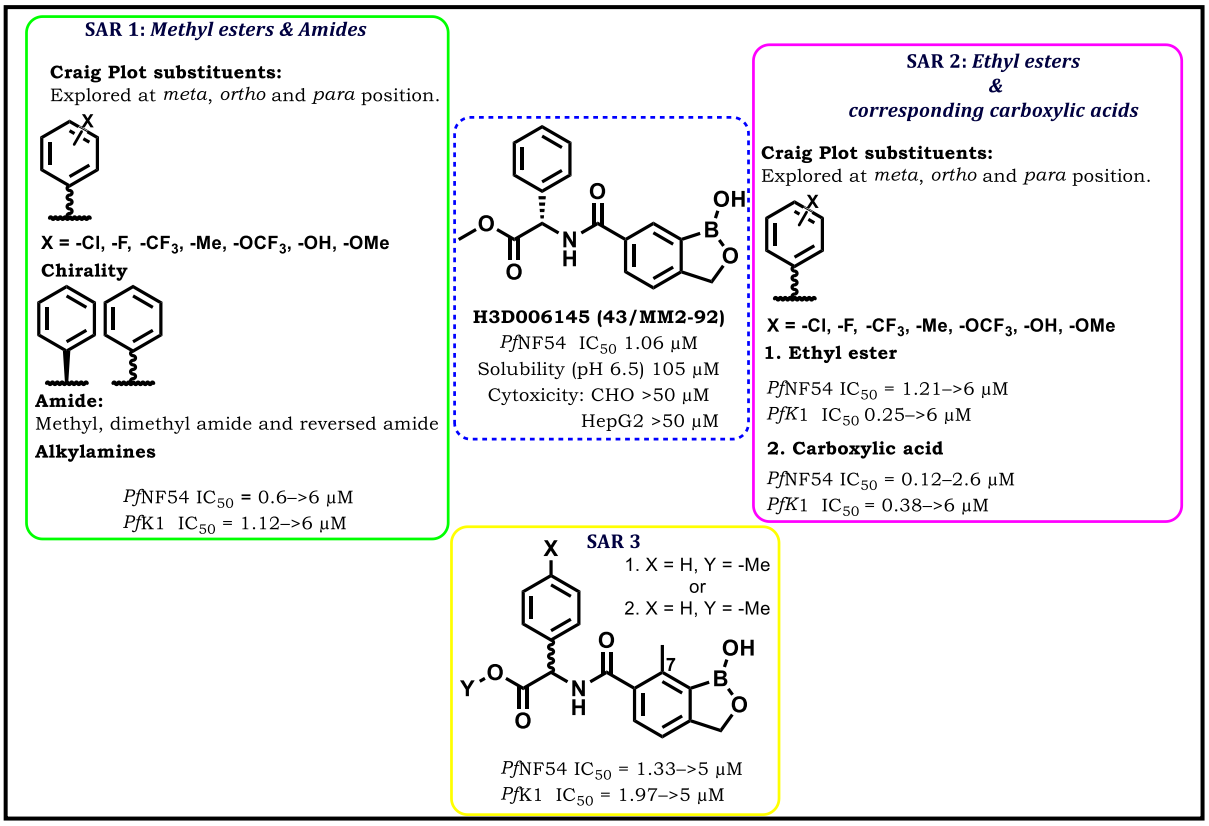

Figure 6.3: SAR design for compounds in the benzoxaboroles series and antiplasmodium activity

Table 6.1: Benzoxaborole compounds exhibiting high antiplasmodium activity

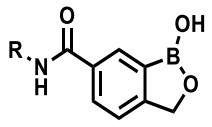

R	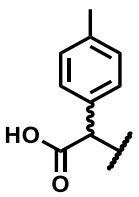	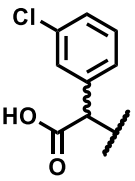	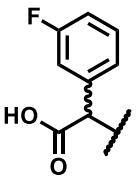
	73/MM2-177	**77/MM4-127**	**79/MM4-89**
*Pf*NF54/K1 IC_{50} (μM)	[a]0.12/>6 ([b]0.19/0.25)	[c]0.39/0.39	[c]0.34/0.48
CHO IC_{50}(μM)/[d]HepG2	>50/-	-/24	-/15
Solubility (pH 6.5, μM)	130	*160	*160

IC_{50} determined at [a]UCT, [b]STPH, and [c]UP. These are mean values from n = 2 determinations. Chloroquine and artesunate were used as controls with the standard *Pf*NF54 IC_{50} values of 0.016 μM and 0.004 μM, respectively. [d]HepG2 cells at a concentration of 2 μM (one biological replicate and technical duplicates) and results reported as percentage inhibition. *Turbidimetric solubility.

Assessment of the cytotoxicity of compounds in this series in CHO (>50 μM) and HepG2 (8.6–25% inhibition) cell lines showed that benzoxaboroles were not cytotoxic and, in selected examples, selectivity indices were between 41 and 413. The majority of compounds in this series displayed high solubility, although a few showed low solubility, in either a miniaturised shake flask method with HPLC at pH 6.5 (<5–200 μM) or using the turbidimetric method (20–200 μM). Assessment of the *in vitro* microsomal stability of select benzoxaborole compounds showed that these compounds are metabolically stable with 91–99%, 90–99% and 87–97% of the compound remaining at 30 min in human, rat, and mouse liver microsomes, respectively. Therefore, the compounds showed long projected half-lives (between 145 and >150 min) across the species and low intrinsic clearance rates (<11.6 CL_{int}, μL/min/mg).

This class of benzoxaboroles is thought to act through a novel MoA relative to clinical antimalarials as the metabolomic data did not show significant changes in

metabolites following incubation of the parasite with these compounds. The ambiguous metaprints derived suggest that the metabolites of the compounds may be other than the ones examined via the hydrophilic metabolomic approach employed here, or that the cellular processes targeted by this compound series do not result in direct cellular metabolic perturbations. This may include cellular processes such as translation or mRNA processing, whose effects do not induce quantifiable metabolites. Further assessment of potential targets or resistance markers (as employed in barcoded resistant mutant lines comprising over 42 parasite lines of *Pf*3D7 and Dd2) revealed that these lines were fully susceptible to this new class of benzoxaboroles. This implies that the new benzoxaboroles pursued in this project exert their antiplasmodium activity through novel MoAs. Retrospective analysis of the binding mode exemplified by selected compounds in a homology model of the *P. falciparum* LeuRS editing domain showed favourable interactions in the active site similar to the previously reported ligand (**AN6426**) of this protein. In summary, benzoxaboroles show antiplasmodium activity and act through a MoA projected to involve inhibition of LeuRS. The carboxylic acid class of compounds in this series exhibited higher antiplasmodium activity than the ethyl and methyl ester series.

The physicochemical properties of the benzoxaborole series were assessed to determine drug-likeness and investigate properties that impact solubility. Benzoxaboroles were compliant with the Lipinski Ro5 and Veber's guidelines: molecular weight = 249.1–373.3 g/mol, clogP < 3, TPSA < 140 $Å^2$, HBA = 4–8, and HBD = 2–4. Overall, the benzoxaboroles met all the guidelines for drug-likeness and developability (PFI < 7).

6.3. Future work and recommendations

Compounds in the Ugi and cyclohexyl series did not yield active inhibitors of the asexual blood and sexual stages of *P. falciparum*. However, the metaprint generated from the weakly active compound **2/MM1-19** showed that the Ugi series compounds may act along the pyrimidine biosynthesis and peptide catabolism pathways. Future studies should attempt to identify compounds with improved activity by exploring a chemical space other than the one interrogated in this thesis. Future work should also attempt to identify and purify *Pf*PPAT for target-based work. The moderate activity shown by compound **28/MM2-145** and the metabolomic results suggesting that this compound acts on the pyrimidine biosynthesis pathway hold promise in identifying a novel class of triazolopyrimidine compounds with novel MoAs. Future work should reattempt to optimize the chiral preparative HPLC mobile phase for the

separation of enantiomers of **28/MM2-145**. SAR exploration should be undertaken to discover novel analogues based on the most active enantiomer.

Benzoxaboroles show antiplasmodium activity and this study has revealed that carboxylic acid analogues display greater antiplasmodium active than corresponding esters. This shows that this scaffold has potential for exploration to identify next-generation antimalarial on the basis that they have a unique chemotype and act against previously unidentified targets. As such, future work should determine if the activity of the esters may be the result of metabolism into carboxylic acid over time. Identification of the target(s) of these compounds remains an ongoing pursuit but a hypothesis around inhibition of *P. falciparum* LeuRS has been made. The series of compounds presented here should also be subjected to resistance selection in order to derive resistant mutants and uncover genetic changes resulting from treatment with these compounds. In conclusion, this benzoxaborole series is: (i) metabolically stable in liver microsomes *in vitro*, (ii) displays sub-micromolar activity, (iii) is selective for the parasite over mammalian cells, and (iv) shows high aqueous solubility, all of which warrant its progression to proof-of-concept *in vivo* efficacy studies in mouse models.

6.4. References

1. de Jonge, B. L.; Walkup, G. K.; Lahiri, S. D.; Huynh, H.; Neckermann, G.; Utley, L.; Nash, T. J.; Brock, J.; San Martin, M.; Kutschke, A., Discovery of inhibitors of 4′-phosphopantetheine adenylyltransferase (PPAT) to validate PPAT as a target for antibacterial therapy. *Antimicrob. Agents Chemother.* **2013**, *57* (12), 6005-6015.

2. Moreau, R. J.; Skepper, C. K.; Appleton, B. A.; Blechschmidt, A.; Balibar, C. J.; Benton, B. M.; Drumm III, J. E.; Feng, B. Y.; Geng, M.; Li, C., Fragment-based drug discovery of inhibitors of phosphopantetheine adenylyltransferase from gram-negative bacteria. *J. Med. Chem.* **2018**, *61* (8), 3309-3324.

3. Skepper, C. K.; Moreau, R. J.; Appleton, B. A.; Benton, B. M.; Drumm III, J. E.; Feng, B. Y.; Geng, M.; Hu, C.; Li, C.; Lingel, A., Discovery and Optimization of Phosphopantetheine Adenylyltransferase Inhibitors with Gram-Negative Antibacterial Activity. *J. Med. Chem.* **2018**, *61* (8), 3325-3349.

4. Allman, E. L.; Painter, H. J.; Samra, J.; Carrasquilla, M.; Llinás, M., Metabolomic profiling of the malaria box reveals antimalarial target pathways. *Antimicrob. Agents Chemother.* **2016**, *60* (11), 6635-6649.

5. Veber, D. F.; Johnson, S. R.; Cheng, H.-Y.; Smith, B. R.; Ward, K. W.; Kopple, K. D., Molecular Properties That Influence the Oral Bioavailability of Drug Candidates. *J. Med. Chem.* **2002**, *45* (12), 2615-2623.

6. Lipinski, C. A.; Lombardo, F.; Dominy, B. W.; Feeney, P. J., Experimental and computational approaches to estimate solubility and permeability in drug discovery and development settings. *Adv Drug Deliv Rev* **2001**, *46* (1-3), 3-26.

7. Newman, H.; Krajnc, A.; Bellini, D.; Eyermann, C. J.; Boyle, G. A.; Paterson, N. G.; McAuley, K. E.; Lesniak, R.; Gangar, M.; von Delft, F.; Brem, J.; Chibale, K.; Schofield, C. J.; Dowson, C. G., High-Throughput Crystallography Reveals Boron-Containing Inhibitors of a Penicillin-Binding Protein with Di- and Tricovalent Binding Modes. *J. Med. Chem.* **2021**, *64* (15), 11379-11394.

Chapter 7: Experimental

7.1. Chemistry

7.1.1. General information on experimental data

All commercially available chemicals were purchased from Sigma-Aldrich (South Africa), AK Scientific (USA), Fluorochem (UK) or Combi-Blocks Limited (USA) and were of analytical grade and thus used without further purification. All solvents used were of analytical grade and dry solvents were used as purchased from the supplier where required. Where necessary, however, ^{1}H NMR and LC-MS were used to ascertain purity. Where applicable, microwave-irradiated reactions were conducted on Discover® SP with maximum pressure 250 psi and power 200 W. Reaction progress was monitored via analytical thin layer chromatography (TLC) sourced from Merck (South Africa) as TLC Silica gel 60 F_{254} aluminium-backed and LC-MS. TLC plates were prepared using optimized solvent mixtures in a 100 mL beaker and were either dried or further developed with staining solutions such as ninhydrin, iodine or potassium permanganate. Developed TLC plates were subsequently visualized under ultraviolet light at 254 nm. Compounds were purified on silica gel chromatography using Merck kieselgel 60: 70 – 230 mesh by gravity column chromatography, preparative-TLC (prep-TLC) plates (silica gel GF, 20 × 20 cm, 2000 microns) sourced from Silicycle inc. (Canada) or flash column chromatography on a Biotage Isolera™ system (Biotage AB, Uppsala, Sweden). Pure enantiomers were obtained from the preparative-HPLC (Waters® 2545 Quaternary Gradient Module HPLC) fitted with a chiral column (IA: particle size 5 µm, 20 mm Φ × 250 mm L preparative column, 4.6 mm Φ × 250 mm L analytical column) eluting with appropriately optimized solvent mixture.

Reported compounds were characterized by ^{1}H NMR, ^{13}C NMR, LC-MS and the melting point was determined. Spectra were recorded on Varian Mercury (^{1}H 300 MHz), Bruker Ultrashield-Plus (^{1}H 400, ^{13}C 101 MHz) or Bruker Ascend™ 600 (^{1}H 600, ^{13}C 151 MHz) instruments. The NMR samples were dissolved in deuterated acetonitrile-d_3 (CD_3CN), dimethyl sulfoxide (DMSO-d_6), methanol-d_4 (MeOD) or chloroform-d ($CDCl_3$). Chemical shifts (δ) are reported in parts per million (ppm) and rounded to two decimal places. Coupling constants (J) are reported in Hertz (Hz) and rounded to two decimal places. Abbreviations used in assigning ^{1}H-NMR signals are: br.s (broad singlet), d (doublet), dd (doublet of doublets), ddd (doublet of doublet of doublets), dt (doublet of triplets), hept (heptet), m (multiplet), q (quartet), s (singlet),

t (triplet), or td (triplet of doublets). Melting points were determined using the Reichert-Jung Thermovar hot stage microscope and were recorded uncorrected.

The HPLC and mass spectra used to determine the purities and molecular ions of target compounds were acquired on an Agilent HPLC system equipped with Agilent 1260® Infinity Binary Pump, Agilent 1260® Infinity Diode Array Detector, Agilent 1290® Infinity Column Compartment, Agilent 1260® Infinity Autosampler, Agilent 6120® Quadrupole LC–MS, and Peak Scientific® Genius 1050 Nitrogen Generator. The column used was an X-bridge® C18, 2.6 µm, 2.1 mm (ID) x 30 mm (length) maintained at 35 °C. The composition and gradient conditions of the mobile phase used at a flow rate of 0.9 mL/min are listed in **Table 7.1**. The injection volume was 2 µL, and the mass spectra were obtained both in the positive and negative mode by electrospray ionization (ESI) and atmospheric pressure chemical ionization (APCI). The diode array detector was programmed to scan the eluents at an absorption wavelength range of 210-640 nm.

Table 7.1: High-performance liquid chromatography (HPLC) gradient conditions

Time (min)	%**A**	%**B**
0 – 0.35	85	15
0.35 – 1.2	85	15
1.2 – 4.5	0	100

A, 10 mM NH_4OAc in buffer (0.4% acetic acid); **B**, 10 mM NH_4OAc (0.4% acetic acid) in 90% MeOH and 10% H_2O

7.2. Synthesis and characterization

7.2.1. General procedure for synthesis of the Ugi series

Carboxylic acid (1 mmol), cyclohexyl isocyanide (0.5 – 1 mmol), 2,5-dimethoxybenzaldehyde (1 mmol) and 2-methoxyethylamine (1 mmol) were added to a microwave tube (10 mL) containing a magnetic stirrer bar. The mixture was subjected to microwave irradiation (<250 psi) at 60 °C for 30 min. The reaction mixture was cooled to 14 – 24 °C, diluted with DCM and washed with $NaHCO_3$. The solution was extracted with DCM (×3), dried on Na_2SO_4, and the filtrate was concentrated under reduced pressure. The resulting crude product was either submitted to column chromatography or prep-TLC elution with an appropriate solvent system to give the desired compound. All compounds obtained racemic mixture but **2** was submitted to a chiral column to obtain pure enantiomers.

N-(2-(2-aminoethoxy)ethyl)-N-(2-(cyclohexylamino)-1-(2,5-dimethoxyphenyl)-2-oxoethyl)thiophene-2-carboxamide, 1/MM1-15

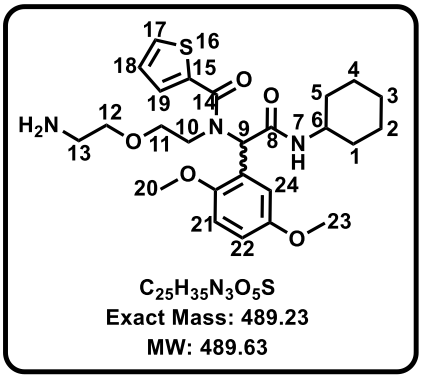

This compound was obtained from thiophene-2-carboxylic acid (352 mg, 2.74 mmol, 1 eq.), 1,5-diamino-3-oxapentane (286 mg, 2.74 mmol, 1 eq.), 2,5-dimethoxybenzaldehyde (457 mg, 2.74 mmol, 1 eq.) and cyclohexyl isocyanide (300 mg, 2.74 mmol, 1 eq.) as a white wax (190 mg, 12%); *Rf* (DCM:MeOH, 8:2) 0.2; ^{1}H NMR (300 MHz, $CDCl_3$) δ 7.45 (dd, *J* = 5.0, 1.1 Hz, 1H, H^{19}), 7.37 (d, *J* = 3.6 Hz, 1H, –NH^7), 7.02 (dd, *J* = 5.0, 1.1 Hz, 1H, H^{17}), 6.95 – 6.76 (m, 3H, $H^{18, 21, 22}$), 6.59 (s, 1H, H^{24}), 6.08 (–NH_2), 5.88 (s, 1H, H^9), 3.88 (m, 1H, H^6), 3.80 – 3.35 (m, 12H, $H^{10, 11, 12, 20, 23}$), 3.05 (m, 2H, H^{13}), 2.00 – 1.54 (m, 5H, $H^{1, 3b, 5}$), 1.36 – 1.09 (m, 5H, $H^{2,3a,4}$). ^{13}C NMR (101 MHz, $CDCl_3$) δ 168.8, 167.5, 153.5, 152.1, 138.1, 129.3, 128.9, 127.0 (2C), 124.4, 116.3 (2C), 114.4, 111.5, 70.8, 67.9, 55.8 (2C), 48.7, 40.6, 33.2, 33.0, 25.5, 25.0 (2C). HPLC-MS (APCI/ESI): Purity = 99%, t_R = 2.343 min, *m/z* $[M+1]^+$ = 490.2, calculated exact mass for $C_{25}H_{35}N_3O_5S$: 489.23.

N-(2-(cyclohexylamino)-1-(2,5-dimethoxyphenyl)-2-oxoethyl)-N-(2-methoxyethyl)-1H-indole-3-carboxamide, 2/MM1-19

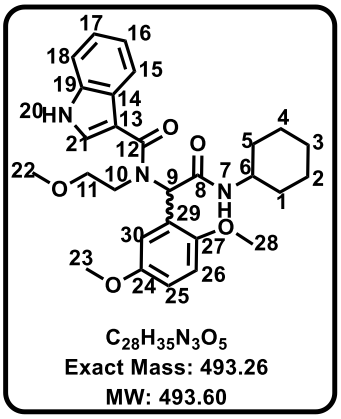

This compound was obtained from 1*H*-indole-3-carboxylic acid (590 mg, 3.64 mmol, 1 eq.), 2-methoxyethylamine (275 mg, 3.64 mmol, 1 eq.), 2,5-dimethoxybenzaldehyde (604 mg, 3.64 mmol, 1 eq.) and cyclohexyl isocyanide (400 mg, 3.64 mmol, 1 eq.) as a white solid (580 mg, 52%); m.p: 155-156 °C; *Rf* (EtOAc:Hex, 7:3) 0.6; ^{1}H NMR (300 MHz, DMSO-d_6) δ 11.49 (d, *J* = 6.0 Hz, 1H, H^{20}), 8.09 (d, *J* = 7.8 Hz, 1H, –NH^7), 7.77 (d, *J* = 6.0 Hz, 1H, H^{21}), 7.49 – 7.39 (m, 2H, $H^{15, 18}$), 7.16 (ddd, *J* = 8.1, 7.0, 1.4 Hz, 1H, H^{17}), 7.10 (ddd, *J* = 8.1, 7.1, 1.3 Hz, 1H, H^{16}), 6.94 – 6.89 (m, 2H, $H^{25, 26}$), 6.68 (s, 1H, H^{30}), 5.93 (s, 1H, H^9), 3.68 (m, 5H, $H^{11, 22}$), 3.59 (s, 3H, H^{28}), 3.08 (s, 3H, H^{23}), 2.92 (m, 1H, H^6), 1.89 – 1.49 (m, 5H, $H^{1, 3b, 5}$), 1.37 – 1.05 (m, 5H, $H^{2, 3a, 4}$). ^{13}C NMR (101 MHz, DMSO-d_6) δ 170.9, 170.6, 153.3, 152.5, 136.0, 127.0, 125.9, 125.4, 122.7, 121.0, 116.5, 113.8 (2C), 111.6, 111.5, 110.9, 77.2, 69.9, 58.5, 55.8, 55.7, 48.9, 45.5, 33.4, 33.15, 25.7, 25.5, 25.3. HPLC-MS (APCI/ESI): Purity = 98%, t_R = 2.866 min, *m/z* $[M+1]^+$ = 494.2, calculated exact mass for $C_{28}H_{35}N_3O_5$: 493.26.

(R)-N-(2-(cyclohexylamino)-1-(2,5-dimethoxyphenyl)-2-oxoethyl)-N-(2-methoxyethyl)-1H-indole-3-carboxamide, 2A/MM1-19A

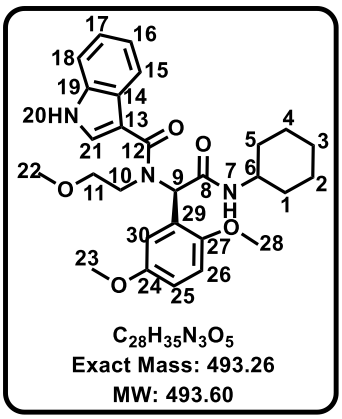

This compound was obtained from **2** on chiral prep-HPLC (t_R = 7.81 min) as a yellow wax; *Rf* (EtOAc:EtOH:Hex, 5:0.5:4.5) 0.3; ^{1}H NMR (300 MHz, $CDCl_3$) δ 9.71 (s, 1H, H^{20}), 8.03 (dd, *J* = 7.8, 1.4 Hz, 1H, H^{15}), 7.37 (d, *J* = 2.7 Hz, 1H, H^{21}), 7.14 (ddd, *J* = 8.3, 7.0, 1.4 Hz, 1H, H^{17}), 7.07 (ddd, *J* = 8.3, 7.0, 1.4 Hz, 1H, H^{16}), 6.90 (dd, *J* = 8.0, 1.5 Hz, 1H, H^{18}), 6.84 (dd, *J* = 8.8, 3.0 Hz, 1H, H^{25}), 6.78 (d, *J* = 3.0 Hz, 1H, H^{30}), 6.71 (d, *J* = 8.9 Hz, 1H, H^{26}), 6.19 (s, 1H, H^9), 4.16 – 3.99 (m, 2H, H^{11}), 3.76 (s, 3H, H^{22}), 3.47 – 3.32 (m, 8H, $H^{10, 23, 28}$), 3.02 – 2.87 (m, 1H, H^6), 2.12 – 1.73 (m, 5H, $H^{1, 3b, 5}$), 1.52 – 1.11 (m, 5H, $H^{2, 3a, 4}$). ^{13}C NMR (101 MHz, $CDCl_3$) δ 170.9, 170.6, 153.3, 152.5, 136.0, 127.0, 125.9, 125.4, 122.7, 121.5, 116.5 113.8 (2C), 111.6, 111.5, 110.9, 77.2, 69.9, 58.5, 55.8, 55.7, 48.9, 45.5, 33.4, 33.2, 25.7, 25.4, 25.3. HPLC-MS (APCI/ESI): Purity = 98%, t_R = 2.866 min, *m/z* $[M+1]^+$ = 494.2, calculated exact mass for $C_{28}H_{35}N_3O_5$: 493.26.

(S)-N-(2-(cyclohexylamino)-1-(2,5-dimethoxyphenyl)-2-oxoethyl)-N-(2-methoxyethyl)-1H-indole-3-carboxamide, 2B/MM1-19B

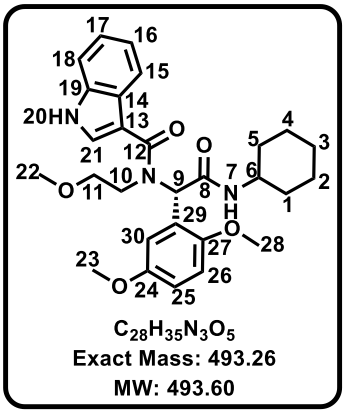

This compound was obtained from **2** on chiral prep-HPLC (t_R = 10.75 min) as a yellow-brown wax; *Rf* (EtOAc:EtOH:Hex, 5:0.5:4.5) 0.3; ^{1}H NMR (300 MHz, $CDCl_3$) δ 9.98 (s, 1H, H^{20}), 8.85 (s, 1H, –NH^7), 8.01 (dd, *J* = 7.9, 1.1 Hz, 1H, H^{15}), 7.35 (d, *J* = 2.7 Hz, 1H, H^{21}), 7.11 (ddd, *J* = 8.0, 7.0, 1.1 Hz, 1H, H^{17}), 7.02 (ddd, *J* = 8.0, 7.0, 1.1 Hz, 1H, H^{16}), 6.84 (dd, *J* = 8.9, 3.0 Hz, 1H, H^{25}), 6.78 (m, 2H, $H^{18, 30}$), 6.70 (d, *J* = 8.9 Hz, 1H, H^{26}), 6.19 (s, 1H, H^9), 4.20 – 3.97 (m, 2H, H^{11}), 3.77 (s, 3H, H^{22}), 3.47 – 3.22 (m, 8H, $H^{10, 23, 28}$), 3.02 – 2.82 (m, 1H, H^6), 2.20 – 1.73 (m, 5H, $H^{1, 3b, 5}$), 1.56 – 1.12 (m, 5H, $H^{2, 3a, 4}$). ^{13}C NMR (101 MHz, $CDCl_3$) δ 170.9, 170.6, 153.3, 152.5, 136.9, 127.1, 125.9, 125.4, 122.6, 121.0, 116.5, 113.8 (2C), 111.6, 111.5, 110.9, 77.2, 69.9, 58.5, 55.8, 55.7, 48.9, 45.5, 33.4, 33.2, 25.7, 25.4, 25.3. HPLC-MS (APCI/ESI): Purity > 99%, t_R = 2.576 min, *m/z* $[M+1]^+$ = 494.2, calculated exact mass for $C_{28}H_{35}N_3O_5$: 493.26.

N-(2-(cyclohexylamino)-2-oxoethyl)-N-(2-methoxyethyl)-1H-indole-3-carboxamide, 15/MM1-85

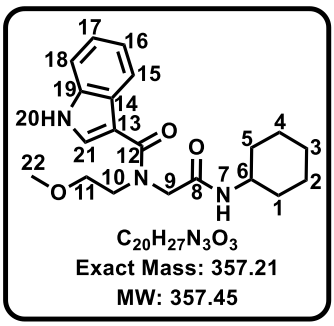

This compound was obtained from 1*H*-indole-3-carboxylic acid (200 mg, 1.24 mmol, 1 eq.), 2-methoxyethylamine (93 mg, 1.24 mmol, 1 eq.), formaldehyde (37 mg, 1.24 mmol, 1 eq.) and cyclohexyl isocyanide (68 mg, 0.62 mmol, 1 eq.) as a light yellow wax (5 mg, 10%); *Rf* (EtOAc: Hex, 3:7) 0.4; ^{1}H NMR (300 MHz, $CDCl_3$) δ 7.53 (s, 1H, H^{21}), 7.43 – 7.34 (m, 2H, H^{15}, H^{18}), 7.25 – 7.20 (m, 2H, H^{16}, H^{17}), 4.20 (s, 2H, H^9), 3.78 (m, 5H, H^6, H^{10}, H^{11}), 3.38 (s, 3H, H^{22}), 1.97 – 1.08 (m, 10H, H^1, H^2, H^3, H^4, H^5). HPLC-MS (APCI/ESI): Purity > 99%, t_R = 2.411 min, *m/z* $[M+1]^+$ = 358.1, calculated exact mass for $C_{20}H_{27}N_3O_3$: 357.45.

N-(2-(cyclohexylamino)-1-(2,5-dimethoxyphenyl)-2-oxoethyl)-N-(2-morpholinoethyl)-1H-indole-3-carboxamide, 16/MM1-86

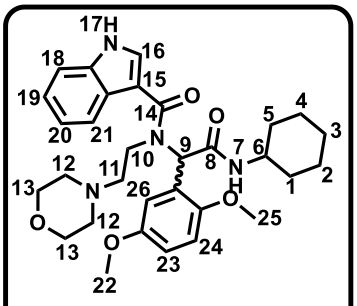

Obtained from 5-chloro-1-methyl-1H-pyrazole-4-carboxylic acid (150 mg, 0.925 mmol, 1 eq.), 2-morpholinoethan-1-amine (120 mg, 0.925 mmol, 1 eq.), 2,5-dimethoxybenzaldehyde (154 mg, 0.925 mmol, 1 eq.) and cyclohexyl isocyanide (50 mg, 0.463 mmol, 0.5 eq.) as a white solid (83 mg, 33%); m.p: 180-183 °C; *Rf* (EtOAc:EtOH:Hex, 6:2:2) 0.5 (prep-TLC); ^{1}H NMR (600 MHz, DMSO-d_6) δ 11.46 (d, J = 2.5 Hz, 1H, -NH^{17}), 7.96 (d, J = 2.5 Hz, 1H, H^{16}), 7.75 (dt, J = 8.0, 1.0 Hz, 1H, H^{18}), 7.42 (dt, J = 8.0, 1.0 Hz, 1H, H^{21}), 7.15 (ddd, J = 8.0, 7.0, 1.0 Hz, 1H, H^{20}), 7.09 (ddd, J = 8.0, 7.0, 1.0 Hz, 1H, H^{19}), 6.97 – 6.86 (m, 2H, H$^{23, 24}$), 6.73 (s, 1H, H^{26}), 5.97 (s, 1H, H^9), 3.68 (s, 4H, H^{25,6}), 3.60 (br.s, 2H, H^{10}), 3.41 (m, 7H, H$^{13, 22}$), 3.32 (br.s, 2H, H^{11}), 2.21 – 1.92 (m, 4H, H^{12}), 1.79 – 1.61 (m, 5H, H^{1,3b,5}), 1.33 – 1.02 (m, 5H, H^{2,3a,4}). ^{13}C NMR (151 MHz, DMSO-d_6) δ 169.5, 167.9, 153.4, 152.5, 136.0, 127.2, 126.6, 125.9, 122.3, 120.9, 120.3, 116.1, 113.9 (2C), 112.3, 112.1, 111.3, 66.5 (2C), 56.2 (2C), 55.9 (2C), 53.8 (2C), 48.3, 32.7, 32.6, 25.7, 25.1, 25.1. HPLC-MS (APCI/ESI): Purity >99%, t_R = 0.884 min, m/z $[M+1]^+$ = 549.2, calculated exact mass for $C_{31}H_{40}N_4O_5$: 548.30.

N-(2-(cyclohexylamino)-1-(2,5-dimethoxyphenyl)-2-oxoethyl)-N-(2-methoxyethyl)benzamide, 17/MM1-56

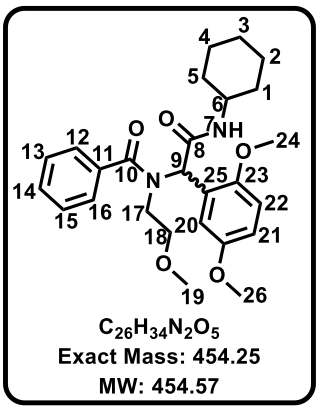

This compound was obtained from benzoic acid (447 mg, 3.66 mmol, 1 eq.), 2-methoxyethylamine (275 mg, 3.66 mmol, 1 eq.), 2,5-dimethoxybenzaldehyde (609 mg, 3.66 mmol, 1 eq.) and cyclohexyl isocyanide (400 mg, 3.66 mmol, 0.5 eq.) as a white solid (765 mg, 34%); m.p: 158-161 °C; *Rf* (EtOAc:Hex, 5:5) 0.35; ^{1}H NMR (600 MHz, DMSO-d_6) δ 7.92 (d, J = 8.0 Hz, 1H, –NH^7), 7.46 – 7.40 (m, 3H, H$^{12, 14, 16}$), 7.33 – 7.28 (m, 2H, H$^{13, 15}$), 6.91 – 6.86 (m, 2H, H$^{21, 22}$), 6.60 (br.s, 1H, H^{20}), 5.32 (s, 1H, H^9), 3.82 – 3.58 (m, 7H, H$^{18a, 19, 24}$), 3.52 – 3.44 (m, 1H, H^{18b}), 3.40 – 3.32 (m, 1H, H^{17a}), 3.25 – 3.17 (m, 1H, H^{17b}), 3.04 (s, 3H, H^{26}), 2.69 – 2.61 (m, 1H, H^6), 1.77 – 1.60 (m, 5H, H$^{1,3b, 5}$), 1.57 – 1.09 (m, 5H, H$^{2, 3a, 4}$). ^{13}C NMR (151 MHz, DMSO-d_6) δ 172.5, 168.7, 153.2, 152.3, 137.5, 129.9, 128.8 (2C), 126.8, 125.5, 116.0, 114.3 (2C), 112.3, 68.9, 61.4, 58.2, 56.1, 55.9, 48.2, 43.9, 32.6 (2C), 25.6,

25.1, 25.0. HPLC-MS (APCI/ESI): Purity 99%, t_R = 2.268 min, *m/z* $[M+1]^+$ = 455.2, calculated exact mass for $C_{26}H_{34}N_2O_5$: 454.25.

N-(2-(cyclohexylamino)-1-(2,5-dimethoxyphenyl)-2-oxoethyl)-N-(2-methoxyethyl)-4-methylbenzamide, 18/MM1-82

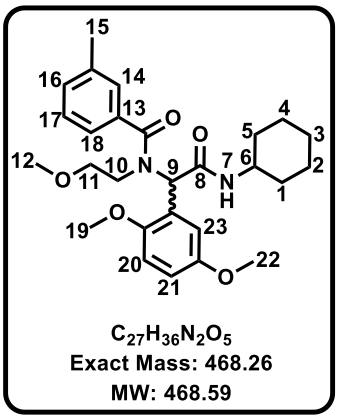

This product was obtained from 4-methylbenzoic acid (150 mg, 1.10 mmol, 1 eq.), 2-methoxyethylamine (83 mg, 1.10 mmol, 1 eq.), 2,5-dimethoxybenzaldehyde (183 mg, 1.10 mmol, 1 eq.), and cyclohexyl isocyanide (60 mg, 1.10 mmol, 0.5 eq.) as a white solid (192 mg, 77%); m.p: 107-110 °C; *Rf* (EtOAc:Hex, 7:3) 0.4; ^{1}H NMR (600 MHz, DMSO-d_6) δ 7.79 (d, *J* = 7.8 Hz, 1H, –NH^7), 7.33 (ddd, *J* = 8.3, 7.5, 1.6 Hz, 1H, H^{18}), 7.26 (d, *J* = 1.6 Hz, 1H, H^{14}), 7.17 – 7.12 (m, 2H, H$^{16, 17}$), 6.95 (d, *J* = 9.0 Hz, 1H, H^{20}), 6.92 (dd, *J* = 9.0, 3.0 Hz, 1H, H^{21}), 6.69 (d, *J* = 3.0 Hz, 1H, H^{23}), 5.40 (s, 1H, H^9), 3.70 – 3.66 (m, 8H, H$^{11, 12, 19}$), 3.29 (m, 2H, H^{10}), 3.05 (s, 3H, H^{22}), 2.81 – 2.74 (m, 1H, H^6), 2.35 (s, 3H, H^{15}), 1.84 – 1.51 (m, 3H, H^{1,3b,5}), 1.57 – 1.05 (m, 5H, H^{2,3a,4}). ^{13}C NMR (151 MHz, DMSO-d_6) δ 172.4, 168.8, 153.4, 152.5, 137.9, 137.6, 130.3, 128.6, 127.3, 125.8, 124.0, 116.3, 114.6 (2C), 112.6, 69.4, 58.2, 56.3, 56.0, 48.3, 44.0, 32.7, 32.6, 25.7, 25.1, 25.0, 21.4. HPLC-MS (APCI/ESI): Purity 97%, t_R = 2.610 min, *m/z* $[M+1]^+$ = 469.2, calculated exact mass for $C_{27}H_{36}N_2O_5$: 468.26.

N-(2-(cyclohexylamino)-1-(2,5-dimethoxyphenyl)-2-oxoethyl)-N-(2-methoxyethyl)-1-methyl-1H-pyrazole-4-carboxamide, 19/MM1-63

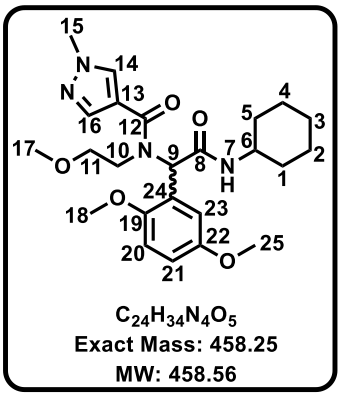

This compound was obtained from 1-methyl-1*H*-pyrazole-4-carboxylic acid (231 mg, 1.83 mmol, 1 eq.), 2-methoxyethylamine (138 mg, 0.56 mmol, 1 eq.), 2,5-dimethoxybenzaldehyde (304 mg, 1.83 mmol, 1 eq.) and cyclohexyl isocyanide (200 mg, 1.83 mmol, 1 eq.) as a clear wax (73 mg, 9%); *Rf* (EtOAc:EtOH:Hex, 4:1:5) 0.5; ^{1}H NMR (300 MHz, $CDCl_3$) δ 7.76 (s, 1H, H^{14}), 7.62 (s, 1H, H^{16}), 6.75 (dd, *J* = 8.9, 2.8 Hz, 1H, H^{21}), 6.71 – 6.62 (m, 2H, H$^{20, 23}$), 5.91 (s, 1H, H^9), 4.06 – 3.88 (m, 2H, H^{11}), 3.85 (s, 3H, H^{15}), 3.68 (s, 3H, H^{25}), 3.58 (s, 3H, H^{18}), 3.33 – 3.18 (m, 5H, H^{10,17}), 2.99 – 2.68 (m, 1H, H^6), 2.07 – 1.54 (m, 5H, H$^{1, 3b, 5}$), 1.44 – 1.09 (m, 5H, H$^{2, 3a, 4}$). ^{13}C NMR (151 MHz, $CDCl_3$) δ 169.4, 168.2, 153.4, 152.2, 140.3, 131.1, 124.8, 118.1, 116.5, 113.9, 111.3, 69.5, 64.0, 58.5, 55.8, 55.8,

48.6, 45.2, 39.2, 33.4, 33.2, 25.6, 25.2 (2C). HPLC-MS (APCI/ESI): Purity 98%, t_R = 2.461 min, *m/z* $[M+1]^+$ = 459.2, calculated exact mass for $C_{24}H_{34}N_4O_5$: 458.25.

5-chloro-N-(2-(cyclohexylamino)-1-(2,5-dimethoxyphenyl)-2-oxoethyl)-N-(2-methoxyethyl)-1-methyl-1H-pyrazole-4-carboxamide, 20/MM1-64

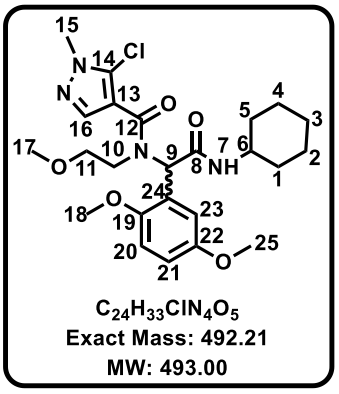

This compound was obtained from 5-chloro-1-methyl-1*H*-pyrazole-4-carboxylic acid (235 mg, 1.83 mmol, 1 eq.), 2-methoxyethylamine (138 mg, 0.56 mmol, 1 eq.), 2,5-dimethoxybenzaldehyde (304 mg, 1.83 mmol, 1 eq.) and cyclohexyl isocyanide (200 mg, 1.83 mmol, 1 eq.) as a yellow gum (193 mg, 21%); m.p: 112-114 °C; *Rf* (EtOAc:EtOH:Hex, 6:3:1) 0.4; 1H NMR (300 MHz, $CDCl_3$) δ 8.33 (s, 1H, –NH^7), 7.60 (s, 1H, H^{16}), 6.81 (dd, *J* = 8.9, 2.8 Hz, 1H, H^{21}), 6.78 – 6.68 (m, 2H, $H^{20, 23}$), 5.81 (s, 1H, H^9), 4.15 – 3.90 (m, 2H, H^{11}), 3.86 (s, 3H, H^{17}), 3.73 (s, 3H, H^{25}), 3.70 (s, 3H, H^{15}), 3.41 – 3.21 (m, 5H, $H^{10, 18}$), 3.04 – 2.78 (m, 1H, H^6), 2.13 – 1.67 (m, 5H, $H^{1,3b,5}$), 1.42 – 1.20 (m, 5H, $H^{2, 3a, 4}$). ^{13}C NMR (151 MHz, $CDCl_3$) δ 168.9, 167.5, 153.4, 152.3, 138.4, 129.0, 124.8, 116.7, 114.7, 114.1, 111.3, 69.3, 63.9, 58.7, 56.1, 55.9, 48.7, 45.3, 36.6, 33.6, 33.2, 25.8, 25.4 (2C). HPLC-MS (APCI/ESI): Purity 97%, t_R = 2.487 min, *m/z* $[M+1]^+$ = 493.1, calculated exact mass for $C_{24}H_{34}N_4O_5$: 492.21.

N-(2-(cyclohexylamino)-1-(2,5-dimethoxyphenyl)-2-oxoethyl)-3,4-dihydroxy-N-(2-methoxyethyl)benzamide, 21/MM1-81

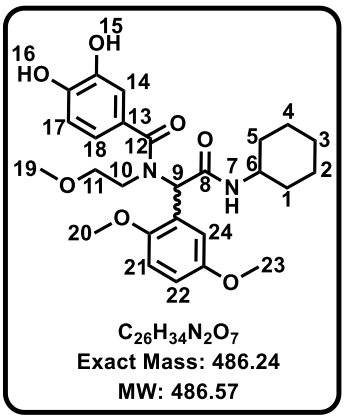

This compound was obtained from 3,4-dihydroxybenzoic acid (150 mg, 0.973 mmol, 1 eq.), 2-methoxyethylamine (73.1 mg, 0.973 mmol, 1 eq.), 2,5-dimethoxybenzaldehyde (162 mg, 0.973 mmol, 1 eq.) and cyclohexyl isocyanide (53.1 mg, 0.487 mmol, 0.5 eq.) as a white solid (43 mg, 18%); m.p: 173-176 °C; *Rf* (EtOAc:EtOH:Hex, 3:1:6) 0.5 (prep-TLC); ^{1}H NMR (300 MHz, $CDCl_3$) δ 7.05 (s, 1H, H^{18}), 6.88 – 6.70 (m, 3H, $H^{14, 21, 22}$), 6.68 – 6.64 (m, 2H, $H^{17, 24}$), 5.77 (s, 1H, H^9), 4.14 – 3.92 (m, 2H, H^{11}), 3.74 (s, 3H, H^{19}), 3.65 (s, 3H, H^{20}), 3.39 (s, 3H, H^{23}), 3.36 – 3.19 (m, 2H, H^{10}), 3.03 – 2.87 (m, 1H, H^6), 2.16 – 1.65 (m, 5H, $H^{1, 3b, 5}$), 1.50 – 1.09 (m, 5H, $H^{2, 3a, 4}$). ^{13}C NMR (151 MHz, $CDCl_3$) δ 175.9, 170.8, 153.4, 152.2, 147.3, 144.7, 127.6, 124.9, 119.9, 116.7, 115.0, 113.9

(2C), 111.5, 69.7, 64.5, 58.7, 55.9, 55.9, 49.3, 45.5, 33.4, 33.2, 25.7, 25.4 (2C). HPLC-MS (APCI/ESI): Purity >95%, t_R = 2.493 min, *m/z* $[M+1]^+$ =487.2, calculated exact mass for $C_{26}H_{34}N_2O_7$: 486.24.

N-(2-(tert-butylamino)-1-(2,5-dimethoxyphenyl)-2-oxoethyl)-N-(2-methoxyethyl)-1H-indole-3-carboxamide, 22/MM1-53

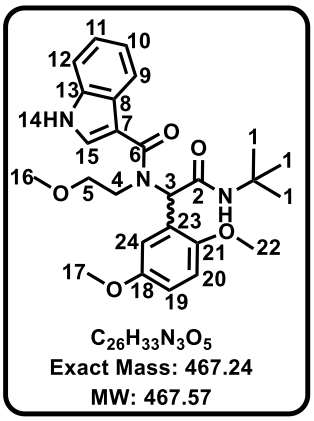

This compound was obtained from 1*H*-indole-3-carboxylic acid (200 mg, 1.20 mmol, 1 eq.), 2-methoxyethylamine (90.4 mg, 1.20 mmol, 1 eq.), 2,5-dimethoxybenzaldehyde (194 mg, 1.10 mmol, 1 eq.) and tert-butyl isocyanide (100 mg, 1.10 mmol, 1 eq.) as a white solid (580 mg, 52%); m.p: 128-133 °C; *Rf* (EtOAc:EtOH:Hex, 3:6.5:0.5) 0.3 (prep-TLC); ^{1}H NMR (600 MHz, CD_3CN) δ 9.81 (s, 1H, -NH^{14}), 7.86 (dd, *J* = 8.1, 1.1 Hz, 1H, H^9), 7.46 (s, 1H, H^{15}), 7.44 – 7.37 (m, 2H, H^{12}, –NH), 7.20 (ddd, *J* = 8.1, 7.0, 1.1 Hz, 1H, H^{11}), 7.16 (ddd, *J* = 8.1, 7.0, 1.1 Hz, 1H, H^{10}), 6.89 – 6.87 (m, 2H, H$^{19, 20}$), 6.80 (br.s, 1H, H^{24}), 5.86 (s, 1H, H^3), 3.72 – 3.63 (m, 4H, H^{5b,16}), 3.60 (s, 3H, H^{22}), 3.46 – 3.38 (m, 1H, H^{5a}), 3.25 – 3.14 (m, 5H, H^{4,17}), 1.43 (s, 9H, H^1 (3 × CH_3)). ^{13}C NMR (151 MHz, CD_3CN) δ 170.9, 170.4, 154.2, 153.3, 136.9, 127.8, 127.1, 126.8, 123.5, 121.6, 121.5, 116.9, 114.9 (2C), 112.8, 112.7, 70.6, 63.5, 58.8, 56.6, 56.2, 52.1, 46.1, 28.9 (3C). HPLC-MS (APCI/ESI): Purity >99%, t_R = 2.517 min, *m/z* $[M+1]^+$ = 468.2, calculated exact mass for $C_{26}H_{33}N_3O_5$: 467.24.

7.2.2. General procedure for synthesis of the cyclohexyl pyrimidines series

2-iodo-4,6-dimethoxypyrimidine, 2.1b

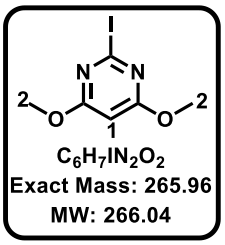

A solution of 2-iodo-4,6-dimethoxypyrimidine **2.1a** (1 eq.) (**Scheme 2.1 Chapter 2**) was prepared in 57% hydroiodic acid (50 eq.) at 0 °C and stirred for 1 h before it was warmed to 24 °C. The reaction was stirred for 12 h, and the yellow reaction mixture was diluted with dichloromethane (DCM), and K_2CO_3 was added. The organic fraction was extracted with DCM (×3), washed with sodium thiosulphate, dried on Na_2SO_4, and the filtrate was concentrated under reduced pressure to give **2.1b**. as a white solid which turned light yellow upon standing. ^{1}H NMR (300 MHz, $CDCl_3$) δ = 5.97 (s, 1H, H^1), 3.92 (s, 6H, H^6). HPLC-MS (APCI/ESI): Purity 99%, t_R = 3.441 min, *m/z* $[M+1]^+$ = 266.9, calculated exact mass for $C_6H_7N_2O_2$: 266.04.

Ethyl (E)-3-(4,6-dimethoxypyrimidin-2-yl)acrylate, 2.1c

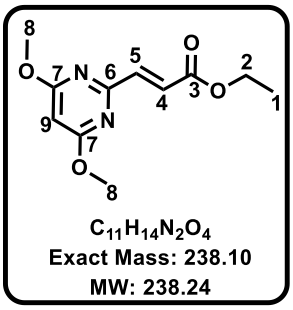

This product was obtained from **2.1b** (1200 mg, 4.5106 mmol), ethyl acrylate (777 mg, 9.0212 mmol, 2 eq.), triethylamine (511 mg, 5.0519 mmol, 1.12 eq.), and 10% Pd/C heated in a sealed tube at 90 °C for 20 h. The product was a white solid (680 mg, 67%); m.p: 71-74°C; *Rf* (EtOAc:Hex, 2:8) 0.8; ^{1}H NMR (300 MHz, $CDCl_3$) δ 7.51 (d, *J* = 15.7 Hz, 1H, H^4), 7.13 (d, *J* = 15.7 Hz, 1H, H^5), 5.98 (s, 1H, H^9), 4.29 (q, *J* = 7.1 Hz, 2H, H^2), 3.97 (s, 6H, H^8), 1.35 (t, *J* = 7.1 Hz, 3H, H^1). HPLC-MS (APCI/ESI): Purity >99%, t_R = 2.578 min, *m/z* $[M+2]^+$ = 240.1, calculated exact mass for $C_{11}H_{14}N_2O_4$: 238.10.

Ethyl 6-(4,6-dimethoxypyrimidin-2-yl)cyclohex-3-ene-1-carboxylate, 2.1d

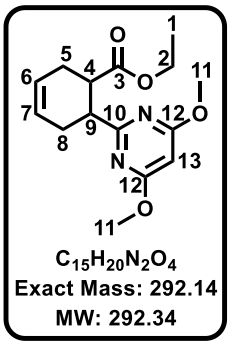

This product was obtained from **2.1c** (680 mg, 2.85 mmol) and butadiene sulfone (6750 mg, 57.09 mmol, 20 eq.) in toluene in a sealed tube heated at 155 °C for 78 h or when **2.1c** was consumed as seen by LC-MS. More butadiene sulfone was added to force the reaction to completion. **2.1d** was obtained as a yellow oil (457 mg, 28%); *Rf* (EtOAc:Hex, 2:8) 0.7; ^{1}H NMR (300 MHz, $CDCl_3$) δ 5.83 (s, 1H, H^{13}), 5.73 (m, 2H, H^6, H^7), 3.99 (q, *J* = 7.1 Hz, 2H, H^2), 3.89 (s, 6H, H^{11}), 3.27 (td, *J* = 10.9, 5.4 Hz, 1H, H^9), 3.13 (td, *J* = 10.9, 5.5 Hz, 1H, H^4), 2.59 – 2.38 (m, 2H, H^8), 2.37 – 2.11 (m, 2H, H^5), 1.08 (t, *J* = 7.1 Hz, 3H, H^1). HPLC-MS (APCI/ESI): Purity 95%, t_R = 2.324 min, *m/z* $[M+1]^+$ = 293.1, calculated exact mass for $C_{15}H_{20}N_2O_4$: 292.14.

Ethyl 2-(4,6-dimethoxypyrimidin-2-yl)cyclohexane-1-carboxylate, 2.1e

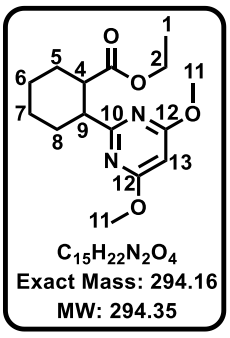

This compound was obtained from a solution of **2.1d** (457 mg, 1.5632 mmol) prepared in MeOH (3 mL) to which was added 20% Pd/C portion-wise under hydrogen and the reaction mixture stirred for 3 h at 0 – 24 °C. After filtration through a celite pad, the solvent was removed *in vacuo* to afford **2.1e** as a clear oil (470 mg, 100%); *Rf* (EtOAc:Hex, 1:9) 0.6; ^{1}H NMR (300 MHz, DMSO-d_6) δ 6.00 (s,1H, H^{13}), 3.91 (q, *J* = 6.8 Hz, 2H, H^2), 3.84 (s, 6H, H^{11}), 2.83 (td, *J* = 11.0, 3.5 Hz, 2H, H^4, H^9), 2.08 – 1.98 (m, 2H, H^8), 1.82 – 1.72 (m, 2H, H^5), 1.50 – 1.21 (m, 4H, H^6, H^7), 1.01 (t, *J* = 7.1 Hz, 3H, H^1). HPLC-MS (APCI/ESI): Purity

92%, t_R = 2.624 min, *m/z* $[M+1]^+$ = 295.1, calculated exact mass for $C_{15}H_{22}N_2O_4$: 294.16.

2-(4,6-dimethoxypyrimidin-2-yl)cyclohexane-1-carboxylic acid, 2.1f

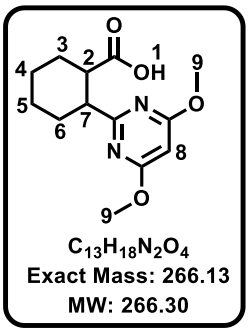

This compound was obtained from a solution of **2.1e** (470 mg, 1.5968 mmol) in MeOH:THF:H_2O (1:1:2) and LiOH.H_2O (134 mg, 3.1936 mmol) under reflux for 6 h. The reaction mixture was cooled and treated with 1M HCl to pH = 3. The aqueous phase was extracted with EtOAc (×3), organics dried on Na_2SO_4 and once filtered, concentrated under reduced pressure. The product was a beige solid (280 mg, 66%); m.p: 124-128 °C; *Rf* (EtOAc:Hex, 3:7) 0.1; ^{1}H NMR (300 MHz, DMSO-d_6) δ 5.99 (s, 1H, H^8), 3.85 (s, 6H, H^9), 2.91 – 2.68 (m, 2H, H^2, H^7), 2.12 – 1.96 (m, 2H, H^6), 1.82 – 1.72 (m, 2H, H^3), 1.49 – 1.18 (m, 4H, H^4, H^5). HPLC-MS (APCI/ESI): Purity >99%, t_R = 2.454 min, *m/z* [M-1] = 265.1 (negative mode), calculated exact mass for $C_{13}H_{18}N_2O_4$: 266.13.

2-(4,6-dimethoxypyrimidin-2-yl)-N-((1-methyl-1H-pyrrol-2-yl)methyl)cyclohexane-1-carboxamide, 3/MM1-75

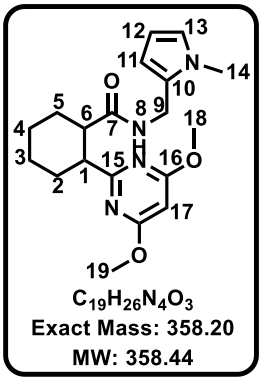

This compound was obtained from **2.1f** (130 mg, 0.49 mmol), EDCI (0.99 mg, 0.73 mmol, 1.5 eq.), *N,N*-Diisopropylethylamine (DIPEA) (95 mg, 0.73 mmol, 1.5 eq.), (1-methyl-1H-pyrrol-2-yl)methanamine (70 mg, 0.63 mmol, 1.3 eq.) and HOBt (140 mg, 0.73 mmol, 1.5 eq.) as a white solid (45 mg, 26%); m.p: 161-162 °C; *Rf* (EtOAc:Hex, 3:7) 0.3; ^{1}H NMR (300 MHz, $CDCl_3$) δ 6.51 (dd, *J* = 3.5, 1.7 Hz, 1H, H^{13}), 5.99 (dd, *J* = 3.5, 1.7 Hz, 1H, H^{12}), 5.93 (dd, *J* = 3.5, 1.7 Hz, 1H, H^{11}), 5.79 (s, 1H, H^{17}), 5.66 (s, 1H, -NH^8), 4.32 (dd, *J* = 15.2, 5.6 Hz, 1H, H^9), 4.22 (dd, *J* = 15.1, 5.6 Hz, 1H, H^9), 3.81 (s, 6H, H^{18}, H^{19}), 3.28 (s, 3H, H^{14}), 3.02 (td, *J* = 11.3, 3.6 Hz, 1H, H^1), 2.72 (td, *J* = 11.8, 3.6 Hz, 1H, H^6), 2.08 – 1.96 (m, 4H, H^2, H^5), 1.83 – 1.21 (m, 4H, H^3, H^4). ^{13}C NMR (151 MHz, $CDCl_3$) δ 174.6, 174.5, 172.1, 128.8, 122.9, 108.5 (2C), 106.9, 86.9, 53.89 (2C), 48.6, 48.1, 34.7, 33.4, 32.8, 29.9, 25.8, 25.5. HPLC-MS (APCI/ESI): Purity > 99%, t_R = 2.514 min, *m/z* $[M+1]^+$ = 359.2, calculated exact mass for $C_{19}H_{26}N_4O_3$: 358.20.

N-(3-chlorobenzyl)-2-(4,6-dimethoxypyrimidin-2-yl)cyclohexane-1-carboxamide, 13/MM1-88

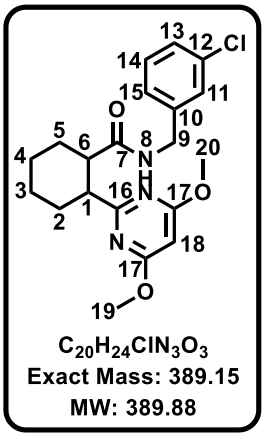

This compound was obtained from **2.1f** (100 mg, 0.38 mmol), EDCI (108 mg, 0.56 mmol, 1.5 eq.), DIPEA (72 mg, 0.56 mmol, 1.5 eq.), (3-chlorophenyl)methanamine (69 mg, 0.48 mmol, 1.3 eq.), and HOBt (76 mg, 0.56 mmol, 1.5 eq.) as a white solid (52 mg, 24%); m.p: 120-123 °C; *Rf* (EtOAc:Hex, 3:7) 0.5; ^{1}H NMR (600 MHz, DMSO-d_6) δ 8.10 (t, J = 6.1 Hz, 1H, -NH^8), 7.22 – 7.21 (m, 2H, H^{13}, H^{14}), 7.08 – 7.06 (m, 1H, H^{11}), 6.99 – 6.93 (m, 1H, H^{15}), 5.93 (s, 1H, H^{18}), 4.23 (dd, J = 15.5, 6.4 Hz, 1H, H^9), 4.09 (dd, J = 15.5, 6.1 Hz, 1H, H^9), 3.83 (s, 6H, H^{19}, H^{20}), 2.96 (td, J = 12.0, 6.1 Hz, 1H, H^1), 2.83 (td, J = 12.3, 6.1 Hz, 1H, H^6), 2.00 – 1.77 (m, 4H, H^2, H^5), 1.45 – 1.29 (m, 4H, H^3, H^4). ^{13}C NMR (151 MHz, DMSO-d_6) δ 175.2, 172.7, 171.5, 143.0, 133.4, 130.2, 127.2, 126.9, 125.9, 87.0, 54.1 (2C), 48.2, 47.4, 41.8, 40.8, 32.7, 30.5, 26.0, 25.8. HPLC-MS (APCI/ESI): Purity 96%, t_R = 2.586 min, *m/z* $[M+1]^+$ = 390.1, calculated exact mass for $C_{20}H_{24}ClN_3O_3$: 389.15.

N-(3,4-difluorobenzyl)-2-(4,6-dimethoxypyrimidin-2-yl)cyclohexane-1-carboxamide, 14/MM1-89

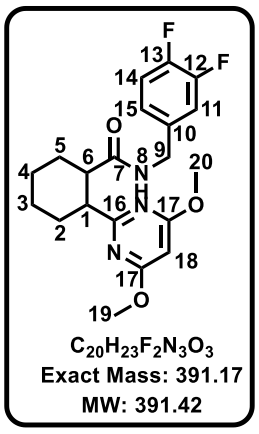

This product was obtained from **2.1f** (100 mg, 0.38 mmol), EDCI (108 mg, 0.56 mmol, 1.5 eq.), DIPEA (72 mg, 0.56 mmol, 1.5 eq.), (3,4-difluorophenyl)methanamine (70 mg, 0.48 mmol, 1.3 eq.), and HOBt (76 mg, 0.56 mmol, 1.5 eq.) as a white solid (45 mg, 31%); m.p: 142-145 °C; *Rf* (EtOAc:Hex, 3:7) 0.4; ^{1}H NMR (400 MHz, $CDCl_3$) δ 6.98 (dt, J = 10.2, 8.2 Hz, 1H, H^{14}), 6.78 (ddd, J = 11.1, 7.6, 2.2 Hz, 1H, H^{11}, couples to -F), 6.75 – 6.70 (m, 1H, H^{15}), 5.80 (s, 1H, H^{18}), 4.37 (dd, J = 15.0, 5.1 Hz, 1H, H^9), 4.09 (dd, J = 15.0, 5.1 Hz, 1H, H^9), 3.84 (s, 6H, H^{19}, H^{20}), 3.03 (td, J = 12.0, 3.7 Hz, 1H, H^1), 2.79 (td, J = 12.0, 3.7 Hz, 1H, H^6), 2.08 – 1.66 (m, 4H, H^2, H^5), 1.50 – 1.29 (m, 4H, H^3, H^4). ^{13}C NMR (101 MHz, $CDCl_3$) δ 175.4, 172.3, 171.7, 151.5, 149.2 (2C), 135.9, 123.5, 117.3, 116.6, 86.8, 54.2 (2C), 49.0, 48.3, 42.4, 32.9, 29.9, 25.9, 25.6. HPLC-MS (APCI/ESI): Purity >99%, t_R = 1.119 min, *m/z* $[M+1]^+$ = 392.1, calculated exact mass for $C_{20}H_{23}F_2N_3O_3$: 391.17.

N-(3,4-dichlorobenzyl)-2-(4-(4-(N-(2-hydroxyethyl)sulfamoyl)phenyl)-6-methylpyrimidin-2-yl)cyclohexane-1-carboxamide Synthesis

Synthesis of compound **4a** involved a slightly different procedure from the preceding cyclohexyl pyrimidines and four major intermediates (**2.2b, 2.2c, 2.2e** and **2.2f**) were isolated and their characterization including that of compound **4a** is given below.

Ethyl (E)-3-(4,6-dimethoxypyrimidin-2-yl)acrylate, 2.2b

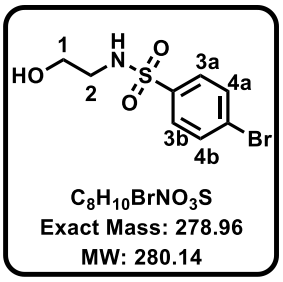

$C_8H_{10}BrNO_3S$
Exact Mass: 278.96
MW: 280.14

To a stirring solution of ethanolamine (717 mg, 11.74 mmol, 1.5 eq.) and DIPEA (2023 mg, 15.65 mmol, 1.12 eq.) in DCM (20 mL) was added 4-bromobenzenesulfonyl chloride (2000 mg, 7.83 mmol). Reaction mixture was then left to stir at 18 °C for 14h. The product was a white wax (1850 mg, 84%); *Rf* (EtOAc:Hex, 8:2) 0.8; ^{1}H NMR (300 MHz, $CDCl_3$) δ 7.74 (d, *J* = 9.0 Hz, 2H, $H^{3a, 3b}$), 7.65 (d, *J* = 9.0 Hz, 2H, $H^{4a, 4b}$), 5.47 (s, 1H, –NH), 3.70 (t, *J* = 6.0 Hz, 2H, H^2), 3.10 (t, *J* = 6.0 Hz, 2H, H^1). HPLC-MS (APCI/ESI): Purity >99%, t_R = 1.972 min, *m/z* $[M+1]^+$ = 281.1, calculated exact mass for $C_8H_{10}BrN_3S$: 278.96.

N-(2-hydroxyethyl)-4-(4,4,5,5-tetramethyl-1,3,2-dioxaborolan-2-yl)benzenesulfonamide, 2.2c

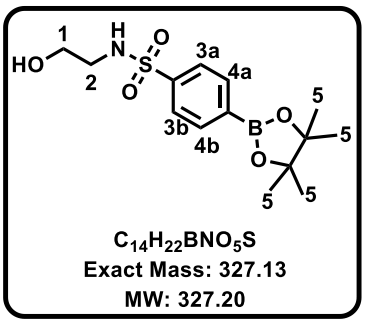

$C_{14}H_{22}BNO_5S$
Exact Mass: 327.13
MW: 327.20

This product was obtained from **2.2b** (1900 mg, 6.78 mmol), bis(pinacolato)diboron (2583 mg, 10.17 mmol, 1.5 eq.), potassium acetate (1997 mg, 20.35 mmol, 3 eq.), and palladium (II) acetate (76.13 mg, 0.34 mmol, 0.05 eq.) in 1,4-dioxane (20 mL) at 80 °C for 12h. The product was a dark brown oil (3100 mg, 52%); *Rf* (EtOAc:Hex, 8:2) 0.5; ^{1}H NMR (300 MHz, $CDCl_3$) δ 7.94 (d, *J* = 7.7 Hz, 2H, $H^{3a, 3b}$), 7.85 (d, *J* = 7.8 Hz, 2H, $H^{4a, 4b}$), 5.16 (s, 1H, –OH), 3.73 – 3.61 (m, 2H, H^2), 3.16 – 3.03 (m, 2H, H^1), 1.35 (s, 12H, H^5). HPLC-MS (APCI/ESI): Purity >99%, t_R = 2.388 min, *m/z* $[M-1]^+$ = 326.1, calculated exact mass for $C_{14}H_{22}BNO_5S$: 327.13.

4-(2-chloro-6-methylpyrimidin-4-yl)-N-(2-hydroxyethyl)benzenesulfonamide, 2.4e

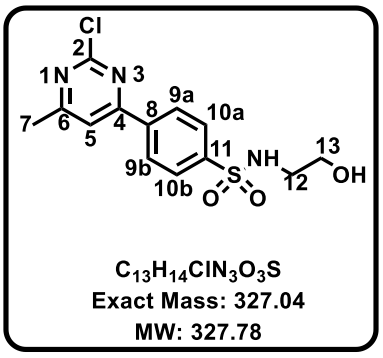

$C_{13}H_{14}ClN_3O_3S$
Exact Mass: 327.04
MW: 327.78

Obtained from 2,4-dichloro-6-methylpyrimidine (200 mg, 1.23 mmol), **2.4c** (602 mg, 1.84 mmol, 1.5 eq.), $Pd(dppf)Cl_2 \cdot DCM$ (20 mg, 0.02 mmol, 0.02 eq.) and cesium carbonate (600 mg, 1.84 mmol, 1.5 eq.) in mixture of 1,4-dioxane: water (4:1) under microwave irradiation at 70 °C for 20 min. The crude reaction mixture was diluted with DCM and passed through a celite pad. The resulting solution was concentrated under reduced pressure, adsorbed on silica and submitted to Biotage flash chromatography eluting with EtOAc (0 – 100%) in hexane and then EtOAc: MeOH 9:1. The product was a yellow solid (240 mg, 40%); *Rf* (EtOAc:Hex, 2:8) 0.5; ^{1}H NMR (600 MHz, MeOD) δ 8.32 (d, *J* = 6.0 Hz, 2H, $H^{10a, 10b}$), 8.01 (d, *J* = 6.0 Hz, 2H, $H^{9a, 9b}$), 7.92 (s, 1H, H^5), 4.83 (s, 1H, –OH), 3.56 (t, *J* = 6.0 Hz, 2H, H^{12}) , 3.06 (t, *J* = 6.0 Hz, 2H, H^{13}), 2.60 (s, 3H, H^7). ^{13}C NMR (151 MHz, MeOD) δ 173.6, 166.4, 162.3, 144.7, 140.3, 129.3 (2C), 127.1 (2C), 116.9, 61.9, 46.3, 23.9. HPLC-MS (APCI/ESI): Purity = 98%, t_R = 2.209 min, *m/z* $[M+1]^+$ = 328.1, calculated exact mass for $C_{13}H_{14}ClN_3O_3S$: 327.04.

Ethyl(E)-3-(4-(4-(N-(2-hydroxyethyl)sulfamoyl)phenyl)-6-methylpyrimidin-2-yl)acrylate, 2.4f

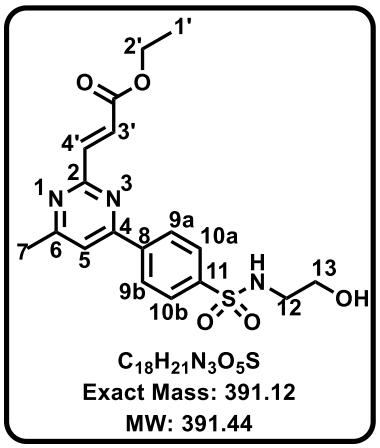

$C_{18}H_{21}N_3O_5S$
Exact Mass: 391.12
MW: 391.44

Obtained from **2.4e** (365 mg, 1.11 mmol), ethyl acrylate (334 mg, 3.34 mmol, 3 eq.), DIPEA (575 mg, 4.45 mmol, 4 eq.), tris(*o*-tolyl)phosphine (102 mg, 0.33 mmol, 0.3 eq.) and palladium (II) acetate (25 mg, 0.11 mmol, 0.1 eq.) under microwave irradiation at 145 °C for 10 min. The crude reaction mixture was diluted with DCM and passed through a celite pad. The resulting solution was concentrated under reduced pressure, adsorbed on silica and submitted to Biotage flash chromatography eluting with MeOH (0 – 10%) in DCM. The product was a beige solid (126 mg, 29%); *Rf* (EtOAc:Hex, 8:2) 0.3; ^{1}H NMR (400 MHz, $CDCl_3$) δ 8.27 (d, 2H, *J* = 8.0 Hz, $H^{10a, 10b}$), 8.02 (d, 2H, *J* = 8.0 Hz, $H^{9a, 9b}$), 7.76 (d, *J* = 15.7 Hz, 1H, $H^{4'}$), 7.53 (s, 1H, H^5), 7.31 (d, *J* = 15.7 Hz, 1H, $H^{3'}$), 5.12 (s, 1H, –OH), 4.31 (q, *J* = 7.1 Hz, 2H, $H^{2'}$), 3.72 (t, *J* = 5.4 Hz, 2H, H^{12}), 3.17 (t, *J* = 5.4 Hz, 2H, H^{13}), 2.65 (s, 3H, H^7), 1.36 (t, *J* = 7.1 Hz, 3H, $H^{1'}$). ^{13}C NMR (101 MHz, $CDCl_3$) δ 168.7, 166.4, 162.9, 162.3, 142.9, 142.1,

140.9, 128.2 (2C), 128.1, 127.8 (2C), 115.9, 61.4, 61.0, 45.4, 24.5, 14.4. HPLC-MS (APCI/ESI): Purity = 93%, t_R = 2.417 min, *m/z* $[M+1]^+$ = 392.1, calculated exact mass for $C_{18}H_{21}N_3O_5S$: 391.12.

N-(3,4-dichlorobenzyl)-2-(4-(4-(N-(2-hydroxyethyl)sulfamoyl)phenyl)-6-methylpyrimidin-2-yl)cyclohexane-1-carboxamide, 4a/MM2-39

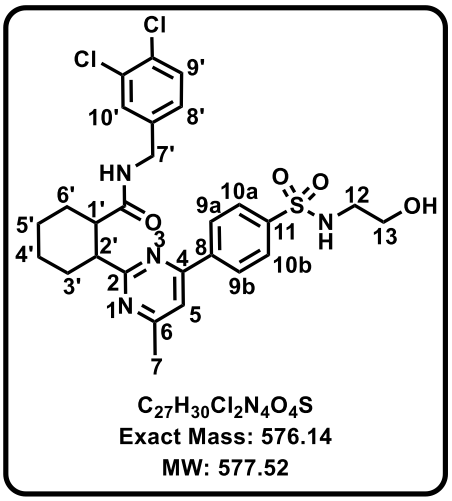

Obtained from a crude mixture of 2-(4-(4-(*N*-(2-hydroxyethyl)sulfamoyl)phenyl)-6-methylpyrimidin-2-yl)cyclohexane-1-carboxylic acid (41 mg) which was dissolved in DCM (1.5 mL) and then EDCI (19.81 mg, 0.15 mmol, 1.5 eq.), DIPEA (18.95 mg, 0.15 mmol, 1.5 eq.), 3,4-dichlorobenzylamine (22.36 mg, 0.13 mmol, 1.3 eq.) and HOBt (28.10 mg, 0.15 mmol, 1.5 eq.) were added. The reaction stirred at 16 °C for 14 h. The crude reaction mixture was concentrated *in vacuo* and submitted to the prep-HPLC. The product was a white solid (1.9 mg, 3%); *Rf* (EtOAc:Hex, 8:2) 0.3; ^{1}H NMR (400 MHz, CD_3CN) δ 8.55 (d, 2H, *J* = 8.0 Hz, $H^{10a, 10b}$), 7.90 (d, 2H, *J* = 8.0 Hz, $H^{9a, 9b}$), 7.59 (d, *J* = 1.8 Hz, 1H, $H^{10'}$), 7.08 (s, 1H, H^5), 7.00 (d, *J* = 8.3 Hz, 1H, $H^{9'}$), 6.89 (s, 1H, –NH), 6.62 (dd, *J* = 8.3, 1.8 Hz, 1H, $H^{8'}$), 5.81 (s, 2H, $H^{7'}$), 5.71 (t, *J* = 6.2 Hz, 1H, –OH), 4.31 (td, *J* = 15.1, 7.5 Hz, 1H, $H^{2'}$), 3.79 (td, *J* = 15.1, 5.1 Hz, 1H, $H^{1'}$), 3.51 (q, *J* = 5.5 Hz, 2H, H^{12}), 3.21 – 2.95 (m, 4H, $H^{3'a}$, $H^{6'a}$, H^{13}), 2.83 (t, *J* = 5.6 Hz, 1H, –NH), 2.48 (s, 3H, H^7), 2.40 – 2.23 (m, 6H, $H^{3'b}$, $H^{6'b}$, $H^{5'}$, $H^{4'}$). ^{13}C NMR (101 MHz, CD_3CN) δ 175.4, 173.3, 168.5, 141.4 (2C), 131.2, 130.3, 129.6, 128.0 (2C), 127.9 (3C), 126.7, 126.6, 119.8, 61.4, 46.5, 45.7, 44.9, 42.3, 33.0, 30.2 (2C), 24.3 (3C). HPLC-MS (APCI/ESI): Purity >98%, t_R = 1.198 min, *m/z* $[M+1]^+$ = 577.1, calculated exact mass for $C_{27}H_{30}Cl_2N_4O_4S$: 576.14.

7.2.3. Azabenzamidazoles series

6-methylpyridine-2,3-diamine, 2.4b

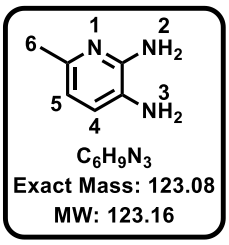

Obtained from 6-methyl-3-nitropyridin-2-amine (1000 mg, 4.83 mmol), hydrazine monohydrate (2418 mg, 48.31 mmol) and 10% Pd/C (35.99 mg, 0.34 mmol) in MeOH (10 mL) at 0 °C and then reflux for 12 h. The product was a brown oil (800 mg, 100%); *Rf* (DCM:MeOH, 8:2) 0.5. ^{1}H NMR (300 MHz, DMSO-d_6) δ 6.60 (d, J = 7.5 Hz, 1H, H^4), 6.20 (d, J = 7.5 Hz, 1H, H^5), 5.28 (s, 2H, –NH$_2^2$), 4.40 (s, 2H, –NH$_2^3$), 2.13 (s, 3H, H^6). HPLC-MS (APCI/ESI): Purity >96%, t_R = 0.122 min, *m/z* [M+1]$^+$ = 124.1, calculated exact mass for $C_6H_9N_3$: 123.08.

5-methyl-1,3-dihydro-2H-imidazo[4,5-b]pyridin-2-one, 2.4c

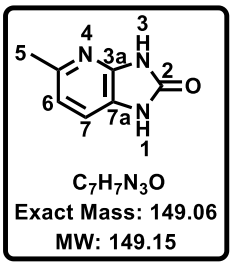

Obtained from **2.4b** (500 mg, 4.06 mmol) and urea (283 mg, 4.71 mmol) in THF (2 mL) under microwave irradiation at 130 °C for 30 min. The product crushed out as a brown solid (350 mg, 58%); m.p: 243-246 °C; This compound was insoluble and *Rf* could not be obtained. ^{1}H NMR (600 MHz, DMSO-d_6) δ 11.10 (s, 1H, -NH^3), 10.63 (s, 1H, -NH^1), 7.10 (d, J = 7.7 Hz, 1H, H^6), 6.77 (d, J = 7.7 Hz, 1H, H^7), 2.36 (s, 3H, H^5); ^{13}C NMR (151 MHz, DMSO-d_6) δ 154.9, 148.4, 144.8, 135.4, 121.7, 115.7, 23.8. HPLC-MS (APCI/ESI): Purity = 99%, t_R = 0.248 min, *m/z* [M+1]$^+$ = 150.1, calculated exact mass for $C_6H_9N_3O$: 149.06.

2-chloro-5-methyl-1H-imidazo[4,5-b]pyridine, 2.4d

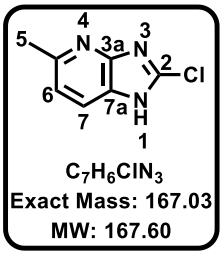

Obtained from **2.4c** (1330 mg, 8.92 mmol) in $POCl_3$ (8.31 mL, 89.2 mmol) heated at 95 °C for 14 h. The product was a beige solid (278 mg, 18%); m.p: 192-194 °C; *Rf* (EtOAc:Hex, 4:6) 0.2; ^{1}H NMR (400 MHz, MeOD) δ 7.83 (d, J = 8.2 Hz, 1H, H^7), 7.18 (d, J = 8.2 Hz, 1H, H^6), 2.60 (s, 3H, H^5). HPLC-MS (APCI/ESI): Purity > 99%, t_R = 0.632 min, *m/z* [M+1]$^+$ = 168.0, calculated exact mass for $C_7H_6ClN_3$: 167.03.

N-(3-chlorobenzyl)-5-methyl-1H-imidazo[4,5-b]pyridin-2-amine, 23/MM1-177

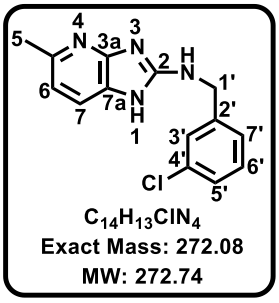

Obtained from **2.4d** (100 mg, 0.60 mmol) and (3-chlorophenyl)methanamine (169 mg, 1.19 mmol, 2 eq.) in EtOH (1 mL) under microwave irradiation at 150 °C for 1 h. The product was a beige solid (46 mg, 28%); *Rf* (DCM:MeOH, 9:1) 0.2; ^{1}H NMR (300 MHz, DMSO-d_6) δ 11.41 (s, 1H, –NH^1), 7.44 – 7.23 (m, 6H, H^6, H^7, H$^{3'}$, H$^{5'}$, H$^{6'}$, H$^{7'}$), 6.71 (s, 1H, –NH exocyclic), 4.52 (d, *J* = 6.0 Hz, 2H, H$^{1'}$), 2.39 (s, 3H, H^5). HPLC-MS (APCI/ESI): Purity = 97%, t_R = 2.183 min, *m/z* [M+1]$^+$ = 273.1, calculated exact mass for $C_{14}H_{13}ClN_4$: 272.08.

(R)-N-(1-(3-chlorophenyl)ethyl)-5-methyl-1H-imidazo[4,5-b]pyridin-2-amine, 24/MM2-83

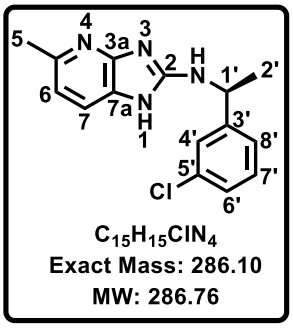

Obtained from **2.4d** (100 mg, 0.60 mmol) and (*S*)-1-(3-chlorophenyl)ethan-1-amine (186 mg, 1.19 mmol, 2 eq.) in EtOH (1 mL) under microwave irradiation at 150 °C for 1 h. The product was a brown oil (40 mg, 23%); m.p: 205-207 °C; *Rf* (EtOAc:Hex:EtOH, 2:7:1) 0.2; ^{1}H NMR (400 MHz, MeOD) δ 7.43 (m, 1H, H$^{4'}$), 7.34 (m, 2H, H^7, H^6), 7.29 (t, *J* = 7.7 Hz, 1H, H$^{7'}$), 7.21 (ddd, *J* = 7.7, 2.1, 1.3 Hz, 1H, H$^{6'}$), 6.81 (dd, *J* = 7.7, 1.3 Hz, 1H, H$^{8'}$), 5.01 (q, *J* = 6.9 Hz, 1H, H$^{1'}$), 2.46 (s, 3H, H^5), 1.56 (d, *J* = 7.0 Hz, 3H, H$^{2'}$). ^{13}C NMR (101 MHz, MeOD) δ 157.2, 149.7, 148.2, 135.4, 131.1, 128.2, 127.2 (2C), 125.4, 119.9, 116.3 (2C), 52.9, 23.5, 23.4. HPLC-MS (APCI/ESI): Purity = 97%, t_R = 2.259 min, *m/z* [M+1]$^+$ = 287.1, calculated exact mass for $C_{15}H_{15}ClN_4$: 286.10.

5-methyl-2-(3-(trifluoromethyl)phenyl)-1H-imidazo[4,5-b]pyridine, 25/MM2-78

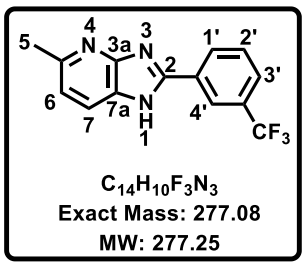

Obtained from **2.4d** (100 mg, 0.60 mmol), 4,4,5,5 tetramethyl-2-(3-(trifluoromethyl)phenyl)-1,3,2-dioxaborolane (136 mg, 0.72 mmol, 1.2 eq.), dppf (48 mg, 0.05 mmol, 0.10 eq.) and cesium carbonate (600 mg, 1.79 mmol, 3.0 eq.) in mixture of 1,4-dioxane:water (4:1) at 70 °C for 18 h. The product was a light yellow wax (29 mg, 18%); *Rf* (EtOAc:Hex, 5:5) 0.5; ^{1}H NMR (300 MHz, MeOD) δ 8.49 (s, 1H, H$^{4'}$), 8.39 (d, *J* = 7.8 Hz, 1H, H$^{1'}$), 7.92 (d, *J* = 7.8 Hz, 1H, H^7), 7.88 – 7.71 (m, 2H, H$^{2'}$, H$^{3'}$), 7.29 (d, *J* = 7.8 Hz, 1H, H^6), 2.65 (s, 3H, H^5). HPLC-MS (APCI/ESI): Purity = 97%, t_R = 2.490 min, *m/z* [M+1]$^+$ = 278.1, calculated exact mass for $C_{14}H_{10}F_3N_3$: 277.08.

(S)-2-(3-chlorophenyl)-2-((5-methyl-1H-imidazo[4,5-b]pyridin-2-yl)amino)ethan-1-ol, 26/MM2-77

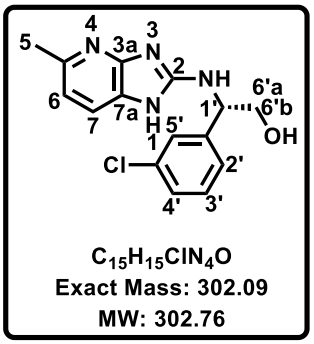

Obtained from **2.4d** (100 mg, 0.60 mmol) and (S)-2-amino-2-(3-chlorophenyl)ethan-1-ol (204 mg, 1.19 mmol, 2 eq.) in EtOH (1 mL) under microwave irradiation at 150 °C for 4h. The product was a beige wax (9 mg, 11%); *Rf* (EtOAc:Hex:EtOH, 1:5:4) 0.5; ^{1}H NMR (600 MHz, MeOD) δ 7.47 (d, *J* = 7.9 Hz, 1H, H^7), 7.33 (m, 3H, $H^{3'}$, $H^{4'}$, $H^{5'}$), 7.24 (d, *J* = 6.0 Hz, 1H, $H^{2'}$), 6.81 (d, *J* = 7.9 Hz, 1H, H^6), 4.97 (dd, *J* = 6.5, 4.8 Hz, 1H, $H^{1'}$), 3.89 (dd, *J* = 11.3, 4.8 Hz, 1H, $H^{6'a}$), 3.82 (dd, *J* = 11.3, 6.5 Hz, 1H, $H^{6'b}$), 2.46 (s, 3H, H^5). ^{13}C NMR (151 MHz, MeOD) δ 157.5, 149.8 (2C), 144.3, 135.4, 130.9, 128.5, 128.2, 126.6, 126.5, 116.3 (2C), 66.6, 59.4, 23.4. HPLC-MS (APCI/ESI): Purity > 99%, t_R = 2.134 min, *m/z* $[M+1]^+$ = 303.0, calculated exact mass for $C_{15}H_{15}ClN_4O$: 302.09.

7.2.4. Triazolopyrimidines series

All the compounds in this series were synthesized from an appropriate substituted benzylamine as exemplified with the synthesis of **28/MM2-145** through intermediates **2.5b** to **38/MM2-141**.

Phenyl (Z)-N-(3-chlorobenzyl)-N'-cyanocarbamimidate, 2.5b

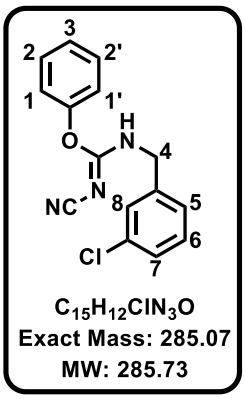

Obtained from diphenyl cyanocarbonimidate (500 mg, 2.10 mmol) and (3-chlorophenyl)methanamine (446 mg, 3.14 mmol, 1.5 eq.) in 2–propanol (10 mL) stirred at 60 °C for 2 h and then 16 °C for 16 h. The product was a white solid (334 mg, 56%); *Rf* (EtOAc:Hex, 2:8) 0.2; ^{1}H NMR (600 MHz, $CDCl_3$) δ 7.85 (br.s, 1H, –NH), 7.42 – 7.23 (m, 8H, H^1, $H^{1'}$, H^2, $H^{2'}$, H^3, H^5, H^6, H^7), 7.00 (s, 1H, H^8), 4.52 (d, *J* = 6.0 Hz, 2H, H^4). ^{13}C NMR (151 MHz, $CDCl_3$) δ 164.1, 151.1, 138.9, 134.9, 130.3 (2C), 129.7, 128.4, 128.2, 126.9, 126.1, 121.6 (2C), 115.7, 45.7. HPLC-MS (APCI/ESI): Purity > 99%, t_R = 2.118 min, *m/z* $[M+1]^+$ = 286.0, calculated exact mass for $C_{15}H_{12}ClN_3O$: 285.07.

N5-(3-chlorobenzyl)-1H-1,2,4-triazole-3,5-diamine, 2.5c

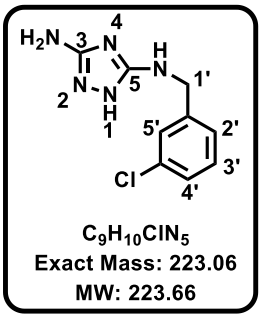

Obtained from **2.5b** (400 mg, 1.40 mmol) and hydrazine monohydrate (175 mg, 3.49 mmol, 2.5 eq.) in MeOH (5 mL) was stirred at 50 °C for 18 h. The product was a white solid (200 mg, 64%); m.p. 184 – 186°C; *Rf* (EtOAc:Hex, 4:6) 0.8; ^{1}H NMR (300 MHz, DMSO-d_6) δ 7.37 – 7.20 (m, 4H, H$^{2'}$, H$^{3'}$, H$^{4'}$, H$^{5'}$), 4.22 (d, *J* = 6.5 Hz, 2H, H$^{1'}$). ^{13}C NMR (151 MHz, DMSO-d_6) δ 161.1, 149.6, 124.3, 121.6, 120.8, 113.1, 62.7, 32.4, 32.2. HPLC-MS (APCI/ESI): Purity > 99%, t_R = 0.475 min, *m/z* $[M+1]^+$ = 224.0, calculated exact mass for $C_9H_{10}ClN_5$: 223.06.

2-((3-chlorobenzyl)amino)-5-methyl-[1,2,4]triazolo[1,5-a]pyrimidin-7(4H)-one, 27/MM1-185

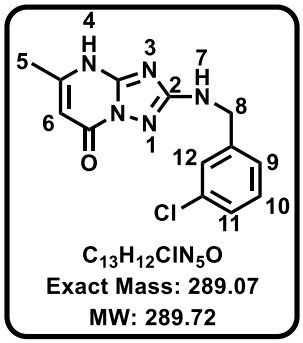

Obtained from **2.5c** (500 mg, 2.10 mmol) and hydrazine monohydrate (446 mg, 3.14 mmol, 1.5 eq.) in 2–propanol (10 mL) was stirred at 60 °C for 2 h and then 16 °C for 16 h. The product was a white solid (334 mg, 56%); m.p: 265-268 °C; *Rf* (EtOAc:Hex, 2:8) 0.2; ^{1}H NMR (300 MHz, DMSO-d_6) δ 12.69 (s, 1H, -NH^4), 7.41 – 7.24 (m, 4H, H^9, H^{10}, H^{11}, H^{12}), 7.18 (t, *J* = 6.5 Hz, 1H, –NH^7), 5.64 (s, 1H, H^6), 4.40 (d, *J* = 6.5 Hz, 2H, H^8), 2.23 (s, 3H, H^5). ^{13}C NMR (151 MHz, DMSO-d_6) δ 161.1, 149.6 (2C), 127.7, 124.3, 121.6 (2C), 120.8, 113.1, 98.4, 62.7, 32.4, 32.2. HPLC-MS (APCI/ESI): Purity > 99%, t_R = 2.183 min, *m/z* $[M+1]^+$ = 290.0, calculated exact mass for $C_{13}H_{12}ClN_5O$: 289.07.

7-chloro-N-(3-chlorobenzyl)-5-methyl-[1,2,4]triazolo[1,5-a]pyrimidin-2-amine, 2.11d

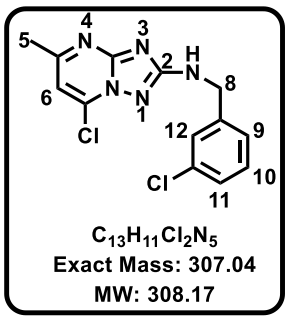

Obtained from **27** (734 mg, 2.53 mmol) in $POCl_3$ (2.33 mg, 15.51 mmol, 10 eq.) at 100 °C for 14 h. The product was a brown wax (603 mg, 78%); *Rf* (DCM: MeOH, 2:8) 0.7; ^{1}H NMR (300 MHz, MeOD) δ 7.41 (dd, *J* = 1.3, 0.6 Hz, 1H, H^{12}), 7.37 – 7.16 (m, 3H, H^9, H^{10}, H^{11}), 7.10 (s, 1H, H^6), 4.56 (s, 2H, H^8), 2.55 (s, 3H, H^5). HPLC-MS (APCI/ESI): Purity = 96%, t_R = 2.471 min, *m/z* $[M+1]^+$ = 308.0, calculated exact mass for $C_{13}H_{11}Cl_2N_5$: 307.04.

tert-butyl(2-((2-((3-chlorobenzyl)amino)-5-methyl-[1,2,4]triazolo[1,5-a]pyrimidin-7-yl)amino)-1-(2-methoxyphenyl)ethyl)carbamate, 38/MM2-141

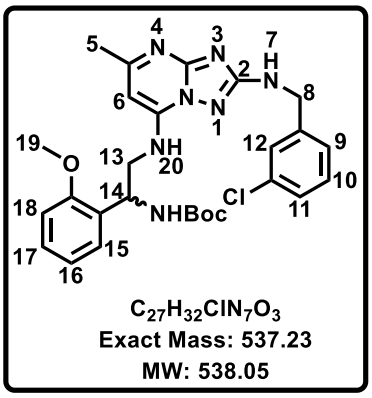

Obtained from **2.11d** (45 mg, 0.15 mmol), tert-butyl (2-amino-1-(2-methoxyphenyl)ethyl)carbamate (39 mg, 0.15 mmol, 1 eq.) and DIPEA (94 mg, 0.73 mmol, 5 eq.) in EtOH (1 mL) under microwave irradiation at 150 °C for 1h. The product was a beige solid (25 mg, 32%); mp: 196-197 °C; *Rf* (DCM:MeOH, 9:1) 0.15; ^{1}H NMR (600 MHz, DMSO-d_6) δ 7.43 – 7.39 (m, 1H, H^{12}), 7.35 – 7.30 (m, 3H, H^{10}, H^{11}, H^{16}), 7.28 – 7.22 (m, 2H, H^9, H^{15}), 7.01 – 6.97 (m, 2H, H^{18}, H^{17}), 6.93 (t, *J* = 6.4 Hz, 1H, –NH^7), 6.87 (t, *J* = 6.5 Hz, 1H, –NH^{20}), 6.11 (s, 1H, H^6), 5.21 – 5.16 (m, 1H, H^{14}), 4.49 (d, *J* = 6.4 Hz, 2H, H^8), 3.86 (s, 3H, H^{19}), 3.57 – 3.49 (m, 1H, H^{13}), 3.48 – 3.38 (m, 1H, H^{13}), 2.36 (s, 3H, H^5), 1.28 (s, 9H, Boc -CH_3). ^{13}C NMR (151 MHz, DMSO-d_6) δ 165.6, 160.9, 155.9, 154.9, 145.4, 143.0, 132.6, 129.5, 128.3, 128.1, 126.5, 126.3, 126.1, 125.4, 120.2, 110.7, 86.7, 77.8, 55.2, 48.5, 45.3, 45.3, 44.9, 27.7 (3C), 24.2. HPLC-MS (APCI/ESI): Purity > 99%, t_R = 1.158 min, *m/z* $[M+1]^+$ = 538.2, calculated exact mass for $C_{27}H_{32}ClN_7O_3$: 537.23.

N7-(2-amino-2-(2-methoxyphenyl)ethyl)-N2-(3-chlorobenzyl)-5-methyl-[1,2,4]triazolo[1,5-a]pyrimidine-2,7-diamine, 28/MM2-145

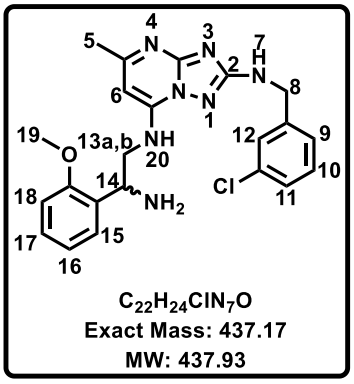

Obtained from **38** (47 mg, 0.09 mmol) stirred in TFA (1 mL) at 25 °C for 4 h. The product was a brown solid (15 mg, 40%); mp: 80-82 °C; *Rf* (DCM:MeOH, 9:1) 0.10; ^{1}H NMR (400 MHz, MeOD) δ 7.39 (s, 1H, H^{12}), 7.35 – 7.19 (m, 6H, H^7, H^9, H^{10}, H^{11}, H^{15}, H^{16}), 6.96 – 6.89 (m, 2H, H^{18}, H^{17}), 6.06 (s, 1H, H^6), 4.52 – 4.47 (m, 3H, H^8, H^{14}), 3.77 (s, 3H, H^{19}), 3.64 (dd, *J* = 13.8, 7.1 Hz, 1H, H^{13a}), 3.58 (dd, *J* = 13.8, 7.0 Hz, 1H, H^{13b}), 2.37 (s, 3H, H^5). ^{13}C NMR (101 MHz, MeOD) δ 166.9, 163.7, 158.4, 156.6, 148.1, 143.9, 135.3, 130.9, 130.6, 130.0, 128.3, 128.3, 127.9 (2C), 126.6, 121.9, 111.8, 89.1, 55.8, 51.1, 46.7, 24.5. HPLC-MS (APCI/ESI): Purity = 98%, t_R = 2.301 min, *m/z* $[M+1]^+$ = 438.1, calculated exact mass for $C_{22}H_{24}ClN_7O$: 437.17.

N7-(2-amino-2-(2-methoxyphenyl)ethyl)-N2-(4-chlorobenzyl)-5-methyl-[1,2,4]triazolo[1,5-a]pyrimidine-2,7-diamine, 29/MM3-144

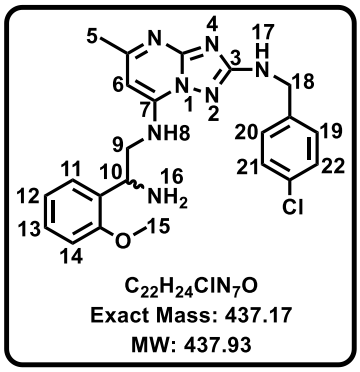

Obtained starting with (4-chlorophenyl)methanamine as a white solid (10 mg, 15%); mp: 108-110 °C; *Rf* (MeOH: DCM, 1:9) 0.4; ^{1}H NMR (400 MHz, MeOD) δ 7.39 – 7.26 (m, 8H, H^{11}, H^{13}, H^{16}, H^{19}, H^{20}, H^{21}, H^{22}), 6.95 (m, 3H, H^{12}, H^{14}, H^{17}), 6.09 (s, 1H, H^{6}), 4.58 – 4.53 (m, 1H, H^{10}), 4.51 (s, 2H, H^{18}), 3.80 (s, 3H, H^{15}), 3.69 (dd, *J* = 14.0, 6.5 Hz, 1H, H^{9a}), 3.63 (dd, *J* = 14.1, 6.5 Hz, 1H, H^{9b}), 2.38 (s, 3H, H^{5}). ^{13}C NMR (101 MHz, MeOD) δ 167.0, 163.7, 158.4, 156.5, 148.0, 140.2, 133.6, 130.5, 129.9 (2C), 129.4 (2C), 129.2, 128.6 (2C), 122.0, 111.9, 89.1, 55.9, 51.3, 46.6, 24.5. HPLC-MS (APCI/ESI): Purity = 99%, t_R = 2.336 min, *m/z* $[M+1]^+$ = 438.1, calculated exact mass for $C_{22}H_{24}ClN_7O$: 437.17.

N7-(2-amino-2-(2-methoxyphenyl)ethyl)-N2-(2-chlorobenzyl)-5-methyl-[1,2,4]triazolo[1,5-a]pyrimidine-2,7-diamine, 30/MM3-189

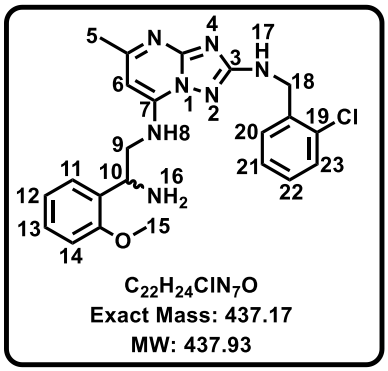

Obtained starting with (2-chlorophenyl)methanamine as a white solid (82 mg, 67%); mp: 95-98 °C; *Rf* (MeOH: DCM, 1:9) 0.4; ^{1}H NMR (600 MHz, MeOD) δ 7.47 (dd, *J* = 8.0, 1.7 Hz, 1H, H^{23}), 7.41 – 7.35 (m, 1H, H^{22}), 7.33 (ddd, *J* = 8.0, 7.8, 1.7 Hz, 1H, H^{21}), 7.28 – 7.20 (m, 3H, H^{11}, H^{20}, H^{12}), 6.93 – 6.91 (m, 2H, H^{13}, H^{14}), 6.07 (s, 1H, H^{6}), 4.63 (s, 2H, H^{18}), 4.50 – 4.47 (m, 1H, H^{10}), 3.78 (s, 3H, H^{15}), 3.62 (dd, *J* = 13.7, 7.0 Hz, 1H, H^{9a}), 3.55 (dd, *J* = 13.8, 7.0 Hz, 1H, H^{9b}), 2.38 (s, 3H, H^{5}). ^{13}C NMR (151 MHz, MeOD) δ 166.9, 163.7, 158.3, 156.6, 148.1, 138.3, 134.1, 130.7, 130.3, 130.0, 129.6, 129.4 (2C), 128.3, 128.0, 121.9, 111.7, 89.1, 55.8, 51.0, 45.2, 24.5. HPLC-MS (APCI/ESI): Purity > 99%, t_R = 2.287 min, *m/z* $[M+1]^+$ = 438.1, calculated exact mass for $C_{22}H_{24}ClN_7O$: 437.17.

N7-(2-amino-2-(2-methoxyphenyl)ethyl)-5-methyl-N2-(3-(trifluoromethyl)benzyl)-[1,2,4]triazolo[1,5-a]pyrimidine-2,7-diamine, 31/MM3-205

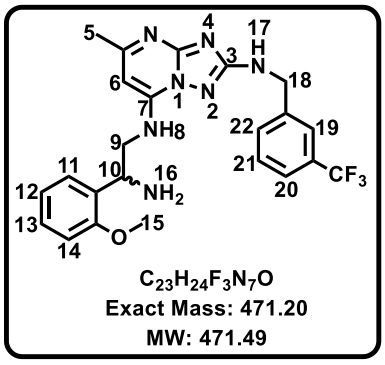

Obtained starting with (3-(trifluoromethyl)phenyl)methanamine as a beige solid (53 mg, 64%); mp: 203-205 °C; *Rf* (MeOH: DCM, 1:9) 0.5;^{1}H NMR (400 MHz, MeOD) δ 7.71 - 7.66 (m, 2H, H^{19}, H^{20}), 7.60 – 7.56 (m, 1H, H^{21}), 7.46 – 7.38 (m, 1H, H^{13}), 7.33 (d, *J* = 7.6 Hz, 1H, H^{22}), 7.28 – 7.20 (m, 1H, H^{12}), 6.95 - 6.88 (m, 2H, H^{14}, H^{11}), 6.08 (s, 1H, H^6), 4.49 (m, 3H, H^{10}, H^{18}), 3.79 (s, 3H, H^{15}), 3.63 (dd, *J* = 13.8, 7.0 Hz, 1H, H^{9a}), 3.56 (dd, *J* = 13.7, 7.0 Hz, 1H, H^{9b}), 2.38 (s, 3H, H^5). ^{13}C NMR (101 MHz, MeOD) δ 167.2, 164.1, 158.6, 156.6, 147.8, 139.6, 133.4, 132.1, 129.6, 129.5 (2C), 128.3, 126.9, 124.0 (2C), 122.3, 112.5, 89.1, 56.1, 52.1, 45.5, 43.9, 24.6. HPLC-MS (APCI/ESI): Purity = 99%, t_R = 2.358 min, *m/z* $[M+1]^+$ = 472.2, calculated exact mass for $C_{23}H_{24}F_3N_7O$: 471.20.

N7-(2-amino-2-(2-methoxyphenyl)ethyl)-5-methyl-N2-(4-(trifluoromethyl)benzyl)-[1,2,4]triazolo[1,5-a]pyrimidine-2,7-diamine, 32/MM3-159

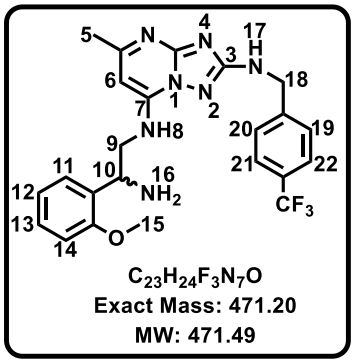

Obtained from (4-(trifluoromethyl)phenyl)methanamine starting substituted benzylamine as a light yellow wax (40 mg, 30%); *Rf* (MeOH: DCM, 1:9) 0.5; ^{1}H NMR (600 MHz, MeOD) δ 7.62 (d, *J* = 8.1 Hz, 2H, H^{21}, H^{22}), 7.56 (d, *J* = 8.1 Hz, 2H, H^{19}, H^{20}), 7.43 (ddd, *J* = 8.6, 7.5, 1.7 Hz, 1H, H^{12}), 7.35 (dd, *J* = 7.6, 1.7 Hz, 1H, H^{11}), 7.10 (dd, *J* = 7.6, 1.7 Hz, 1H, H^{14}), 7.01 (ddd, *J* = 8.6, 7.6, 1.7 Hz, 1H, H^{13}), 6.38 (s, 1H, H^6), 4.83 – 4.79 (m, 1H, H^{10}), 4.65 (s, 2H, H^{18}), 4.14 (dd, *J* = 14.6, 7.0 Hz, H^{9a}), 4.03 (dd, *J* = 14.7, 7.0 Hz, H^{9b}), 3.89 (s, 3H, H^{15}), 2.50 (s, 3H, H^5). ^{13}C NMR (151 MHz, MeOD) δ 165.2, 161.8, 158.7, 149.3, 145.0, 132.6, 130.1 (2C), 128.8 (2C), 126.4, 126.4, 126.4, 122.6, 122.5, 122.4, 112.7, 91.2, 56.2, 52.2, 46.7, 45.2, 21.4. HPLC-MS (APCI/ESI): Purity >99%, t_R = 2.305 min, *m/z* $[M+1]^+$ = 472.1, calculated exact mass for $C_{23}H_{24}F_3N_7O$: 471.20.

N7-(2-amino-2-(2-methoxyphenyl)ethyl)-5-methyl-N2-(2-(trifluoromethyl)benzyl)-[1,2,4]triazolo[1,5-a]pyrimidine-2,7-diamine, 33/MM3-167

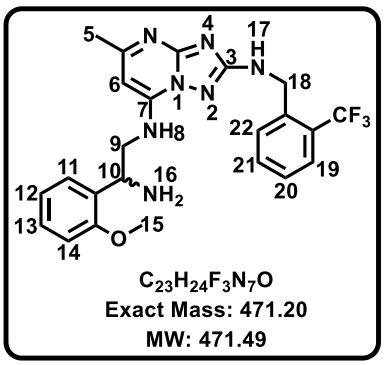

Obtained from (2-(trifluoromethyl)phenyl)methanamine starting substituted benzylamine as a beige solid (53 mg, 64%); mp: 153-155 °C; *Rf* (MeOH: DCM, 1:9) 0.5; ^{1}H NMR (400 MHz, MeOD) δ 7.72 – 7.68 (m, 2H, H^{19}, H^{20}), 7.56 (ddd, *J* = 8.6, 7.7, 1.9 Hz, 1H, H^{21}), 7.46 – 7.36 (m, 2H, H^{12}, H^{22}), 7.33 (dd, *J* = 7.6, 1.8 Hz, 1H, H^{11}), 7.08 (dd, *J* = 8.3, 1.7 Hz, 1H, H^{14}), 7.00 (ddd, *J* = 8.0, 7.5, 1.7 Hz, 1H, H^{13}), 6.10 (s, 1H, H^6), 4.80 – 4.71 (m, 3H, H^{10}, H^{18}), 3.90 – 3.81 (m, 5H, H^9, H^{15}), 2.40 (s, 3H, H^5). ^{13}C NMR (101 MHz, MeOD) δ 167.2, 164.2, 158.6, 156.6, 147.8, 139.6, 133.4, 132.1, 129.6, 129.5 (2C), 128.3, 126.9, 124.0 (2C), 122.3, 112.5, 89.1, 56.1, 52.1, 45.5, 43.9, 24.6. HPLC-MS (APCI/ESI): Purity = 96%, t_R = 2. 358 min, *m/z* $[M+1]^+$ = 472.2, calculated exact mass for $C_{23}H_{24}F_3N_7O$:

N7-(2-amino-2-(2-methoxyphenyl)ethyl)-5-methyl-N2-(3-methylbenzyl)-[1,2,4]triazolo[1,5-a]pyrimidine-2,7-diamine, 34/MM4-75

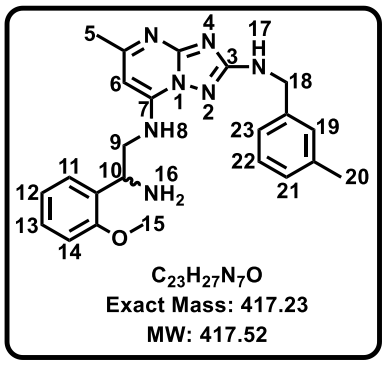

Obtained starting with *m*-tolylmethanamine as a white solid (21 mg, 46%); mp: 146-147 °C; *Rf* (MeOH: DCM, 1:9) 0.8; ^{1}H NMR (300 MHz, MeOD) δ 7.34 – 7.11 (m, 5H, H^{11}, H^{19}, H^{20}, H^{21}, H^{22}, H^{23}), 7.04 – 6.88 (m, 3H, H^{12}, H^{13}, H^{14}), 6.08 (s, 1H, H^6), 4.54 – 4.44 (m, 3H, H^{10}, H^{18}), 3.78 (s, 3H, H^{15}), (dd, *J* = 13.8, 7.0Hz, 1H, H^{9a}), 3.54 (dd, *J* = 13.8, 7.0Hz, 1H, H^{9b}), 2.38 (s, 3H, H^5), 2.31 (s, 3H, H^{20}). ^{13}C NMR (101 MHz, MeOD) δ 167.1, 163.6, 158.3, 156.5, 148.1, 141.1, 139.1, 130.6, 130.0 (2C), 129.3, 128.9, 128.6, 128.3, 125.3, 121.9, 111.7, 89.1, 55.8, 51.1, 47.3, 24.5, 21.5. HPLC-MS (APCI/ESI): Purity = 95%, t_R = 0.784 min, *m/z* $[M+1]^+$ = 418.2, calculated exact mass for $C_{23}H_{27}N_7O$: 417.23.

N7-(2-amino-2-(2-methoxyphenyl)ethyl)-5-methyl-N2-(4-methylbenzyl)-[1,2,4]triazolo[1,5-a]pyrimidine-2,7-diamine, 35/MM4-19

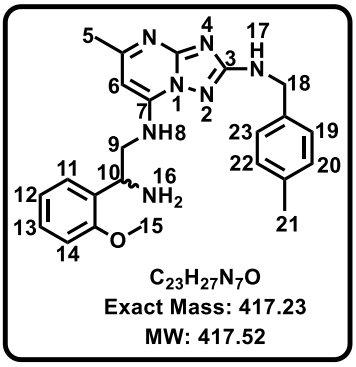

Obtained starting with *p*-tolylmethanamine as a white solid (26 mg, 22%); mp: 84-85 °C; *Rf* (MeOH: DCM, 1:9) 0.6; ^{1}H NMR (600 MHz, MeOD) δ 7.43 (ddd, *J* = 8.9, 7.6, 1.7 Hz, 1H, H^{12}), 7.33 (dd, *J* = 7.6, 1.7 Hz, 1H, H^{11}), 7.24 (d, *J* = 7.8 Hz, 2H, H^{19}, H^{23}), 7.13 - 7.08 (m, 3H, H^{13}, H^{20}, H^{22}), 7.01 (dd, *J* = 7.5, 1.7 Hz, 1H, H^{14}), 6.10 (s, 1H, H^6), 4.58 – 4.55 (m, 1H, H^{10}), 4.50 (s, 2H, H^{18}), 3.96 (dd, *J* = 14.7, 7.6 Hz, 1H, H^{9a}), 3.93 (dd, *J* = 14.7, 7.6 Hz, 1H, H^{9b}), 3.90 (s, 3H, H^{15}) 2.40 (s, 3H, H^5), 2.30 (s, 3H, H^{21}). ^{13}C NMR (151 MHz, MeOD) δ 165.7, 162.3, 157.2, 154.7, 146.4, 136.6, 136.3, 130.9, 128.6, 128.3 (2C), 126.8 (2C), 121.5, 120.9, 111.2, 87.7, 54.8, 50.9, 45.6, 43.5, 22.9, 19.7. HPLC-MS (APCI/ESI): Purity > 99%, t_R = 2.309 min, *m/z* $[M+1]^+$ = 418.2, calculated exact mass for $C_{23}H_{27}N_7O$: 417.23.

N7-(2-amino-2-(2-methoxyphenyl)ethyl)-5-methyl-N2-(2-methylbenzyl)-[1,2,4]triazolo[1,5-a]pyrimidine-2,7-diamine, 36/MM4-34

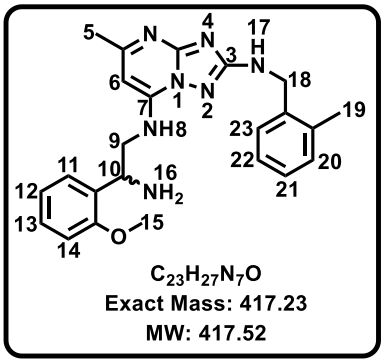

Obtained starting with *o*-tolylmethanamine as a white solid (38 mg, 39%); mp: 132-135 °C; *Rf* (MeOH: DCM, 1:9) 0.8; ^{1}H NMR (600 MHz, MeOD) δ 7.33 (m, 2H, H^{23}, H^{20}), 7.27 – 7.21 (m, 1H, H^{22}), 7.18 – 7.09 (m, 3H, H^{11}, H^{12}, H^{21}), 6.93 (m, 2H, H^{13}, H^{14}), 6.07 (s, 1H, H^6), 4.56 – 4.46 (m, 3H, H^{10}, H^{18}), 3.79 (s, 3H, H^{15}), 3.63 (dd, *J* = 13.9, 6.2 Hz, 1H, H^9), 3.55 (dd, *J* = 13.8, 7.0 Hz, 1H, H^9), 2.38 (s, 3H, H^5), 2.35 (s, 3H, H^{19}). ^{13}C NMR (151 MHz, MeOD) δ 167.1, 163.8, 158.7, 156.2, 147.8, 138.0, 137.7, 132.4, 130.0 (2C), 129.7, 128.2 (2C), 122.9, 122.4, 112.6, 89.1, 56.2, 52.3, 47.1, 44.9, 24.4, 21.1. HPLC-MS (APCI/ESI): Purity > 99%, t_R = 0.699 min, *m/z* $[M+1]^+$ = 418.2, calculated exact mass for $C_{23}H_{27}N_7O$: 417.23.

N7-(2-amino-2-(2-methoxyphenyl)ethyl)-N2-benzyl-5-methyl-[1,2,4]triazolo[1,5-a]pyrimidine-2,7-diamine, 37/MM3-140

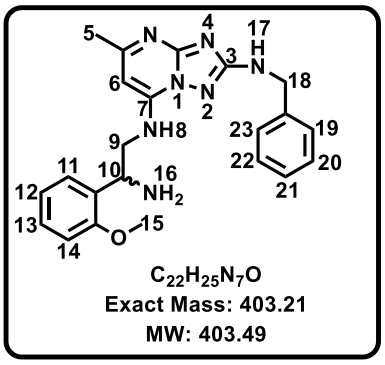

Obtained starting with benzylamine as a beige solid (72 mg, 82%); mp: 192-195 °C; *Rf* (MeOH: DCM, 1:9) 0.7; ^{1}H NMR (300 MHz, MeOD) δ 7.48 – 7.17 (m, 7H, H^{11}, H^{12}, H^{19}, H^{20}, H^{21}, H^{22}, H^{23}), 7.10 (ddd, *J* = 8.4, 7.5, 1.0 Hz, 1H, H^{13}), 7.01 (dd, *J* = 7.5, 1.0 Hz, 1H, H^{14}), 6.13 (s, 1H, H^6), 4.85 – 4.83 (m, 1H, H^{10}), 4.55 (s, 2H, H^{18}), 3.99 (dd, *J* = 13.7, 6.38, 1H, H^{9a}), 3.93 (dd, *J*= 13.7, 6.71, 1H, H^{9b}), 3.89 (s, 3H, H^{15}), 2.41 (s, 3H, H^5). HPLC-MS (APCI/ESI): Purity = 98%, t_R = 2.233 min, *m/z* $[M+1]^+$ = 404.2, calculated exact mass for $C_{22}H_{25}N_7O$: 403.21.

N2-(3-chlorobenzyl)-N7-(3,4-dimethoxyphenethyl)-5-methyl-[1,2,4]triazolo[1,5-a]pyrimidine-2,7-diamine, 39/MM3-75

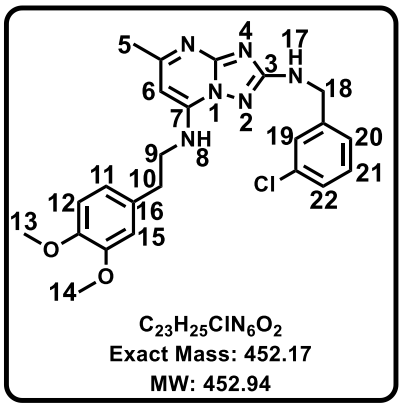

Obtained from **2.11d** (100 mg, 0.325 mmol). The product was a white solid (36 mg, 48%); mp: 156-157 °C; Rf (EtOAc: Hexane, 6:4) 0.50; ^{1}H NMR (400 MHz, DMSO-d_6) δ 7.44 – 7.23 (m, 5H, $H^{17,}$ $H^{19,}$ $H^{20,}$ $H^{21,}$ H^{22}), 7.10 (t, *J* = 6.5 Hz, 1H, H^8), 6.88 – 6.76 (m, 3H, H^{11}, H^{12}, H^{15}), 6.10 (s, 1H, H^6), 4.45 (d, *J* = 6.5 Hz, 2H, H^{18}), 3.69 (s, 3H, H^{14}), 3.68 (s, 3H, H^{13}), 3.52 (q, *J* = 6.9 Hz, 2H, H^9), 2.83 (t, *J* = 7.2 Hz, 2H, H^{10}), 2.30 (s, 3H, H^5). ^{13}C NMR (101 MHz, DMSO-d_6) δ 165.7, 161.3, 155.2, 148.7, 147.4, 145.7, 143.5, 132.9, 131.2, 130.0, 126.9, 126.5, 125.9, 120.8, 112.8, 111.9, 87.1, 55.5, 55.4, 45.0, 42.9, 34.3, 24.5. HPLC-MS (APCI/ESI): Purity = 99%, t_R = 1.184 min, *m/z* $[M+1]^+$ = 453.1, calculated exact mass for $C_{23}H_{25}ClN_6O_2$: 452.17.

N7-(2-amino-2-phenylethyl)-N2-(3-chlorobenzyl)-5-methyl-[1,2,4]triazolo[1,5-a]pyrimidine-2,7-diamine, 40/ MM3-59

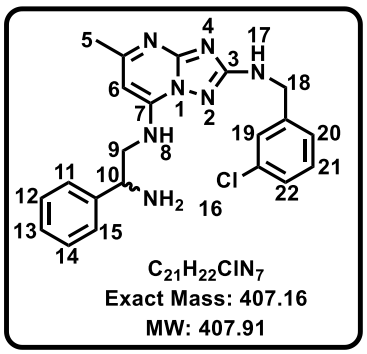

Obtained from **2.11d** (100 mg, 0.325 mmol). The product was a white solid (40 mg, 30%); mp: 78-81 °C; *Rf* (EtOAc: Hexane, 6:4) 0.20; ^{1}H NMR (400 MHz, DMSO-d_6) δ 7.46 – 7.38 (m, 3H, H^{16}, H^{19}), 7.36 – 7.15 (m, 9H, H^8, H^{11}, H^{12}, H^{13}, H^{14}, H^{15}, H^{17}, H^{20}, H^{21}, H^{22}, H^{23}), 6.13 (s, 1H, H^6), 4.45 (d, *J* = 6.4 Hz, 2H, H^{18}), 4.20 – 4.12 (m, 1H, H^{10}), 3.49 (dd, *J* = 13.1, 8.3 Hz, 1H, H^{9a}), 3.40 (dd, *J* = 13.1, 8.3 Hz, 1H, H^{9b}), 2.30 (s, 3H, H^5). ^{13}C NMR (101 MHz, DMSO-d_6) δ 165.7, 161.3, 155.1, 145.7, 143.4, 143.3, 132.9, 130.0, 128.2 (2C), 127.2, 126.9, 126.8 (2C), 126.5, 125.9, 87.4, 54.3, 48.5, 45.0, 24.5. HPLC-MS (APCI/ESI): Purity = 99%, t_R = 1.307 min, *m/z* $[M+1]^+$ = 408.2, calculated exact mass for $C_{21}H_{22}ClN_7$: 407.16.

***N7-(2-amino-2-(3-chlorophenyl)ethyl)-N2-(3-chlorobenzyl)-5-methyl-[1,2,4]triazolo[1,5-a]pyrimidine-2,7-diamine, 41/* MM3-139**

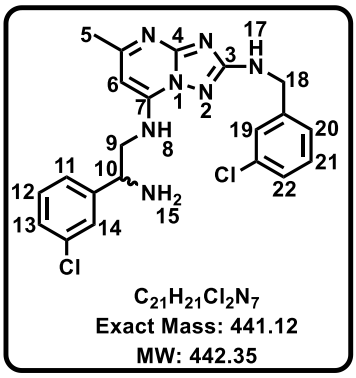

Obtained from **2.11d** (100 mg, 0.325 mmol). The product was a white solid (55 mg, 56%); mp: 100-103 °C; Rf (MeOH: DCM, 9:1) 0.20; ^{1}H NMR (600 MHz, DMSO-d_6) δ 8.60 (s, 2H, H^{15}), 7.67 (s, 1H, H^{14}), 7.49 – 7.26 (m, 8H, H^{11}, H^{12}, H^{13}, H^{19}, H^{20}, H^{21}, H^{22}), 6.33 (s, 1H, H^6), 4.66 – 4.60 (m, 1H, H^{10}), 4.50 (d, *J* = 6.4 Hz, 2H, H^{18}), 3.93 (dd, *J* = 14.5, 7.5 Hz, 1H, H^9), 3.81 (dd, *J* = 14.5, 6.3 Hz, 1H, H^9), 2.38 (s, 3H, H^5). ^{13}C NMR (151 MHz, DMSO-d_6) δ 164.9, 158.3, 158.1, 146.5, 142.8, 137.4, 133.4, 132.9, 130.6, 130.1 (2C), 129.0, 127.7 (2C), 126.8, 126.7, 125.8, 88.8, 52.7, 44.9, 22.2. HPLC-MS (APCI/ESI): Purity = 99%, t_R = 2.416 min, *m/z* $[M+1]^+$ = 442.0, calculated exact mass for $C_{21}H_{21}Cl_2N_7$: 441.12.

N2-(3-chlorobenzyl)-N7-(3-methoxyphenethyl)-5-methyl-[1,2,4]triazolo[1,5-a]pyrimidine-2,7-diamine, 42/MM3-60

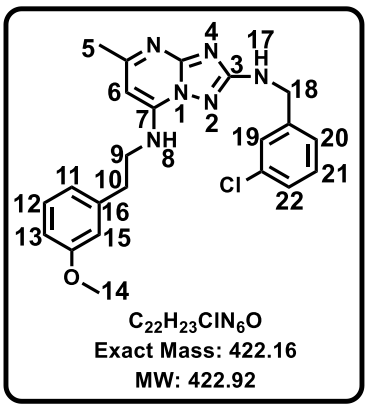

Obtained from **2.11d** (100 mg, 0.325 mmol). The product was a white solid (70 mg, 51%); mp: 152-154 °C; Rf (EtOAc: Hexane, 6:4) 0.50; ^{1}H NMR (400 MHz, DMSO-d_6) δ 7.42 – 7.23 (m, 5H, H^{12}, H^{19}, H^{20}, H^{21}, H^{22}), 7.19 (t, *J* = 7.7 Hz, 1H, H^{17}), 7.10 (t, *J* = 6.6 Hz, 1H, H^8), 6.87 – 6.73 (m, 3H, H^{11}, H^{13}, H^{15}), 6.14 (s, 1H, H^6), 4.46 (d, *J* = 6.5 Hz, 2H, H^{18}), 3.70 (s, 3H, H^{14}), 3.53 (t, *J* = 7.2 Hz, 2H, H^9), 2.88 (t, *J* = 7.4 Hz, 2H, H^{10}), 2.31 (s, 3H, H^5). ^{13}C NMR (101 MHz, DMSO) δ 165.7, 161.4, 159.3, 155.2, 145.6, 143.5, 140.4, 132.9, 130.0, 129.4, 126.9, 126.5, 125.9, 121.1, 114.5, 111.8, 87.1, 54.9, 45.0, 42.7, 34.7, 24.5. HPLC-MS (APCI/ESI): Purity = 99%, t_R = 1.191 min, *m/z* $[M+H]^+$ = 423.1, calculated exact mass for $C_{22}H_{23}ClN_6O$: 422.16.

7.2.5. General procedure for benzoxaboroles synthesis

7.2.5.1. Synthesis of the methyl and ethyl esters, amides and alkyl benzoxaboroles series

Method A: To a solution of 1-hydroxy-1,3-dihydrobenzo[c][1,2]oxaborole-6-carboxylic acid (1 mmol, 1 eq.), EDCI (0.15 mmol, 1.5 eq.) and HOBt (0.15 mmol, 1.5 eq.) in DMF (1 mL) was stirred for 30 min at 0 °C. To this solution amine (0.13 mmol, 1.3 eq.) and DIPEA (2 mmol, 1.0 eq.) were added and reaction stirred at 20 °C for 14 h.
Method B: To a solution of 1-hydroxy-1,3-dihydrobenzo[c][1,2]oxaborole-6-carboxylic acid (1 mmol, 1.0 eq.) and HATU (1.5 mmol, 1.5 eq.) in DMF (2 mL) was added DIPEA (2 mmol, 2.0 eq.). The mixture was stirred at 24 °C for 30 min, and then amine (1.5 mmol, 1.5 eq.) was added. The resulting mixture was stirred at 24 °C for 1 h. Reaction mixture was left to stir at 24 °C for 14 h.
Method C: To a solution of 1-hydroxy-1,3-dihydrobenzo[c][1,2]oxaborole-6-carboxylic acid (1 mmol, 1.0 eq.), amine (1.5 mmol, 1.5 eq.) and triethylamine (2 mmol, 2.0 eq.) in DMF (2 mL) was added T3P® (1.5 mmol, 1.5 eq.). The mixture was stirred at 24 °C for 14 h.

Work-up (*Method A, B and C*): At the end of the reaction time, reaction mixture was diluted with EtOAc (2 mL) and then toluene (3 x 5 mL) while concentrating it under

reduced pressure. The residue was taken up into EtOAc (5 mL) and water was added (5 mL) followed by extraction in EtOAc (3 x 5 mL). The organic layer was washed with brine (10 mL), dried on Na_2SO_4, and concentrated under reduced pressure. The resulting residue was adsorbed on isolute and submitted to reverse-phased Biotage eluting with MeOH (0 – 100%) in water to afford the desired amides **43-71** and **81-97**.

7.2.5.2. Hydrolysis

To a solution of an ester (1 mmol, 1 eq.) in dioxane:H2O (3:1) was added $LiOH{\cdot}H_2O$ (2.5 mmol, 2.5 eq.) at 24 °C. The reaction mixture was left to stir for 12 h and to the solution, 1 N HCl was added dropwise to solution pH = 5. The resulting solution was extracted with EtOAc (3 x 5 mL) and the combined organic layer was washed with brine (10 mL), dried on Na_2SO_4, and concentrated under reduced pressure. The resulting residue was adsorbed on isolute and submitted to reverse-phased Biotage eluting with MeOH (0 – 100%) in water. Fractions containing the product were combined and concentrated *in vacuo* to afford desired carboxylic acids **72** – **80**.

Methyl(R)-2-(1-hydroxy-1,3-dihydrobenzo[c][1,2]oxaborole-6-carboxamido)-2-phenylacetate, 43/MM2-92

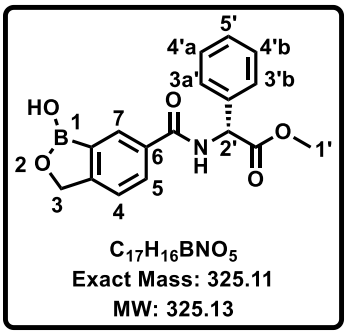

Obtained through method A as a white solid (57 mg, 16%); m.p: 142-143 °C; *Rf* (EtOAc:Hex:EtOH, 3:6:1) 0.15; ^{1}H NMR (600 MHz, MeOD) δ 8.15 (s, 1H, H^7), 7.95 (d, *J* = 8.0 Hz, 1H, H^5), 7.50 – 7.45 (m, 3H, $H^{3'a, 3'b,}$ H^4), 7.43 – 7.32 (m, 3H, $^{H4'a, 4'b,}$ $H^{5'}$), 5.72 (s, 1H, $H^{2'}$), 5.12 (s, 2H, H^3), 3.76 (s, 3H, $H^{1'}$). ^{13}C NMR (151 MHz, MeOD) δ 172.8, 170.3, 158.9, 137.5, 134.5, 131.3, 130.6, 129.9 (2C), 129.6, 129.1 (2C), 122.5 (2C), 72.3, 58.9, 53.1. HPLC-MS (APCI/ESI): Purity > 99%, t_R = 2.309 min, *m/z* $[M+1]^+$ = 326.1, calculated exact mass for $C_{17}H_{16}BNO_5$: 325.11.

2-amino-N-(1-hydroxy-1,3-dihydrobenzo[c][1,2]oxaborol-6-yl)-2-phenylacetamide, 44/MM4-26

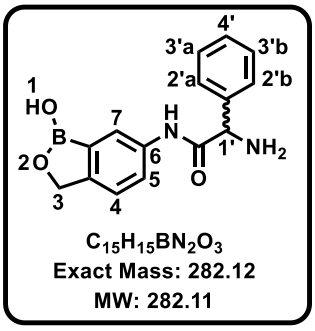

Obtained through method C as an orange solid (120 mg, 63% over two steps); m.p: 196-198°C; *Rf* (DCM:MeOH, 9:1) 0.1; ^{1}H NMR (600 MHz, MeOD) δ 7.79 (s, 1H, H^{7}), 7.62 (d, *J* = 8.3, 1H, H^{5}), 7.57 (d, *J* = 7.5 Hz, 2H, $H^{2'a, 2'b}$), 7.48 - 7.41 (m, 3H, $H^{3'a, 3'b}$, $H^{4'}$), 7.31 (d, *J* = 8.3 Hz, 1H, H^{4}), 5.02 (s, 2H, H^{3}), 4.95 (s, 1H, $H^{1'}$). ^{13}C NMR (151 MHz, MeOD) δ 168.9, 151.3, 138.2, 136.5, 130.6 (2C), 130.4 (2C), 128.9 (2C), 124.2, 122.6 (2C), 72.0, 59.1. HPLC-MS (APCI/ESI): Purity > 99%, t_R = 1.206 min, *m/z* $[M+1]^+$ = 283.1, calculated exact mass for $C_{15}H_{15}BN_2O_3$: 282.12.

Methyl(R)-2-(1-hydroxy-1,3-dihydrobenzo[c][1,2]oxaborole-6-carboxamido)-2-phenylacetate, 45/MM2-91

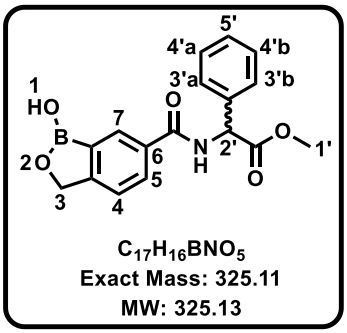

Obtained through method A as a white solid (37 mg, 10%); m.p: 178-181°C; *Rf* (DCM:MeOH, 9:1) 0.2; ^{1}H NMR (400 MHz, MeOD) δ 8.14 (s, 1H, H^{7}), 7.94 (d, *J* = 8.0 Hz, 1H, H^{5}), 7.50 – 7.32 (m, 5H, $H^{3'a, 3'b,}$ $H^{4'a, 4'b,}$ H^{4}), 5.73 (s, 1H, $H^{2'}$), 5.11 (s, 2H, H^{3}), 3.75 (s, 3H, $H^{1'}$). ^{13}C NMR (101 MHz, MeOD) δ 171.4, 168.9, 157.4, 136.1, 132.7, 129.8 (2C), 129.2 (2C), 128.5, 128.2, 127.6, 121.0 (2C), 70.8, 57.5, 51.7. HPLC-MS (APCI/ESI): Purity > 99%, t_R = 2.309 min, *m/z* $[M+1]^+$ = 326.1, calculated exact mass for $C_{17}H_{16}BNO_5$: 325.11.

Methyl (R)-2-(1-hydroxy-1,3-dihydrobenzo[c][1,2]oxaborole-6-carboxamido)-2-phenylacetate, 45A/MM2-224A

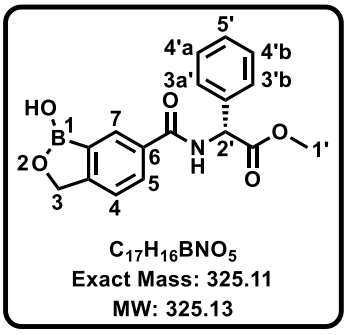

Obtained from reversed-phase chiral HPLC purification of ***45/MM2-91*** as a white solid (19 mg, 17%); m.p: 180-183°C; $[a]^{20}_D$ = +58.9; *Rf* (EtOAc:Hex:EtOH, 3:6:1) 0.15; ^{1}H NMR (400 MHz, MeOD) δ 8.15 (s, 1H, H^7), 7.95 (d, *J* = 8.0 Hz, 1H, H^5), 7.50 – 7.48 (m, 3H, $H^{4,}$ $H^{3'a,\ 3'b}$), 7.44 – 7.31 (m, 3H, $H^{4'a,\ 4'b,}$ $H^{5'}$), 5.72 (s, 1H, $H^{2'}$), 5.12 (s, 2H, H^3), 3.75 (s, 3H, $H^{1'}$). ^{13}C NMR (101 MHz, MeOD) δ 172.8, 170.3, 158.9, 137.5, 134.3, 131.3, 130.7, 129.9 (2C), 129.6, 129.1 (2C), 122.5 (2C), 72.3, 58.9, 53.1. HPLC-MS (APCI/ESI): Purity > 99%, t_R = 2.309 min, *m/z* $[M+1]^+$ = 326.1, calculated exact mass for $C_{17}H_{16}BNO_5$: 325.11.

Methyl (S)-2-(1-hydroxy-1,3-dihydrobenzo[c][1,2]oxaborole-6-carboxamido)-2-phenylacetate, 45B/MM2-224B

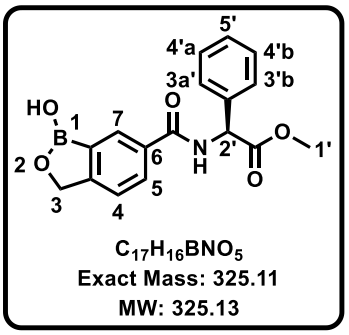

Obtained from reversed-phase chiral HPLC purification of ***45/MM2-91*** as a white solid (19 mg, 17%); m.p: 130-132°C; $[a]^{20}_D$ = -61.3; *Rf* (EtOAc:Hex:EtOH, 3:6:1) 0.15; ^{1}H NMR (400 MHz, MeOD) δ 8.17 (s, 1H, H^7), 7.97 (d, *J* = 8.0 Hz, 1H, H^5), 7.53 – 7.46 (m, 3H, $H^{3'a,\ 3'b,}$ H^4), 7.46 – 7.33 (m, 3H, $H^{4'a,\ 4'b,}$ $H^{5'}$), 5.74 (s, 1H, $H^{2'}$), 5.14 (s, 2H, H^3), 3.77 (s, 3H, $H^{1'}$). ^{13}C NMR (101 MHz, MeOD) δ 172.8, 170.2, 158.9, 137.5, 134.1, 131.4, 130.7, 129.9 (2C), 129.6, 129.1 (2C), 122.5 (2C), 72.3, 58.9, 53.1. HPLC-MS (APCI/ESI): Purity > 99%, t_R = 2.321 min, *m/z* $[M+1]^+$ = 326.1, calculated exact mass for $C_{17}H_{16}BNO_5$: 325.11.

Methyl 2-(1-hydroxy-1,3-dihydrobenzo[c][1,2]oxaborole-6-carboxamido)-2-(p-tolyl)acetate, 46/MM2-174

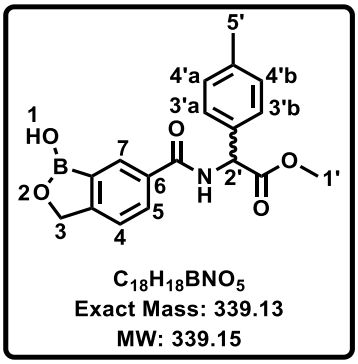

Using method B, the product was obtained as a white solid (64 mg, 33%); *Rf* (EtOAc:Hex:EtOH, 3:6:1) 0.25; m.p: 160-162 °C; ^{1}H NMR (400 MHz, DMSO-d_6) δ 9.28 (s, 1H, H^1), 9.12 (d, *J* = 7.1 Hz, 1H, –NH), 8.26 (s, 1H, H^7), 7.99 (d, *J* = 8.0, 1H, H^5), 7.48 (d, *J* = 8.0 Hz, 1H, H^4), 7.37 (d, *J* = 7.9 Hz, 2H, H$^{3'a, 3'b}$), 7.20 (d, *J* = 7.8 Hz, 2H, H$^{4'a, 4'b}$), 5.62 (d, *J* = 7.1 Hz, 1H, H$^{2'}$), 5.04 (s, 2H, H^3), 3.65 (s, 3H, H$^{1'}$), 2.31 (s, 3H, H$^{5'}$). ^{13}C NMR (101 MHz, DMSO-d_6) δ 180.6, 176.3, 166.5, 146.9, 139.6, 139.5, 138.5 (2C), 137.5 (2C), 130.6, 124.6 (2C), 79.4, 66.1, 65.9, 61.6, 30.1. HPLC-MS (APCI/ESI): Purity = 98%, t_R = 2.369 min, *m/z* $[M+1]^+$ = 340.0, calculated exact mass for $C_{18}H_{18}BNO_5$: 339.13.

Methyl 2-(1-hydroxy-1,3-dihydrobenzo[c][1,2]oxaborole-6-carboxamido)-2-(m-tolyl)acetate, 47/MM2-196

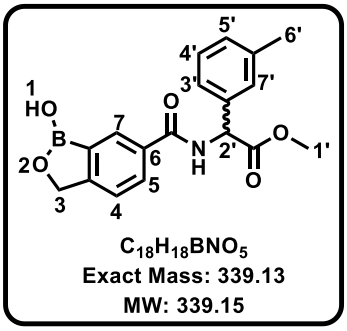

Obtained through method C as a yellow solid (74 mg, 38%); m.p: 141-143 °C; *Rf* (DCM:MeOH, 9:1) 0.8; ^{1}H NMR (400 MHz, DMSO-d_6) δ 9.33 (s, 1H, H^1), 9.19 (d, *J* = 7.1 Hz, 1H, -NH), 8.27 (s, 1H, H^7), 7.99 (d, *J* = 8.0 Hz, 1H, H^5), 7.49 (d, *J* = 8.0 Hz, 1H, H^4), 7.33 – 7.23 (m, 3H, H$^{3'}$, H$^{4'}$, H$^{7'}$), 7.21 – 7.14 (m, 1H, H$^{5'}$), 5.62 (d, *J* = 7.1 Hz, 1H, H$^{2'}$), 5.04 (s, 2H, H^3), 3.66 (s, 3H, H$^{1'}$), 2.32 (s, 3H, H$^{6'}$). ^{13}C NMR (101 MHz, DMSO-d_6) δ 171.2, 166.9, 157.2, 137.8, 136.1, 132.6, 130.31, 130.2, 128.9, 128.5, 125.4, 121.2 (2C), 69.9, 56.9, 52.3, 52.3, 21.0. HPLC-MS (APCI/ESI): Purity = 97%, t_R = 2.391 min, m/z $[M+1]^+$ = 340.2, calculated exact mass for $C_{18}H_{18}BNO_5$: 339.13.

Methyl 2-(1-hydroxy-1,3-dihydrobenzo[c][1,2]oxaborole-6-carboxamido)-2-(o-tolyl)acetate, 48/MM4-81

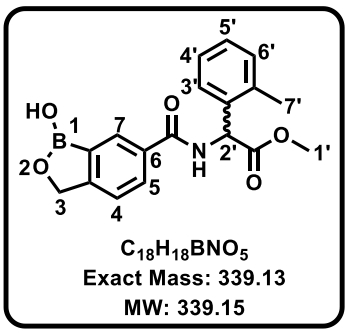

Obtained through method C as a white solid (50 mg, 26%); m.p: 109-112 °C; *Rf* (DCM:MeOH, 9:1) 0.8; ^{1}H NMR (600 MHz, MeOD) δ 8.14 (s, 1H, H^7), 7.94 (d, *J* = 8.0 Hz, 1H, H^5), 7.47 (d, *J* = 8.0 Hz, 1H, H^4), 7.33 (dd, *J* = 7.2, 1.3 Hz, 1H, $H^{6'}$), 7.27 – 7.24 (m, 2H, $H^{3'}$, $H^{4'}$), 7.24 – 7.17 (m, 1H, $H^{5'}$), 5.98 (s, 1H, $H^{2'}$), 5.12 (s, 2H, H^3), 3.76 (s, 3H, $H^{1'}$), 2.47 (s, 3H, $H^{7'}$). ^{13}C NMR (151 MHz, MeOD) δ 173.2, 170.3, 158.9, 138.3, 135.9, 134.1, 131.8, 131.4, 130.7, 129.6, 128.3, 127.5, 122.5 (2C), 72.3, 55.5, 53.0, 19.4. HPLC-MS (APCI/ESI): Purity >99%, t_R = 2.376 min, m/z $[M+1]^+$ = 340.1, calculated exact mass for $C_{18}H_{18}BNO_5$: 339.13.

Methyl 2-(4-fluorophenyl)-2-(1-hydroxy-1,3-dihydrobenzo[c][1,2]oxaborole-6-carboxamido)acetate, 49/MM2-201

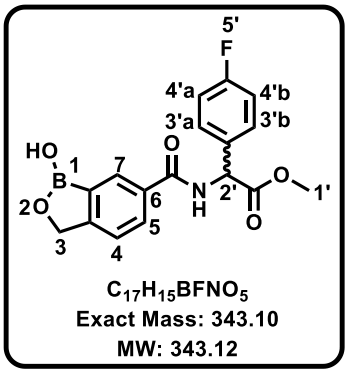

Obtained through method A as a beige solid (64 mg, 33%); m.p: 141-143 °C; *Rf* (DCM:MeOH, 9:1) 0.6; ^{1}H NMR (300 MHz, MeOD) δ 8.14 (s, 1H, H^7), 7.95 (d, *J* = 8.0 Hz, 1H, H^5), 7.57 – 7.43 (m, 3H, $H^{3'a, 3'b}$, H^4), 7.19 – 7.05 (m, 2H, $H^{4'a, 4'b}$, coupling with -F), 5.73 (s, 1H, $H^{2'}$), 5.12 (s, 2H, H^3), 3.76 (s, 3H, $H^{1'}$). ^{13}C NMR (101 MHz, MeOD) δ 172.6, 170.2, 158.9, 134.0, 133.7, 131.2 (2C), 131.1, 130.6, 122.5 (2C), 116.7 (2C), 116.5, 72.2, 58.1, 53.2. HPLC-MS (APCI/ESI): Purity >99%, t_R = 2.370 min, *m/z* $[M+1]^+$ = 344.1, calculated exact mass for $C_{17}H_{15}BFNO_5$: 343.12.

Methyl 2-(3-fluorophenyl)-2-(1-hydroxy-1,3-dihydrobenzo[c][1,2]oxaborole-6-carboxamido)acetate, 50/MM4-44

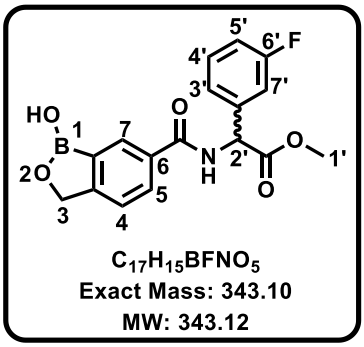

Obtained through method C as a beige solid (117 mg, 61%); m.p: 149-150 °C; *Rf* (DCM:MeOH, 9:1) 0.6; ^{1}H NMR (400 MHz, MeOD) δ 8.16 (s, 1H, H^{7}), 7.96 (d, *J* = 8.0 Hz, 1H, H^{5}), 7.49 (d, *J* = 8.0 Hz, 1H, H^{4}), 7.41 (t, *J* = 7.8 Hz, 1H, $H^{4'}$), 7.34 – 7.22 (m, 2H, $H^{3'}$, $H^{7'}$), 7.10 (td, *J* = 7.8, 2.6 Hz, 1H, $H^{5'}$, couples to -F), 5.77 (s, 1H, $H^{2'}$), 5.13 (s, 2H, H^{3}), 3.77 (s, 3H, $H^{1'}$). ^{13}C NMR (101 MHz, MeOD) δ 172.2, 170.2, 159.0, 140.2, 140.2, 134.03, 131.7, 131.6, 131.4, 130.7, 125.0, 122.5 (2C), 116.4, 72.3, 58.2, 53.2. HPLC-MS (APCI/ESI): Purity >99%, t_R = 2.356 min, *m/z* $[M+1]^+$ = 344.2, calculated exact mass for $C_{17}H_{15}BFNO_5$: 343.12.

Methyl 2-(2-fluorophenyl)-2-(1-hydroxy-1,3-dihydrobenzo[c][1,2]oxaborole-6-carboxamido)acetate, 51/MM4-64

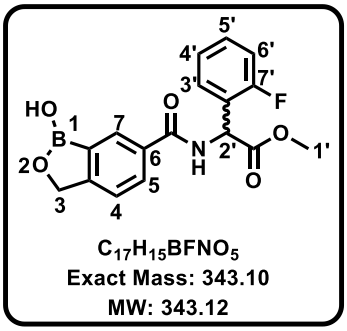

Obtained through method B as a white wax (73 mg, 37%); *Rf* (DCM:MeOH, 9:1) 0.6; ^{1}H NMR (600 MHz, MeOD) δ 8.12 (s, 1H, H^{7}), 7.93 (d, *J* = 8.0 Hz, 1H, H^{5}), 7.62 – 7.46 (m, 3H, H^{4}, $H^{6'}$, $H^{5'}$), 7.39 – 7.31 (m, 2H, $H^{3'}$, $H^{4'}$), 6.10 (s, 1H, $H^{2'}$), 5.12 (s, 2H, H^{3}), 3.77 (s, 3H, $H^{1'}$). ^{13}C NMR (151 MHz, MeOD) δ 172.1, 170.2, 158.9, 135.5, 135.4, 133.9, 131.1, 130.9, 130.6, 130.6, 125.5, 122.5 (2C), 116.7, 72.2, 58.9, 53.3. HPLC-MS (APCI/ESI): Purity = 95%, t_R = 2.330 min, *m/z* $[M+1]^+$ = 344.0, calculated exact mass for $C_{17}H_{15}BFNO_5$: 343.12.

Methyl 2-(1-hydroxy-1,3-dihydrobenzo[c][1,2]oxaborole-6-carboxamido)-2-(4-methoxyphenyl)acetate, 52/MM3-160

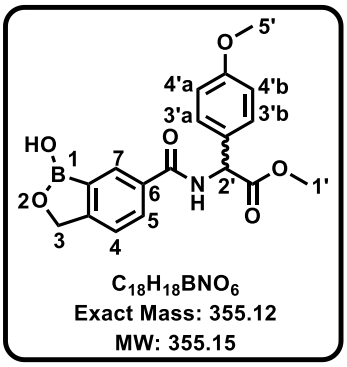

Obtained through method B as a beige solid (95 mg, 48%); m.p: 167-169 °C; *Rf* (DCM:MeOH, 9:1) 0.4; ^{1}H NMR (300 MHz, MeOD) δ 8.14 (s, 1H, H^7), 7.95 (d, *J* = 8.0 Hz, 1H, H^5), 7.47 (d, *J* = 8.0 Hz, 1H, H^4), 7.39 (d, *J* = 9.0 Hz, 2H, H$^{3'a, 3'b}$), 6.94 (d, *J* = 9.0 Hz, 2H, H$^{4'a, 4'b}$), 5.64 (s, 1H, H$^{2'}$), 5.12 (s, 2H, H^3), 3.80 (s, 3H, H$^{5'}$), 3.75 (s, 3H, H$^{1'}$). ^{13}C NMR (101 MHz, MeOD) δ 173.1, 170.2, 161.4, 158.9, 134.2, 131.4, 130.7, 130.4, 129.3 (2C), 122.5 (2C), 115.3 (2C), 72.3, 58.4, 55.8, 52.9. HPLC-MS (APCI/ESI): Purity >99%, t_R = 2.351 min, *m/z* $[M+1]^+$ = 356.1.

Methyl 2-(1-hydroxy-1,3-dihydrobenzo[c][1,2]oxaborole-6-carboxamido)-2-(3-methoxyphenyl)acetate, 53/MM4-15

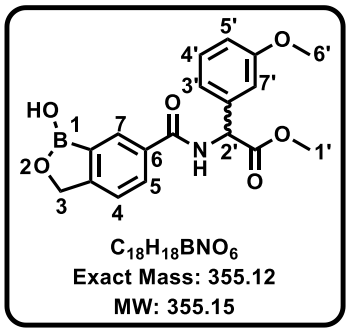

Obtained through method C as a white solid (47 mg, 24%); m.p: 150-152 °C; *Rf* (DCM:MeOH, 9:1) 0.4; ^{1}H NMR (600 MHz, MeOD) δ 8.15 (s, 1H, H^7), 7.95 (d, *J* = 8.0 Hz, 1H, H^5), 7.47 (d, *J* = 8.0 Hz, 1H, H^4), 7.30 (t, *J* = 7.6 Hz, 1H, H$^{4'}$), 7.07 – 7.02 (m, 2H, H$^{3'}$, H$^{7'}$), 6.92 (dt, *J* = 7.6, 2.6 Hz, 1H, H$^{5'}$), 5.69 (s, 1H, H$^{2'}$), 5.11 (s, 2H, H^3), 3.80 (s, 3H, H$^{1'}$), 3.75 (s, 3H, H$^{6'}$). ^{13}C NMR (151 MHz, MeOD) δ 172.7, 170.2, 161.5, 158.9, 138.8, 134.1, 131.4, 130.9, 130.7, 122.5 (2C), 121.2, 115.1, 114.7, 72.3, 58.8, 55.8, 53.1. HPLC-MS (APCI/ESI): Purity >99%, t_R = 0.919 min, *m/z* $[M+1]^+$ = 356.1, calculated exact mass for $C_{18}H_{18}BNO_6$: 355.15.

Methyl 2-(1-hydroxy-1,3-dihydrobenzo[c][1,2]oxaborole-6-carboxamido)-2-(2-methoxyphenyl)acetate, 54/MM4-46

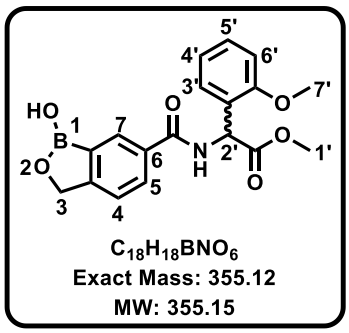

Obtained through method C as a yellow solid (47 mg, 24%); m.p: 94-97 °C; *Rf* (DCM:MeOH, 9:1) 0.4; ^{1}H NMR (400 MHz, MeOD) δ 8.10 (s, 1H, H^7), 7.93 (d, *J* = 8.0 Hz, 1H, H^5), 7.47 (d, *J* = 8.0 Hz, 1H, H^4), 7.36 – 7.32 (m, 2H, H$^{3'}$, H$^{4'}$), 7.04 (d, *J* = 8.4 Hz, 1H, H$^{6'}$), 6.97 (t, *J* = 8.4 Hz, 1H, H$^{5'}$), 6.02 (s, 1H, H$^{2'}$), 5.12 (s, 2H, H^3), 3.88 (s, 3H, H$^{7'}$), 3.73 (s, 3H, H$^{1'}$), ^{13}C NMR (101 MHz, MeOD) δ 163.7, 160.6, 149.4, 149.3, 124.9, 122.8 (2C), 121.6, 121.1, 120.9, 116.4, 113.0, 112.4, 102.9, 62.8,

46.8, 44.5, 43.5. HPLC-MS (APCI/ESI): Purity = 95%, t_R = 2.330 min, *m/z* $[M+H]^+$ = 356.1, calculated exact mass for $C_{18}H_{18}BNO_6$: 355.15.

Methyl 2-(1-hydroxy-1,3-dihydrobenzo[c][1,2]oxaborole-6-carboxamido)-2-(4-hydroxyphenyl)acetate, 55/MM3-8

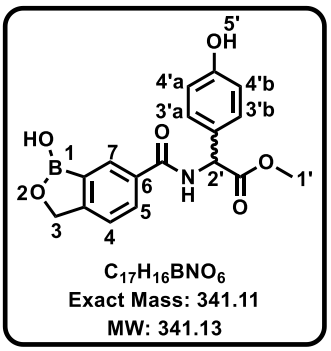

Obtained through method B as a beige solid (29 mg, 15%); m.p: 164-167 °C; *Rf* (DCM:MeOH, 9:1) 0.4; ^{1}H NMR (600 MHz, MeOD) δ 8.14 (s, 1H, H^7), 7.94 (d, *J* = 8.0 Hz, 1H, H^5), 7.46 (d, *J* = 8.0 Hz, 1H, H^4), 7.29 (d, *J* = 12.0 Hz, 2H, $H^{3'a, 3'b}$), 6.80 (d, *J* = 12.0 Hz, 2H, $H^{4'a, 4'b}$), 5.58 (s, 1H, $H^{2'}$), 5.12 (s, 2H, H^3), 3.74 (s, 3H, $H^{1'}$). ^{13}C NMR (101 MHz, MeOD) δ 173.2, 170.3, 159.0, 158.9, 134.2, 131.3, 130.7, 130.4 (2C), 127.9, 122.4 (2C), 116.6 (2C), 72.3, 58.5, 52.9. HPLC-MS (APCI/ESI): Purity >99%, t_R = 2.114 min, *m/z* $[M+1]^+$ = 342.0, calculated exact mass for $C_{17}H_{16}BNO_6$: 341.11.

Methyl 2-(1-hydroxy-1,3-dihydrobenzo[c][1,2]oxaborole-6-carboxamido)-2-(3-hydroxyphenyl)acetate, 56/MM4-101

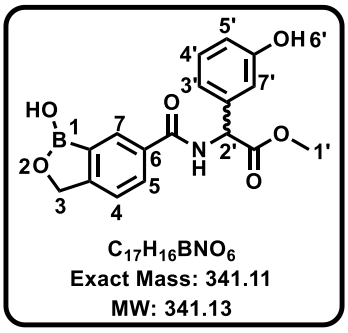

Obtained through method C as a beige solid (68 mg, 35%); m.p: 100-102 °C; *Rf* (DCM:MeOH, 9:1) 0.4; ^{1}H NMR (600 MHz, DMSO-d_6) δ 9.50 (s, 1H, $-OH^6$), 9.28 (s, 1H, H^1), 9.12 (d, *J* = 6.9 Hz, 1H, -NH), 8.27 (s,1H, H^7), 7.99 (d, *J* = 8.0 Hz, 1H, H^5), 7.48 (d, *J* = 8.0 Hz, 1H, H^4), 7.18 (t, *J* = 7.8 Hz, 1H, $H^{4'}$), 6.91 – 6.85 (m, 2H, $H^{3'}$, $H^{7'}$), 6.77 – 6.72 (m, 1H, $H^{5'}$), 5.56 (d, *J* = 6.9 Hz, 1H, $H^{2'}$), 5.04 (s, 2H, H^3), 3.66 (s, 3H, $H^{1'}$). ^{13}C NMR (151 MHz, DMSO-d_6) δ 180.5, 176.4, 157.9, 156.6, 146.8, 142.0, 139.7, 139.6, 138.9, 130.6, 128.3, 124.6, 124.6, 79.4, 66.4, 61.6, 51.9. HPLC-MS (APCI/ESI): Purity = 97%, t_R = 2.183 min, m/z $[M+1]^+$ = 342.1, calculated exact mass for $C_{17}H_{16}BNO_6$: 341.11.

Methyl 2-(1-hydroxy-1,3-dihydrobenzo[c][1,2]oxaborole-6-carboxamido)-2-(3-hydroxyphenyl)acetate, 57/MM4-108

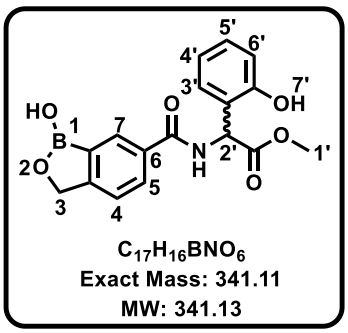

Obtained through method C as a white solid (68 mg, 35%); m.p: 100-102 °C; *Rf* (DCM:MeOH, 9:1) 0.4; ^{1}H NMR (600 MHz, DMSO-d_6) δ 9.51 (s, 1H, H$^{7'}$), 9.30 (s, 1H, H^1), 9.14 (d, J = 6.8 Hz, 1H, -NH), 8.27 (s, 1H, H^7), 7.99 (d, J = 8.0 Hz, 1H, H^5), 7.48 (d, J = 8.0 Hz, 1H, H^4), 7.16 – 6.91 (m, 3H, H$^{3'}$, H$^{4'}$, H$^{6'}$), 6.77 – 6.72 (m, 1H, H$^{5'}$), 5.53 (d, J = 6.8 Hz, 1H, H$^{2'}$), 5.02 (s, 2H, H^3), 3.60 (s, 3H, H$^{1'}$). ^{13}C NMR (151 MHz, DMSO-d_6) δ 177.6, 176.4, 159.9, 157.6, 146.8, 142.0, 139.7, 139.6, 138.9, 130.6, 128.3, 124.6, 124.6, 79.4, 66.4, 61.6, 51.9. HPLC-MS (APCI/ESI): Purity >99%, t_R = 2.132 min, m/z $[M+1]^+$ = 342.0, calculated exact mass for $C_{17}H_{16}BNO_6$: 341.11.

Methyl 2-(1-hydroxy-1,3-dihydrobenzo[c][1,2]oxaborole-6-carboxamido)-2-(4-(trifluoromethyl)phenyl)acetate, 58/MM3-9

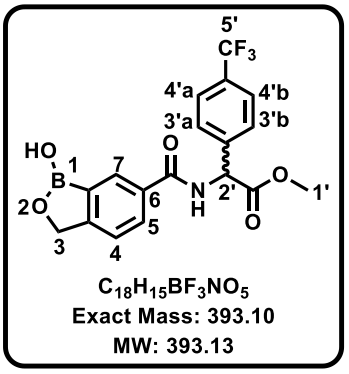

Obtained through method B as a beige solid (75 mg, 68%); m.p: 134-136 °C; *Rf* (DCM:MeOH, 9:1) 0.3; ^{1}H NMR (400 MHz, MeOD) δ 8.16 (s, 1H, H^7), 7.97 (d, J = 8.0 Hz, 1H, H^5), 7.74 – 7.65 (m, 4H, H$^{3'a, 3'b,}$ H$^{4'a, 4'b}$), 7.49 (d, J = 8.0 Hz, 1H, H^4), 5.86 (s, 1H, H$^{2'}$), 5.13 (s, 2H, H^3), 3.78 (s, 3H, H$^{1'}$). ^{13}C NMR (101 MHz, MeOD) δ 171.9, 170.2, 159.0, 142.1, 133.9, 131.3, 130.6, 129.8 (3C), 126.7, 126.7 (2C), 122.5 (2C), 72.3, 58.3, 53.3. HPLC-MS (APCI/ESI): Purity >99%, t_R = 2.489 min, *m/z* $[M+1]^+$ = 394.0, calculated exact mass for $C_{18}H_{15}BF_3NO_5$: 393.10.

Methyl 2-(1-hydroxy-1,3-dihydrobenzo[c][1,2]oxaborole-6-carboxamido)-2-(3-(trifluoromethyl)phenyl)acetate, 59/MM4-14

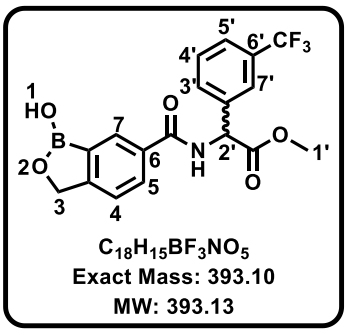

Obtained through method C as a white solid (123 mg, 56%); m.p: 149-152 °C; *Rf* (DCM:MeOH, 9:1) 0.8; ^{1}H NMR (600 MHz, MeOD) δ 8.17 (s, 1H, H^7), 7.97 (d, *J* = 8.0 Hz, 1H, H^5), 7.82 (s, 1H, H$^{7'}$), 7.76 (d, *J* = 8.0 Hz, 1H, H^4), 7.66 (d, *J* = 7.8 Hz, 1H, H$^{5'}$), 7.60 (t, *J* = 7.8 Hz, 1H, H$^{4'}$), 7.48 (d, *J* = 7.9 Hz, 1H, H$^{3'}$), 5.87 (s, 1H, H$^{2'}$), 5.13 (s, 2H, H^3), 3.78 (s, 3H, H$^{1'}$). ^{13}C NMR (151 MHz, MeOD) δ 172.0, 170.1, 159.1, 139.2, 133.9, 132.9, 131.4, 130.7, 130.6, 126.3, 126.2, 125.9, 125.9, 122.5 (2C), 72.3, 58.2, 53.3. HPLC-MS (APCI/ESI): Purity = 97%, t_R = 2.417 min, m/z $[M+1]^+$ = 394.1, calculated exact mass for $C_{18}H_{15}BF_3NO_5$: 393.10.

Methyl 2-(1-hydroxy-1,3-dihydrobenzo[c][1,2]oxaborole-6-carboxamido)-2-(2-(trifluoromethyl)phenyl)acetate, 60/MM4-16

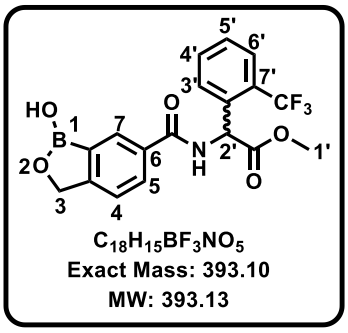

Obtained through method C as a white solid (47 mg, 21%); m.p: 129-133 °C; *Rf* (DCM:MeOH, 9:1) 0.7; ^{1}H NMR (600 MHz, MeOD) δ 8.12 (s, 1H, H^7), 7.93 (d, *J* = 8.0 Hz, 1H, H^5), 7.79 (d, *J* = 8.0 Hz, 1H, H^4), 7.74 – 7.65 (m, 2H, H$^{5'}$, H$^{6'}$), 7.60 – 7.55 (m, 1H, H$^{4'}$), 7.47 (d, *J* = 8.0 Hz, 1H, H$^{3'}$), 6.10 (s, 1H, H$^{2'}$), 5.12 (s, 2H, H^3), 3.76 (s, 3H, H$^{1'}$). ^{13}C NMR (151 MHz, MeOD) δ 172.2, 170.3, 159.0, 135.4, 133.9, 133.8, 131.4, 131.1, 130.7, 130.2, 127.5 (2C), 127.4, 122.5 (2C), 72.3, 54.9, 53.3. HPLC-MS (APCI/ESI): Purity >99%, t_R = 2.438 min, m/z $[M+1]^+$ = 394.1, calculated exact mass for $C_{18}H_{15}BF_3NO_5$: 393.10.

Methyl 2-(4-chlorophenyl)-2-(1-hydroxy-1,3-dihydrobenzo[c][1,2]oxaborole-6-carboxamido)acetate, 61/MM3-175

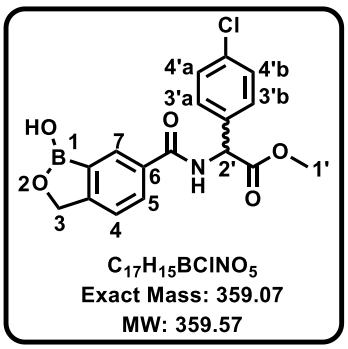

Obtained through method B as a beige solid (83 mg, 41%); m.p: 150-153 °C; *Rf* (DCM:MeOH, 9:1) 0.5; ^{1}H NMR (300 MHz, MeOD) δ 8.16 (s, 1H, H^{7}), 7.96 (d, *J* = 8.0 Hz, 1H, H^{5}), 7.51 – 7.44 (m, 3H, H^{4}, $H^{3'a, 3'b}$), 7.40 (d, *J* = 9.0 Hz, 2H, $H^{4'a, 4'b}$), 5.74 (s, 1H, $H^{2'}$), 5.13 (s, 2H, H^{3}), 3.76 (s, 3H, $H^{1'}$). ^{13}C NMR (101 MHz, MeOD) δ 172.4, 170.2, 158.9, 136.4, 135.5, 134.0 (2C), 131.3, 130.8, 130.6, 129.9 (2C), 122.5 (2C), 72.2, 58.1, 53.2. HPLC-MS (APCI/ESI): Purity >99%, t_R = 2.416 min, *m/z* $[M+1]^+$ = 360.0.

Methyl 2-(3-chlorophenyl)-2-(1-hydroxy-1,3-dihydrobenzo[c][1,2]oxaborole-6-carboxamido)acetate, 62/MM4-12

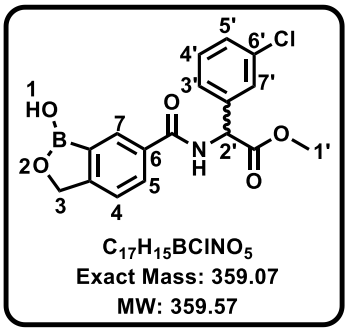

Obtained through method B as a white solid (124 mg, 77%); m.p: 143-145 °C; *Rf* (DCM:MeOH, 9:1) 0.7; ^{1}H NMR (400 MHz, DMSO-d_6) δ 9.34 (s, 1H, H^{1}), 9.31 (d, *J* = 7.2 Hz, 1H, -NH), 8.27 (s, 1H, H^{7}), 7.99 (d, *J* = 8.0 Hz, 1H, H^{5}), 7.59 (s, 1H, $H^{7'}$), 7.53 – 7.40 (m, 4H, H^{4}, $H^{3'}$, $H^{4'}$, $H^{5'}$), 5.75 (d, *J* = 7.2 Hz, 1H, $H^{2'}$), 5.05 (s, 2H, H^{3}), 3.67 (s, 3H, $H^{1'}$). ^{13}C NMR (101 MHz, DMSO-d_6) δ 170.7, 166.9, 157.3, 138.8, 133.1, 132.4, 130.4, 130.2, 130.1, 128.2, 128.1, 127.2, 121.3 (2C), 69.9, 56.3, 52.5. HPLC-MS (APCI/ESI): Purity **>** 99%, t_R = 2.402 min, *m/z* $[M+1]^+$ = 360.0, calculated exact mass for $C_{17}H_{15}BClNO_5$: 359.07.

Methyl 2-(2-chlorophenyl)-2-(1-hydroxy-1,3-dihydrobenzo[c][1,2]oxaborole-6-carboxamido)acetate, 63/MM4-07

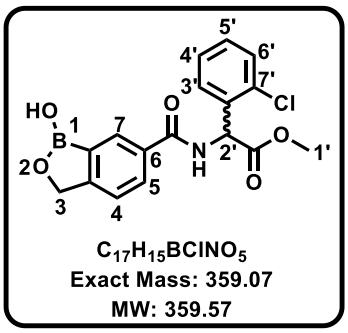

Obtained through method B as a white solid (38 mg, 38%); m.p: 90-92 °C; *Rf* (DCM:MeOH, 9:1) 0.7; ^{1}H NMR (600 MHz, MeOD) δ 8.13 (s, 1H, H^{7}), 7.94 (d, *J* = 8.0 Hz, 1H, H^{5}), 7.51 – 7.44 (m, 3H, H^{4}, $H^{6'}$, $H^{5'}$), 7.39 – 7.31 (m, 2H, $H^{3'}$, $H^{4'}$), 6.18 (s, 1H, $H^{2'}$), 5.11 (s, 2H, H^{3}), 3.77 (s, 3H, $H^{1'}$). ^{13}C NMR (151 MHz, MeOD) δ 172.1, 170.2, 158.9, 135.5, 135.4, 133.9, 131.3, 131.1, 130.9, 130.6, 130.2, 128.5, 122.5

(2C), 72.2, 55.9, 53.3. HPLC-MS (APCI/ESI): Purity = 97%, t_R = 2.350 min, m/z $[M+1]^+$ = 360.1, calculated exact mass for $C_{17}H_{15}BClNO_5$: 359.07.

Ethyl 2-(1-hydroxy-1,3-dihydrobenzo[c][1,2]oxaborole-6-carboxamido)-2-phenylacetate, 64/MM3-57

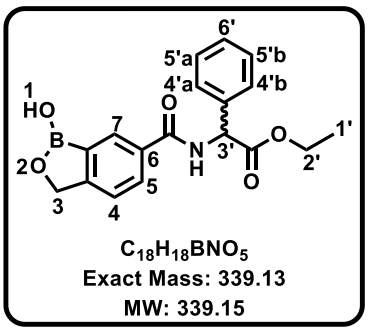

Obtained through method C as a white wax (202 mg, 35%); *Rf* (EtoAc:Hexane 3:7) 0.5; ^{1}H NMR (400 MHz, DMSO-d_6) δ 9.31 (s, 1H, H^1), 9.19 (d, *J* = 7.1 Hz, 1H, -NH), 8.27 (s, 1H, H^7), 7.99 (d, *J* = 8.0 Hz, 1H, H^5), 7.49 (m, 3H, H^4, $H^{4'a, 4'b}$), 7.45 – 7.31 (m, 3H, $H^{5'a, 5'b}$, $H^{6'}$), 5.64 (d, *J* = 7.1 Hz, 1H, $H^{3'}$), 5.04 (s, 2H, H^3), 4.13 (q, *J* = 7.1 Hz, 2H, $H^{2'}$), 1.15 (t, *J* = 7.1 Hz, 3H, $H^{1'}$). HPLC-MS (APCI/ESI): Purity >99%, t_R = 2.440 min, m/z $[M+1]^+$ = 340.2, calculated exact mass for $C_{18}H_{18}BNO_5$: 339.13.

Ethyl 2-(4-chlorophenyl)-2-(1-hydroxy-1,3-dihydrobenzo[c][1,2]oxaborole-6-carboxamido)acetate, 65/MM4-50

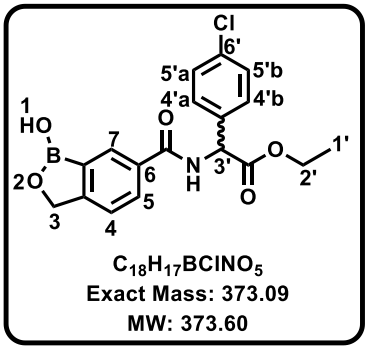

Obtained through method C as a white solid (137 mg, 63%); m.p: 103-105; *Rf* (DCM:MeOH, 9:1) 0.4; ^{1}H NMR (600 MHz, DMSO-d_6) δ 9.29 (s, 1H, H^1), 9.20 (d, *J* = 7.2 Hz, 1H, -NH), 8.26 (s, 1H, H^7), 7.98 (d, *J* = 8.0 Hz, 1H, H^5), 7.52 (d, *J* = 12 Hz, 2H, $H^{5'a, 5'b}$), 7.49 (d, *J* = 8.0 Hz, 1H, H^4), 7.46 (d, *J* = 12 Hz, 2H, $H^{4'a, 4'b}$), 5.68 (d, *J* = 7.2 Hz, 1H, $H^{3'}$), 5.05 (s, 2H, H^3), 4.14 (q, *J* = 7.1 Hz, 2H, $H^{2'}$), 1.15 (t, *J* = 7.1 Hz, 3H, $H^{1'}$). ^{13}C NMR (151 MHz, DMSO-d_6) δ 170.2, 166.8, 157.2, 135.4, 132.8, 132.5, 130.2 (2C), 130.0, 128.4 (2C), 121.2 (2C), 69.9, 61.0, 56.3, 48.7, 13.9. HPLC-MS (APCI/ESI): Purity >99%, t_R = 2.479 min, m/z $[M+1]^+$ = 374.1, calculated exact mass for $C_{18}H_{17}BClNO_5$: 373.09.

Ethyl 2-(3-chlorophenyl)-2-(1-hydroxy-1,3-dihydrobenzo[c][1,2]oxaborole-6-carboxamido)acetate, 66/MM4-93

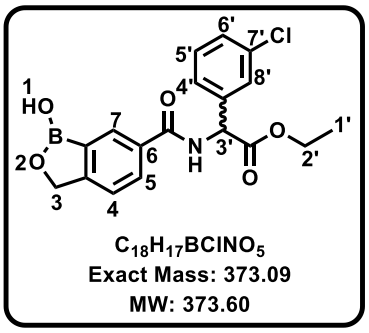

Obtained through method C as a light-yellow solid (161 mg, 75%); m.p: 149-151; *Rf* (DCM:MeOH, 9:1) 0.4; ^{1}H NMR (400 MHz, DMSO-d_6) δ 9.24 (d, J = 7.2 Hz, 1H, -NH), 8.27 (s, 1H, H^7), 7.99 (d, J = 8.0 Hz, 1H, H^5), 7.59 (s, 1H, H$^{8'}$), 7.53 – 7.40 (m, 4H, H^4, H$^{4'}$, H$^{5'}$, H$^{6'}$), 5.70 (d, J = 7.2 Hz, 1H, H$^{3'}$), 5.05 (s, 2H, H^3), 4.15 (q, J = 6.9 Hz, 2H, H$^{2'}$), 1.16 (t, J = 7.0 Hz, 3H, H$^{1'}$). ^{13}C NMR (101 MHz, DMSO-d_6) δ 179.6, 176.4, 166.7, 148.3, 142.5, 141.9, 139.8, 139.7, 139.5, 137.6, 136.6, 130.7, 122.5 (2C), 79.4, 70.6, 65.9, 23.4. HPLC-MS (APCI/ESI): Purity >99%, t_R = 2.474 min, m/z $[M+1]^+$ = 374.1, calculated exact mass for $C_{19}H_{17}BClNO_5$: 373.09.

Ethyl 2-(2-chlorophenyl)-2-(1-hydroxy-1,3-dihydrobenzo[c][1,2]oxaborole-6-carboxamido)acetate, 67/MM4-114

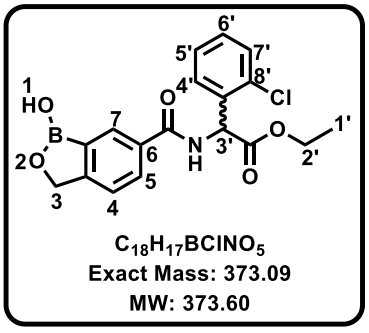

Obtained through method C as a yellow gum (116 mg, 55%); *Rf* (DCM:MeOH, 9:1) 0.4; ^{1}H NMR (400 MHz, MeOD) δ 8.14 (s, 1H, H^7), 7.95 (d, J = 7.9 Hz, 1H, H^5), 7.59 – 7.52 (m, 1H, H$^{6'}$), 7.49 - 7.47 (m, 2H, H^4, H$^{5'}$), 7.37 - 7.32 (m, 2H, H$^{3'}$, H$^{4'}$), 6.15 (s, 1H, H$^{3'}$), 5.12 (s, 2H, H^3), 4.16 (q, J = 6.7 Hz, 2H, H$^{2'}$), 1.15 (t, J = 7.0 Hz, 3H, H$^{1'}$). HPLC-MS (APCI/ESI): Purity >99%, t_R = 2.430 min, m/z $[M+1]^+$ = 374.1, calculated exact mass for $C_{19}H_{17}BClNO_5$: 373.09.

Ethyl 2-(1-hydroxy-1,3-dihydrobenzo[c][1,2]oxaborole-6-carboxamido)-2-(m-tolyl)acetate, 68/MM4-105

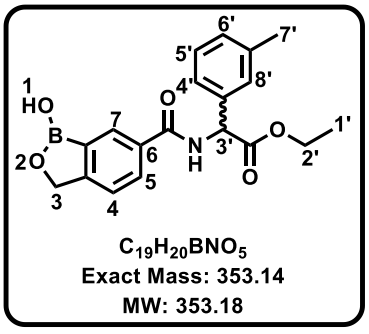

Obtained through method C as a yellow solid (117 mg, 59%); *Rf* (DCM:MeOH, 9:1) 0.7; m.p: 96-98 °C; ^{1}H NMR (400 MHz, DMSO-d_6) δ 9.29 (s, 1H, H^1), 9.10 (d, J = 7.1 Hz, 1H, -NH), 8.27 (s, 1H, H^7), 7.99 (d, J = 8.0 Hz, 1H, H^5), 7.48 (d, J = 8.0 Hz, 1H, H^4), 7.32 – 7.25 (m, 3H, H$^{4'}$, H$^{5'}$, H$^{8'}$), 7.21 – 7.14 (m, 1H, H$^{6'}$), 5.59 (d, J = 7.1 Hz, 1H, H$^{3'}$), 5.04 (s, 2H, H^3), 4.13 (q, J = 7.0 Hz, 2H, H$^{2'}$), 2.32 (s, 3H, H$^{7'}$), 1.15 (t, J = 7.0 Hz, 3H, H$^{1'}$). ^{13}C NMR (101 MHz, DMSO-d_6) δ 180.1, 176.4, 166.6, 147.1, 145.6, 139.7, 139.6, 138.3, 137.9, 134.8, 130.6, 122.2 (2C), 79.4, 70.3, 66.5,

52.8, 30.5, 23.4. HPLC-MS (APCI/ESI): Purity >99%, t_R = 2.449 min, m/z $[M+1]^+$ = 354.2, calculated exact mass for $C_{19}H_{20}BNO_5$: 354.14.

Ethyl 2-(1-hydroxy-1,3-dihydrobenzo[c][1,2]oxaborole-6-carboxamido)-2-(m-tolyl)acetate, 69/MM4-100

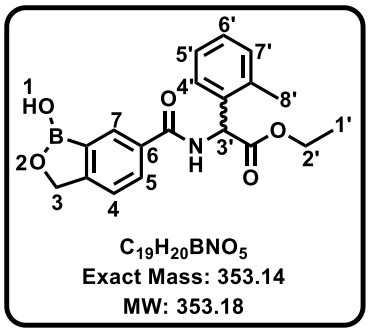

Obtained through method C as a light-yellow solid (67 mg, 34%); *Rf* (DCM:MeOH, 9:1) 0.7; m.p: 98-101 °C; ^{1}H NMR (400 MHz, DMSO-d_6) δ 9.40 (s, 1H, H^1), 9.22 (d, *J* = 7.3 Hz, 1H, -NH), 8.38 (s, 1H, H^7), 8.10 (d, *J* = 8.0 Hz, 1H, H^5), 7.60 (d, *J* = 8.0 Hz, 1H, H^4), 7.45 (dd, *J* = 7.1, 1.0 Hz, 1H, $H^{7'}$), 7.42 – 7.30 (m, 3H, $H^{4'}$, $H^{5'}$, $H^{6'}$), 5.96 (d, *J* = 7.3 Hz, 1H, $H^{3'}$), 5.16 (s, 2H, H^3), 4.28 (q, *J* = 7.1 Hz, 2H, $H^{2'}$), 2.50 (s, 3H, $H^{8'}$), 1.28 (t, *J* = 7.1 Hz, 3H, H1'). ^{13}C NMR (101 MHz, DMSO-d_6) δ 170.8, 166.9, 157.1, 136.6, 134.9, 132.6, 130.4, 130.2, 130.1, 128.1, 127.5, 126.1, 121.1 (2C), 69.9, 60.9, 53.7, 18.9, 13.9. HPLC-MS (APCI/ESI): Purity = 98%, t_R = 2.435 min, m/z $[M+1]^+$ = 354.1, calculated exact mass for $C_{19}H_{20}BNO_5$: 354.14.

Ethyl 2-(3-fluorophenyl)-2-(1-hydroxy-1,3-dihydrobenzo[c][1,2]oxaborole-6-carboxamido)acetate, 70/MM4-56

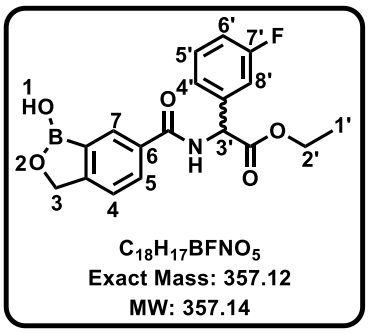

Obtained through method C as a yellow solid (96 mg, 48%); *Rf* (DCM:MeOH, 9:1) 0.5; m.p: 148-150 °C; ^{1}H NMR (600 MHz, MeOD) δ 8.14 (s, 1H, H^7), 7.95 (d, *J* = 8.0 Hz, 1H, H^5), 7.52 – 7.45 (m, 2H, H^4, $H^{5'}$), 7.40 (ddd, *J* = 7.3, 5.3, 1.2 Hz, 1H, $H^{6'}$), 7.21 (td, *J* = 7.6, 1.2 Hz, 1H, $H^{4'}$), 7.17 (dd, *J* = 8.3, 1.2 Hz, 1H, $H^{8'}$, couples to -F), 6.02 (s, 1H, $H^{3'}$), 5.12 (s, 2H, H^3), 4.24 (q, *J* = 7.1 Hz, 2H, $H^{2'}$), 1.23 (t, *J* = 7.1 Hz, 3H, $H^{1'}$). ^{13}C NMR (151 MHz, MeOD) δ 171.6, 170.2, 162.9, 158.9, 134.1, 131.6, 131.6, 130.6, 125.7, 125.7, 122.5 (2C), 116.7, 72.3, 62.9, 52.6, 52.6, 14.3. HPLC-MS (APCI/ESI): Purity >99%, t_R = 2.413 min, m/z $[M+1]^+$ = 358.0, calculated exact mass for $C_{18}H_{17}BFNO_5$: 357.12.

Ethyl 2-(2-fluorophenyl)-2-(1-hydroxy-1,3-dihydrobenzo[c][1,2]oxaborole-6-carboxamido)acetate, 71/MM4-55

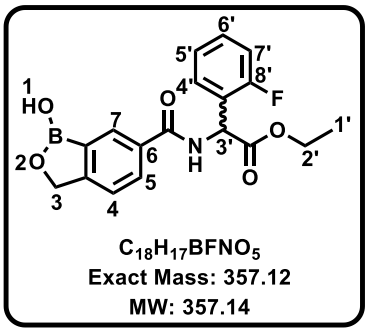

Obtained through method C as a yellow solid (91 mg, 45%); *Rf* (DCM:MeOH, 9:1) 0.5; m.p: 143-145 °C; ^{1}H NMR (300 MHz, MeOD) δ 8.16 (s, 1H, H^7), 7.96 (d, *J* = 8.0 Hz, 1H, H^5), 7.53 – 7.20 (m, 4H, H^4, $H^{4'}$, $H^{6'}$, $H^{7'}$), 7.16 – 7.04 (m, 1H, $H^{5'}$), 5.74 (s, 1H, $H^{3'}$), 5.13 (s, 2H, H^3), 4.24 (q, *J* = 7.1, 2H, $H^{2'}$), 1.24 (t, *J* = 7.1 Hz, 3H, $H^{1'}$). HPLC-MS (APCI/ESI): Purity >99%, t_R = 2.389 min, m/z $[M+1]^+$ = 358.1, calculated exact mass for $C_{18}H_{17}BFNO_5$: 357.12.

Methyl(R)-2-(1-hydroxy-1,3-dihydrobenzo[c][1,2]oxaborole-6-carboxamido)-2-phenylacetate, 72/MM2-173

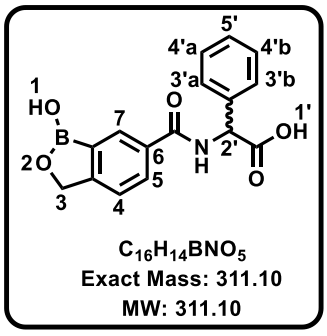

Obtained from hydrolysis of **64/MM3-57** as a white solid (29 mg, 43%); m.p: 154-157°C; ^{1}H NMR (400 MHz, MeOD) δ 8.13 (s, 1H, H^7), 7.94 (d, *J* = 8.0 Hz, 1H, H^5), 7.50 – 7.32 (m, 5H, $H^{3'a, 3'b}$, $H^{4'a, 4'b}$, H^4), 5.73 (s, 1H, $H^{2'}$), 5.12 (s, 2H, H^3). ^{13}C NMR (101 MHz, MeOD) δ 171.4, 168.9, 157.4, 136.1, 132.7, 129.8, 129.2 (2C), 128.5, 128.2, 127.6 (2C), 121.0 (2C), 70.8, 57.5. HPLC-MS (APCI/ESI): Purity >99%, t_R = 1.021 min, *m/z* $[M+1]^+$ = 312.1, calculated exact mass for $C_{17}H_{16}BNO_5$: 311.10.

Methyl(R)-2-(1-hydroxy-1,3-dihydrobenzo[c][1,2]oxaborole-6-carboxamido)-2-phenylacetate, 73/MM2-177

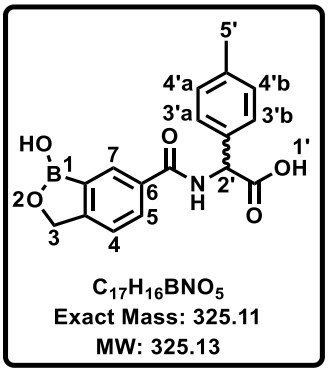

Obtained from hydrolysis of **49/MM2-201** as a white solid (32 mg, 29%); *Rf* (EtOAc:Hex, 7:3) 0.35; m.p: 210-212 °C; ^{1}H NMR (400 MHz, MeOD) δ 7.93 (s, 1H, H^7), 7.65 (d, *J* = 7.7 Hz, 1H, H^5), 7.40 (d, *J* = 7.8 Hz, 2H, $H^{3'a, 3'b}$), 7.17 – 7.08 (m, 3H, H^4, $H^{4'a, 4'b}$), 5.40 (s, 1H, $H^{2'}$), 2.30 (s, 3H, $H^{5'}$). ^{13}C NMR (101 MHz, MeOD) δ 177.0, 170.3, 154.7, 139.1, 137.7, 132.7, 130.4, 129.8, 128.8, 128.2, 126.5 (2C), 121.3 (2C), 70.2, 60.6, 21.2. HPLC-MS (APCI/ESI): Purity >99%, t_R = 2.206 min, *m/z* $[M+1]^+$ = 326.1, calculated exact mass for $C_{17}H_{16}BNO_5$: 325.11.

2-(1-hydroxy-1,3-dihydrobenzo[c][1,2]oxaborole-6-carboxamido)-2-(m-tolyl)acetic acid, 74/MM4-134

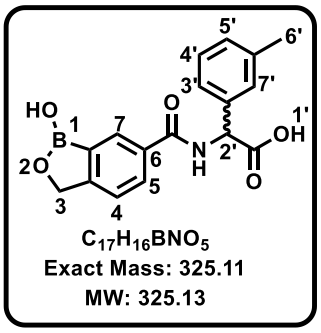

Obtained from hydrolysis of **68/MM4-105** as a white solid (53 mg, 58%); m.p: 196-197 °C; ^{1}H NMR (600 MHz, MeOD) δ 7.93 (s, 1H, H^7), 7.65 (d, *J* = 7.8, 1H, H^5), 7.35 (d, *J* = 7.9 Hz, 1H, H^4), 7.31 (d, *J* = 7.7 Hz, 1H, H$^{3'}$), 7.20 – 7.09 (m, 2H, H$^{4'}$, H$^{7'}$), 7.03 (d, *J* = 7.6 Hz, 1H, H$^{5'}$), 5.39 (s, 1H, H$^{2'}$), 4.88 (s, 2H, H^3), 2.32 (s, 3H, H$^{6'}$). ^{13}C NMR (101 MHz, MeOD) δ 179.1, 176.4, 166.6, 147.1, 145.6, 142.1, 139.7, 139.6, 138.3, 137.9, 134.8, 130.6, 121.6 (2C), 77.4, 68.3, 30.4. HPLC-MS (APCI/ESI): Purity = 96%, t_R = 2.236 min, m/*z* $[M+1]^+$ = 326.1, calculated exact mass for $C_{18}H_{18}BNO_5$: 325.11.

2-(1-hydroxy-1,3-dihydrobenzo[c][1,2]oxaborole-6-carboxamido)-2-(o-tolyl)acetic acid, 75/MM4-137

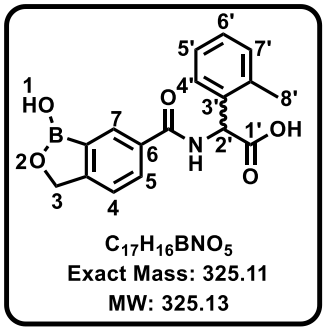

Obtained from hydrolysis of **69/MM4-100** as as a white solid (33 mg, 61%); m.p: 198-201 °C; ^{1}H NMR (300 MHz, MeOD) δ 7.90 (s, 1H, H^7), 7.62 (d, *J* = 7.9 Hz, 1H, H^5), 7.48 – 7.38 (m, 1H, H$^{7'}$), 7.19 – 7.04 (m, 4H, H^4, H$^{4'}$, H$^{5'}$, H$^{6'}$), 5.65 (s, 1H, H$^{2'}$), 4.86 (s, 2H, H^3), 2.58 (s, 3H, H$^{8'}$). ^{13}C NMR (101 MHz, MeOD) δ 171.8, 167.9, 157.1, 136.6, 134.9, 132.7, 130.6, 130.1, 130.1, 128.1, 127.5, 126.1, 121.1 (2C), 69.9, 53.7, 18.9. HPLC-MS (APCI/ESI): Purity >99%, t_R = 2.248 min, m/*z* $[M+1]^+$ = 326.0, calculated exact mass for $C_{17}H_{16}BNO_5$: 325.14.

2-(4-chlorophenyl)-2-(1-hydroxy-1,3-dihydrobenzo[c][1,2]oxaborole-6-carboxamido)acetic acid, 76/MM4-86

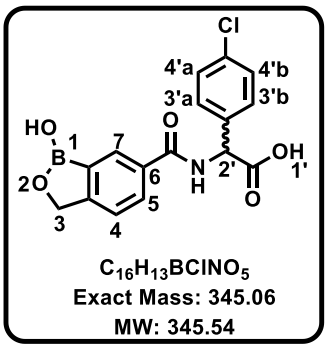

Obtained from hydrolysis of **65/MM4-50** as a beige solid (74 mg, 71%); m.p: 138-140 °C; ^{1}H NMR (300 MHz, MeOD) δ 8.16 (s, 1H, H^7), 7.97 (d, *J* = 8.0 Hz, 1H, H^5), 7.56 – 7.45 (m, 3H, H^4, H$^{4'a, 4'b}$), 7.45 – 7.33 (d, *J* = 9.0 Hz, 2H, H$^{3'a, 3'b}$), 5.69 (s, 1H, H$^{2'}$), 5.13 (s, 2H, H^3), 3.35 (s, 1H, H$^{1'}$). HPLC-MS (APCI/ESI): Purity = 96%, t_R = 2.233 min, *m/z* $[M+1]^+$ = 346.0, calculated exact mass for $C_{16}H_{13}BClNO_5$: 346.06.

2-(3-chlorophenyl)-2-(1-hydroxy-1,3-dihydrobenzo[c][1,2]oxaborole-6-carboxamido)acetic acid, 77/MM4-127

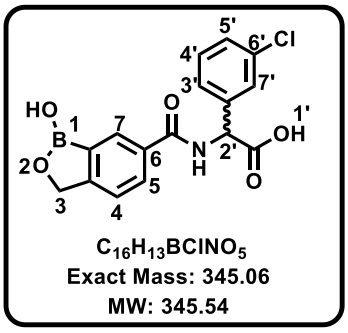

Obtained from hydrolysis of **66/MM4-93** as a white solid (70 mg, 76%); m.p: 143-145 °C; *Rf* (DCM:MeOH, 9:1) 0.4; ^{1}H NMR (400 MHz, DMSO-d_6) δ 9.35 (s, 1H, H^1), 9.14 (d, *J* = 7.5 Hz, 1H, -NH), 8.27 (s, 1H, H^7), 7.99 (d, *J* = 7.9 Hz, 1H, H^5), 7.59 (s, 1H, H$^{7'}$), 7.53 – 7.36 (m, 4H, H^4, H$^{3'}$, H$^{4'}$, H$^{5'}$), 5.62 (d, *J* = 7.5 Hz, 1H, H$^{2'}$), 5.05 (s, 2H, H^3). ^{13}C NMR (101 MHz, DMSO-d_6) δ 171.4, 166.6, 157.2, 139.9, 132.9, 132.7, 130.3, 130.1, 130.1, 127.9, 127.8 127.03, 121.3 (2C), 69.9, 56.4. HPLC-MS (APCI/ESI): Purity = 97%, t_R = 2.227 min, m/z $[M+1]^+$ = 346.1, calculated exact mass for $C_{16}H_{13}BClNO_5$: 345.06.

2-(2-chlorophenyl)-2-(1-hydroxy-1,3-dihydrobenzo[c][1,2]oxaborole-6-carboxamido)acetic acid, 78/MM4-136

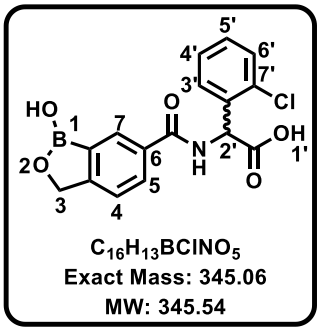

Obtained from hydrolysis of **67/MM4-114** as a white solid (47 mg, 44%); m.p: 160-163 °C; ^{1}H NMR (400 MHz, MeOD) δ 8.14 (s, 1H, H^7), 7.95 (d, *J* = 7.9 Hz, 1H, H^5), 7.54 (dd, *J* = 8.0, 1.1 Hz, 1H, H^6), 7.49 – 7.47 (m, 2H, H^4, H$^{5'}$), 7.37 – 7.32 (m, 2H, H$^{3'}$, H$^{4'}$), 6.15 (s, 1H, H$^{2'}$), 5.12 (s, 2H, H^3). ^{13}C NMR (101 MHz, MeOD) δ 173.2, 170.0, 158.9, 136.1, 135.5, 134.2, 131.4, 130.9 (2C), 130.7, 130.6, 128.4, 122.5 (2C), 72.3, 55.9. HPLC-MS (APCI/ESI): Purity >99%, t_R = 2.102 min, m/z $[M+1]^+$ = 346.1, calculated exact mass for $C_{16}H_{13}BClNO_5$: 345.06.

2-(3-fluorophenyl)-2-(1-hydroxy-1,3-dihydrobenzo[c][1,2]oxaborole-6-carboxamido)acetic acid, 79/MM4-89

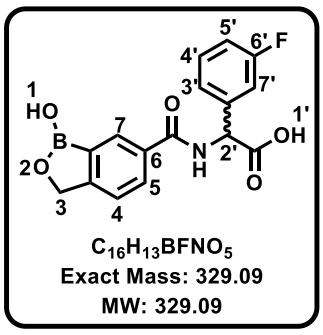

Obtained from hydrolysis of **70/MM4-56** as a light yellow solid (39 mg, 47%); m.p: 132-135 °C; ^{1}H NMR (400 MHz, DMSO-d_6) δ 9.34 (s, 1H, H^1), 9.17 (d, *J* = 7.6 Hz, 1H, -NH), 8.27 (s, 1H, H^7), 7.99 (d, *J* = 8.0 Hz, 1H, H^5), 7.60 – 7.46 (m, 2H, H^4, H$^{7'}$), 7.42 – 7.36 (m, 1H, H$^{4'}$), 7.26 – 7.21 (m, 2H, H$^{3'}$, H$^{5'}$), 5.91 (d, *J* = 7.6 Hz, 1H, H$^{2'}$), 5.04 (s, 2H, H^3). ^{13}C NMR (101 MHz, DMSO-d_6) δ 171.2, 166.6, 161.3, 158.9, 157.2, 132.6, 130.1, 130.1, 129.6, 124.5, 121.3 (2C), 115.5, 115.3, 69.9, 50.1. HPLC-MS

(APCI/ESI): Purity > 99%, t_R = 1.950 min, *m/z* $[M+1]^+$ = 330.1, calculated exact mass for $C_{16}H_{13}BFNO_5$: 329.09.

2-(2-fluorophenyl)-2-(1-hydroxy-1,3-dihydrobenzo[c][1,2]oxaborole-6-carboxamido)acetic acid, 80/MM4-87

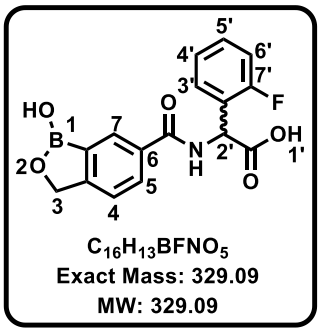

Obtained from hydrolysis of **71/MM4-55** as a white gum (61 mg, 70%); ^{1}H NMR (300 MHz, MeOD) δ 8.16 (s, 1H, H^7), 7.96 (d, *J* = 8.0 Hz, 1H, H^5), 7.54 – 7.21 (m, 3H, H^4, $H^{5'}$, $H^{6'}$), 7.16 – 7.04 (m, 1H, $H^{3'}$), 6.96 (ddd, *J* = 8.3, 7.6, 1.8 Hz, 1H, $H^{4'}$), 5.74 (s, 1H, $H^{2'}$), 5.13 (s, 2H, H^3). ^{13}C NMR (101 MHz, MeOD) δ 169.8, 166.9, 157.3, 135.6, 134.6, 132.4, 130.2, 130.1, 129.8, 127.0, 126.1, 124.6, 121.3 (2C), 69.9, 56.3. HPLC-MS (APCI/ESI): Purity = 96%, t_R = 1.913 min, m/z $[M+1]^+$ = 330.0, calculated exact mass for $C_{16}H_{13}BFNO_5$: 329.09.

1-hydroxy-N-(2-(methylamino)-2-oxo-1-phenylethyl)-1,3-dihydrobenzo[c][1,2]oxaborole-6-carboxamide, 81/MM3-136

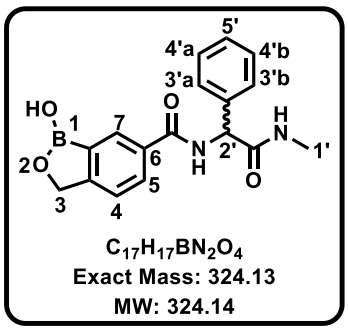

Obtained through method A as a beige solid (15 mg, 8.23%); m.p: 216-218°C; *Rf* (EtOAc: Hex: EtOH, 3:6:1) 0.6; ^{1}H NMR (400 MHz, MeOD) δ 8.16 (s, 1H, H^7), 7.96 (d, *J* = 8.0 Hz, 1H, H^5), 7.52 - 7.46 (m, 3H, H^4, $H^{3'a, 3'b}$), 7.41 – 7.31 (m, 3H, $H^{4'a, 4'b}$, $H^{5'}$), 5.64 (s, 1H, $H^{2'}$), 5.12 (s, 2H, H^3), 2.77 (s, 3H, $H^{1'}$). ^{13}C NMR (101 MHz, MeOD) δ 173.1, 169.8, 158.9, 139.0, 134.2, 131.2, 130.5, 129.8 (2C), 129.3, 128.8 (2C), 122.5 (2C), 72.2, 59.3, 26.5. HPLC-MS (APCI/ESI): Purity >99%, t_R = 2.317 min, *m/z* $[M+1]^+$ = 325.1, calculated exact mass for $C_{17}H_{17}BN_2O_5$: 324.14.

N-(2-(dimethylamino)-2-oxo-1-phenylethyl)-1-hydroxy-1,3-dihydrobenzo[c][1,2]oxaborole-6-carboxamide, 82/MM4-60

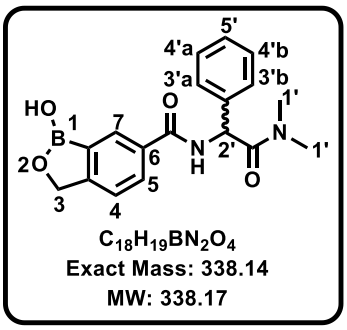

Obtained through method A as a beige solid (12 mg, 22%); m.p: 179-181°C; *Rf* (DCM:MeOH, 9:1) 0.2; ^{1}H NMR (600 MHz, MeOD) δ 8.13 (s, 1H, H^{7}), 7.94 (d, *J* = 8.0 Hz, 1H, H^{5}), 7.49 – 7.43 (m, 3H, H^{4}, $H^{3'a, 3'b}$), 7.40 – 7.34 (m, 3H, $H^{4'a, 4'b}$, $H^{5'}$), 6.09 (s, 1H, $H^{2'}$), 5.10 (s, 2H, H^{3}), 3.01 (s, 6H, $H^{1'}$). ^{13}C NMR (151 MHz, MeOD) δ 171.9, 169.4, 158.9, 137.8, 134.3, 131.2, 130.5, 130.1 (2C), 129.6, 129.4 (2C), 122.5 (2C), 72.2, 56.3, 37.4, 36.4. HPLC-MS (APCI/ESI): Purity >99%, t_R = 2.295 min, *m/z* $[M+1]^+$ = 339.1, calculated exact mass for $C_{18}H_{19}BN_2O_4$: 338.14.

Methyl(S)-2-(1-hydroxy-1,3-dihydrobenzo[c][1,2]oxaborole-6-carboxamido)-2-phenylacetate, 83/MM2-90

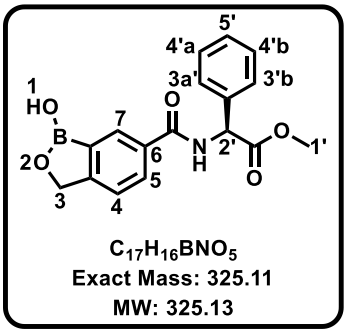

Obtained through method B a white solid (52 mg, 28%); m.p: 130-132°C; *Rf* (EtOAc:Hex:EtOH, 3:6:1) 0.15; ^{1}H NMR (600 MHz, MeOD) δ 8.15 (s, 1H, H^{7}), 7.95 (d, *J* = 8.0 Hz, 1H, H^{5}), 7.49 – 7.46 (m, 3H, $H^{3'a, 3'b,}$ H^{4}), 7.41 – 7.34 (m, 3H, $H^{4'a, 4'b,}$ $H^{5'}$), 5.72 (s, 1H, $H^{2'}$), 5.12 (s, 2H, H^{3}), 3.75 (s, 3H, $H^{1'}$). ^{13}C NMR (151 MHz, MeOD) δ 172.8, 170.2, 158.9, 137.5, 134.2, 131.4, 130.7, 129.9, 129.6, 129.1, 122.5 (2C), 72.3, 58.9, 53.1. HPLC-MS (APCI/ESI): Purity = 96%, t_R = 2.321 min, *m/z* $[M+1]^+$ = 326.1, calculated exact mass for $C_{17}H_{16}BNO_5$: 325.11.

1-hydroxy-N-(2-hydroxy-2-methylpropyl)-1,3-dihydrobenzo[c][1,2]oxaborole-6-carboxamide, 84/MM2-124

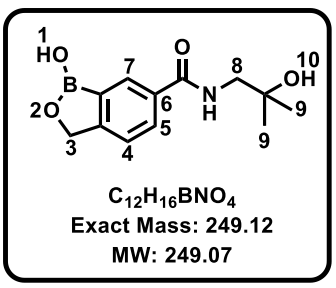

Obtained through method A as a cream wax (25 mg, 18%); *Rf* (DCM:MeOH, 9:1) 0.25; ^{1}H NMR (300 MHz, CD_3CN) δ 8.19 (s, 1H, H^{7}), 7.93 (d, *J* = 8.0 Hz, 1H, H^{5}), 7.48 (d, *J* = 8.0 Hz, 1H, H^{4}), 7.19 (s, 1H, H^{10}), 5.07 (s, 2H, H^{3}), 3.37 (d, *J* = 6.1 Hz, 2H, H^{8}), 1.19 (s, 6H, H^{9} (2 × CH_3)). ^{13}C NMR (151 MHz, CD_3CN) δ 169.2, 158.6, 134.8, 130.8, 130.2, 122.5 (2C), 118.3, 71.6, 51.5, 27.6 (2C). HPLC-MS (APCI/ESI): Purity = 97%, t_R = 0.308 min, *m/z* $[M+1]^+$ = 250.1, calculated exact mass for $C_{12}H_{16}BNO_4$: 249.12.

1-hydroxy-N-(2-hydroxypropyl)-1,3-dihydrobenzo[c][1,2]oxaborole-6-carboxamide, 85/MM2-123

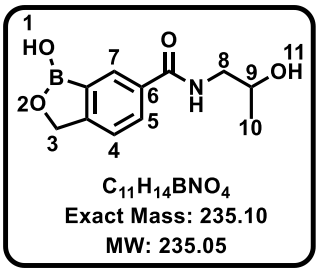

Obtained through method A as a white solid (41 mg, 16%); m.p: 175-178°C; *Rf* (DCM:MeOH, 9:1) 0.15; ^{1}H NMR (300 MHz, MeOD) δ 8.13 (s, 1H, H^7), 7.95 (d, *J* = 8.0 Hz, 1H, H^5), 7.48 (d, *J* = 8.0 Hz, 1H, H^4), 5.12 (s, 2H, H^3), 4.54 (s, 1H, H^{11}), 4.04 - 3.91 (m, 1H, H^9), 3.48 – 3.31 (m, 3H, H^8, 1–OH), 1.21 (d, *J* = 6.3 Hz, 3H, H^{10}). ^{13}C NMR (151 MHz, MeOD) δ 170.7, 158.6, 134.8, 131.0, 130.2, 126.4, 122.5 (2C), 72.2, 67.6, 21.0. HPLC-MS (APCI/ESI): Purity = 96%, t_R = 0.253 min, *m/z* $[M+1]^+$ = 236.1, calculated exact mass for $C_{11}H_{14}BNO_4$: 235.10.

1-hydroxy-N-(2-methoxyethyl)-1,3-dihydrobenzo[c][1,2]oxaborole-6-carboxamide, 86/MM2-119

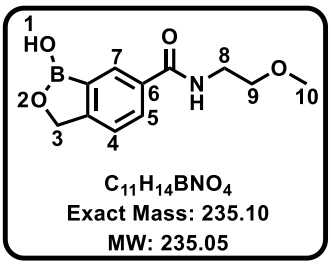

Obtained through method A as a light brown gum (20 mg, 15%); (EtOAc:Hex:EtOH, 3:6:1) 0.3; ^{1}H NMR (600 MHz, MeOD) δ 8.10 (s, 1H, H^7), 7.92 (d, *J* = 8.0 Hz, 1H, H^5), 7.45 (d, *J* = 8.0 Hz, 1H, H^4), 5.11 (s, 2H, H^3), 3.59 – 3.56 (m, 4H, H^8, H^9), 3.38 (s, 3H, H^{10}). ^{13}C NMR (151 MHz, MeOD) δ 170.5, 158.5, 134.7, 130.9, 130.1, 122.4 (2C), 72.2, 72.0, 58.9, 40.7. HPLC-MS (APCI/ESI): Purity = 95%, t_R = 0.469 min, *m/z* $[M+1]^+$ = 236.1, calculated exact mass for $C_{11}H_{14}BNO_4$: 235.10.

Methyl(R)-2-(1-hydroxy-1,3-dihydrobenzo[c][1,2]oxaborole-6-carboxamido)-2-phenylacetate, 87/MM2-44

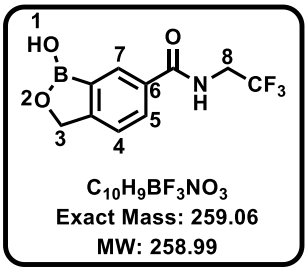

Obtained through method A as a clear solid (5.5 mg, 4%); *Rf* (DCM:MeOH, 9:1) 0.10; ^{1}H NMR (600 MHz, MeOD) δ 8.13 (s, 1H, H^7), 7.95 (d, *J* = 8.0 Hz, 1H, H^5), 7.50 (d, *J* = 7.9 Hz, 1H, H^4), 5.12 (s, 2H, H^3), 4.09 (q, *J* = 9.3 Hz, 2H, H^8, couples to -CF_3). ^{13}C NMR (151 MHz, MeOD) δ 170.6, 159.0, 133.7, 131.1, 130.3, 124.7, 122.6 (2C), 72.2, 42.1. HPLC-MS (APCI/ESI): Purity > 99%, t_R = 0.218 min, *m/z* $[M+1]^+$ = 260.1, calculated exact mass for $C_{10}H_9BF_3NO_3$: 259.06.

rac-(R)-1-hydroxy-N-(2-hydroxy-1-phenylethyl)-1,3-dihydrobenzo[c][1,2]oxaborole-6-carboxamide, 88/MM2-130

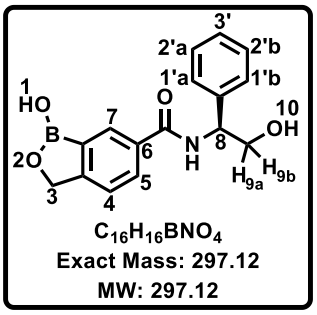

Obtained through method A as a light yellow wax (35 mg, 11%); (EtOAc:Hex:EtOH, 3:6:1) 0.6; ^{1}H NMR (300 MHz, MeOD) δ 8.17 (s, 1H, H^7), 7.96 (d, *J* = 8.1 Hz, 1H, H^5), 7.52 – 7.20 (m, 6H, $H^{1'a,\ 1'b,}$ $H^{2'a,\ 2'b,}$ $H^{3',}$ H^4), 5.26 – 5.16 (m, 1H, H^8), 5.12 (s, 2H, H^3), 3.90 – 3.88 (m, 1H, H^{9a}), 3.86 – 3.84 (m, 1H, H^{9b}), 3.35 (s, 1H, H^{10}). HPLC-MS (APCI/ESI): Purity = 98%, t_R = 2.044 min, *m/z* $[M+1]^+$ = 298.0, calculated exact mass for $C_{16}H_{16}BNO_4$: 297.12.

Methyl2-cyclohexyl-2-(1-hydroxy-1,3-dihydrobenzo[c][1,2]oxaborole-6-carboxamido)acetate, 89/MM2-165

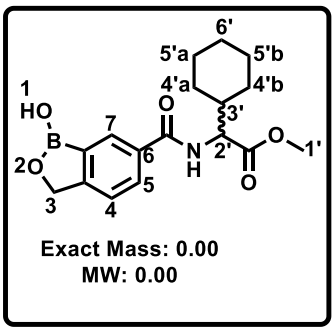

Obtained through method A as a white solid (17 mg, 18%); m.p: 100-101°C; *Rf* (DCM:MeOH, 9:1) 0.30; ^{1}H NMR (300 MHz, MeOD) δ 8.11 (s, 1H, H^7), 7.92 (d, *J* = 8.0 Hz, 1H, H^5), 7.47 (d, *J* = 8.0 Hz, 1H, H^4), 5.12 (s, 2H, H^3), 4.50 (d, *J* = 7.4 Hz, 1H, $H^{2'}$), 3.74 (s, 3H, $H^{1'}$), 1.85 – 1.01 (m, 11H, H3′, $H^{4'a,\ 4'b}$, $H^{5'a,\ 5'b}$, $H^{6'}$). HPLC-MS (APCI/ESI): Purity = 95%, t_R = 2.469 min, *m/z* $[M+1]^+$ = 332.1, calculated exact mass for $C_{17}H_{22}BNO_5$: 331.16.

Methyl 4-(1-hydroxy-1,3-dihydrobenzo[c][1,2]oxaborole-6-carboxamido)benzoate, 90/MM3-85

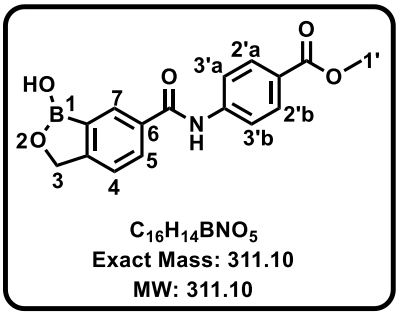

Obtained through method B as a white solid (10 mg, 5.72%); m.p: 232-234 °C; *Rf* (DCM:MeOH, 9:1) 0.25; ^{1}H NMR (400 MHz, MeOD) δ 8.24 (s, 1H, H^7), 8.09 – 7.98 (m, 3H, $H^{5,}$ $H^{3'a,\ 3'b}$), 7.87 (d, *J* = 8.0 Hz, 2H, $H^{2'a,\ 2'b}$), 7.55 (d, *J* = 8.0 Hz, 1H, H^4), 5.16 (s, 2H, H^3), 3.90 (s, 3H, $H^{1'}$). HPLC-MS (APCI/ESI): Purity 99%, t_R = 1.182 min, *m/z* $[M+1]^+$ = 312.1, calculated exact mass for $C_{16}H_{14}BNO_5$: 311.10.

Methyl 5-(1-hydroxy-1,3-dihydrobenzo[c][1,2]oxaborole-6-carboxamido)pyrazine-2-carboxylate, 91/MM3-11

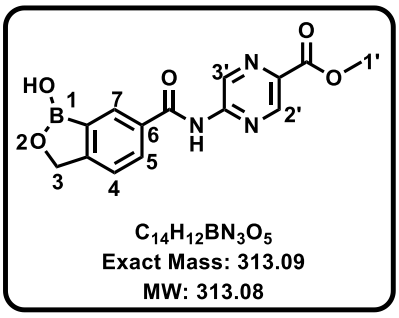

Obtained through method B as a white solid (24 mg, 14%); m.p: 179-183 °C; *Rf* (DCM:MeOH, 9:1) 0.2; ^{1}H NMR (400 MHz, DMSO-d_6) δ 9.39 (s, 1H, H$^{2'}$), 8.59 (s, 1H, H$^{3'}$) 8.40 (s, 1H, H^7), 8.06 (d, *J* = 8.0 Hz, 1H, H^5), 7.56 (d, *J* = 8.0 Hz, 1H, H^4), 5.06 (s, 2H, H^3), 3.87 (s, 3H, H$^{1'}$). HPLC-MS (APCI/ESI): Purity >99%, t_R = 2.317 min, *m/z* $[M+1]^+$ = 311.1, calculated exact mass for $C_{16}H_{14}BNO_5$: 313.09.

Methyl (1-hydroxy-1,3-dihydrobenzo[c][1,2]oxaborole-6-carbonyl)phenylalaninate, 92/MM3-42

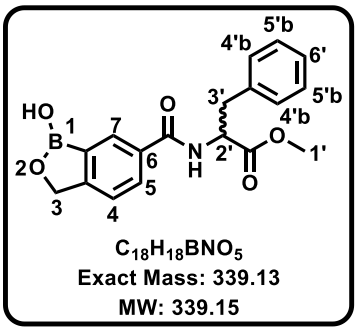

Obtained through method B as a white solid (42 mg, 44%); m.p: 68-70 °C; *Rf* (DCM:MeOH, 9:1) 0.8; ^{1}H NMR (600 MHz, MeOD) δ 8.02 (s, 1H, H^7), 7.83 (d, *J* = 8.0 Hz, 1H, H^5), 7.44 (d, *J* = 8.0, 1H, H^4), 7.31 – 7.24 (m, 4H, H$^{4'a,\ 4'b}$, H$^{5'a,\ 5'b}$), 7.21 – 7.18 (m, 1H, H$^{6'}$), 5.11 (s, 2H, H^3), 4.89 – 4.83 (m, 1H, H$^{2'}$), 3.73 (s, 3H, H$^{1'}$), 3.30 (dd, *J* = 12.0, 6.0 Hz, 1H, H$^{3'}$), 3.12 (dd, *J* = 12.0, 6.0 Hz, 1H, H$^{3'}$). ^{13}C NMR (151 MHz, MeOD) δ 173.7, 170.3, 158.9, 138.5, 134.3, 131.1, 130.3, 130.2 (2C), 129.5 (2C), 127.9, 122.5 (2C), 72.3, 55.9, 52.8, 38.2. HPLC-MS (APCI/ESI): Purity >99%, t_R = 2.381 min, *m/z* $[M+1]^+$ = 340.1, calculated exact mass for $C_{18}H_{18}BNO_5$: 339.15.

Methyl (1-hydroxy-1,3-dihydrobenzo[c][1,2]oxaborole-6-carbonyl)tyrosinate, 93/MM3-10

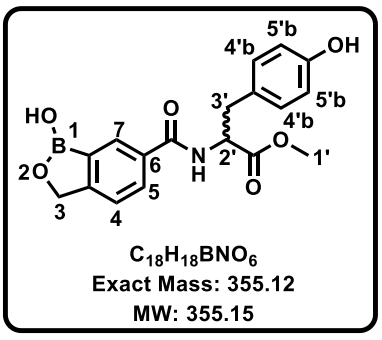

Obtained through method B as a white solid (64 mg, 32%); m.p: 188-190 °C; *Rf* (EtOAc: Hex, 5:5) 0.5; ^{1}H NMR (400 MHz, MeOD) δ 8.03 (s, 1H, H^7), 7.84 (d, *J* = 8.0 Hz, 1H, H^5), 7.45 (d, *J* = 8.0 Hz, 1H, H^4), 7.07 (d, 2H, *J* = 8.0 Hz, H$^{4'a,\ 4'b}$), 6.70 (d, 2H, *J* = 8.0 Hz, H$^{5'a,\ 5'b}$), 5.11 (s, 2H, H^3), 4.82 – 4.78 (m, 1H, H$^{2'}$), 3.72 (s, 3H, H$^{1'}$), 3.18 (dd, *J* = 13.9, 5.4 Hz, 1H, H$^{3'}$), 3.02 (dd, *J* = 14.0, 5.4 Hz, 1H, H$^{3'}$). ^{13}C NMR (101 MHz, MeOD) δ 173.9, 170.4, 158.8, 157.4, 134.3, 131.2 (2C), 131.1, 130.3, 129.1, 122.5 (2C), 116.3 (2C), 72.2, 56.2, 52.7, 37.4. HPLC-MS

(APCI/ESI): Purity >99%, t_R = 2.160 min, *m/z* $[M+1]^+$ = 356.1, calculated exact mass for $C_{18}H_{18}BNO_6$: 355.12.

7.2.5.2. Synthesis of the 7-methyl benzoxaboroles series

Ethyl 3-hydroxy-2-methylbenzoate, 2.15b

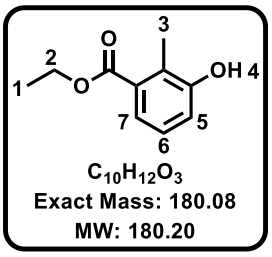

To a solution of 3-hydroxy-2-methylbenzoic acid (5 g, 32.86 mmol) in EtOH (40 mL) was added thionyl chloride (3.58 mL, 49.29 mmol, 1.5 eq.) drop-wise at 0 °C. Reaction mixture was left to stir at 81 °C for 14 h. At this time point reaction mixture was cooled and concentrated under reduced pressure. The resulting crude was submitted to Biotage flash chromatography eluting with EtOAc:Hexane (1:9) to afford **2.15b** was obtained as a light brown wax (5.98 g, 100% (quantitative)); (EtOAc:Hex, 1:9) 0.4; ^{1}H NMR (300 MHz, DMSO-d_6) δ 9.70 (s, 1H, H^4), 7.16 (dd, *J* = 7.7, 1.5 Hz, 1H, H^7), 7.08 (t, *J* = 9.0 Hz, 1H, H^6), 6.98 (dd, *J* = 7.9, 1.5 Hz, 1H, H^5), 4.25 (q, *J* = 7.1 Hz, 2H, H^2), 2.27 (s, 3H, H^3), 1.29 (t, *J* = 7.1 Hz, 3H, H^1). HPLC-MS (APCI/ESI): Purity >99%, t_R = 0.925 min, *m/z* $[M+1]^+$ = 181.2, calculated exact mass for $C_{10}H_{12}O_3$: 180.08.

Ethyl 3-hydroxy-2-methylbenzoate, 2.15c

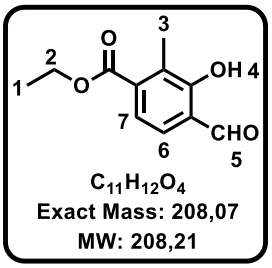

To a solution of **2.15b** (6.60 g, 27.14 mmol) in THF (30 mL) were added $MgCl_2$ (10.46 g, 109.88 mmol), TEA (20.42 mL, 146.54 mmol) and (HCHO)n (9.80 g). The mixture was immediately heated to 80 °C and was stirred for 14 h. The reaction mixture was cooled to 15 °C. To it were added ice H_2O (20 mL) and then 12 N HCl (10 mL) slowly. The mixture was stirred for 1 h and then extracted with EtOAc (25 mL x 3). The combined organic layer was washed with sat. $NaHCO_3$ to neutral, dried over Na_2SO_4, filtered and concentrated under reduced pressure to give crude. This was submitted to Biotage eluting with EtOAc (0-40%) in Hexane and pooled fractions afforded **2.15c** was a light yellow oil (4.89 g, 64%); (EtOAc:Hex, 3:7) 0.7; ^{1}H NMR (300 MHz, DMSO-d_6) δ 10.11 (s, 1H, H^5), 7.69 (d, *J* = 8.1 Hz, 1H, H^7), 7.32 (d, *J* = 8.1 Hz, 1H, H^6), 4.32 (q, *J* = 7.1 Hz, 2H, H^2), 2.31 (s, 3H, H^3), 1.32 (t, *J* = 7.1 Hz, 3H, H^1). HPLC-MS (APCI/ESI): Purity = 97%, t_R = 1.072 min, *m/z* $[M+1]^+$ = 209.1, calculated exact mass for $C_{10}H_{12}O_3$: 208.21.

Ethyl 4-formyl-2-methyl-3-(((trifluoromethyl)sulfonyl)oxy)benzoate, 2.15d

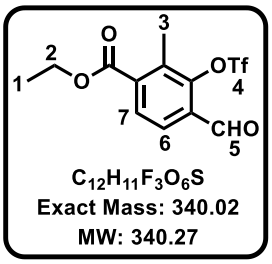

To a solution of **2.15c** (4.6 g, 22 mmol) in DCM (10 mL) was slowly added trifluoromethanesulfonic anhydride (5.6 mL, 33 mmol) and triethylamine (9.24 mL, 66 mmol) at 0 °C. The reaction mixture was then warmed to 26 °C and stirred for 3 hours. Thereafter, 10 mL water was added to the reaction mixture and the solution extracted with DCM (3x10 mL). The combined organic solution was dried on Na_2SO_4 and then filtered and concentrated under reduced pressure to give a brown solid residue. This was adsorbed on silica and submitted to Biotage flash chromatography eluting with EtOAc in hexane (2:8). Fractions containing the product were pooled and concentrated under reduced pressure to give **2.15d** (3.5 g, 47%) as a white wax; *Rf* (EtOAc:Hex, 2:8) 0.6; confirmed with HPLC-MS (APCI/ESI): Purity = 90%, t_R = 2.610 min, *m/z* $[M+1]^+$ = 341.1, calculated exact mass for $C_{10}H_{12}O_3$: 340.02.

Ethyl 1-hydroxy-7-methyl-1,3-dihydrobenzo[c][1,2]oxaborole-6-carboxylate, 2.14f

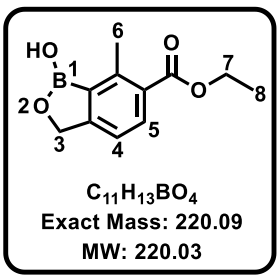

To a solution of ethyl 4-formyl-2-methyl-3-(4,4,5,5-tetramethyl-1,3,2-dioxaborolan-2-yl)benzoate in MeOH:THF (Solvent 1:19, 20 mL) was added $NaBH_4$ (catalytic, 104 mg) in portions at 0 °C. Then the reaction mixture was stirred at 25 °C for 1 h. HPLC showed the starting material was consumed. The reaction solution was adjusted to pH = 4 with 2 M HCl. The organic layer was removed *in vacuo*. The residue was taken into DCM:MeOH (5:5) and the resulting solid was filtered to afford **2.14f** (1.48 g) as a white solid used in the next step without further purification; ^{1}H NMR (300 MHz, DMSO-d_6) δ 9.20 (s, 1H, H^1), 7.88 (d, *J* = 7.9 Hz, 1H, H^5), 7.31 (d, *J* = 7.9 Hz, 1H, H^4), 4.99 (s, 2H, H^3), 4.28 (q, *J* = 7.1 Hz, 2H, H^7), 2.67 (s, 3H, H^6), 1.31 (t, *J* = 7.1 Hz, 3H, H^8).

1-hydroxy-7-methyl-1,3-dihydrobenzo[c][1,2]oxaborole-6-carboxylic acid, 2.15g

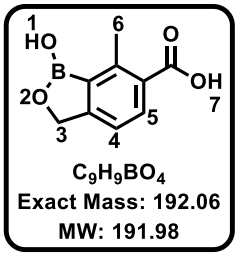

To a solution of **2.14f** in H_2O (10 mL) was added 1N NaOH and heated at 40 °C for 3 h. Reaction mixture was left to stir at 24 °C for 14 h. LCMS showed product **C** formation. The reaction mixture was treated with 2N HCl to pH = 2. The solid was filtered and washed with water. The cake was dried to give the acid **C** (808 mg, 63%) as a white solid; ^{1}H NMR (300 MHz, DMSO-d_6) δ 12.76 (s, 1H, H^7), 9.16 (s, 1H, H^1), 7.90 (d, J = 7.9 Hz, 1H, H^5), 7.28 (d, J = 8.0 Hz, 1H, H^4), 4.98 (s, 2H, H^3), 2.68 (s, 3H, H^6).

Methyl 2-(1-hydroxy-7-methyl-1,3-dihydrobenzo[c][1,2]oxaborole-6-carboxamido)-2-phenylacetate, 94/MM4-141

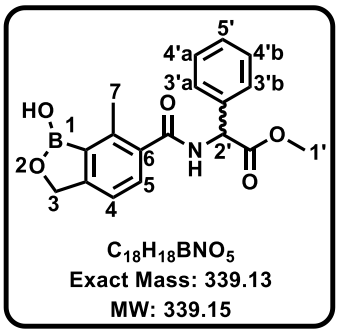

Using method B, the product was obtained as a beige solid (88 mg, 65%); m.p: 152-154 °C; *Rf* (DCM:MeOH, 9:1) 0.5;^{1}H NMR (300 MHz, MeOD) δ 7.51 – 7.30 (m, 6H, H^5, H$^{3'a,\ 3'b}$, H$^{4'a,\ 4'b}$, H$^{5'}$), 7.22 (d, J = 7.8 Hz, 1H, H^4), 5.68 (s, 1H, H$^{2'}$), 5.04 (s, 2H, H^3), 3.75 (s, 3H, H$^{1'}$), 2.51 (s, 3H, H^7). ^{13}C NMR (101 MHz, MeOD) δ 173.1, 172.6, 156.8, 141.4, 137.3, 136.3, 131.2, 129.9 (2C), 129.6, 129.0 (2C), 119.4 (2C), 71.8, 58.7, 53.0, 17.8. HPLC-MS (APCI/ESI): Purity >99%, t_R = 2.352 min, *m/z* $[M+1]^+$ = 340.1, calculated exact mass for $C_{18}H_{18}BNO_5$: 339.13.

Methyl 2-(1-hydroxy-7-methyl-1,3-dihydrobenzo[c][1,2]oxaborole-6-carboxamido)-2-phenylacetate, 95/MM4-144

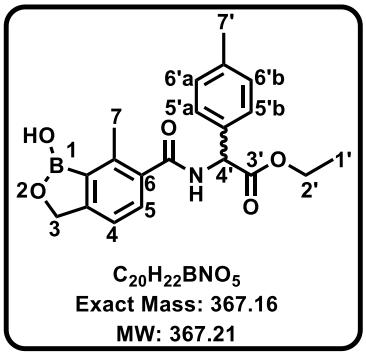

Obtained from **2.15g** using method B as a white solid (58 mg, 61%); m.p: 118-120 °C; *Rf* (DCM:MeOH, 8:2) 0.5; ^{1}H NMR (400 MHz, MeOD) δ 7.44 (d, J = 7.7 Hz, 1H, H^5), 7.33 (d, J = 8.0 Hz, 2H, H$^{5'a,\ 5'b}$), 7.23 – 7.20 (m, 3H, H^4, H$^{6'a,\ 6'b}$), 5.60 (s, 1H, H$^{4'}$), 5.04 (s, 2H, H^3), 4.21 (q, J = 7.1 Hz, 2H, H$^{2'}$), 2.51 (s, 3H, H^7), 2.34 (s, 3H, H$^{7'}$), 1.23 (t, J = 7.1 Hz, 3H, H$^{1'}$). ^{13}C NMR (101 MHz, MeOD) δ 173.0, 172.3, 156.8, 141.4, 139.6, 136.4, 134.3, 131.2, 130.5 (2C), 128.9 (2C), 119.4 (2C), 71.8, 62.7, 58.6, 21.2, 17.8, 14.4. HPLC-MS (APCI/ESI): Purity = 97%, t_R = 2.486 min, *m/z* $[M+1]^+$ = 368.2, calculated exact mass for $C_{20}H_{22}BNO_5$: 367.16.

Methyl 2-(1-hydroxy-7-methyl-1,3-dihydrobenzo[c][1,2]oxaborole-6-carboxamido)-2-phenylacetate, 96/MM4-150

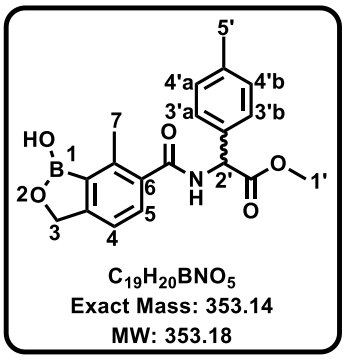

Obtained from **2.15g** using method B a yellow solid (64 mg, 70%); m.p: 137-139 °C; *Rf* (EtOAc:Hexane, 4:6) 0.4; ^{1}H NMR (300 MHz, MeOD) δ 7.46 (d, *J* = 7.7 Hz, 1H, H^5), 7.38 – 7.30 (m, 5H, $H^{3'a, 3'b}$, $H^{4'a, 4'b}$, H^4), 5.68 (s, 1H, $H^{2'}$), 5.04 (s, 2H, H^3), 3.76 (s, 3H, $H^{1'}$), 2.51 (s, 3H, H^7), 2.34 (s, 3H, $H^{5'}$). ^{13}C NMR (101 MHz, MeOD) δ 173.1, 172.6, 158.7, 141.4, 137.3, 136.3, 131.2, 129.9 (2C), 129.6, 129.0 (2C), 119.4 (2C), 71.8, 58.7, 53.0, 21.2, 17.8. HPLC-MS (APCI/ESI): Purity >99%, t_R = 2.476 min, *m/z* $[M+1]^+$ = 354.1, calculated exact mass for $C_{19}H_{20}BNO_5$: 353.14.

Methyl 2-(1-hydroxy-7-methyl-1,3-dihydrobenzo[c][1,2]oxaborole-6-carboxamido)-2-phenylacetate, 97/MM4-148

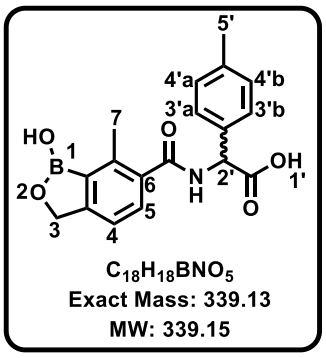

Obtained from hydrolysis of **95** (0.163 mmol, 60 mg, 1 eq.) with $LiOH{\cdot}H_2O$ (0.490 mmol, 21 mg, 3 eq.) in THF:H_2O (4:1) the product was obtained as a white solid (41 mg, 73%); m.p: 227-229 °C; ^{1}H NMR (400 MHz, MeOD) δ 7.44 (d, *J* = 7.7 Hz, 1H, H^5), 7.37 – 7.30 (d, *J* = 8.0 Hz, 2H, $H^{3'a, 3'b}$), 7.23 – 7.20 (m, 3H, H^4, $H^{4'a, 4'b}$), 5.60 (s, 1H, $H^{2'}$), 5.04 (s, 2H, H^3), 2.51 (s, 3H, H^7), 2.34 (s, 3H, $H^{5'}$). ^{13}C NMR (101 MHz, MeOD) δ 173.0, 172.3, 156.8, 141.4, 139.6, 136.4, 134.3, 131.2, 130.5 (2C), 128.9, 119.4 (2C), 71.8, 62.7, 58.6, 21.2, 17.8. HPLC-MS (APCI/ESI): Purity >99%, t_R = 2.237 min, *m/z* $[M+1]^+$ = 340.1, calculated exact mass for $C_{18}H_{18}BNO_5$: 339.13.

7.3. Biological Assays

7.3.1. Antiplasmodium activity evaluation protocols

7.3.1.1. The modified [^{3}H]-hypoxanthine incorporation assay for asexual blood stage parasites conducted at STPH

Compounds were screened against chloroquine (CQ)-sensitive (CQS) *Pf*NF54 and CQ resistant (CQR) multidrug-resistant (K1) strains of *P. falciparum in vitro* using the modified [^{3}H]-hypoxanthine incorporation assay.[258] *P. falciparum* was cultivated in a variation of the medium previously described,[136, 259] consisting of RPMI 1640 supplemented with 0.5% ALBUMAX® II, 25 mM Hepes, 25 mM $NaHCO_3$ (pH 7.3), 0.36 mM hypoxanthine and 100 µg/mL neomycin. Human erythrocytes served as host cells. Cultures were maintained at 37 °C in an atmosphere of 3% O_2, 4% CO_2 and 93% N_2 in humidified modular chambers. Compounds were dissolved by sonication in DMSO (10 mg/mL) and diluted in hypoxanthine-free culture medium. Infected erythrocytes (100 µL per well with 2.5% haematocrit and 0.3% parasitemia) were added to each drug titrated in 100 µL duplicates over a 64-fold range. After 48 h incubation, 0.5 µCi of [^{3}H]hypoxanthine in 50 µL medium was added and plates were incubated for an additional 24 h. Parasites were harvested onto glass-fiber filters and radioactivity was counted using a Betaplate liquid scintillation counter (Wallac, Zurich). The results were recorded as counts per minute (cpm) per well at each drug concentration and expressed as a percentage of the untreated controls. Fifty percent inhibitory concentrations (IC_{50}) were estimated by linear interpolation.[260]

7.3.1.2. The modified LDH assay for asexual blood stage parasites conducted at UCT

The test samples were tested in triplicate on two occasion against the CQS *P*NF54 and CQR K1 strains. Continuous *in vitro* cultures of asexual erythrocyte stages of *P. falciparum* were maintained using the method of Trager and Jensen (1976) with modifications.[136] Quantitative assessment of antiplasmodium activity *in vitro* was determined via the parasite lactate dehydrogenase assay using a modified method described by Makler *et al.*[261]

The test samples were prepared to a 10mM stock solution in 100% DMSO and sonicated to enhance solubility. Samples were tested as a suspension if not completely dissolved. Stock solutions were stored at -20°C. Further dilutions were prepared on the day of the experiment. CQ and artesunate were used as the reference drug in all experiments. A full dose-response was performed for all compounds to determine the concentration inhibiting 50% of parasite growth (IC_{50}–value). In a 96 well plate, test samples were serially diluted 2-fold from the highest concentration in complete medium to give 10 concentrations to evaluate. Thereafter, an equivalent volume of parasite stock at 2% parasitemia was added to each well, to a final volume of 200µL with a hematocrit of 1%. The same dilution technique was used for all samples. The highest concentration of solvent to which the parasites were exposed to had no measurable effect on the parasite viability. Control compounds were tested at a starting concentration of 1000 ng/mL. Each plate also contained blank and control populations, comprising of non-parasitised red blood cells (RBCs) and parasitised red blood cells respectively, to create reference points at representing 0% and 100% survival.

Plates were incubated for 72 h, then flash-frozen at -80 °C. A duplicate plate with each well containing 100 µL of Malstat reagent and 25 µL of nitroblue tetrazolium solution was prepared for each plate containing parasites. The parasite plates were thawed and the contents carefully resuspended. A volume of 20 µL was transferred from each parasite plate well to the corresponding well in the duplicate plate. Plates were left in the dark for 20 minutes to allow the dye to develop, then plates were analysed on a spectrophotometer at 620 nm. The IC_{50}-values were obtained using a non-linear dose-response curve fitting analysis via GraphPad Prism v.4.0 software.

7.3.1.3. The SYBR Green assay for asexual blood stage parasites conducted at UP

Asexual *Pf*NF54 (drug susceptible) and K1 (drug resistant) parasite strains were cultivated under previously described conditions.[136] Parasites were maintained at 5% hematocrit (A+/O+ human erythrocytes) in complete culture media [RPMI 1640 (Sigma-Aldrich) supplemented with 25 mM HEPES, 20 mM D-glucose, 200 µM hypoxanthine, 0.2% (w/v) sodium bicarbonate, 24 µg/mL gentamicin, and 0.5% (w/v) AlbuMAX II)] and kept under hypoxic conditions (90% N_2, 5% O_2, and 5% CO_2) at 37 °C with agitation. D-sorbitol [5% (w/v)] was used to synchronize parasite

cultures, resulting in predominantly (>95%) ring stages, when required. Parasite progression and morphology of asexual blood stages were monitored microscopically using Giemsa-stained thin smears.

The SYBR Green I assay enabled analysis of synchronized *in vitro Pf* NF54 and K1 parasites (1% parasitemia, 1% hematocrit) exposed to drug pressure for 96 h at 90% N_2, 5% O_2, and 5% CO_2 with CQ the positive control for inhibition of parasite proliferation. Parasite proliferation was determined once the 96 h incubation had elapsed by adding equal volumes (100 µL) of parasite suspension and SYBR Green I lysis buffer (0.2% µL/ml of 10 000x SYBR Green I, 20 mM Tris-HCl, pH 7.5, 5 mM EDTA, 0.008% saponin (w/v) and 0.08% Triton x-100) and incubated for 1 h at room temperature in the dark. Fluorescence was quantified with the GloMaxR-Multi+Detection System at 485/538 nm and used as a direct measure of proliferation.[200] Data for preliminary hit identification was performed for one biological replicate in technical triplicates whereas three independent biological replicates of technical triplicates were performed for dose–response evaluation.[262]

7.3.1.4. *In vitro* activity against gametocyte stage

The *in vitro* gametocyte activity was investigated in luciferase reporter line-based assay of the transgenic *Pf*NF54. In this luciferase assay a transgenic parasite line NF54-*Pf*S16-GFP-Luc was used to enable stage-specific assessment of gametocytocidal activity. Gametocytes were prepared according to the procedure reported by Reader *et al.*[263] Experiments were performed on days 5 (representing >90% of either early stage I - III) and 10 (representing mature stage IV/V gametocytes). In each experiment, assays were set up with the use of 2 to 3% gametocytaemia, 1.5% haematocrit culture and 48 h drug pressure in a gas chamber (90% N_2, 5% O_2, and 5% CO_2) and temperature maintained at 37 °C. Luciferase activity was determined in 30 µl parasite lysates by adding 30 µl luciferin substrate (Promega Luciferase Assay System) at room temperature and detection of resultant bioluminescence at an integration constant of 10s with the GloMax®-Multi+ Detection System with Instinct® Software. Methylene blue (5 µM) and MMV390048 (5 µM) were included as controls.

7.3.2. Cytotoxicity evaluation protocol

7.3.2.1. *In vitro* cytotoxicity evaluation against Chinese Hamster Ovarian (CHO) cell line

The *in vitro* cytotoxicity of the synthesized compounds was evaluated against the CHO cancer cell line using the MTT [3-(4,5-dimethylthiazolyl-2)-2,5-diphenyltetrazolium bromide] assay, which is a colorimetric assay based on assessing the cell metabolic activity.[264] The synthesized compounds were assayed in triplicate. Stock solutions of 2 mg/mL of test samples in DMSO were prepared with poorly soluble samples being tested as suspensions. The compounds were kept at -20 °C until required. In all experiments, emetine was used as a reference drug.
Starting from an initial concentration of 100 µg/mL, ten-fold serial dilutions were made in complete medium to give 6 concentrations to the lowest concentration of 0.001 µg/mL. The cell viability was not affected by the highest concentration of the solvent to which the cells were exposed. The full dose-response curves were plotted using a non-linear dose-response curve fitting analysis via GraphPad Prism v.4.0 software. By this, the minimum concentration required for 50% inhibition (IC_{50}) values were determined for each compound.

7.3.2.2. *In vitro* cytotoxicity evaluation against Caucasian hepatocellular carcinoma cells (HepG2) cells

HepG2 were maintained according to the previously described conditions.[200] Cells were grown in Dulbecco's Modified Eagle's Medium (DMEM) (HyClone) supplemented with 5% Fetal Bovine Serum (heat inactivated) and 1 % Penicillin/Streptomycin (Sigma-Aldrich) at 37 °C at 5% CO_2. Cell viability was monitored microscopically with 0.2% Trypan-Blue. Cells were trypsinised with 1x Trypsin-EDTA (Sigma) and ~100 000 cells were plated in 96-well plates and grown for 24 h. The cells were treated at 2 µM compound concentration and incubated for 48 h at 37 °C and 5% CO_2. Cytotoxicity was determined using the CytoSelect™. LDH Cytotoxicity Assay Kit (Cell Biolabs Inc., CBA-241) which was added to the supernatant. Absorbance was measured at 450 nm. Data obtained were analysed in Excel and experiments were performed in technical duplicates for one biological repeats (n=1).

7.3.3. Metabolic Stability Assay

Metabolic stability was conducted using the one-time point assay.[265] The metabolic stability assay was performed in duplicate in a 96-well micro titre plate. The test compounds (0.1 μM) were incubated (37 °C) in mouse, rat and pooled human liver microsomes (final protein concentration of 0.4 mg/mL; XenoTech, Lenexa, KS) suspended in 0.1 M phosphate buffer (pH 7.4) for 30 minutes, in the presence and absence of the cofactor NADPH (1 mM). The reactions were quenched by the addition of ice-cold acetonitrile containing an internal standard (carbamazepine, 0.0236 μg/mL). The samples were centrifuged, and the supernatant was filtered and analysed by means of HPLC-MS/MS (Agilent Rapid Resolution HPLC, AB SCIEX 4500 MS). The relative loss of parent compound over time was monitored and plots were prepared for each compound of concentration versus time to determine the first order rate constant for compound depletion. This was used to calculate the degradation half–life and *in vitro* intrinsic clearance value.

7.3.4. Chemical Rescue Experiment

Cultures were prepared and maintained according to the procedure captured in section **7.3.1.2**. However, in order to determine the effect of the CoA precursors on the PPAT compound IC_{50} values, the precursors were prepared to 20 x the final desired concentration in complete medium. A dose-response experiment was prepared for each compound as described in **7.3.1.2** above. A fixed volume of 10 μL of each precursor was added to each well to yield the desired final concentration, and plates were incubated and developed as described in **7.3.1.2**. The effect of the precursors was determined by comparing the IC_{50} of the proposed PPAT compound alone to the IC_{50} of the same compound in the presence of the precursor.

7.3.5. Beta-hematin inhibition assay

Selected proposed PPAT inhibitors were evaluated for the potential for inhibition of beta-hematin formation in an established assay procedure.[225] Hundred microliters of a solution containing water/305.5 μM NP-40/DMSO at a v/v ratio of 70%/20%/10%, respectively, was added to every well in columns 2 - 12 of a 96-well plate. To column 1 was added 140 μL of water and 40 μL of 305.5 μM NP-40. Twenty microliters of the test compounds (20 mM), that is, the synthesized compounds and control, was added to column 1 in duplicate. One hundred microliters of the test

solution was diluted to column 11, with column 12 left as a blank (0 μM of compound). A 178.8 μL aliquot of hematin (hemin) stock was suspended in 20 mL of a 1 M acetate buffer, pH 4.8 and 100 μL of this hematin suspension added into each well. Plates were then incubated for ~5 hours at 37 oC after which 32 μL of pyridine solution (20% water, 20% acetone, 10% 2M HEPES buffer (pH 7.4), 50% pyridine) was added followed by addition of 60 μL of acetone to all wells. Plates were again read at 405 nm on a Thermo Scientific Multiscan Go Microplate Spectrophotometer. The IC_{50} values were determined using GraphPad Prism 9.

7.3.6. Solubility Determination

7.3.6.1. HPLC Kinetic Solubility

A miniaturised shake flask method was used to perform the solubility assay. From 10 mM stock solutions of the test compounds in DMSO, calibration standards (10 - 220 μM in DMSO) were prepared. The 10 mM stock solutions were also used to spike (1:50) duplicate aqueous samples in phosphate buffered saline (pH 6.5). The DMSO was dried off in a GeneVac (MiVac, 90 min, 37 °C) after which the samples were incubated while shaking for 20 hours at 25 °C. Thereafter, the solutions were filtered, and their absorbance measured using HPLC-DAD (Agilent 1200 Rapid Resolution HPLC with a diode array detector). The calibration standards were used to plot the calibration curves, which were used to determine the solubility of the aqueous samples.

7.3.6.2. Turbidimetric (Kinetic) Solubility

Stock solutions (10 mM) of test compounds were prepared by dissolving in DMSO. Serial dilutions of the test compounds were prepared in a 96-well microtitre plate in DMSO in triplicate from the stock solutions starting from 8 mM to 0.25 mM on a predilution plate. This was followed by secondary serial dilutions in triplicate in either DMSO or PBS buffer (0.01M ph 7.4), by pipetting 4 μL aliquots from the predilution plate to corresponding wells in the secondary plate to make up to the final volume of 200 μL in each well. The serial dilutions in DMSO only wells (total volume 200 μM) were controls. The plate was covered and incubated for 2 hours in an oven maintained at 37 °C. The absorbance values of the wells were then measured by a UV-Visible Multiscan Go 1510-05438 spectrometer (Thermo Scientific) at 620 nM, i.e. the wavelength the compounds are not expected to absorb. The obtained

values were then corrected by subtracting the absorbance of the blank wells containing only DMSO. The corrected absorbance values were plotted as a function of concentration using Microsoft ® Office Excel from which the concentration was determined to identify solubility. This was the value where the concentration of the compound deviate from zero or the baseline.

7.3.7. Culturing for Metabolomics

7.3.7.1. Parasite culture maintenance

*Pf*3D7 strain was maintained under standard culture conditions at 2%hematocrit with O-positive human erythrocytes according to the conditions described by Allman *et al.*[127] Ring-stage developing parasites were suspended in 5% sorbitol (Sigma-Aldrich) over three subsequent developmental cycles to synchronize parasites within 4 to 6 h, as previously described. *P. falciparum* cultures were collected by centrifugation at 1,500 x *g* for 5 min at 25 °C, and the parasitized RBC pellet was resuspended in a 10 x volume of 5% sorbitol, followed by incubation at 37 °C for 10 min. Following incubation, the cells were pelleted and washed in 50 ml of complete medium, prior to placement of the parasites back into culture flasks at 2% hematocrit and 2% parasitemia.

7.3.7.2. Sample preparation for metabolomics

Hydrophilic metabolite changes following compound intervention were profiled according to the procedure by Allman *et al.*[127] Treatments were performed on 1 x 10^8 MACS-purified, synchronized trophozoite parasite-infected RBCs (24-36 h post invasion) in 5 mL RPMI. Compounds were added at a concentration of 10 x 3 IC_{50} 72 h and incubated for 2.5 h. All treatment conditions were performed as technical triplicates and included an untreated control. Subsequently, PBS washes were performed, and infected RBCs were extracted with 90% methanol containing 0.5 mM $^{13}C^{15}N$-labelled aspartate as an internal standard, then dried under nitrogen and stored at -80 °C. Process blanks were generated at the time of extraction in technical triplicates. Samples were then resuspended in high-performance liquid chromatography (HPLC) grade water containing 1 mM chlorpropamide as an additional internal standard and analyzed by ultra-high-performance liquid chromatography mass spectrometry UHPLC-MS as described.[127, 266]

7.3.7.3. Data Analysis

Following negative ionization analysis of hydrophilic extracts on a Thermo Exactive Plus Orbitrap, sample data were converted and transferred for analysis.[266] Targeted peak picking from a curated list of 298 metabolites was achieved using el-MAVEN software[267], followed by normalization and analysis via RStudio and Metaboanalyst[268]. Data visualization was performed with the Hyperspec (http://hyperspec.r-forge.r-project.org) and Suprahex R[269] scripting packages in RStudio. Metabolomic profiling through hierarchical clustering for identification of related metabolic signatures was performed using the Ward method, based on the Pearson correlation coefficients, by the Hyperspec R integrated heatmap function.

7.3.8. DNA Barcoded resistant mutants studies

7.3.8.1. Parasite culture preparation

Two vials of the barcoded pool were thawed two weeks before starting the assay to allow for expansion of the parasite lines. These pool cultures were then combined, and the culture allowed to expand to ~300 mL. On day 1 of the assay, 1-3% ring stage parasitaemia of the culture was prepared. A 10 mL sample was collected from the bulk culture prior to dispensing into 6 well plates and each compound was screened against duplicate 5 mL cultures. After the cultures had settled, the media was removed and replaced with fresh media containing the query compound at 3 x IC_{50}. Growth over the course of 14 days was monitored by flow cytometry (Cytoflex, Beckman Coulter) with parasites stained in a 96 well plate using 1 x SYBR green. At day 14, the cultures were harvested, and red blood cells lysed by saponin (0.1%). Parasite pellets were collected by centrifugation (3000 rpm, 5min) and washed once with PBS, before resuspending in 100 µl phosphate-buffered saline (PBS) and freezing at -20 ˚C.

7.3.8.2. Sample preparation and barcode amplification

Barcode amplification and indexing was performed with two sequential polymerase chain reaction (PCR) and for this assay, PCR1 was performed directly on the parasite pellet resuspended in PBS. Water was included as a control.

Ampure clean-up

Beads were allowed to reach room temperature before use, and then vortexed well to resuspend. The PCR product was mixed with 1.8 vol ampure beads in a 96 well round-bottom plate and incubated for 10 mins. Magnetic was applied on 96 well-plate holder for 5 min and the supernatant was removed. While on magnet, 200 µl of fresh 80% ethanol was added to rinse (repeated twice). Ethanol was removed and beads were allowed to dry for 2-5 min. Elution was performed in 30 µl water for 10 mins off magnet. The plate was returned to magnet and eluate was collected.

7.3.8.3. Sample preparation and submission for sequencing

Indexed and purified samples were quantified via picogreen assay in duplicate by adding 1 µl of sample to 100 µl of picoGreen Mix in black 96-well plates (Greiner Bio-One). Wells were sealed, mixed and incubated at room temperature for 2 mins before reading on a FLUOstar Omega plate reader (BMG Labtech). DNA standards including 14, 7, 3.5, 1.75, 0.88, 0.44, 0.22 (ng/µl) were used to generate a standard curve. Sample concentrations were generated using MARS data analysis software. 25 ng of each sample were combined before being diluted to 4 nM for MiSeq submission.

Direct amplification libraries were submitted for loading on MiSeq supplied as both the 4 ˚C and -20 ˚C components of the MiSeq kit (BCSO0012). For sequencing the following Miseq conditions were applied:

Spike in 50 % PhiX

Run at low cluster density aiming for 400 k/mm^2.

Pass conditions: % PF≥ 85 (Cluster density range tolerated if PF≥85%: 350-600 k/mm^2)

150 bp paired-end reads

7.3.8.4. Data analysis

De-multiplexing and generation of FASTQ files were done on the Illumina cloud (BaseSpace). FASTQ files were downloaded and processed by custom scripts that generated a count matrix for each molecular barcode that identifies a mutant line. Only intact barcodes flanked by the correct genomic sequence context were counted. Barcode counts were further processed in R to produce plots and statistical analysis of counts to reveal the effect of drugs on the composition of the population of mutant

lines over time. The statistical analysis was performed using DeSeq2 for RNAseq analysis.

7.4. References

1. Desjardins, R. E.; Canfield, C.; Haynes, J.; Chulay, J., Quantitative assessment of antimalarial activity in vitro by a semiautomated microdilution technique. *Antimicrob. Agents Chemother.* **1979**, *16* (6), 710-718.

2. Trager, W.; Jensen, J. B., Human malaria parasites in continuous culture. *Science* **1976**, *193* (4254), 673-675.

3. Dorn, A.; Stoffel, R.; Matile, H.; Bubendorf, A.; Ridley, R. G., Malarial haemozoin/β-haematin supports haem polymerization in the absence of protein. *Nature* **1995**, *374* (6519), 269-271.

4. Huber, W.; Koella, J. C., A comparison of three methods of estimating EC50 in studies of drug resistance of malaria parasites. *Acta Trop* **1993**, *55* (4), 257-61.

5. Makler, M.; Ries, J.; Williams, J.; Bancroft, J.; Piper, R.; Gibbins, B.; Hinrichs, D., Parasite lactate dehydrogenase as an assay for Plasmodium falciparum drug sensitivity. *Am. J. Trop. Med.* **1993**, *48* (6), 739-741.

6. Verlinden, B. K.; Niemand, J.; Snyman, J.; Sharma, S. K.; Beattie, R. J.; Woster, P. M.; Birkholtz, L.-M., Discovery of Novel Alkylated (bis)Urea and (bis)Thiourea Polyamine Analogues with Potent Antimalarial Activities. *J. Med. Chem.* **2011**, *54* (19), 6624-6633.

7. Leshabane, M.; Dziwornu, G. A.; Coertzen, D.; Reader, J.; Moyo, P.; van der Watt, M.; Chisanga, K.; Nsanzubuhoro, C.; Ferger, R.; Erlank, E., Benzimidazole Derivatives Are Potent against Multiple Life Cycle Stages of Plasmodium falciparum Malaria Parasites. *ACS Infect. Dis.* **2021**, *7* (7), 1945-1955.

8. Reader, J.; Botha, M.; Theron, A.; Lauterbach, S. B.; Rossouw, C.; Engelbrecht, D.; Wepener, M.; Smit, A.; Leroy, D.; Mancama, D., Nowhere to hide: interrogating different metabolic parameters of Plasmodium falciparum gametocytes in a transmission blocking drug discovery pipeline towards malaria elimination. *Malar. J.* **2015**, *14* (1), 1-17.

9. Mosmann, T., Rapid colorimetric assay for cellular growth and survival: application to proliferation and cytotoxicity assays. *J. Immunol. Methods* **1983**, *65* (1-2), 55-63.

10. Bertrand, M.; Jackson, P.; Walther, B., Rapid assessment of drug metabolism in the drug discovery process. *Eur. J. Pharm. Sci.* **2000**, *11*, S61-S72.

11. Sandlin, R. D.; Fong, K. Y.; Wicht, K. J.; Carrell, H. M.; Egan, T. J.; Wright, D. W., Identification of β-hematin inhibitors in a high-throughput screening effort

reveals scaffolds with in vitro antimalarial activity. *Int J Parasitol Drugs Drug Resist* **2014**, *4* (3), 316-325.

12. Allman, E. L.; Painter, H. J.; Samra, J.; Carrasquilla, M.; Llinás, M., Metabolomic profiling of the malaria box reveals antimalarial target pathways. *Antimicrob. Agents Chemother.* **2016**, *60* (11), 6635-6649.

13. Murithi, J. M.; Owen, E. S.; Istvan, E. S.; Lee, M. C.; Ottilie, S.; Chibale, K.; Goldberg, D. E.; Winzeler, E. A.; Llinás, M.; Fidock, D. A., Combining stage specificity and metabolomic profiling to advance antimalarial drug discovery. *Cell Chem. Biol.* **2020**, *27* (2), 158-171.

14. Agrawal, S.; Kumar, S.; Sehgal, R.; George, S.; Gupta, R.; Poddar, S.; Jha, A.; Pathak, S., El-MAVEN: a fast, robust, and user-friendly mass spectrometry data processing engine for metabolomics. In *High-throughput metabolomics*, Springer: 2019; pp 301-321.

15. Chong, J.; Soufan, O.; Li, C.; Caraus, I.; Li, S.; Bourque, G.; Wishart, D. S.; Xia, J., MetaboAnalyst 4.0: towards more transparent and integrative metabolomics analysis. *Nucleic Acids Res.* **2018**, *46* (W1), W486-W494.

16. Fang, H.; Gough, J., supraHex: an R/Bioconductor package for tabular omics data analysis using a supra-hexagonal map. *Biochem. Biophys. Res. Commun.* **2014**, *443* (1), 285-289.